EQUIVALENCE MEASUREMENT STUDIES (SECTIONS 1 - 4)

Phillip A. Bello, et al

CNR, Incorporated

Prepared for:

Rome Air Development Center

April 1975

RADC-TR-75-95, Volume I (of two)
Final Technical Report
April 1975

EQUIVALENCE MEASUREMENT STUDIES
(Sections 1 - 4)

CNR, Inc.

Rome Air Development Center
Air Force Systems Command
Griffiss Air Force Base, New York 13441

UNCLASSIFIED

SECURITY CLASSIFICATION OF THIS PAGE (When Data Entered)

REPORT DOCUMENTATION PAGE		READ INSTRUCTIONS BEFORE COMPLETING FORM
1. REPORT NUMBER RADC-TR-75-95, Volume I (of one)	2. GOVT ACCESSION NO.	3. RECIPIENT'S CATALOG NUMBER
4. TITLE (and Subtitle) EQUIVALENCE MEASUREMENT STUDIES (Sections 1 - 4)		5. TYPE OF REPORT & PERIOD COVERED Final Technical Report April 1973 - May 1974 6. PERFORMING ORG. REPORT NUMBER N/A
7. AUTHOR(s) Phillip A. Bello Louis A. Jankauskas Leslie W. Pickering		8. CONTRACT OR GRANT NUMBER(s) F30602-73-C-0267
9. PERFORMING ORGANIZATION NAME AND ADDRESS CNR, Inc. 20 Wells Ave. Newton, MA 02159		10. PROGRAM ELEMENT, PROJECT, TASK AREA & WORK UNIT NUMBERS 62702F 45191812
11. CONTROLLING OFFICE NAME AND ADDRESS Rome Air Development Center (DCLD) Griffiss AFB, NY		12. REPORT DATE April 1975 13. NUMBER OF PAGES 369
14. MONITORING AGENCY NAME & ADDRESS(if different from Controlling Office) Same		15. SECURITY CLASS. (of this report) UNCLASSIFIED 15a. DECLASSIFICATION/DOWNGRADING SCHEDULE N/A

16. DISTRIBUTION STATEMENT (of this Report)

Approved for public release; distribution unlimited.

17. DISTRIBUTION STATEMENT (of the abstract entered in Block 20, if different from Report)

Same

18. SUPPLEMENTARY NOTES

RADC Project Engineer:
Charles N. Meyer (DCLD)
AC 315 330-2859

19. KEY WORDS (Continue on reverse side if necessary and identify by block number)

Channel Quality Monitoring; HF Channel; Troposcatter Channel; Line-of-sight Microwave Relay Channel; Satellite Ionospheric Scintillation Channel; Advanced Data Transmission Modems

20. ABSTRACT (Continue on reverse side if necessary and identify by block number)

This report describes the results of an investigation concerned with developing and evaluating concepts for channel quality monitoring of advanced digital data transmission techniques over four fading dispersive channels of interest to military communications: the line-of-sight ground point-to-point microwave relay, troposcatter, satellite ionospheric scintillation, and high-frequency long haul channels. The study emphasis is on a monitoring subsystem called the Media Quality Unit (MQU) which continually estimates long- and short-term error rates for a nondegraded receiver and by comparison with actual error rate as

DD FORM 1 JAN 73 1473 EDITION OF 1 NOV 65 IS OBSOLETE

UNCLASSIFIED

SECURITY CLASSIFICATION OF THIS PAGE (When Data Entered)

measured by a Performance Monitor Unit (PMU) allows estimation of receiver degradation trends and classification of outages into receiver-, media, or interference-caused. Major effort was devoted to development and analysis of MQU techniques which utilize the received information-bearing signal alone as a source of channel information since continuous on-line operation is possible and no special probing signals are required. However, some attention is given to special probing signals and their application to each of the channels of interest. For all channel parameter and error rate estimation techniques, the measurement accuracy was determined as a function of processing bandwidth, averaging time, and channel parameters. Consideration is given to implementation alternatives for the MQU in terms of analog, digital hardware, and small computer processing.

PREFACE

This final report, covering the period April 1973 to May 1974, was prepared by CNR, Inc., of Newton Massachusetts, under Contract F30602-73-C-0267 with Rome Air Development Center, Griffiss Air Force Base, New York.

This study was carried out by Dr. P. A. Bello, Dr. L. E. Jankauskas, and Dr. L. W. Pickering. The project was directed by Dr. P. A. Bello.

The authors wish to acknowledge the ready and willing assistance of RADC project engineer, Mr. C. N. Meyer. The project was originally administered by the Signal Processing Section of RADC under the direction of Mr. Miles Bickelhaupt and subsequently transferred to the Digital Technical Control Group under Mr. D. Iram.

CONTENTS

CONTENTS (Continued)

CONTENTS (Continued)

CONTENTS (Continued)

CONTENTS (Continued)

ILLUSTRATIONS

ILLUSTRATIONS (Continued)

ILLUSTRATIONS (Continued)

ILLUSTRATIONS (Continued)

ILLUSTRATIONS (Continued)

ILLUSTRATIONS (Continued)

ILLUSTRATIONS (Continued)

TABLES

EVALUATION:

The projected conversion of the Defense Communications System (DCS) from an analog FDM-FM to a digital TDM-PCM facility has accentuated the need for automated communications performance monitoring and assessment. A leading problem in this area is the development and evaluation of concepts for channel quality monitoring of advanced digital data transmission techniques over channels of interest to military communications. A principal area of emphasis is estimating receiver degradation trends and classification of outages into receiver-, media- or interference- caused.

The results of the study suggest detailed design development and testing of experimental models of media quality units for those channels having mandated interest. At the time of this writing that would be the LOS channel only, although the results for tropo, HF and ionospheric scintillation are also interesting.

For LOS links the recommended equipment contains the following subsystems: (1) Media sensor; (2) system function estimator; (3) short-term error rate estimations; (4) interference-presence detection; and (5) narrowband interference detection. Two kinds combinations might be advantageously implemented. The first, essentially, employs the received data signal alone without special probing signals and the second employs special probes. A mini-computer would be used for short-term error rate estimation to provide feasibility for evaluating different error rate estimation algorithms with different LOS modems.

The study results are going to be used as inputs to on-going efforts in project 2155, System Control Improvements. Two particular applications are presently envisioned. First, the report will be provided as a reference for the phase II 2155 effort "Automated Performance Monitoring and Assessment for

Digital Microwave Systems." The second possible application of report results is presently in the formulation stages and would be contingent on evolving 2155 requirements and the response to them generated under the projects' third phase which is now only in the basic planning stage.

Charles N. Meyer

CHARLES N. MEYER
Project Engineer

Because of the size of this report, it has been divided into 2 volumes. Vol I contains Sections 1 through 4. Vol II contains Sections 5 through 6 and Appendixes A, B & C.

This report has been reviewed by the RADC Information Office (OI) and is releasable to the National Technical Information Service (NTIS). At NTIS it will be releasable to the general public, including foreign nations.

This technical report has been reviewed and approved for publication.

APPROVED: Charles N Meyer

CHARLES N. MEYER
Project Engineer

APPROVED: Fred I Diamond

FRED I. DIAMOND
Technical Director
Communications & Navigation Division

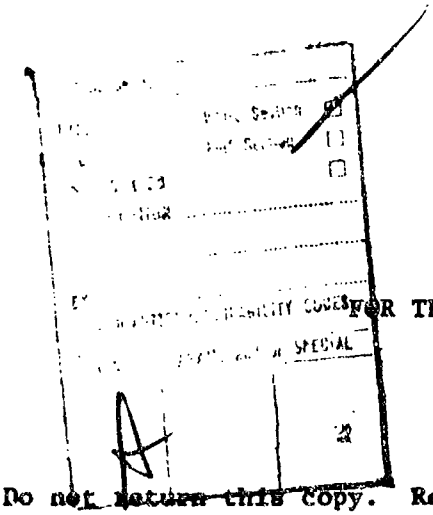

FOR THE COMMANDER: John P Huss

JOHN P. HUSS
Acting Chief, Plans Office

Do not return this copy. Retain or destroy.

SECTION 1

SUMMARY, CONCLUSIONS, AND RECOMMENDATIONS

The effective technical control of the projected digital DCS (Defense Communication System) requires continuous on-line monitoring of the channel not only to isolate faults but, more important, to identify degradation trends and their causes so that corrective action may be taken before excessive degradation has occurred. This final report presents the results of a study involved with the conception and critical performance analysis of such monitoring techniques for four types of radio links: line-of-sight (LOS) microwave relay links, troposcatter links, satellite links subjected to ionospheric scintillation, and HF links.

The term Media Quality Unit (MQU) has been coined here to describe the monitoring subsystem which implements the new monitoring techniques arrived at in the present study. The MQU continually estimates the long- and short-term error rate performance of a nondegraded receiver by means of algorithms applied to appropriate channel measurements taken as near as possible to the antennas of the diversity receivers. An additional function of the MQU is the detection and identification of propagation and interference outages to prevent them from being misinterpreted as receiver faults.

In this section a summary is presented of the report with appropriate references to the detailed discussions in Sections 2 through 6. Following this, conclusions and recommendations for additional work following from the study are presented.

1.1 Channel Modeling

An MQU estimates continually in real time the error rate performance that is achievable with the given channel conditions if the radio receiver, diversity combiner, and modem were properly functioning. For meaningful MQU concepts to be developed, relationships must be established between error rates for various classes of modems and the time-variant dispersive characteristics of the propagation media of interest.

Section 2 is concerned with modeling the characteristics of the radio channels of interest (HF, troposcatter, LOS, satellite

ionospheric scintillation) so that the relationships between important channel parameters and digital modem performance discussed in subsequent sections are made evident.

The discussion is general at first, and then proceeds to a discussion of specific channels. Thus, attention is first given to the system function characterization of radio channels, including "instantaneous" input-output relationships, channel correlation functions, gross channel parameters, and statistics. Following this, attention is focused on the specific channels of interest: HF, troposcatter, line-of-sight radio relay, and satellite ionospheric scintillation channels. Both typical and atypical channel characteristics and advanced digital modem techniques are discussed. Table 1-1 has been compiled as a compact summary of some of the salient characteristics of LOS, troposcatter, satellite ionospheric scintillation, and HF links.

While we do not wish to repeat the material in this table, it is worth making some comments on the LOS channel which must be treated in a different fashion for monitoring. The most harmful source of fading on LOS ground microwave relay links is due to refractive anomalies which create multiple path transmission. The multipath fading on LOS channels is extremely slow with fade depths of 40 dB lasting for seconds -- a hundred or more times longer than a troposcatter channel. However, it is important to note that even in a 40-dB fade the SNR is respectable for a LOS link (say 20 dB) while for a troposcatter link, a 40-dB fade would result in negative dB SNR's. Thus, in monitoring a LOS channel so as to predict modem performance, considerable attention must be paid to the dispersive character of the channel during a deep fade although no such attention is required for a troposcatter link since additive noise has dominated performance well before the 40-dB fade is reached. Thus, while a few nanoseconds would be considered to cause negligible degradation due to frequency-selective fading in a 14-MHz band for a troposcatter link, this need not be true for the LOS link because, as shown in [1.1], the degree of frequency selectivity increases with the fade depth. Because of the slowness of fading and the possible importance of frequency selectivity during fades, the LOS channel error rate performance should be estimated on an instant-by-instant basis. Error rates averaged over the fading are not meaningful for this channel.

In modeling the channel to compute the performance of advanced modems, it is necessary to distinguish between "conventional" and "in-band" diversity communications.

TABLE 1-1

A SUMMARY OF RANGES OF CHANNEL PARAMETERS FOR FOUR LINKS

Channel	Multipath Spread	Doppler Spread	Statistical Models	Comments
Line-of-Sight Ground Microwave Relay	0 to a few nanoseconds	0 to a few millihertz	A few discrete amplitude and phase-variable paths when multipath fading occurs. Single path under more common non-fading conditions.	14-MHz bandwidth typical. 60-dB SNR typical for nonfaded channel. Currently 1 bit/sec/Hz modems being field-tested using baseband duobinary combined with FM radio. 2 bits/sec/Hz and higher modems being investigated. Dual space diversity used to force outages due to deep fades of 40 dB or more to be very rare. Frequency-selective fading exists during deeper fades. Outage may exist at much less than 40 dB due to selective fading.
Troposcatter Links	RMS values from 0.1 to 0.5 μs	RMS values from 0.1 to 20 Hz	Continuum of independently fluctuating complex Gaussian paths.	7-MHz bandwidth. Hourly median SNR's vary over range of 30 dB or more over a season. Quadruple space diversity used. Only experimental modems built. 3 Mb/s achieved and 6 - 12 Mb/s under development with adaptive nonlinear feedback equalizer.
Satellite Ionospheric Scintillation	A fraction of the reciprocal of the carrier frequency	Fraction of 1 Hz for ground-to-stationary satellite	Single path with nonzero-mean Gaussian fluctuating quadrature components.	Same bandwidth allocations and data rates as ground microwave relay. Margin against fading not large. Fading predominant at VHF and decreasing in severity as frequency increases. At 1.6 GHz

TABLE 1-1 (Continued)

Channel	Multipath Spread	Doppler Spread	Statistical Models	Comments
				6-dB fades may occur. Negligible fading 4 - 8 GHz. Space and time-diversity being considered.
HF	Fraction of ms to 4 ms excluding auroral paths	RMS values from a fraction of a Hz to a few Hz	Several discrete paths with complex Gaussian fading.	3 - 4 kHz bandwidth. SNR's quite variable. SSB transmission. Both noise-limited and medium-limited performances may occur on same link at different times. Advanced modems use codem techniques for 2400 b/s. Dual frequency diversity sometimes available using independent sidebands.

In the former case, clearly identified diversity channels exist, each involving transmitters and/or receivers, e.g., quadruple space diversity for troposcatter links. In the latter case, the decision variables at the receiver may be put in a form mathematically identical to the decision variables resulting from conventional diversity combining.

In-band diversity can only be achieved when the signaling elements occupy a bandwidth over which frequency-selective fading occurs and/or a time duration over which time-selective fading occurs. The word signaling element here is interpreted broadly to include all portions of the received signal involved in making a digital decision. In particular, all the energy in a block code would be included in this definition of signaling element.

The use of in-band diversity is under serious consideration for advanced modems on all fading dispersive channels. The utilization of codes to obtain in-band diversity has been pioneered by D. Chase [1.2] and applied by him to the HF channel [1.3] and the troposcatter channel [1.4]. It has been suggested that the nonlinear feedback equalizer achieves in-band diversity [1.5] and such a modem is currently being implemented for use on troposcatter links by Sylvania for the U.S. Army. Also, Raytheon has devised and built for RADC a modem which attempts to extract in-band diversity. In all cases, the objective of the signal processing is to achieve close to maximum likelihood demodulation of the received digital signals.

1.2 Channel Quality Monitoring

Section 3 is concerned with developing the rationale for the basic signal processing functions of the MQU, elucidating the procedures whereby the MQU is used in cooperation with the Performance Monitor Unit (PMU) to establish degradation trends and identify outages, and presenting implementing alternatives.

Lack of attention to the fading dispersive character of a radio channel has frequently led in the past to modems whose performances have been greatly degraded by the time-selective (fast) and frequency-selective fading properties of the channel. Such degradations become manifest in the appearance of symbol distortion, intersymbol interference, crosstalk between channels, and degraded phase references. However, for each of the radio channels of interest in the present study, good designs are possible wherein the performance would be rarely determined by the time- and frequency-selective fading distortion.

Thus, in estimating the performance of a modem based upon the channel characteristics, major attention has been given to performance limited by flat-flat fading, i.e., no frequency-selective and time-selective distortion of symbols. This point of view is sensible because the major benefit of the MQU will be to alert the controller to the existence of degradation trends and sudden faults occurring in the receiving equipment. The occasional outage caused by the propagation medium is worth noting so that misdirected corrective action will not be initiated. However, there is probably little technical control action other than rerouting that would normally be taken per se during brief propagation outages.

Primarily, then, one needs to detect the presence of propagation outages due to excessive multipath and Doppler spread rather than provide a precise error rate prediction during such highly disturbed conditions. Thus, more detailed consideration was given to the error rate behavior for well-designed modems under normal channel conditions, i.e., where performance is not determined by excessive time- and frequency-selective fading or unexpected additive disturbances. Both conventional and in-band diversity operation of modems are considered.

1.2.1 Error Rate Estimation Under Normal Conditions

For conventional operation it is shown that measurements of the instantaneous SNR's on the diversity receivers can be used to estimate the error rates for a nondegraded modem without making any apriori judgments about the statistics of the channel fluctuations. It is assumed, however, that the noises on the diversity receivers are statistically independent and random-phased, an assumption which is likely to be true in most cases of normal operation. The procedure is called the "conditional error probability" method and assumes the availability of a computable conditional error probability expression that relates a specified modem's error rate to the diversity channel's instantaneous SNR's for a particular diversity-combining method.

In the case of Gaussian noise, these conditional error probability expressions have already been derived for FSK and PSK modems assuming several methods of diversity combining. Several are presented in Section 3.1 and additional references given. For example, for maximal ratio predetection diversity combining, Gaussian noise and differentially coherent binary PSK,

$$P_c(\gamma_1, \gamma_2, \ldots, \gamma_M) = \frac{1}{2} \exp\left(- \sum_{m=1}^{M} \gamma_m\right) \tag{1.1}$$

where $P_c(\cdot)$ is the conditional error probability, $\gamma_m(t)$ is the instantaneous SNR on the m^{th} diversity branch, and M is the order of diversity. Short- and long-term error rate estimates are obtained by estimating $\{\gamma_m(t);\ m=1,2,\ldots,M\}$, computing $P_c(\gamma_1,\gamma_2,\ldots,\gamma_M)$, and performing short- and long-term averages, as indicated in Figure 1.1.

At low error rates, the reliable estimation of average error rates takes an inordinate amount of time. An error amplification technique has been conceived to artifically increase the conditional error rate so as to reduce the average error rate measurement variance. A simple extrapolation procedure is then used to estimate the correct error rate from the measured amplified error rate. The theoretical basis for this technique comes from a theorem proven in Section 3.1. It is shown that at high SNR and for a wide class of fading and additive noise statistics the average error rate takes the form

$$P_e \longrightarrow \frac{C}{\Gamma_1 \Gamma_2 \ldots \Gamma_M} \tag{1.2}$$

where Γ_m is the average SNR on the m^{th} diversity receiver and C is a constant dependent on the modem, diversity combiner, and fading statistics at low signal levels.

The error amplification technique involves dividing the m^{th} diversity receiver instantaneous SNR, $\gamma_m(t)$, by a factor $r_m > 1$, carrying out the error rate estimate with these factors, and then dividing the resulting average error rate by the product $r_1 r_2 \ldots r_M$. Mathematically,

$$\hat{P}_e = \frac{1}{\prod_{m=1}^{M} r_m} \left\langle P_c\left(\frac{\gamma_1}{r_1}, \frac{\gamma_2}{r_2}, \ldots, \frac{\gamma_M}{r_M}\right)\right\rangle \tag{1.3}$$

where $\hat{P}_e$ is an estimate of P_e and $\langle\ \rangle$ denotes a time average.

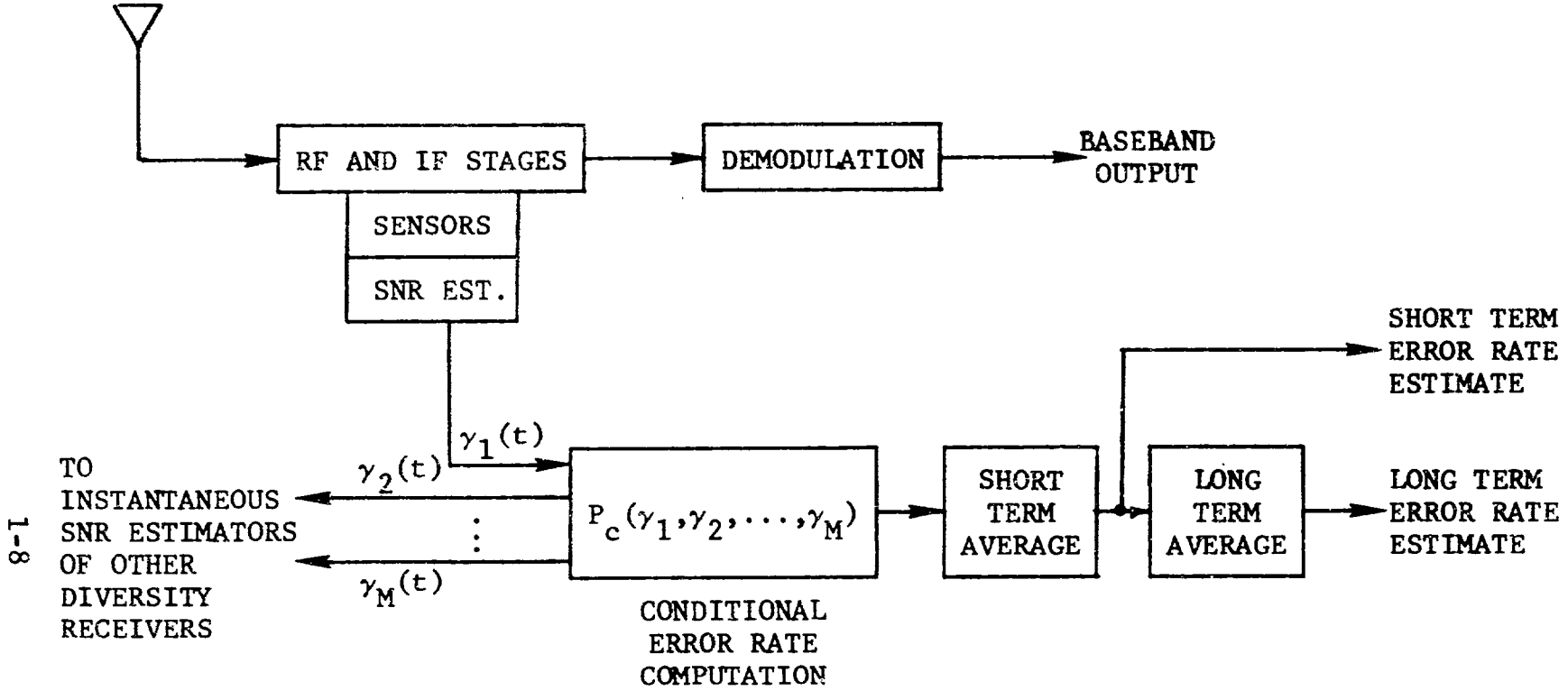

Figure 1.1 The Conditional Error Probability Method for Estimating Nondegraded Modem Performance

A similar error rate estimation procedure, called the "threshold" method, is discussed in Section 3.1 applicable to the high SNR case. In the threshold method, γ_M is compared against a threshold X_m and an estimate $\hat{P}_X$ is made of the probability P_X of the joint event $\{\gamma_m < X_m;\ m=1,2,\ldots,M\}$. It is shown in 3.1 that the desired error rate estimate is given by

$$\hat{P}_e = \hat{P}_X \frac{\int\int\cdots\int P_c(\gamma_1,\gamma_2,\ldots,\gamma_M)d\gamma_1 d\gamma_2\cdots d\gamma_M}{X_1X_2\cdots X_M} \tag{1.4}$$

Since $P_c(\gamma_1,\gamma_2,\ldots,\gamma_M)$ is a known function (dependent on the modem, diversity combiner, and additive noise statistics), the multiple integral is a constant that can be computed. For example, in the case of predetection diversity combining, Gaussian noise, and binary DPSK, we readily find from (1.1) that

$$\int\int\cdots\int P_c(\gamma_1,\gamma_2,\ldots,\gamma_M)d\gamma_1 d\gamma_2\cdots d\gamma_M = \frac{1}{2} \tag{1.5}$$

which leads to

$$\hat{P}_e = \frac{\hat{P}_X}{2\prod_{m=1}^{M} X_m} \tag{1.6}$$

The proof that this result is true for a wide variety of fading and additive noise statistics at high SNR follows from the same theorem used to prove (1.2). The use of the threshold technique is limited to the same region of applicability as the error amplification technique.

If one is willing to assume that the fading statistics are known except for some average channel parameters, in some cases the averages over the fading can be carried out analytically to obtain explicit formulae for error probability as a function of these average parameters. Then measurement of the average parameters and their use in these formulae allow an estimation of error probability. This approach, which is called the "formula" approach, is evaluated in Section 5 for some specific cases.

It is pointed out in Section 2.1.3 that complex Gaussian fading statistics appear to be the best general model available. Fortunately, there exist a considerable number of evaluations of error probability assuming complex Gaussian statistics. To use the formula approach for error rate estimation in the case of correlated fading on the diversity channels it is necessary to measure the complex cross-correlation coefficients between the diversity channels in addition to the average SNR's on each branch.

The error rate estimation procedure described above is applicable to conventional modems not employing in-band diversity. For modems employing in-band diversity techniques (in addition to conventional diversity) which attempt to achieve near-maximum likelihood demodulation, a procedure is derived in Section 3.1 for error rate estimation analogous to that described above for conventional modems. In this case, an estimate is made of the "instantaneous" total received signal power $s_m(t)$ to noise power for the m^{th} receiver, instead of just the SNR at the center of the band. The average error rate is estimated by

$$P_e = \langle P_c(s_1, s_2, \ldots, s_M) \rangle \tag{1.7}$$

where $P_c(s_1, s_2, \ldots, s_M)$ is an appropriate conditional error probability expression. Unfortunately, amplification, threshold, and formula approaches cannot be applied to estimate error rate as in conventional diversity combining unless one is willing to make an estimate of the "equivalent" order of in-band diversity. However, this is a heuristic concept which needs further analysis to be applied to the present real-time estimation needs.

1.2.2 Error Rate Estimation for Atypical Conditions

The techniques discussed above will provide error rate predictions for a properly functioning receiver that can be continually compared with actual performance as determined at the demodulator output by a PMU (performance monitor unit). This comparison will reveal trends in the receiver degradation or sudden failures. However, there will always be occasional propagation or interference conditions outside normal design conditions which will cause the error rate to increase beyond acceptable values, and it is important to detect these situations so that they will not be interpreted as receiver degradation.

We consider in sequence the effects of excessive Doppler spread, excessive multipath spread, and interference.

1.2.2.1 Effect of Doppler Spread

If Doppler spreads become too large (i.e., fast fading), two types of nonidealities occur in data reception:

a) Pulse distortion resulting in destruction of orthogonality relationships and crosstalk in parallel subchannels.

b) Channel measurement degradation, resulting in imperfect predetection diversity combining and coherent detection.

In either case, one may show that the rms Doppler spread* B is the fundamental channel parameter not only determining the onset of fast fading degradation but also frequently allowing a quantitative estimate of performance degradation. The importance of b) is illustrated by examining the effects of fast fading on performance due to channel measurement degradation. One may carry out similar calculations for a), but for channels and modems of interest in this study the effects of b) dominate.

Differential phase-shift-keying is used almost universally on modern HF modems. Fast fading will introduce differential phase errors. It is shown in Section 3 that if $P_e(S)$ is the error rate for M'ary DPSK with any order of diversity, assuming zero Doppler spread and Gaussian noise, the error rate with complex Gaussian fading and an rms Doppler spread B is $P_e(S_{eff})$, where

$$S_{eff} = \frac{S}{1 + S(\pi B\Delta)^2/2} \quad ; \quad (\pi B\Delta)^2/2 << 1 \qquad (1.8)$$

and Δ is the pulse width. The amount of SNR degradation in dB caused by the Doppler spread is

*It is assumed that the mean Doppler shift is tracked and compensated for with some form of AFC. Additional degradation will result from uncompensated Doppler shift. The rms Doppler spread is twice the standard deviation of the power spectrum of a received carrier when normalized to unit area.

$$10 \log \frac{S}{S_{eff}} = 10 \log(1 + S(\pi B\Delta)^2/2) \tag{1.9}$$

The amount of degradation increases with the SNR. For 1-dB degradation

$$B\Delta = \frac{1}{\sqrt{40S}} \tag{1.10}$$

For a numerical example, note that in HF communications, pulse widths vary from 10 to 20 ms. For a 20-ms pulse width we see from (1.10) that for less than 1-dB degradation at 20-dB SNR the rms Doppler spread must satisfy the inequality

$$B < 0.71 \text{ Hz} \tag{1.11}$$

For other channels of interest, the pulse widths would be orders of magnitude smaller and Doppler spread would always have negligible effect for DPSK communications. However, Doppler spread could still have an undesirable effect when phase references are established for coherent detection and predetection diversity combining, because long averaging times are used to extract the phase reference, e.g., as in the case of a filtered pilot tone. The predominant effect of the averaging is the group delay Δ_{gr} suffered by the fading pilot tone. This will produce decorrelation between the complex fading on the data signal and that on the pilot tone. It is shown in Section 3 that if the error rate for coherent detection and any order of diversity without decorrelation (again, Gaussian noise and complex Gaussian fading assumed) is $P_e(S)$, the error rate with decorrelation is given by $P_e(S_{eff})$, where

$$S_{eff} = \frac{S}{1 + S(\pi B\Delta_{gr})^2} \tag{1.12}$$

For 8-GHz troposcatter links, Doppler spreads of 20 Hz are possible though not common. For < 1 dB degradation at 20-dB SNR, only 560 μs of group delay would be tolerable.

For more complicated channel measurement schemes, such as those using decision-directed operations and the implicit ones used in adaptive equalizers, the same general comments apply. The product of the Doppler spread by the group delay of the measurement process must be sufficiently small.

1.2.2.2 Effect of Multipath Spread

We consider now the effects of excessive multipath spread. As the multipath spread increases beyond modem design values, the following nonidealities will occur:

a) Excessive intersymbol interference

b) Pulse distortion, destruction of orthogonality, and crosstalk in parallel subchannels

c) Degradation of channel measurement functions

The major effect of these nonidealities is to produce an irreducible error rate. Unfortunately, the relationship between modem performance and channel parameters is considerably more complex than for channel measurement degradation due to excessive Doppler spread. Generally speaking, as the rms multipath spread L increases, all the nonidealities become successively worse so that although it is not usually possible to relate error rate uniquely to rms multipath spread alone, one may always use the size of L as a flag to signal the presence of atypical multipath spreads.

Section 3 considers the kinds of channel parameters needed to predict modem average error rate. These calculations are useful for HF and troposcatter links. They may not be very important for the satellite ionospheric scintillation channel which appears to have negligible multipath. Average calculations over the fading are probably not meaningful for the LOS microwave relay, as mentioned previously. However, Section 3 does point out the new channel parameters needed to specify the relationship between excessive frequency-selective fading and modem performance for the LOS channel.

Performance analyses of FSK, DPSK, and PSK modems in the presence of frequency-selective fading have been carried out by Bello [1.6] - [1.8], Bello and Nelin [1.9][1.10], Bello and Ehrman [1.11][1.12], and Bello and Crystal [1.13]. Section 3 draws upon these varied calculations to present a brief summary of the relationship between channel characteristics and modem performance in the presence of frequency-selective fading.

In discussing these relationships, the modem type is distinguished according to the presence or absence of the following features:

1) Bandlimited or rectangular signaling pulses
2) Phase-continuous or discontinuous operation
3) The existence of receiver time gates
4) Conventional or "in-band" diversity operations

When the signaling pulses do not have slowly decreasing spectral tails, as for a rectangular pulse, but have their energy well-confined to a given bandwidth W, the first few terms of the frequency power series model [see (2.14)] are adequate to characterize the frequency-selective fading. Thus, for the quadratically selective fading model, it may be shown that in addition to the rms multipath spread the third and fourth moments of the delay power spectrum $Q(\xi)$ are the essential parameters needed to evaluate error rates due to frequency-selective fading. $Q(\xi)$ describes the profile of received power versus path delay.

For the LOS microwave relay channel, strictly bandlimited communications is involved because the transmission of data with attention to high bits/sec/Hz operation is of prime interest. As mentioned previously, channel parameters averaged over the fading are of doubtful significance for LOS channels. In this case, the parameters of interest are the coefficients in the power series channel model themselves. It is demonstrated that for moderate distortion the output of a phase detector or frequency discriminator may be determined from these coefficients.

In the case of rectangular pulses and conventional modems and for in-band diversity modems, it is shown that the essential channel parameters needed to determine error rates due to frequency-selective fading are various integrals involving the delay power spectrum $Q(\xi)$. Only in the case of channel measurement errors due to frequency-selective fading do we have a direct performance prediction possible from the rms multipath spread parameter L.* However, degradation in all cases will increase with L and it should be possible to flag atypical frequency-selective distortion with a measured value of L.

*The rms multipath spread is twice the standard deviation of the delay power spectrum when normalized to unit area.

1.2.2.3 Interference

It is assumed that under normal operating conditions interfering signals will not be present. When they are present, it is essential, as a minimum, to flag this condition. Additional information concerning the gross structure and specific statistical parameters of the noise would be helpful in identifying the source of noise and, if desired, estimating modem performance.

The presence of an interfering signal can be determined by an increase in the power level of the received signal when averaged over the fading. Of course, this procedure will only be effective if no changes took place in the transmitted power and if nonstationary changes in fading conditions are sufficiently small over the averaging time used to establish the power level. The former type of change would not normally be a problem since it should be monitored at the transmitter and telemetered to a central technical control facility. The latter type of changes are unavoidable and their harm depends upon the degree of nonstationarity. There will generally be an optimum averaging time to estimate power level since too long a time causes nonstationary effects to degrade performance while too short an integration time does not average out the fading fluctuations sufficiently. Section 4 presents calculations of the effectiveness of interference detection by examination of changes in measured average power with attention given to the effects of nonstationarity.

The presence of interference can sometimes be recognized by the change in shape of the power spectrum if the interference is not broadband. A simple method for distinguishing between narrowband and broadband interference is to examine the centroid and rms bandwidth of the received power spectrum. A narrowband interfering signal at band center will cause the rms bandwidth to become smaller, while a narrowband interfering signal off band center will cause a shift in the centroid of the power spectrum. Thus the centroid and rms bandwidth are useful parameters for distinguishing between narrowband and broadband interference. Of course, if a full spectrum estimation is carried out, a variety of pattern recognition techniques could be employed for making such a distinction. Section 4 examines the effectiveness of an algorithm using measured centroid and rms bandwidth to detect the presence of a narrowband signal.

The only general study of the effect of arbitrary noise on modem performance over fading channels has been carried out by Bello [1.14][1.15]. As discussed previously, it has been proven

in Section 3.1 that the error rate is primarily dependent only on the average noise power at high SNR's for some rather general classes of fading and additive noise statistics. This suggests that reasonably tight bounds on error rate can be achieved with minimal knowledge of the statistics of the interference, as has been demonstrated in [1.14] and [1.15].

Unlike Gaussian noise, the statistics of noise at the output of a filter are not simply related to those at the input and to the filter transfer function. In fact, no general formulae exist at the present time for relating input and output statistics when non-Gaussian noise is filtered. The only general theorem useful in this regard is the Central Limit Theorem which allows the filter output to be approximated by Gaussian noise when there are a large number of independent noise fluctuations in one time constant of the filter.

Since all receivers employ filters for discriminating against noise, it is necessary to deal with the noise components of decision variables in bounding performance if non-Gaussian noise is to be handled. One may then try to work backward from the parameters of the noise components of decision variables to those of the broadband input noise, or else assume the existence of processing operations which allow the direct estimation of decision variable noise parameters.

Section 3 reviews briefly the relation between moments of noise parameters and error rates and Section 5 presents evaluations of upper and lower bounds on error rates when such minimal noise statistics are known, as average noise power, crest factor, and threshold exceedance probabilities.

1.2.3 Media Quality Unit

Section 3.2 presents first an overview of channel monitoring techniques to place the proposed techniques in proper perspective. Consideration is given to the role of self-test units, interface applique units, in-service operation, and out-of-service operation. The rationale is given for the study emphasis on estimation techniques utilizing the received information-bearing signal alone with sensor signals picked off as close to the antenna as possible. Very simply put, if channel measurements are taken too far into the receiver, there is the likelihood of receiver degradation corrupting the channel measurements, making difficult the estimation of a nondegraded receiver performance.

Drawing upon the results of the study, a signal processing structure has been conceived for establishing receiver degradation trends and discriminating between media and receiver-induced performance degradation. This structure is sketched in Figure 1.2 for the most complex case, the quadruple diversity troposcatter channel. For the other channels, some simplifications of this structure are possible; e.g., for the LOS channel, no average error rate estimation and no gross (i.e., average) channel parameter estimation would be carried out.

Examination of Figure 1.2 reveals that two basic subsystems, labeled MQU (media quality unit) and PMU (performance monitor unit), are used to eventually reach conclusions with regard to degradation trends, cause of outage, and the existence of intermittent faults. The PMU estimates the actual raw error rate of the digital signal passed forward to decryption, decoding, and demultiplexing operations. The effective design and operation of this unit is a subject outside the scope of the present study, where it is merely assumed that such a unit exists. The primary purpose of the MQU, which is the focus of the present study, is to provide error rate estimates for a hypothetical nondegraded receiver based upon information concerning the media characteristics. A comparison of the MQU and PMU average and short-term error rate estimates then allows an estimation of receiver degradation trends, performance margins, and intermittent faults. Of course, it also allows an identification of abrupt outages caused by receiver malfunction. A secondary purpose of the MQU is to provide an indication and identification of the rare outages caused by excessive Doppler spread (i.e., fast fading), multipath spread (i.e., frequency-selective distortion), and interference.

The inputs to the MQU come from appropriate pickoffs at RF or IF for each of the diversity receivers. As pointed out previously, the pickoff should be as close to the antenna as feasible to avoid confusing receiver degradation with channel impairments. AGC (automatic gain control) complicates some channel measurement functions by providing a variable gain not existing in the media itself. To account for such gains, it is assumed that those AGC voltages affecting the signal level used as input to the MQU are also picked off and that gain vs. AGC calibration curves are stored in the MQU where they are periodically updated.

The picked-off signals are filtered and brought to baseband by the media and noise sensors, in preparation for further processing in the MQU. If the received information-bearing signal alone

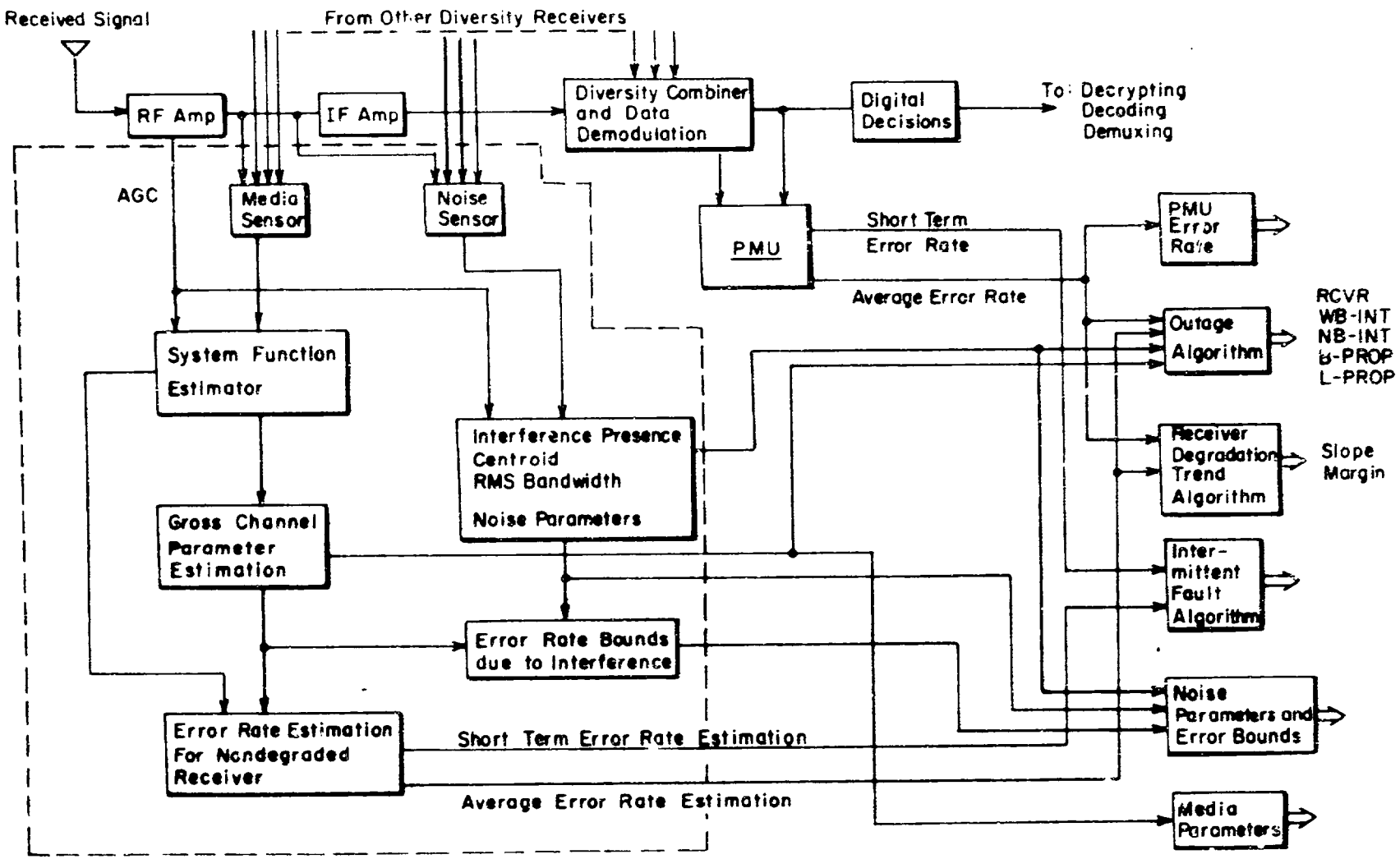

Figure 1.2 Proposed Signal Processing Structure for Establishing Receiver Degradation Trends and Discriminating Between Media and Receiver Induced Degradation

is to be used for channel measurements, the output of the system function estimator would be estimates of the squared magnitude of the transfer functions for the diversity channels at one or more frequencies within the signal bandwidth. A detailed analysis of the use of short-term power measurements to achieve estimates of the squared magnitude of the channel transfer function is presented in Section 4. Figure 1.3 shows a possible signal processing structure for one diversity channel and one frequency location within the diversity channel. Obvious time-multiplexed serial and/or parallel processing arrangements may be used to handle all diversity channels and all frequency samples required. The bandwidth of h(t) is selected small enough so that little frequency selectivity occurs over its passband. The time constant of k(t) is much longer than that of h(t) to average out the data noise fluctuations but short enough not to average over the fading. With specified shapes for h(t),k(t), it is shown in Section 4 that it is possible to optimize the bandwidth of the predetection filter h(t) and the time constant of the postdetection filter k(t) so as to minimize the combined effects of data noise, noise, frequency-selective fading, and time-selective fading.

If special probing signals are used, the Sensor system function estimator processing shown in Figure 1.3 would have to be replaced by an appropriate probe demodulator, such as the correlation processor shown in Figure 6.1 of Section 6. However, the remainder of the structure shown in Figure 1.2 would stay the same. For purposes of discussion, we assume that only the information-bearing signal is used to obtain channel information and that the squared magnitude of the diversity channel transfer functions are determined at selected frequencies by a structure like that shown in Figure 1.3.

With the aid of noise power measurements and removal of AGC gain fluctuations, one may scale the squared-magnitude transfer function measurements so that they will represent instantaneous SNR's for each diversity branch. As discussed in Section 3.1 and analyzed in Section 5, one may use these instantaneous SNR's in appropriate algorithms to estimate the average and short-term error rate for a nondegraded receiver. Multipath and Doppler spread can also be estimated from the squared magnitude of the diversity channels' transfer functions, as discussed and analyzed in Section 4. These parameters can be used to flag outages due to excessive multipath and Doppler spread. However, as discussed in Section 3.1, only with special probing signals which yield estimates of the complex transfer function and/or impulse response can enough information be obtained to estimate error rates due to excessive multipath.

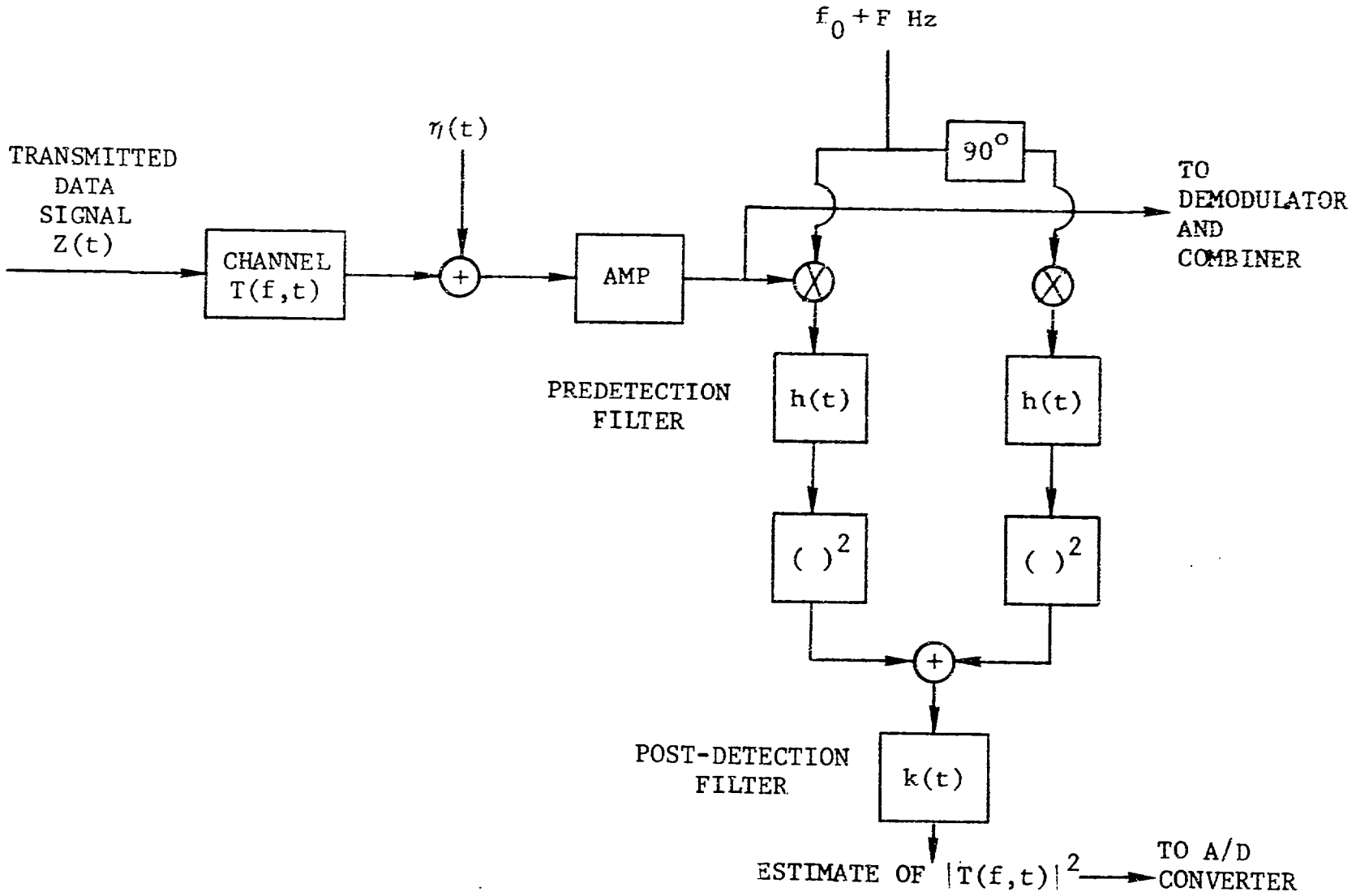

Figure 1.3 Estimator of the Magnitude Squared of the Channel Transfer Function for One Diversity Channel

The noise sensor would utilize out-of-band noise or time-multiplexed signal-free slots to estimate noise parameters (see Section 4.5) for determining bounds on error rate (see Section 5) when an interfering signal has been flagged by the interference-present detector. The latter detector compares the measured average received power on each diversity channel for two adjacent time intervals, looking for significant changes in power level (see Section 4.4.3). Additional information on interference presence is available from the narrowband interference detector which uses changes in the centroid or rms bandwidth of the received signal as a detection criterion (see Section 4.4.2 for an analysis). If noise slots are available adjacent to the signal band, they also can provide information concerning the presence of an interfering signal.

Under normal conditions, excessive multipath and Doppler spread or interference will not be present. When this is the case, the average and short-term error rates estimated by the MQU are compared with those measured for the receiver by the PMU. A steady and increasing departure of these error rates will indicate the presence of a degradation trend in the receiver. A comparison of short-term error rates will allow a determination of whether the receiver degradation is due to an intermittent receiver fault.

When an outage occurs, the measurements shown in Figure 1.2 should allow it to be categorized into one of the following:

- Receiver outage
- Wideband interference
- Narrowband interference
- Propagation, due to excessive Doppler spread (B)
- Propagation, due to excessive multipath spread (L)

Because of the slowness of fading on the links of interest, it is clear that a considerable amount of the signal processing indicated in Figure 1.2 can be carried out by small computers. However, the sensor uses analog processing and, except for HF channels, the short-term power measurement used to estimate the squared-magnitude transfer functions would have to be implemented with hardware.

Section 3.3 discusses implementation of the MQU assuming the information-bearing signal alone is use to derive channel

information. It focuses on the hardware and computation requirements and shows how these depend upon the media parameters. In accordance with both the emphasis of the work statement and the current trends in technology, the implementation discussed is as digital as is reasonably possible, and the digital processing is done by programmed hardware (computer) whenever possible.

The goal of this section was to delineate the implementation problems of potential media quality units and to show the division between analog, hardwired digital, and programmed digital hardware for each case. The discussion is brief and approximate due to time limitations but arrives at useful conclusions nonetheless.

Examination of the problem of estimating the squared magnitude of the channel transfer function indicates that, except for HF channels, analog filters should be used for the predetection filtering operation h(t). However, aside from the possible use of hardware digital processing for squaring and postdetection filtering, the remainder of the signal processing to extract channel parameters and error probabilities is well within the capabilities of modern minicomputers having a hardware multiply/divide, such as the Nova and the PDP-11. The centroid and rms bandwidth computation for detection of a narrowband signal requires the use of analog processing only to determine $\dot{x}$ and $\dot{y}$, derivatives of the in-phase and quadrature components of the received signal. Table 1-2 displays the computational burden in terms of multiplications needed per second for major subsystems of the MQU assuming that the squared-magnitude channel transfer function and the in-phase and quadrature derivatives of the received signal have already been determined. The table is presented for a fast fading quadruple diversity troposcatter channel which represents the worst case channel for computational burden. A sampling rate of 500/second is assumed for the input data to the computer.

Consider several points from this table:

1) The computation burden is essentially a linear function of both the order of diversity and the Doppler bandwidth.

2) The estimation of input power spectrum centroid and rms bandwidth imposes half the computation burden. It would be unnecessary to calculate these quantities on all diversity paths if it were assumed that an interference would be

TABLE 1-2

ROUGH ESTIMATES OF COMPUTATIONAL BURDEN FOR KEY SUBSYSTEMS OF MQU FOR THE EXTREME CASE OF A QUADRUPLE MAXIMAL RATIO COMBINED DIVERSITY TROPOSCATTER LINK UNDERGOING FAST FADING

Subsystem	Computation Burden	Comments
Estimation of $\|T(f,t)\|^2$, $\dot{x},\dot{y}$	Input/Output only	These functions are performed in hardware prior to computer and sampled at 500 times/sec for inputting to the computer
Estimation of RMS Doppler Spread and RMS Multipath Spread	6,000 multiplies/ second	Differentiation technique
Estimation of Total Power Centroid and RMS Bandwidth	12,000 multiplies/ second	Assumes extreme case of four receivers
Conditional Error Probability	3,000 multiplies/ second	Error function or exponential function of maximal ratio combined diversity variables
TOTAL	21,000 multiplies/ second	

received by all diversity branches. In any case, quadruple diversity is usually obtained with two transmitting and two receiving antennas. Also, this computation is fairly simple and can be easily implemented in digital hardware.

3) Twenty-one thousand multiplies per second corresponds to just under 50 microseconds per multiply. Modern minicomputers, such as the Data General Nova Series or the PDP-11, with hardware multiply/divide have multiplication times in the range from 5 to 20 microseconds. Thus it appears that a safety factor of about 2.5 is available.

An important warning should be inserted here. The discussion of computation burden has focused on multiplications alone and on multiplications that must be done at the input rate. This focus was chosen because these multiplications are probably more than half of the total computation load. But a safety factor must be allowed on top of the estimates in the table. Before attempting to implement these techniques, the burden of other operations, especially input-output control, should be examined to insure that the processor chosen can handle the task.

1.3 Channel Measurement Techniques Utilizing the Received Information-Bearing Signal Alone

The proposed MQU incorporates a number of channel measurement functions as discussed in Section 1.2.3 and illustrated in Figure 1.2. Section 4 is devoted to the definition and detailed analysis of various measurement techniques designed to carry out the necessary measurement functions. Expressions are derived for estimation errors and biases as a function of measurement time and bandwidth, multipath and Doppler spread, including the effects of additive noise and data noise.

Initially, consideration is given to the measurement of the squared magnitude of the transfer function of a channel, $|T(f,t)|^2$, via short-term power measurement in a bandwidth of the order of coherence bandwidth of the channel. Optimum values of predetection and postdetection bandwidths are shown to exist minimizing the combined effects of unfiltered data noise and frequency-selective distortion.* Filter bandwidths and integration times are evaluated for specific filter shapes. Numerical

*It is shown that the data noise dominates the additive noise contributions.

evaluations of performance are carried out for the HF, LOS, Troposcatter, and Satellite Ionospheric Scintillation channels. As pointed out several times in preceding sections, the harmful LOS fading is the deep fading and particular attention must be focused on measuring the LOS channel during deep fades. Thus, pre- and post-detection filter optimization should be carried out at the maximum fade depth of interest.

Table 1-3 presents computed values of normalized rms error in measurement of $|T(f,t)|^2$ together with optimum pre- and post-detection filters and assumed rms multipath and Doppler spreads for the channels of interest. For the LOS channel, the rms error is conditioned on and normalized to various fading depths varying from 10 to 40 dB. For the other channels, the rms error is normalized to the average value of $|T(f,t)|^2$. We note that for the LOS channel the maximum fade depth at which measurements are desired to be accurate have noticeable influence on the predetection filter bandwidth and postdetection filter integration time. It is interesting to note that at a 40-dB fade depth the measurement error is comparable to that of a troposcatter channel even though the latter has Doppler spreads and multipath spreads very much larger. This phenomenon is due to the increased time- and frequency-selective fading present during deep fades.

For all but the HF channel, a highly accurate estimation of $|T(f,t)|^2$ is seen to be possible. It should be noted, however, that the estimation errors given in Table 1-3 assume that the multipath and Doppler spreads for which the filters are optimized are those existing in the link. Since multipath and Doppler spread may vary from the design value, the minimum error will not necessarily be reached. Graphs are presented in Section 4 showing the variation in estimation error as the true multipath and Doppler spreads depart from their design values. Highly accurate measurements are still possible over a wide swing in these parameters, except for the HF channel.

Biases in estimation of $|T(f,t)|^2$ exist, but these are smaller in size than the rms fractional errors and may be removed once estimation of the rms multipath spread, L, rms Doppler spread, B, and SNR are obtained. Unfortunately, small errors in estimation of B and L cannot always be obtained for the HF channel so that bias correction will have limited success on the HF channel.

Techniques are proposed and analyzed in Section 4.3 for the measurement of the gross channel parameters of Doppler spread,

TABLE 1-3

RMS FRACTIONAL ERROR IN ESTIMATING SQUARED MAGNITUDE OF CHANNEL TRANSFER FUNCTION USING RECEIVED INFORMATION-BEARING SIGNAL ALONE

Channel	Filter Bandwidth* (Hz)	Filter Time Constant** (s)	RMS Multipath Spread (s)	RMS Doppler Spread (Hz)	RMS Fractional Error†
LOS, 10 dB Fade	3.43×10^{5}	2.27	10^{-8} ††	0.003	1.09×10^{-3}
LOS, 20 dB Fade	1.82×10^{5}	1.06	10^{-8}	0.003	2.49×10^{-3}
LOS, 30 dB Fade	8.64×10^{4}	0.49	10^{-8}	0.003	5.04×10^{-3}
LOS, 40 dB Fade	3.93×10^{4}	0.227	10^{-8}	0.003	1.09×10^{-2}
Troposcatter	1.14×10^{5}	0.059	0.3×10^{-6}	1.0	1.9×10^{-2}
Satellite Iono. Scintillation (1 GHz)	10.1×10^{6}	0.088	10^{-9}	0.2	1.6×10^{-3}
HF Not Transauroral	1.5×10^{2}	0.53	10^{-3} ††	0.5	1.7×10^{-1}

* Optimum predetection filter - 6 dB bandwidth - double tuned filter.

** Optimum postdetection filter integration time for rectangular impulse response.

† For the LOS channel, the rms error is conditioned on and normalized to the signal at the fade depth. For the other channels, the rms error is normalized to the average value of the squared magnitude of the channel transfer function.

†† Two path channel models assumed for computational purposes.

multipath spread, SNR, and diversity branch correlation coefficient utilizing the estimated $|T(f,t)|^2$. Three different techniques are examined for Doppler and multipath spread measurement, called the Differentiation, Correlation, and Level-crossing techniques. These techniques assume that zero-mean complex Gaussian statistics (e.g., Rayleigh envelope statistics) satisfactorily model the fading. This assumption is reasonable for troposcatter, HF links, and VHF ionospheric scintillation links. However, at UHF and above, a nonfading component will exist for the ionospheric scintillation channel and statistics may depart from complex Gaussian. In such a case, special probing signals and coherent processing techniques would be required for multipath and Doppler spread estimation.

Figures 1.4 and 1.5 present curves of standard deviation and bias for the estimation of rms Doppler spread and multipath spread for the troposcatter channel. These curves are for the differentiation method which was found to be only slightly worse than the level-crossing technique, but easier to analyze. The correlation technique was found to be inferior to both of these.

Figure 1.4 deals with estimation of rms Doppler spread. It is assumed in these curves that the $|T(f,t)|^2$ estimator filters have been optimized for the rms Doppler and multipath spread design values of $B_D = 1$ Hz and $L_D = 0.3$ μs and that no attempt has been made to correct the biases in the estimate of $|T(f,t)|^2$. The curves show how the rms estimation errors and biases vary as the true multipath and Doppler spread may vary from the design values. We note that bias errors are negligible until the Doppler spread get to 0.1 Hz at which point they cause the mean Doppler spread to be 0.12 Hz. For detection of atypical fading conditions, measuring high Doppler spread is of more interest and we note that bias error is negligible for Doppler spreads exceeding 0.4 Hz. The standard deviation of the estimator is around 0.08 Hz at $B = 2$ Hz and decreases as B decreases, indicating reliable estimation for the range of 0.1 to 2 Hz rms Doppler spread. For fast fading tropo links, the filter estimating $|T(f,t)|^2$ would be optimized for a higher fading rate and acceptable performance would be achieved over a considerable range.

The estimation time of 10 minutes has a dominant effect on the rms value of the estimation error as it does for all estimators which average over the fading. For all cases, the standard deviation expressed as a fraction of the true value, i.e., the rms fractional error, δ, takes the form

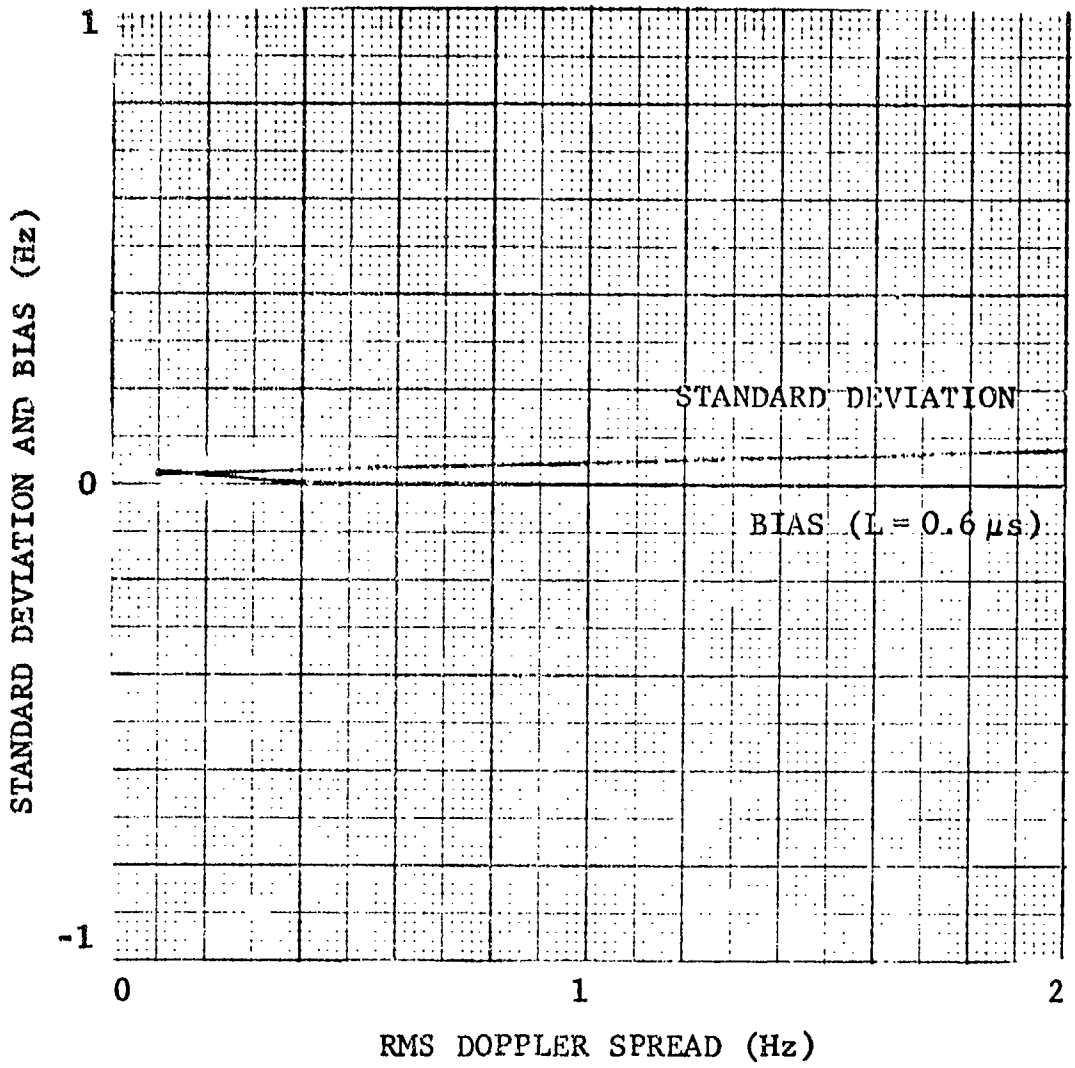

ESTIMATION TIME: 10 minutes
DESIGN RMS DOPPLER SPREAD: 1 Hz
DESIGN RMS MULTIPATH SPREAD: 0.3 μs

Actual rms multipath spread varied from 0.6 to 0.1 μs with L = 0.6 μs producing worst case bias in estimating B

Figure 1.4 Error Standard Deviation and Bias in Estimation of RMS Doppler Spread, B, from Bias Uncorrected Estimates of $|T(f,t)|^2$. (Troposcatter channel and differentiation technique assumed)

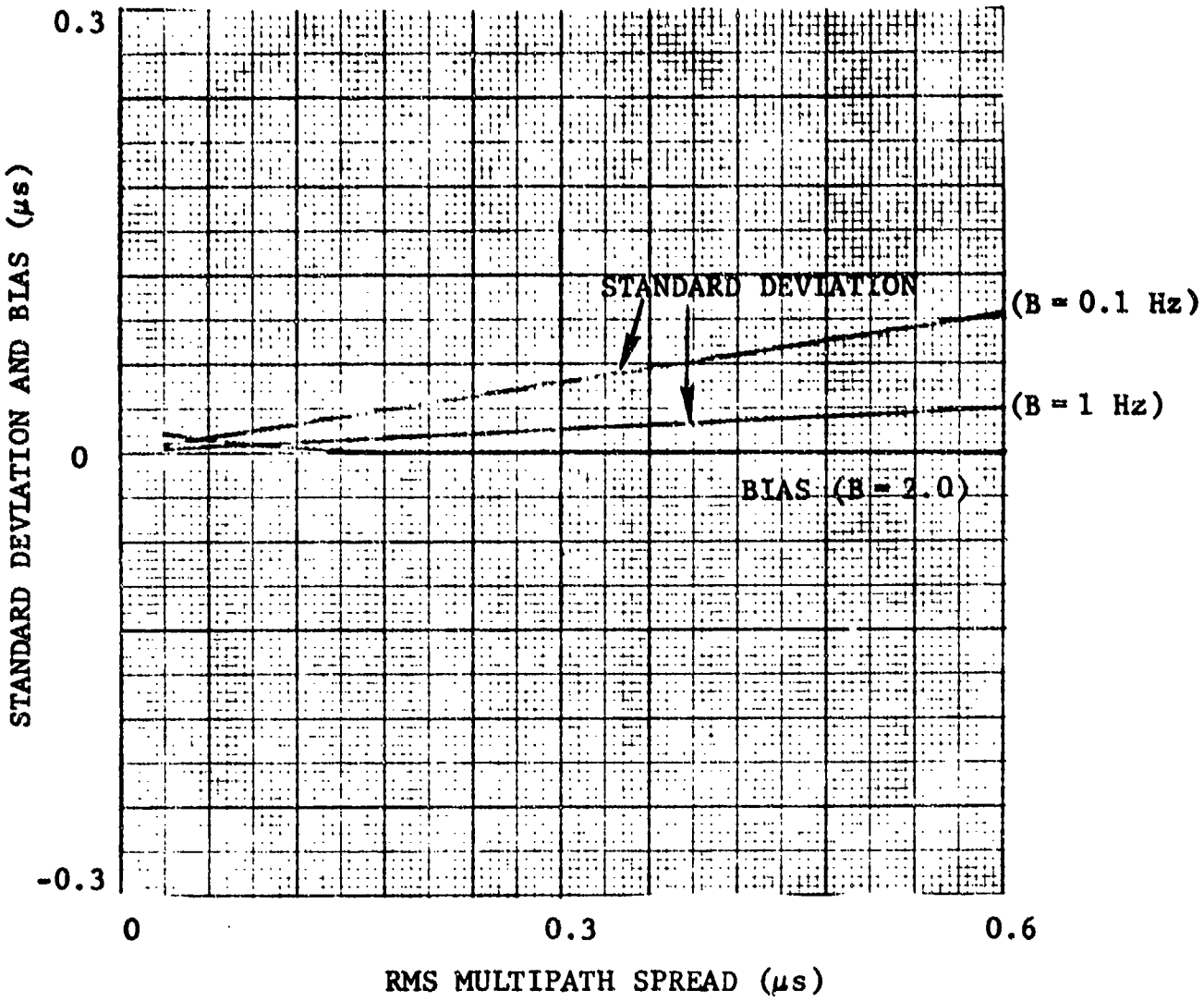

ESTIMATION TIME: 10 minutes
DESIGN RMS DOPPLER SPREAD: 1 Hz
DESIGN RMS MULTIPATH SPREAD: 0.3 μs

Actual rms Doppler spread varied from 0.1 to 2.0 Hz with B = 2 Hz producing worst case bias in estimating L

Figure 1.5 Error Standard Deviation and Bias in Estimation of RMS Multipath Spread from Bias Uncorrected Estimates of $|T(f,t)|^2$. (Troposcatter channel and differentiation technique assumed)

$$\delta = \frac{A}{\sqrt{K}} \tag{1.13}$$

where A is a function usually weakly dependent upon the channel, and K is the number of independent samples of the channel fluctuations used in carrying out the average. This number is given usually somewhat conservatively by

$$K = BT_0 \tag{1.14}$$

where T_0 is the averaging time. Doubling the averaging time will reduce δ by $\sqrt{2}$. Also, an increase in the Doppler spread by a factor of 2 will decrease δ by $\sqrt{2}$. The absolute value of the rms error will, of course, increase by $\sqrt{2}$. The increase in estimator standard deviation with B in Figure 1.4 is this $\sqrt{B}$ relationship.

Figure 1.5 presents curves of error standard deviation and bias vs. rms multipath spread in μs with rms Doppler spread as a parameter. The biases do not cause any serious problem unless the multipath spread gets too low, which is the correct direction for estimation of atypical multipath spread. The standard deviation of the error can become considerable if the fading rate is too slow as evidenced by the figure and (1.13). This problem must be faced whether special probing signals are used or not, however.

Figure 1.6 presents the standard deviation and bias of the error in estimating the correlation coefficient between the envelopes of two diversity channels. From these curves we conclude that considerable measurement time or large Doppler spreads are required to estimate a correlation coefficient that is close to unity even though the bias error is negligible. Since correlation close to unity is the atypical case that produces system performance loss, this is an unfortunate situation which places a limit on the utility of the "formula" approach for estimating error rate.

Similar calculations may be carried out for the ionospheric scintillation channel and for the same Doppler spreads the measurement of rms Doppler spread would show the same behavior as in Figure 1.4 except that the bias would be negligible because of the reduced multipath spread of this channel.

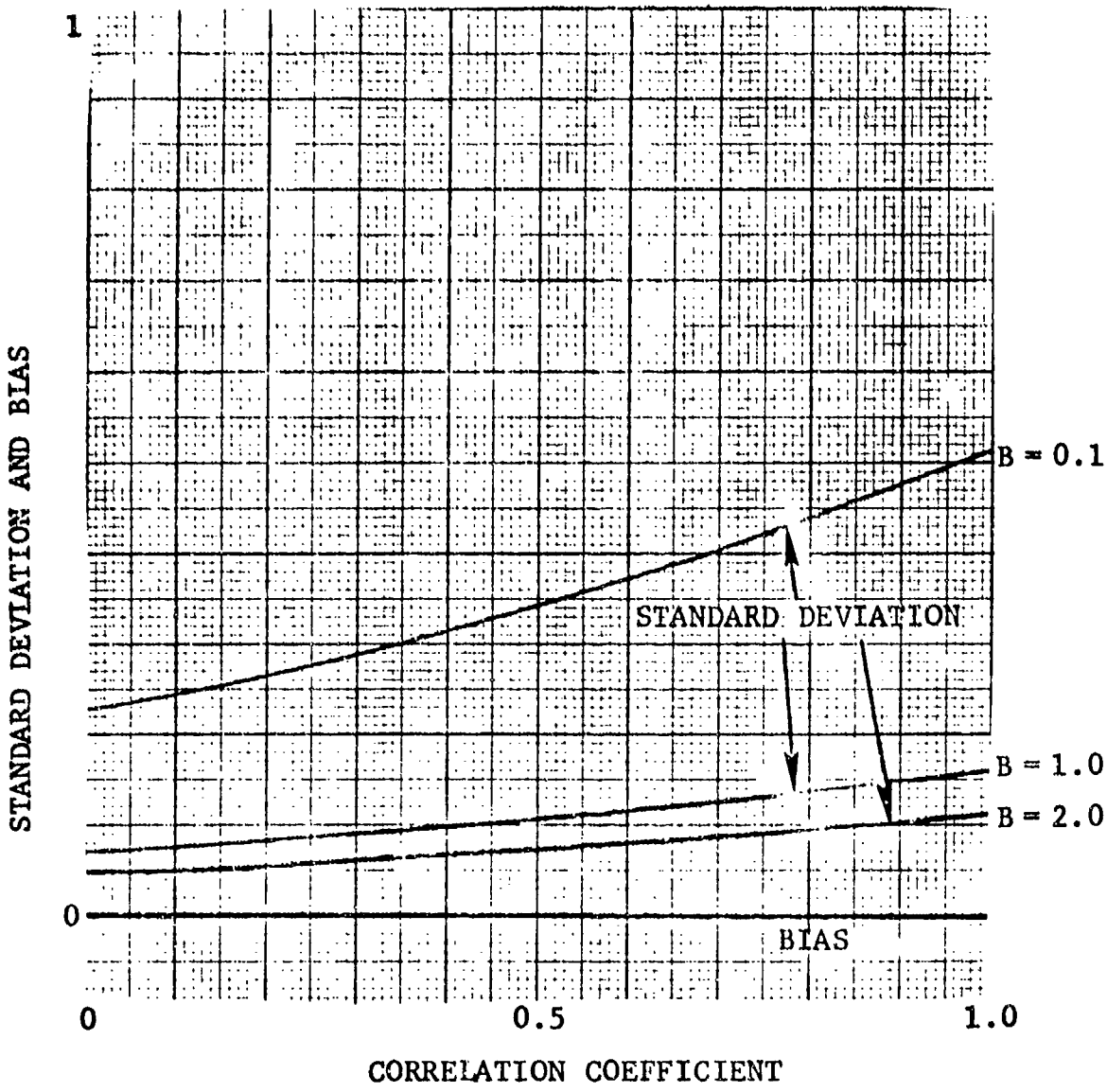

ESTIMATION TIME: 10 minutes
DESIGN RMS DOPPLER SPREAD: 1 Hz
DESIGN RMS MULTIPATH SPREAD: 0.3 μs

Figure 1.6 Error Standard Deviation and Bias in Estimation of Branch Envelope Correlation Coefficient from Bias Uncorrected $|T(f,t)|^2$ Estimates. (Troposcatter channel assumed)

Figures 1.7 - 1.9 present curves for the HF channel analogous to those for the troposcatter channel. Figure 1.7 plots the standard deviation and bias of the Doppler spread estimator as a function of B in the range 0.1 to 2 Hz for values of L from 0.1 ms to 2 ms. We observe that large bias errors occur. A similar problem is faced in the measurement of rms multipath, as shown in Figure 1.8. Finally, the performance of the correlation coefficient estimation is also poor, as shown in Figure 1.9.

The estimation of average SNR turns out to be unbiased and to have a standard deviation which is given by

$$\sigma \approx \frac{\Gamma(1+\epsilon)}{\sqrt{K}} \quad ; \qquad K \approx B T_0 \tag{1.15}$$

for all the channels where, even for HF, ϵ is small compared to unity. Thus, provided enough Doppler spread and/or measurement time is available, reliable measurement of the average SNR at least can be carried out for the HF channel using the received signal alone for measurement.

1.4 Detection of Interference

The problem of detecting the presence of an interfering signal by in-band processing alone is treated in Section 4.4. Two basic procedures are analyzed. In one procedure, the centroid and rms bandwidth of the power spectrum of the received signal are examined to see if they have changed significantly from their a priori known values. This procedure is effective in the measurement of the presence of a narrowband interference. In the other procedure, an attempt is made to detect a sudden change in received power level. The effectiveness of this procedure is analyzed considering the influence of channel nonstationarities which could be confused with a change in power level.

It is a reasonable intuitive notion, when the data is totally totally swamped out by the narrowband interference, that the rms bandwidth of the received signal will be equal to that of the interference, and its centroid will be equal to the frequency offset (difference between interference and data carrier frequencies) of the interference.

Optimal procedures for detecting the presence of narrowband interference can be based on the observations of both f_R, the

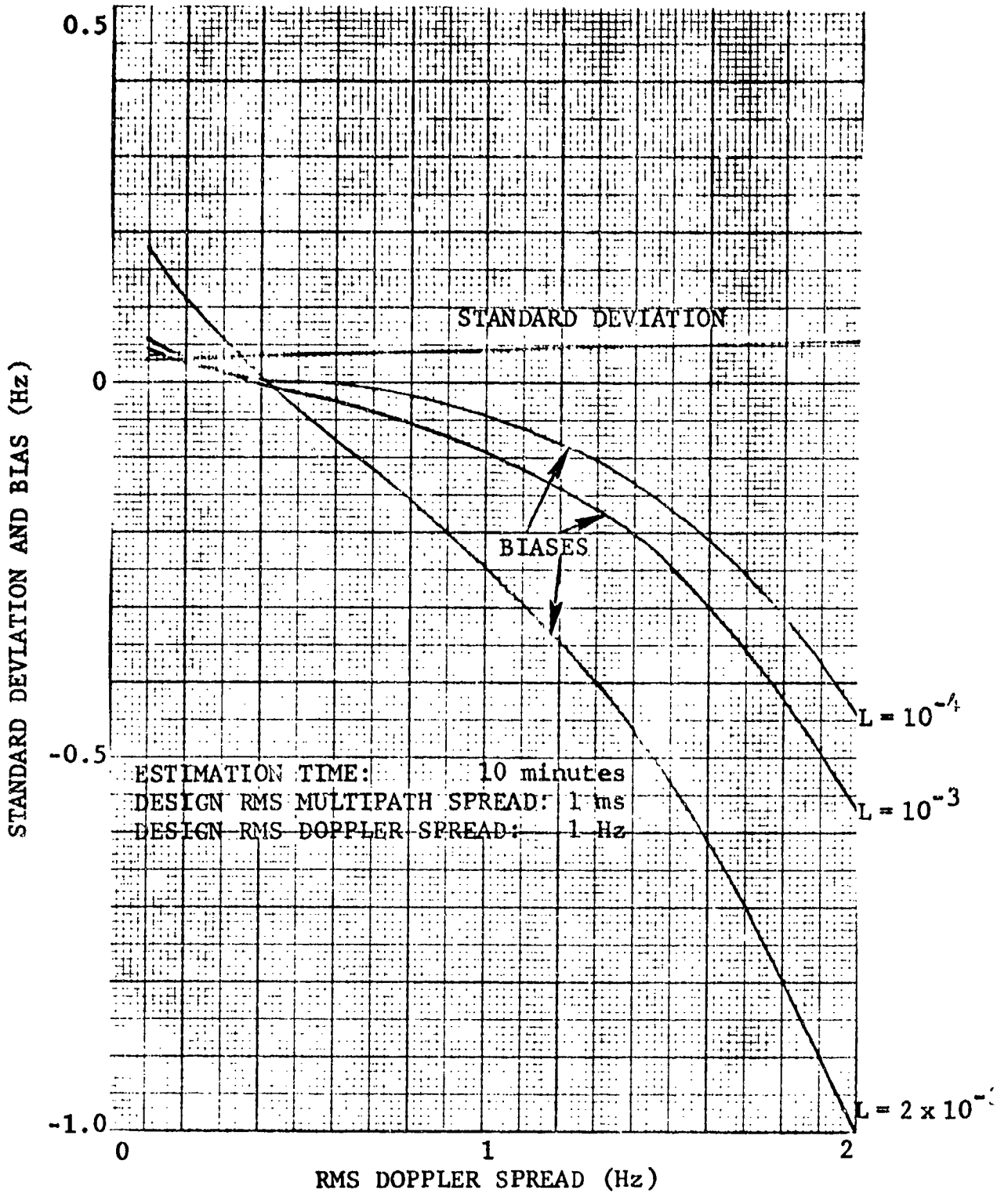

Figure 1.7 Error Standard Deviation and Bias in Estimation of RMS Doppler Spread from Bias Uncorrected Estimates of $|T(f,t)|^2$. (HF channel assumed)

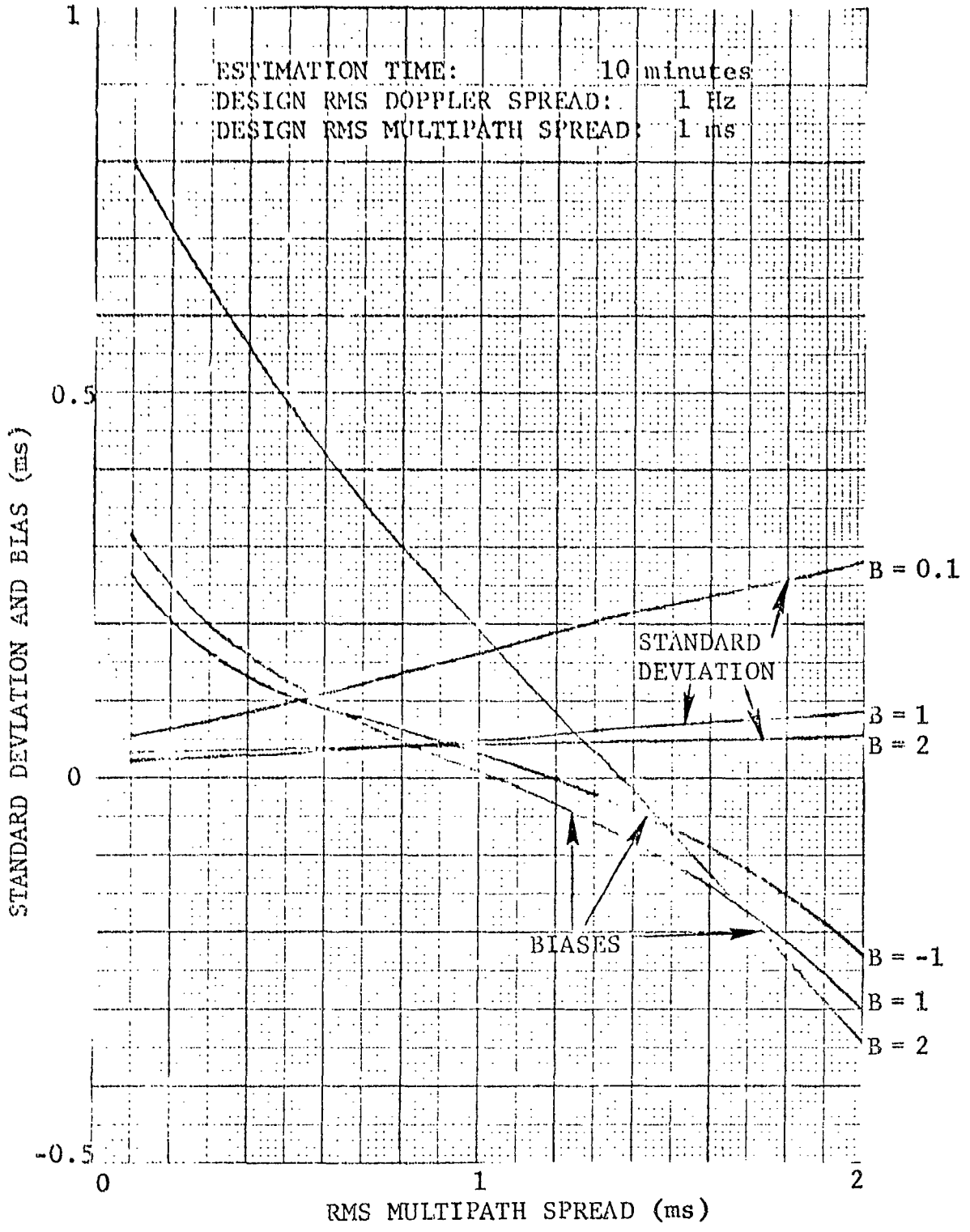

Figure 1.8 Standard Deviation and Bias in Estimation of RMS Multipath Spread from Bias Uncorrected Estimates of $|T(f,t)|^2$. (HF channel assumed)

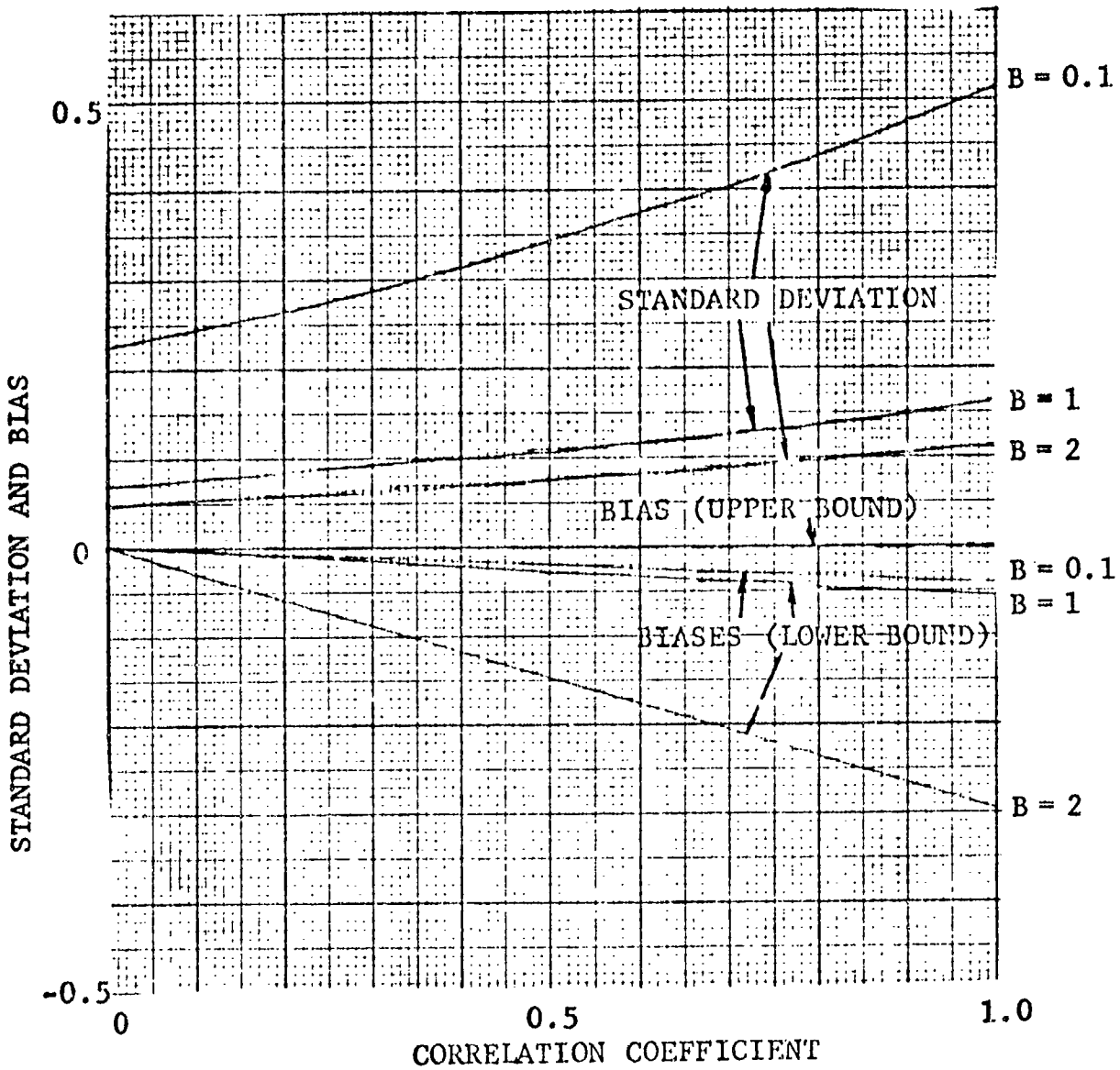

ESTIMATION TIME: 10 minutes
DESIGN RMS DOPPLER SPREAD: 1 Hz
DESIGN RMS MULTIPATH SPREAD: 1 ms

Figure 1.9 Standard Deviation and Bias in Estimation of Branch Envelope Correlation Coefficient from Bias Uncorrected $|T(f,t)|^2$ Estimates. (HF channel assumed)

frequency centroid of the total received signal, and B_R, its rms bandwidth. Decision-theoretic concepts have been applied to the development of a detection technique utilizing estimates of these quantities. The effectiveness of any such scheme must depend, of course, on the reliability of the estimates, and this is discussed at some length in Section 4.4.

The detection schemes which are discussed and evaluated in this report are suboptimal in the sense that there are idealized detectors, not necessarily implementable, that can do better. Nevertheless, the calculated detector operating characteristics for the detection schemes discussed here show good performance Their relation to the optimal detectors is given detailed discussion.

The best narrowband interference detector studied employs the strategy shown in Figure 1.10. From the received signal in-phase and quadrature components, estimates are formed of the rms bandwidth B_s and centroid of the received signal relative to the carrier frequency f_s. Thresholds are selected based upon the a priori known interference-free rms bandwidth and centroid (averaged over the fading). Usually the a priori centroid will be at the center of the band, i.e., at $f_s = 0$. The decision rule is: decide that a narrowband interference is present if either the rms bandwidth drops below a specified threshold or else the centroid exceeds another threshold, and decide no interference when both of these events do not occur. Figure 1.11 shows plots of probability of detection, P_D, vs. probability of false alarm, P_F, for this detector. In the example shown, the interference power is 10 dB below the signal power level. The difference between the carrier frequency of the interference and that of the data equals 0.4 times the data signal rms bandwidth. The rms bandwidth of the interfering signal is assumed 0.1 times that of the data signal. A family of curves is drawn for different $B T_0$ products.* Note that a $B T_0$ product of 100 (at a 1-Hz Doppler spread this corresponds to 100 seconds) yields a detection probability of 0.998 and a false alarm probability of 0.01. Performance improves rapidly with increasing averaging time.

The other scheme for interference detection involved the successive measurement of power (averaged over channel fading)

*In Section 4.5, B_c is used for the channel's rms Doppler spread.

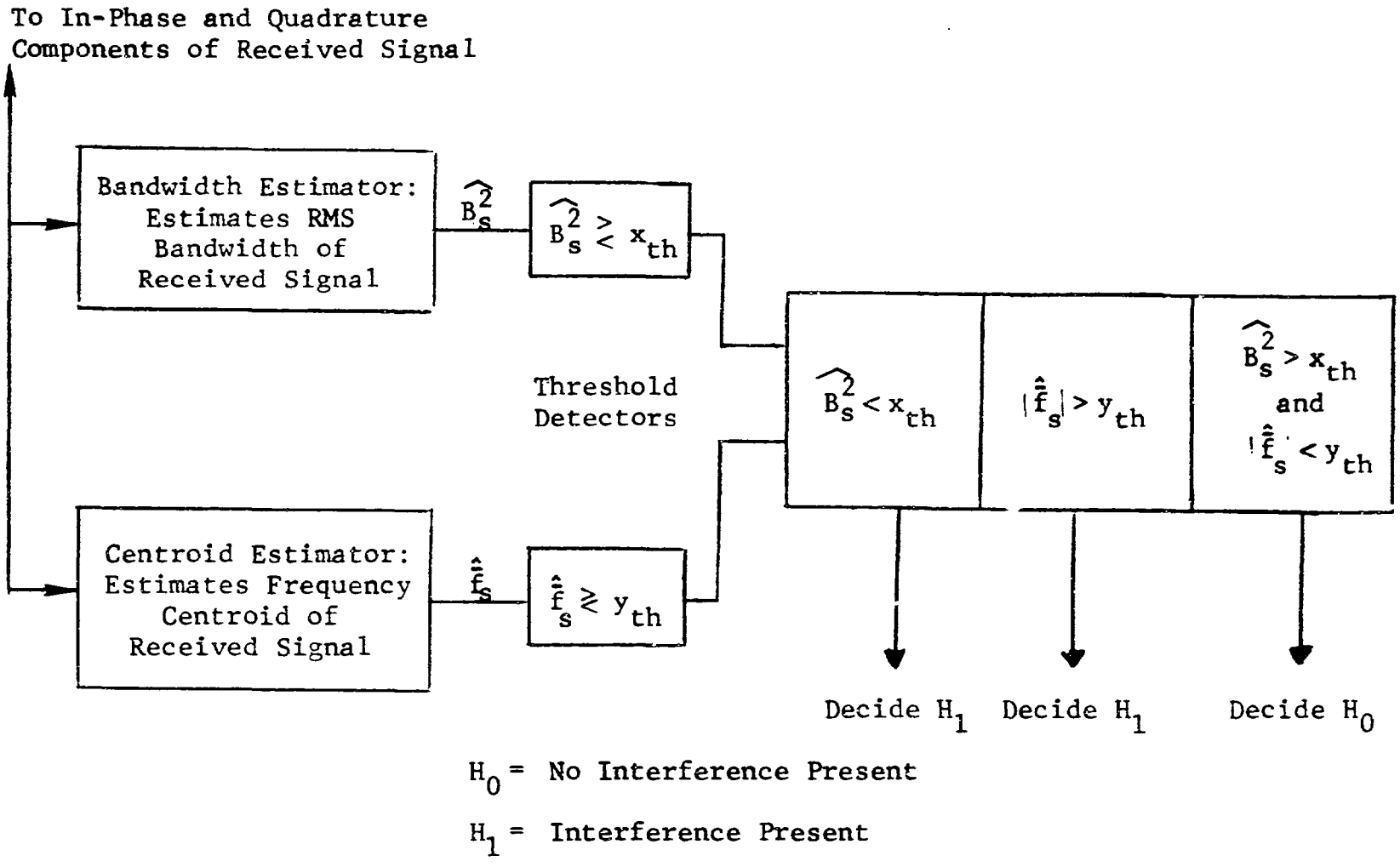

H_0 = No Interference Present

H_1 = Interference Present

Figure 1.10 Signal Processing in Narrowband Interference Detector

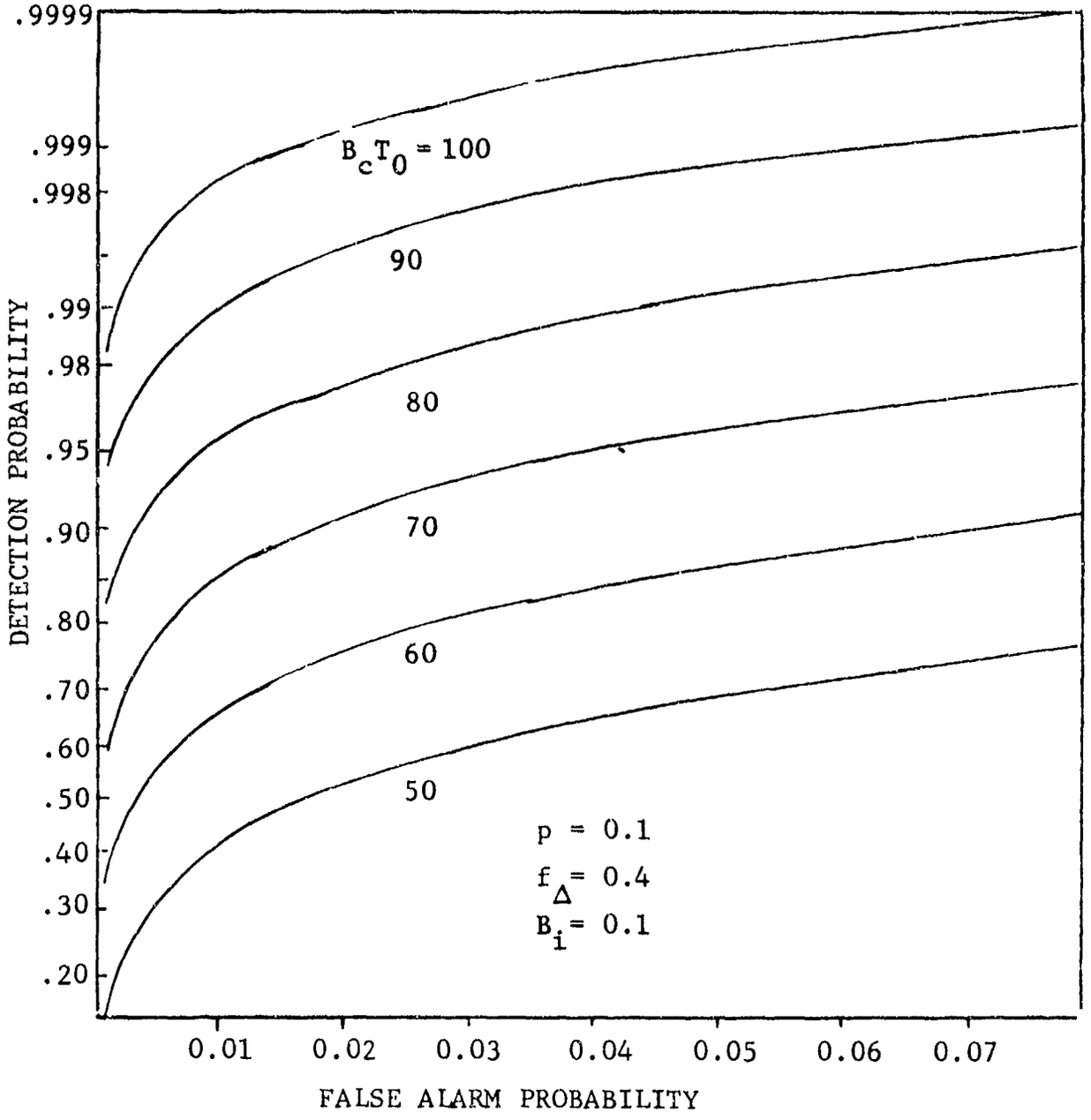

$$B_i = \frac{\text{RMS BANDWIDTH OF INTERFERENCE}}{\text{RMS BANDWIDTH OF DATA}}$$

$$p = \frac{\text{INTERFERENCE POWER}}{\text{TOTAL POWER IN RECEIVED SIGNAL}}$$

$$f_\Delta = \frac{\text{DIFFERENCE IN CARRIER FREQUENCIES OF INTERFERENCE \& DATA}}{\text{RMS BANDWIDTH OF DATA}}$$

B_c = CHANNEL DOPPLER SPREAD

T_0 = INTEGRATION TIME USED TO PROCESS

Figure 1.11 Operating Characteristic of Narrowband Signal Detector

in the received signal with an averaging time T and a comparison of these powers. If they differed sufficiently, an interference was said to be present; otherwise not. Because of slow changes in the transmission loss, the averaging time T cannot be too large, lest decreasing transmission loss be identified with the presence of an interference or, conversely, increasing loss mask the presence of an interference. On the other hand, if T is too small, unaveraged channel fluctuations will result in poor detector performance.

The evaluation of the effectiveness of such a detection scheme is hampered by the lack of definitive knowledge on nonstationary characteristics. Fortunately, some measurement of nonstationary changes was carried out by Bello, et al. [1.16] for a troposcatter channel. The curves in [1.16] indicate that 3% to 96% cumulative distribution of the 20-minute median transmission loss change is contained roughly in the - 3 dB to + 3 dB range and 1% to 99% in the $\pm$ 4 dB range. As a typical large value for the detection performance curves in Section 4 we have used the values $\pm$ 2 dB/20 minutes.

Numerical results are indicated in Figure 1.12. The curves marked "0" indicate the performance that would be obtained in the absence of any channel nonstationarities. For this case, the symmetry in the P_F and P_D curves exists because the initial threshold was chosen so that the (P_F, P_D) pair fell along the line $P_D = 1 - P_F$ of the receiver operating characteristic. With the threshold so set, the other curves indicate how the detectability is affected by linear nonstationary changes with transmission slopes $\pm$ 2 dB/20 minutes. We see, in the case of + 2 dB/20 minutes and 0 dB, that the detection probability rises slightly more rapidly than in the stationary case, but that P_F falls more slowly until finally it begins to rise with increasing observation time. By 1000 seconds, the nonstationarity has taken over fully. We note, however, that there is an "optimum" point on the P_F curve where it bottoms out. This point is at an observation time of 200 seconds and corresponds to $P_F = 0.0666$ and $P_D = 0.9985$ whereas the curves for - 2 dB have the values $P_F = 0.0065$ and $P_D = 0.96$ at the same point.

The performance improves when the fading is faster. This is clear from an examination of the curve in Figure 1.13 which corresponds to B = 10 Hz in contrast to Figure 1.12 for which B = 1 Hz. It is clear that the "optimum" time takes place at T = 200 seconds as before; this time, however, the probability of false alarm has decreased to 0.109×10^{-5} whereas the probability

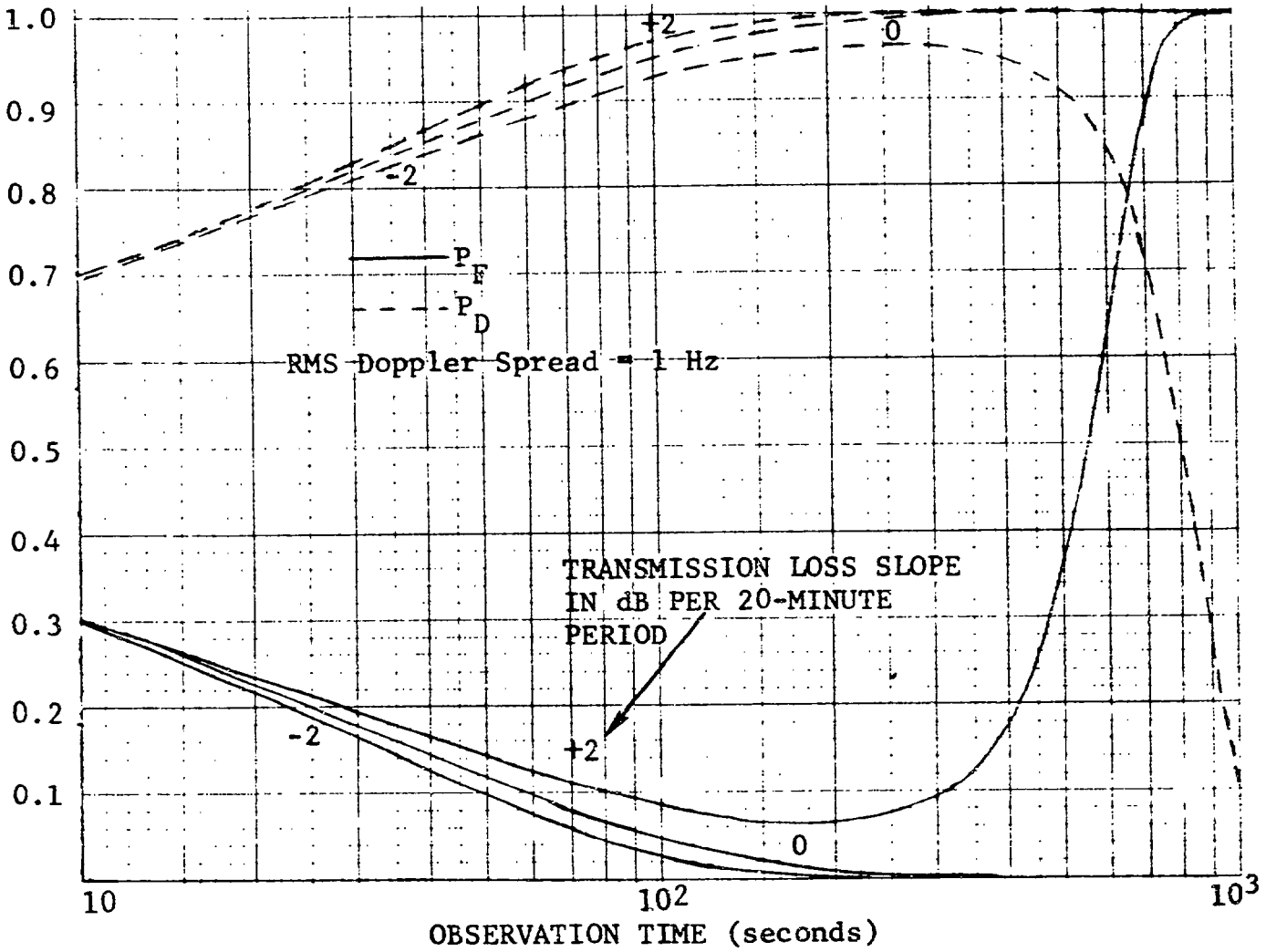

Figure 1.12 Plots of Interference Detectability for Nonstationary Changes on Tropo Channel. Interference Power = Signal Power

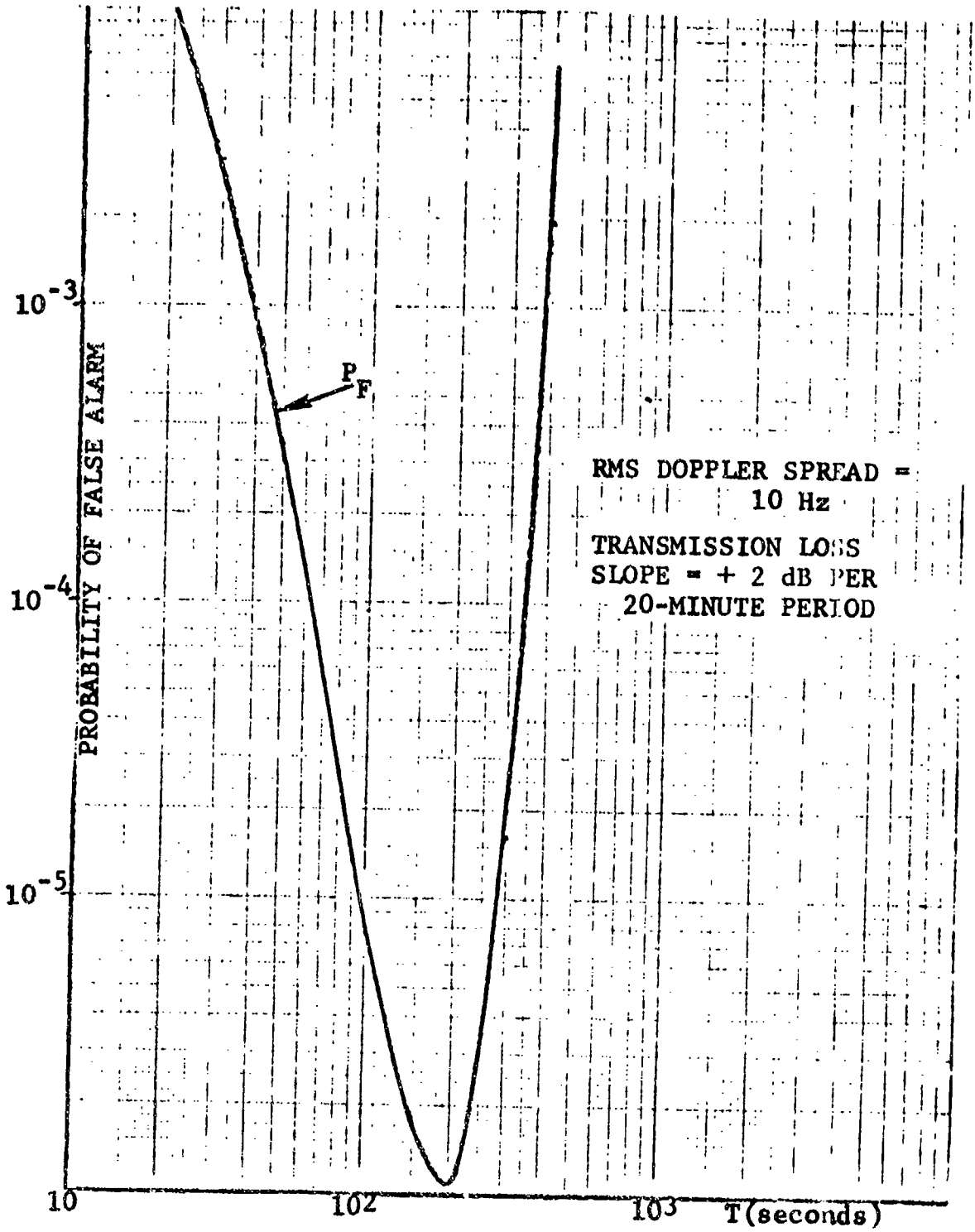

Figure 1.13 Probability of False Alarm vs. Observation Time for Nonstationary Changes in Power Level with Doppler Spread ≈ 10 Hz and Interference Power Equal to Signal Power

of detection is essentially unity near the optimum point (to within five decimal places). These results indicate some potential utility to the detection of noise by measurement of change of power level, but there are important situations where nonstationary channel changes can disrupt fixed threshold schemes detecting a weak interfering signal. However, performance in the presence of nonstationarities improves as SNR decreases or B increases.

1.5 Measurement of Noise Parameters

In Section 4.5 we analyze techniques for interference measurement when idle frequency or time slots are available. By the latter it is meant that the transmitted data signals have frequency slots or time slots that are idle in the sense that they carry no data power. One useful variant of the time slot idea is the "temporary-service-interrupt". This can provide a rapid means of determining, in the presence of communication impairment, whether or not additive interference is the main contributor to the degradation. It also provides the means of developing estimates for error rate bounds, even in the presence of interference for which there is available only a bare minimum of statistical information. This latter topic is discussed at some length in Section 5.7.

It is demonstrated, following [1.17], that the use of idle time slots in the data (with a temporary service interrupt being a special case) is the most general and useful method for accumulating interference data. The reason for this is that the interference is picked off and analyzed in just such a way that its final form coincides with the form it takes on in the receiver's decision circuitry. Figure 1.14 shows an example of the signal processing operations involved. If a service interrupt is involved, it would be necessary to set the AGC voltage at some typical average value due to possible nonlinear effects caused by spikes of noise because the statistics of the measured noise would be affected by the gain of the receiver up to the point of pickoff. The manner in which this interference variable is processed, and the reliability of the measurements of the various pertinent interference parameters, is discussed in detail in Section 4.5. It is pointed out from the results in [1.17] that the probability of error for FSK, PSK, and DPSK matched filter communication systems in complex Gaussian fading diversity channels depend directly on the joint probability density function of the generalized interference variables U and V, where U and V are given by

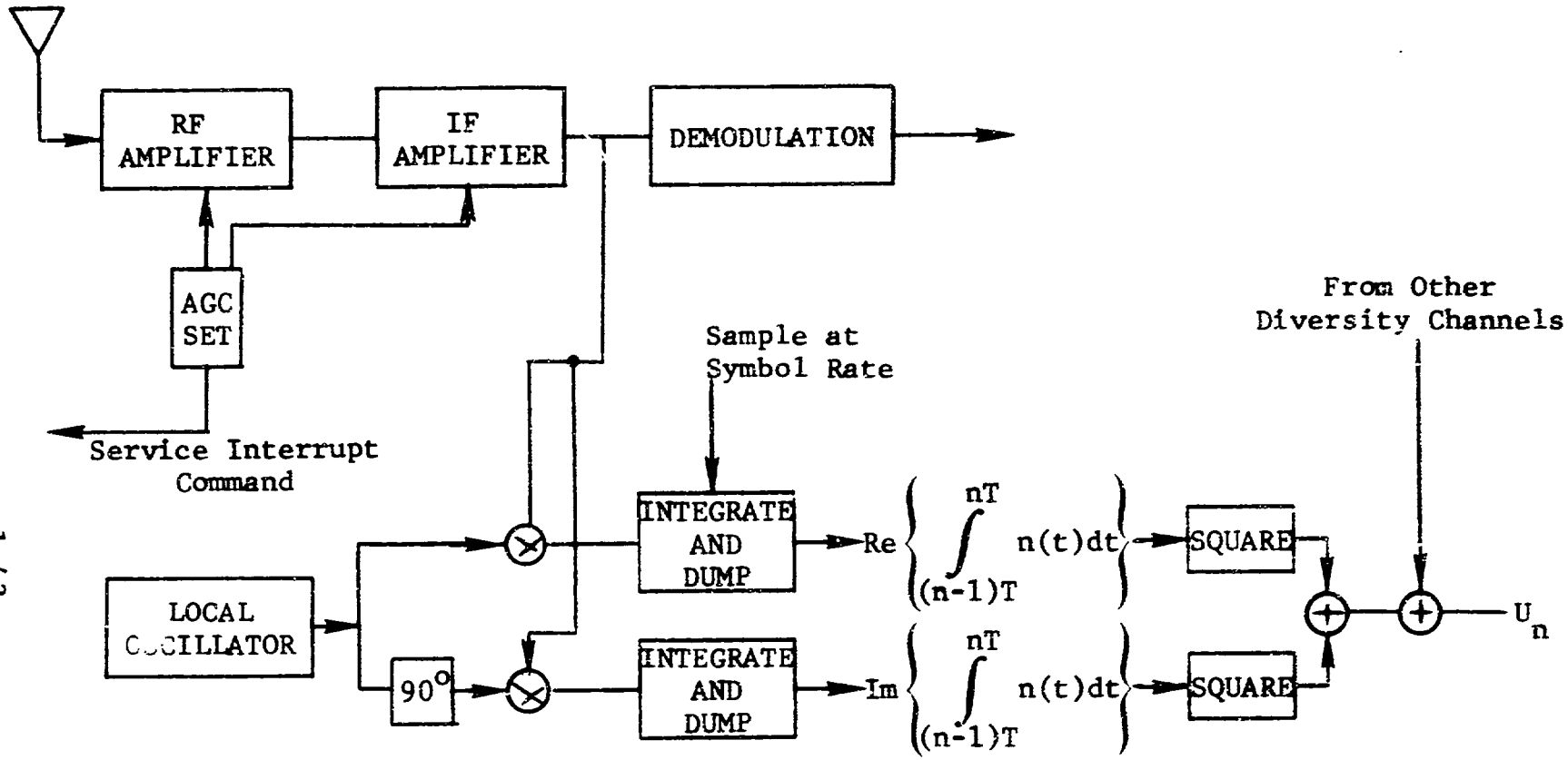

Figure 1.14 Interference Measurement in Idle Time Slots

$$U = \sum_{k=1}^{k=M} |\xi_k|^2 \qquad V = \sum_{k=1}^{k=M} |\eta_k|^2 \tag{1.16}$$

In this expression, the index k just indicates summation over the M diversity branches, whereas the value of ξ and η are linearly related to matched filter sampled output noise. Clearly, then, an accurate measurement of the joint pdf for U and V would lead to accurate predictions of error rate. However, it is shown in Section 5.7 that some pairs of gross parameters of the U or V statistics suffice to determine surprisingly close upper and lower bounds. These parameters are mean noise power and peak/average noise power ratio or mean noise power and the probability of exceeding some threshold measured in units of noise power. It is also assumed that the ratio of peak noise to the average signal power that would exist in the absence of interference is constrained to some value by receiver dynamic range.

Estimates are selected for these parameters and expressions developed for the standard deviation of the estimators as a function of measurement time and processing bandwidth. The error in measurement of peak noise power and threshold probability were examined for different classes of noise distribution and, as expected, distributions with long "tails" require more measurement time to achieve a given accuracy. However, the measurement times involved to achieve satisfactory accuracy would in almost all cases of interest be considerably smaller than that required to estimate media channel parameters. This comes about because the fading is usually much slower than the noise fluctuations of interest and the essential determinant in estimator variance is the number of independent samples of the parent population selected.

1.6 Error Rate Estimation Utilizing Channel Measurements Based Upon Received Information-Bearing Signal Alone

Section 5 of this report deals with the specification and analysis of techniques for predicting the error rates for the fading channels of interest. A variety of techniques are considered varying in complexity and performance. It is pointed out in Section 2 that the LOS channel should be analyzed on a quasi-stationary basis because bad performance occurs only during deep fades which, by link design, are (hopefully) made to be rare. It is more meaningful, for channel quality monitoring, to estimate the error rate on a short-term basis due to the observed

channel strength and frequency selectivity, than to average over an assumed stationary fading channel because the fading is too slow to obtain meaningful averages over the time duration of the fading state. Thus, the results here should be regarded as applicable to the HF, Troposcatter, and Satellite Scintillation channels although strictly for comparison purposes we have presented average error rate estimate for the LOS channel also. When the fading is flat over the typical DCS LOS system bandwidth of 14 MHz, a very reliable estimate of quasi-stationary error rate is obtainable by using the measured $|T(f,t)|^2$ in an appropriate error rate formula. When frequency selectivity is present, such presence may be determined from measurements of $|T(kF,t)|^2$. However, quasi-stationary error rates cannot be estimated knowing $|T(f,t)|^2$ alone.

The error rate estimation techniques conceived and analyzed are concerned in the main with normal or typical channel conditions in which the modem performance is not determined by excessive multipath spread, excessive Doppler spread, or interference. As discussed in Section 1.2.1, for conventional diversity combining, the estimation techniques conceived fall into three categories:

1) Conditional Error Rate Method
2) Threshold Probability Method
3) Formula Method

For in-band diversity modems, only the conditional error rate method is applicable.

In the case of the conditional error rate estimator, one general case and two special cases are identified. The general case is applicable to any fading statistics, diversity combining, and modem technique provided the noises are statistically independent. In order to evaluate the effectiveness of the error rate estimation techniques, some fading statistics, diversity combining, modem, and additive noise statistics must be assumed. For purposes of analysis, predetection maximal ratio combining, binary DPSK, complex Gaussian fading and additive noises were assumed throughout.

One special case studied corresponded to the case of high SNR where it was possible to amplify the apparent conditional error rate before averaging by reducing the measured instantaneous SNR's and yet recover a good estimate of the true error rate by reducing the measured amplified error rate by a known

factor. This approximate technique is needed because error rates are difficult to measure at high SNR's.

The other special case studied is an alternate approach to reducing the estimation variance at high SNR. However, it is more restrictive in that it assumes some specific receiver and modem structure, namely, predetection maximal ratio diversity combining and incoherent or differentially coherent detection, and it assumes that any correlation between fading on the diversity channels may be neglected. In order to obtain error rate estimates for other diversity combining and modem techniques, one would have to apply theoretical adjustment factors already computed for error rates due to complex Gaussian fading, as discussed in Section 5.

Figure 1.15 presents curves of error probability for binary DPSK transmission, complex Gaussian fading and additive noise, and predetection diversity combining with non, dual, and quadruple diversity. Slow nonselective fading is assumed. Also plotted is the standard deviation of the error rate estimate using the conditional error rate method. The standard deviation of the estimator, when the error amplification technique is used, is shown in dashed lines for non, dual, and quadruple diversity.

These curves when properly interpreted are applicable to the four channels of interest. First, the product of $BT = 600$ for these curves, where B is the rms Doppler spread in Hz and T is the averaging time in seconds. Thus, the measurement time needed to achieve the estimator standard deviations will vary with the channel's Doppler spread. We have presented a table of measurement times for $BT = 600$ in Figure 1.15, assigning appropriate Doppler spreads to each channel. As the reader was forewarned, note the ridiculously long time of 1650 minutes required to measure the average error rate for a LOS channel.

Some comments are in order with regard to applying Figure 1.15 to the HF channel. The error rate estimator uses estimates of $|T(f,t)|^2$ as the basic input. It was assumed that filters were properly optimized for measurement of $|T(f,t)|^2$ for each of the channels. When this was done, it was found that the estimator standard deviations were very little different for the four channels of interest, satisfying the presentation of the single figure. However, bias errors in the estimator were found to be significant on the HF channel but negligible on the others. Thus, the accuracy implied by Figure 1.15 cannot be achieved for the HF channel unless special probing signals are used; otherwise the biases will generally be intolerably high.

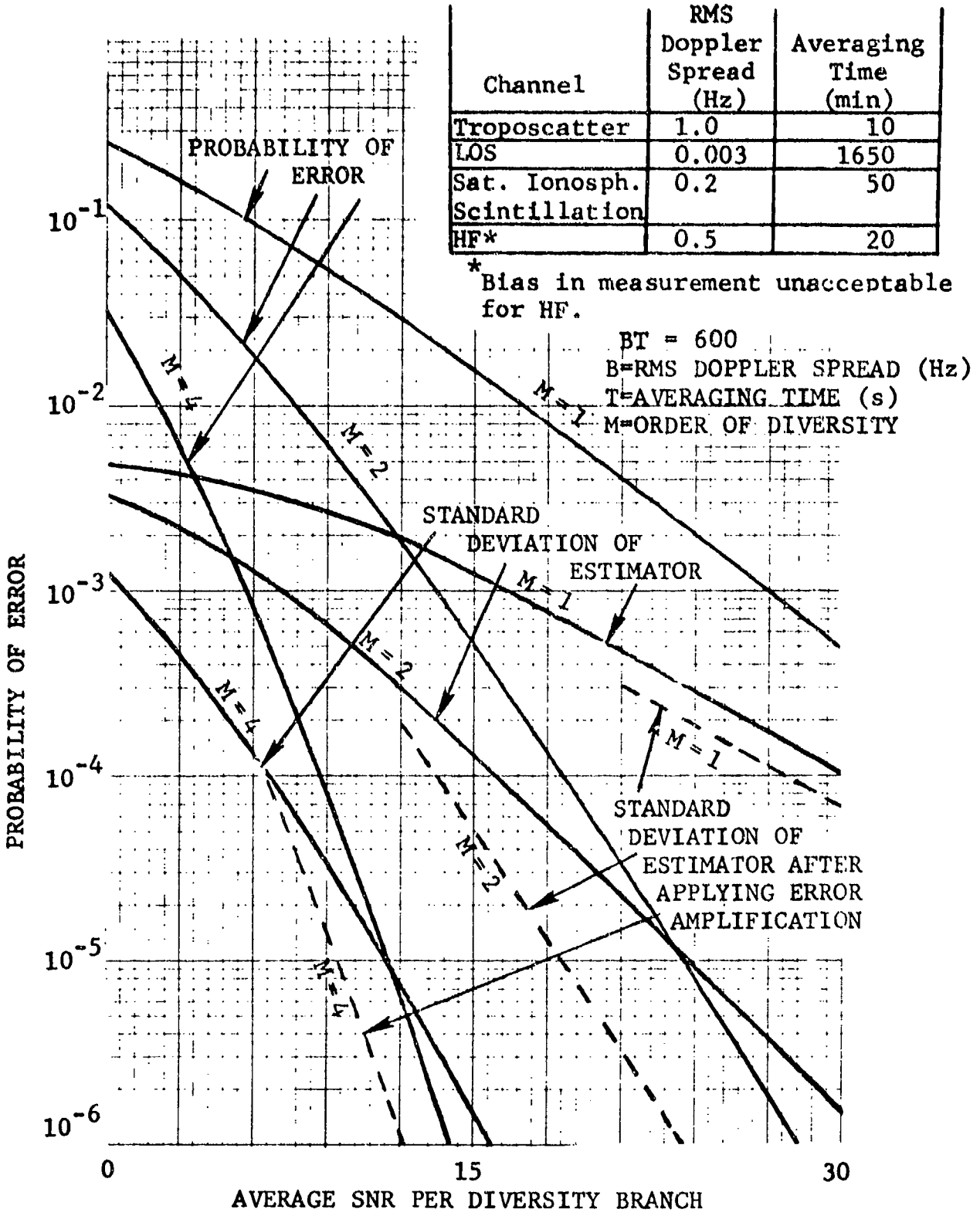

Channel	RMS Doppler Spread (Hz)	Averaging Time (min)
Troposcatter	1.0	10
LOS	0.003	1650
Sat. Ionosph. Scintillation	0.2	50
HF*	0.5	20

*Bias in measurement unacceptable for HF.

Figure 1.15 Error Probability and Standard Deviation of Error Probability Estimation Using the Conditional Error Rate Method. Slow, Nonselective Fading; Predetection Maximal Ratio Combining and DPSK Modulation

With the above provisos and BT = 600, we note that fairly accurate measurement of error rate can be achieved for arbitrary fading statistics on the diversity channels down to low error rates if the error amplification technique is used when SNR's become large. When the diversity becomes very large, however, low error rates can be achieved at low SNR's where the error amplification technique would not be applicable. In such a case, if no assumptions are to be made about fading statistics, there is no recourse but averaging longer to obtain the desired reduction in estimator variance. However, if too long a measurement time is used, channel nonstationarities will begin to have effect and the calculations in Figure 1.15 would have to be used with care since they assumed stationary channel fluctuations. Keeping the above cautions in mind, we note that error standard deviations of 1/6 the desired error rate can be achieved for quadruple diversity, 1/10 for dual diversity, and less for nondiversity.

The threshold method is applicable to general fading statistics but assumes high SNR as in the error amplification approach. Its performance is close to that provided by the error amplification technique shown in Figure 1.15 and, thus, was not plotted.

The formula approach assumes the existence of a formula relating average error rate to channel parameters and statistics. About the only formulas of a general nature that may be derived are those for complex Gaussian fading statistics. Complete specification of such statistics is possible via the complex correlation matrix of the complex time-varying gains defining the diversity channel fading. However, such a general matrix cannot be measured using the received information-bearing signal alone as a probing signal. In one particular case of interest, dual diversity and incoherent or differentially coherent detection, only the magnitude of the correlation coefficient is needed and this can be estimated by operating on the received signal alone. However, only relatively high correlations cause significant degradations and, as we have seen, it is difficult to measure correlation coefficients when they are high. Thus, the formula approach would seem to be most useful when statistical dependencies of the fading on diversity channels may be ignored and when the fading statistics are known. In such a case, they provide the simplest and most accurate estimation technique.

In the case of modems employing in-band diversity, only the conditional error rate method applies for channel measurement. However, the measurement of $\int |T_m(f,t)|^2 df$ is used as input instead of $|T_m(f,t)|^2$; m=1,2,...,M. We have not carried out specific

evaluations for such modems. However, we note that such modems are equivalent to a conventional modem operating at a sufficiently high order of diversity and, thus, our general comments centering on Figure 1.15 apply here, with the exception that the error amplification technique is not rigorously applicable. If one is willing to define and measure the "equivalent in-band diversity" then all the techniques discussed above may be applied. In lieu of this heuristic approach, the only general technique to use is the Conditional Error Rate Method.

Some consideration was given to error rate prediction for an FDM-FM system including irreducible error rate due to multipath. A formula approach may be used based upon prior work of Bello [1.12][1.18] which provided error rates as a function of SNR and rms multipath spread assuming complex Gaussian fading and independent diversity channels. Calculations were carried out for the troposcatter channel.

The estimation of short-term error rate can be quite useful in distinguishing error bursts due to the channel from those due to an intermittent receiver fault. Consideration was given to the effectiveness of measurement of short-term error rate using a small averaging time with the conditional error rate method. Except for the HF channel, the calculations show that the rms value of the difference between a short-term error rate estimate (via the conditional error rate method) and a true counted error rate over the same averaging time interval, will be small compared to the average error rate for averaging time intervals of the order of the fading time constant of the channel and for average error rates down to 10^{-6}. Thus, burst error rates exceeding the average error rate of the channel will be easily identifiable.

1.7 Measurement Techniques Using Special Probing Signals

The use of special probing signals for channel measurements is discussed in Section 6. It is pointed out that the coherent processing possible with such techniques allows data noise and additive noise to be very much smaller than for the estimators discussed above which use the received information-bearing signal alone as the source of channel information. As a result, one may be generous in allowing more noise through to essentially remove distortion effects.

Both in-service and out-of-service probing is considered. For out-of-service probing, the output SNR's of all good system function estimators are related to the input SNR by

$$\rho_{out} \approx \frac{\rho_{in}}{S} \tag{1.17}$$

where S, called the spread factor of the channel, is defined by

$$S = B_{tot} L_{tot} \tag{1.18}$$

where B_{tot} is the total Doppler spread and L_{tot} is the total multipath spread of the channel. For all the channels of interest

$$S \lll 1 \tag{1.19}$$

It follows that excellent measurement accuracy is possible for the system functions of the channel [e.g., for T(f,t)] with out-of-service probing because the communication system is designed so that $\rho_{in} \gg 1$. Thus, the channel parameters of the HF channel (e.g., B) can be measured very well with out-of-service probing although they could only be measured very poorly when the received data signal was the probe.

In-service probing is clearly preferable to out-of-service probing. Various methods of in-service probing are examined depending on how the data signal and probing signal are combined. The most practical arrangements are those that do not require special formatting of the data signal. In this connection, the transmission of a wideband probing signal in the same band as the data is an interesting possibility.

An examination of this type of probing revealed that it was feasible for the LOS, Troposcatter, and Satellite Ionospheric Scintillation channels but questionable for the HF channel. The probing signal must be set low enough not to interfere with the data but not so low that the data noise appearing at the channel measuring equipment output is intolerable. It is shown that if a data/prober SNR of ρ_{DP} and a measurement output SNR of ρ_{MD} due to data noise is desired, then the spread factor of the channel must satisfy the inequality

$$S \leq \frac{1}{\rho_{MD}\,\rho_{DP}} \tag{1.20}$$

Typical values that might be selected are

$$\rho_{MD} = \rho_{DP} = 100 \tag{1.21}$$

which leads to $S \leq 10^{-4}$. But the HF channel with Doppler spreads of 1 - 2 Hz and multipath spreads of 1 - 2 ms has S lying in the range $10^{-3} < S < 4 \times 10^{-3}$. This implies that $\rho_{MD} = \rho_{DP}$ cannot exceed 12 to 15 dB or, alternatively, if ρ_{DP} is set at 20 dB, then ρ_{MD} would vary from 4 to 10 dB.

We now review the practical system function measurement possibilities for each of the channels of interest. First, as we have just pointed out, the HF channel is not a good candidate for wideband in-band in-service probing. However, because of the use of SSB with multiple subcarriers, it is easy to insert a pilot tone at the band edge (in fact, an unmodulated tone is usually transmitted for AFC). This would allow the measurement of the transfer function at one frequency. If the transfer function is desired at more than one frequency, additional tones would have to be transmitted, reducing channel capacity.

In the other channels, transmitted signals are constant envelope and nonlinear essentially hardlimiting amplifiers are used at certain points in the transmitter. An analysis of the output of a hard limiter containing a probing signal plus a constant envelope data signal reveals that if the probing signal is 20 - 30 dB below the data signal, the limiter output will contain the desired probing signal suppressed by 6 dB. Only one other spurious output component would be of sufficient size to offset channel measurement, but it is shown that as long as the data signal remains wideband when its modulation index is doubled, this spurious component may be neglected. It follows that either PN or parallel tone in-band probing is feasible for LOS and tropo channels.

For satellite ionospheric scintillation channels, multipath is not a factor of importance, and a single low-level tone placed adjacent to the data signal can be used to characterize the channel.

The error rate estimation techniques discussed in Section 1.6 based upon processing estimated values of the squared magnitude of the channel transfer function may obviously be used when the actual complex transfer function or impulse response is known. Moreoever, the bias errors which were especially troublesome for HF channels will vanish and variances of the estimation errors will reduce. The latter reduction will not be so dramatic as the reduction of biases because the unaveraged channel fluctuations represent the major source of estimation error variance.

An important benefit of the use of special probing signals comes from the ability to measure the delay power spectrum $Q(\xi)$ which was shown to be necessary for estimating the irreducible error probability produced by excessive multipath in troposcatter modems.

With regard to LOS modems, measurement of the complex transfer function at three frequencies will allow construction of a quadratically frequency-selective model and, from this model, an estimation of "instantaneous" error rates including the effect of selective fading.

1.8 Conclusions

As a result of the study summarized above, the following conclusions have been reached:

- The MQU as conceived in this study has the potential for estimating the error rate for a normally functioning receiver and, by comparison with a PMU output, of allowing the determination of receiver degradation trends. Also, it has the potential for distinguishing between three basic causes of outages: interference, excessive multipath and/or Doppler spread, or receiver failure.
- The use of the received information-bearing signal alone as a source of channel information (called data signal probing) for the MQU is effective for the LOS, Troposcatter, and Satellite Ionospheric Scintillation channels, but only minimally for the HF channel. Accurate estimates of error rates for the LOS channel in the presence of frequency-selective fading and for the troposcatter channel in the presence of excessive multipath spread cannot be obtained with data signal probing. However, the presence of these disturbing conditions may at least be detected. Reliable error

rate estimates for a normally functioning receiver can be obtained for the typical situation where the performance is not limited by time- or frequency-selective distortion.

- The use of special probing signals allows the MQU to estimate time-varying error rates for the LOS channel in the presence of frequency-selective fading and the troposcatter channel in the presence of excessive multipath spread. Error rate estimation for the HF channel also becomes possible.
- The MQU should pick off its input signals as close as possible to the receiving antennas.
- A special wideband probing signal may be transmitted in the same band as the data signal if its strength is selected correctly for the LOS, Troposcatter and Satellite channels, but not for the HF channel. In the latter case only noninterfering tones seem feasible for probing signals. For the LOS channel it appears sufficient to transmit three tones in a 14-MHz band to measure parameters needed to calculate error rate.
- With regard to implementation, only the basic system function measurement (squared-magnitude transfer function in the data probing signal case and complex transfer function or impulse response measurement in the special probing signal case) need be done with analog and/or digital hardware. All the rest of the computations can be handled with a typical current minicomputer having hardware multiply/divide, such as the Nova or PDP-11.
- The Conditional Error Rate method of estimating error rates is preferred because it provides an adequately accurate error rate estimate with no detailed assumptions made about the fading statistics.
- Detection of the presence of a narrowband interference appears feasible through measurement of the centroid and rms bandwidth of the received signal and applying the detection algorithm proposed in this study.
- Detection of the presence of an interfering signal through estimating changes in average power level can be effective if the channel is not too nonstationary and the fading rate fast enough. Calculations for

troposcatter channels indicate the approach to have some promise pending the availability of more definitive information on nonstationary path loss variations.

- The measurement of a few noise parameters, e.g., moments, peak/average, average, and threshold exceedance probability can provide remarkably close upper and lower bounds to error rate in fading channels.

1.9 Recommendations

In view of the positive results arrived at during this study on the calculated performance of various channel measurement techniques used in the MQU (e.g., see Figures 1.4, 1.5, 1.15, and 5.8), the general recommendation is made that detailed design, development, and testing of experimental models of troposcatter, LOS, HF, and Ionospheric Scintillation channel MQU's be carried out with diversity configurations as appropriate. If this recommendation is carried out, the effectiveness of the MQU may be demonstrated both in classifying sources of degradation into the three major categories of receiver-caused, propagation-caused, and interference-caused, and in estimating receiver degradation trends.

We consider the troposcatter channel first. The recommended equipment contains the following subsystems and signal processing operations:

- media sensor
- system function estimator
- multipath spread estimation
- Doppler spread estimation
- SNR estimation
- average error rate estimation for nondegraded receiver
- short-term estimation for nondegraded receiver
- interference-presence detection
- narrowband interference detection

The media sensor picks off signal power at the RF or IF level and filters it in a narrowband predetection filter (see Figure 1.3). For the advanced high-speed troposcatter data modems inband diversity would be employed, and error rate estimation with the MQU would require the media sensor to either examine the short-term power in narrow bands at several spaced frequencies within the data signal spectrum or else use a wideband predetection filter (see

Section 5.6). The latter approach is recommended as being simpler and probably more effective (p. 5-93). As pointed out in Section 3.2.2, it is desirable to select the pickoff location of the media sensor unit as near to the antenna as reasonable to avoid confusing front-end-produced degradations with channel-produced degradation. However, consideration must be given to the possible degradation in effective noise temperature for the communications receiver caused by coupling too much energy to the media sensor at low RF signal levels.

The system function estimator estimates the squared-magnitude of the time-variant channel transfer function by computing the short-term power at the output of the narrowband predetection filter of the media sensor (Figures 1.3, 4.1, and Section 4.1). With suitable optimization of the time constants of the pre- and post-detection filters, useful estimates of the channel's squared-magnitude transfer function can be obtained (e.g., 2% error, Table 1-3). Hardware implementation of the squaring and post-detection filtering is recommended (Section 3.3.1, pp. 3-48 and 3-49).

It is recommended that the gross channel parameters of multipath spread, Doppler spread, and SNR in addition to average and short-term error rate estimates be carried out with the aid of a minicomputer having a hardware multiply/divide. The feasibility of this type of implementation is discussed in Sections 3.3.3 and 3.3.4. The computer provides the flexibility for changing the algorithms for channel parameter measurement and error rate estimation to accommodate a wide variety of troposcatter channels, diversity-combining methods, and modem techniques. It also allows the comparative testing of competing estimation algorithms such as the conditional error rate (Section 3.1, pp. 3-2 to 3-7; also Sections 5.1.2 and 5.1.3), threshold (Section 3.1, pp. 3-9 to 3-11; also Section 5.2), error rate amplification (pp. 3-7 and 3-8), and short-term or burst error rate (Section 5.1.4) measurement techniques.

The detection of the presence of an interfering signal by measuring a sufficient change in power level and the detection of a narrowband interference through measuring sufficient changes in the centroid and rms bandwidth of the received signal are discussed in detail in Section 4.4 and reviewed in Section 1.4. The calculation of detection performance shows promise in these detection methods (see Figures 1.11, 1.12, and 1.13; also Section 4.4). Thus, it is recommended that these detection techniques be implemented also. Implementation of these interference detectors

requires the addition to the above hardware and computer of little more than hardware differentiators for the in-phase and quadrature components of the received signal (see Figure 3.6 and Section 4.3.3).

To check out the effectiveness of the MQU in categorizing sources of degradation and estimating receiver degradation trends, it will be necessary ultimately to have available a digital troposcatter modem and radio. Conventional digital troposcatter modems not employing in-band diversity are already available, and advanced modems utilizing in-band diversity should be available in the near future. However, even in the absence of a modem, the Rake prober and the troposcatter simulators available at RADC may be used for checking out channel and interference measurement functions of the MQU.

In addition to application to the troposcatter channel, it has been demonstrated that the MQU concept should be quite useful in the LOS, Satellite, and HF channels. Our attention has focused on the troposcatter channel in detail because of the somewhat greater complexity of the required MQU. Since LOS links are of major importance in the DCS, we also summarize below our recommendations for the application of MQU concepts to such links.

For LOS links, the recommended equipment contains the following subsystems:

- media sensor
- system function estimator
- short-term error rate estimation
- interference-presence detection
- narrowband interference detection

As has been discussed frequently in this study (p. 1-2, p. 1-25, p. 1-44, p. 1-45, Section 2.2.2, p. 4-1, p. 5-1), measurement of error rates and channel parameters averaged over the fading, while meaningful for troposcatter links, are not meaningful for LOS links. In the latter case, only short-term or quasi-stationary measurements of error rates and channel parameters is recommended.

It is recommended that two kinds of media sensor/system function estimator combinations be implemented. First, it is recommended that the techniques discussed above for use on the troposcatter channel (pp. 1-54, 1-55) be implemented. These employ the received data signal alone without special probing

signals and invoke short-term power spectral estimation in several frequency bands by analogous hardware to obtain an estimate of the squared-magnitude of the channel transfer function (Figures 1.3, 4.1, and Section 4.1). Measurement accuracies of 1% are attainable (see Table 1-3). Such measurements will allow a determination of the presence and degree of frequency selective fading and, thus, aid in properly isolating the source of degradation.

The second media sensor/system function estimator combination that should be implemented involves the use of special probing signals and the measurement of the complex transfer function (amplitude and phase). As pointed out in several places (e.g., pp. 3-21, 3-22, 5-1), only the complex transfer function allows the estimation of short term error rates in the presence of frequency selective fading on LOS links. Either low-level multiple tone or pseudo-noise probing signals should be effective and allow in-service probing with little disturbance to the data signal, as discussed in Section 6.2. The final decision will have to be based upon relative complexity and cost and should be part of the design study.

The detection of the presence of an interfering signal and of a narrowband interference should be implemented as discussed above for the troposcatter channel (paragraph beginning on the bottom of p. 1-55).

It is recommended that a minicomputer be used for short term error rate estimation based upon the measured complex transfer function characteristics obtained from the media sensor/system function estimator hardware. This will provide the flexibility for evaluating different error rate estimation algorithms with different LOS modems.

SECTION 1

REFERENCES

[1.1] "Line-of-Sight Technical Investigation," Final Report by CNR, Inc., on RADC Contract F30602-73-C-0244. (AD006104)

[1.2] D. Chase, "A Class of Algorithms for Decoding Block Codes with Channel Measurement Information," IEEE Trans. on Info. Theory, Vol. IT-18 (January 1972).

[1.3] D. Chase, "A Combined Coding and Modulation Approach Over Dispersive Channels," IEEE Trans. on Comm., pp. 159-174 (March 1973).

[1.4] "Coding/Mux Overhead Study," Final Report by CNR, Inc., on RADC Contract F30602-73-C-0271.

[1.5] P. Monsen, "Digital Transmission Performance on Fading Dispersive Diversity Channels," IEEE Trans. on Comm., Vol. COM-21, pp. 33-39 (January 1973).

[1.6] P. A. Bello, "Comparative Evaluation of High Speed Digital Data Transmission Techniques over the Troposcatter Channel," ADCOM Research Report No. 16 (30 September 1964).

[1.7] P. A. Bello, "Selective Fading Limitations of the Kathryn Modem and Some System Design Considerations, IEEE Trans. on Comm. Tech., Vol. COM-13, No. 3, pp. 320-333 (September 1965).

[1.8] P. A. Bello, "Some Signal Design Considerations for HF PSK Modems," ADCOM Research Report No. 10 (30 September 1964).

[1.9] P. A. Bello and B. D. Nelin, "Predetection Diversity Combining with Selectively Fading Channels," IRE Trans. on Comm. Systems, Vol. CS-10, No. 1, pp. 32-42 (March 1962).

[1.10] P. A. Bello and B. D. Nelin, "The Effect of Frequency-Selective Fading on the Binary Error Probabilities of Incoherent and Differentially-Coherent Matched Filter Receivers," IEEE Trans. on Comm. Systems, Vol. CS-11, No. 2, pp. 170-186 (June 1963).

[1.11] P. A. Bello and L. Ehrman, "Performance of an Energy Detection FSK Digital Modem for Troposcatter Links," IEEE Trans. on Comm. Tech., Vol. COM-17, No. 3, pp. 368-379 (June 1969).

[1.12] P. A. Bello and L. Ehrman, "Error Rates in Diversity FDM-FM Digital Troposcatter Transmission," IEEE Trans. on Comm. Tech., Vol. COM-17, No. 2, pp. 183-191 (April 1969).

[1.13] P. A. Bello and T. Crystal, "A Class of Efficient High-Speed Digital Modems for Troposcatter Links," IEEE Trans. on Comm. Tech., Vol. COM-17, No. 2, pp. 162-183 (April 1969).

[1.14] P. A. Bello, "Error Probabilities Due to Atmospheric Noise and Flat Fading in HF Ionospheric Communication Systems," IEEE Trans. on Comm. Tech. (September 1965).

[1.15] P. A. Bello, "Bounds on the Error Rate of FSK and PSK Receivers due to Non-Gaussian Noise in Fading Channels," IEEE Trans. on Information Theory, Vol. IT-12, No. 3, pp. 315-326 (July 1966).

[1.16] P. A. Bello, et al., "Modeling and Data Analysis -- Short and Medium Range Digital Troposcatter Tests," Signatron, Inc., Final Technical Report, RADC-TR-69-233, Vol. 1, Figure 3-27 (October 1969). (AD875992)

[1.17] P. A. Bello, "Error Probabilities Due to Atmospheric Noise and Flat Fading in HF Ionospheric Communication Systems," IEEE Trans. on Communication Technology, Vol. COM-13, No. 3, pp. 266-279 (September 1965).

[1.18] P. A. Bello and B. D. Nelin, "The Effect of Frequency-Selective Fading on Intermodulation Distortion and Sub-Carrier Phase Stability in Frequency Modulation Systems," IEEE Trans. on Comm. Systems, pp. 87-101 (March 1964).

SECTION 2

CHANNEL MODELING

The major objective of this program is the development and comparative analysis of concepts for determining the quality of certain radio transmission media for digital data transmission. As has been discussed in Section 1, such media quality units (MQU's) show great potential for determining the existence of degradation trends, outages and performance margins caused by equipment malfunction while at the same time preventing propagation media induced performance loss from being interpreted as equipment malfunction.

An MQU should estimate continually in real time the error rate performance that is achievable with the given channel conditions if the radio receiver, diversity combiner, and modem were perfectly functioning. For meaningful MQU concepts to be developed, relationships must be established between error rates for various classes of modems and the time-variant dispersive characteristics of the propagation media of interest, with proper regard being taken for the additive disturbances on the channel.

This section of the report is concerned with modeling the characteristics of the radio channels of interest (HF, troposcatter, LOS, satellite ionospheric scintillation) so that the relationships between important channel parameters and digital modem performance discussed in subsequent sections are made evident.

The discussion is general at first, and then proceeds to a discussion of specific channels. Thus, Section 2.1 discusses the system function characterization of radio channels, including "instantaneous" input-output relationships, channel correlation functions, gross channel parameters, and statistics. Section 2.2 focuses attention on the specific channels of interest: HF, troposcatter, line-of-sight radio relay, and satellite ionospheric scintillation channels. Both typical and atypical channel characteristics and advanced digital modem techniques are discussed.

2.1 System Function Characterization of Random Time-Variant Channels

The propagation channels of interest here are linear and their behavior may be described on an "instantaneous" input-output basis with the aid of system functions, as discussed in Section 2.1.1. Section 2.1.2 introduces channel correlation functions to provide the simplest second-order statistical description of these channels on a quasi-stationary basis. Section 2.1.3 summarizes various statistical channel models that have been useful plus the minimal kind of statistical information needed for performance estimation at high SNR. Section 2.1.4 discusses two basic canonic models that will be used in defining essential parameters characterizing the radio channels of interest.

2.1.1 System Functions

There exists a variety of system functions for characterizing the input-output behavior of linear time-varying systems. The most general discussion of these system functions and their relationships has been presented in [2.1]. For the purposes of the present brief discussion, it is sufficient to confine attention to the time-variant transfer function $T(f,t)$ and the time-variant impulse response $g(t,\xi)$. For simplicity of presentation, we shall use complex envelope representation throughout. Thus, the input signal would be represented by the complex signal $z(t)$. The real signal would be a narrowband process with envelope $|z(t)|$ and with phase $\measuredangle z(t)$ measured with respect to carrier phase $2\pi f_0 t$, where f_0 is the carrier frequency.

In complex notation, the input-output relationships corresponding to the use of $T(f,t)$, $g(t,\xi)$ are

$$w(t) = \int Z(f)\, T(f,t)\, e^{j2\pi ft}\, df \tag{2.1}$$

$$w(t) = \int z(t-\xi)\, g(t,\xi)\, d\xi \tag{2.2}$$

where $w(t)$ is the output signal (complex) and $Z(f)$ is the spectrum of $z(t)$.

The transfer function $T(f,t)$ and impulse response $g(t,\xi)$ are Fourier transform pairs,

$$T(t,f) = \int_{-\infty}^{\infty} g(t,\xi)\, e^{-j2\pi f\xi}\, d\xi \tag{2.3}$$

$$g(t,\xi) = \int_{-\infty}^{\infty} T(f,t)\, e^{j2\pi f\xi}\, df \tag{2.4}$$

It is readily seen that the time-variant transfer function at the frequency f (actually f Hz away from carrier frequency f_0) is just equal to the complex modulation observed on a received RF carrier transmitted at $f_0 + f$ Hz. Thus, the time-varying envelope of this received carrier is $|T(f,t)|$ and the time-varying phase of this received carrier measured with respect to the input carrier phase is $\measuredangle T(f,t)$.

While $g(t,\xi)$ may be described formally as the response at time t to an impulse input at $t-\xi$, it is helpful in modeling radio channels to regard $g(t,\xi)$ as the differential complex time-varying gain associated with path delays in the delay interval $(\xi, \xi+d\xi)$ in a differencial tapped delay line interpretation of (2.2).

With the use of delta functions, the integral formulations above include as a special case the idealized radio channel consisting of a finite number K of discrete paths, i.e.,

$$g(t,\xi) = \sum_{k=1}^{K} G_k(t)\, \delta(\xi - \xi_k) \tag{2.5}$$

for which (2.2) and (2.3) become

$$w(t) = \sum_{k=1}^{K} G(t)\, z(t - \xi_k) \tag{2.6}$$

$$W(f) = \sum_{k=1}^{K} G(t)\, e^{-j2\pi f\xi_k} \tag{2.7}$$

The tapped delay line interpretation of $g(t,\xi)$ is particularly evident in (2.5) through (2.7).

The discrete model is particularly useful in modeling the HF, LOS radio relay, and satellite ionospheric scintillation channels. The integral formulation is appropriate for scatter

channels, such as the troposcatter link and scatter portions of the line-of-sight and surface scatter channels.

2.1.2 _ lation Functions

While the fluctuations in radio channels are due to non-stationary statistical phenomena, on a short enough time scale and for small enough bandwidths the fluctuations in time and frequency can be approximately characterized as statistically stationary. For want of a better word, this approximate stationarity is called quasi-stationarity. A mathematical basis for defining quasi-stationary radio channels is presented by Bello in [2.2].

When the time-variant transfer nction is idealized to have stationary fluctuations in time and frequency, the channel is said to be [2.2] wide-sense-stationary-uncorrelated-scattering (WSSUS). For the WSSUS channel

$$\overline{T^*(f,t)T(f+\Omega,t+\tau)} = R(\Omega,\tau) \tag{2.8}$$

i.e., the cross-correlation function between the complex envelopes of received carriers transmitted Ω Hz apart is dependent only on the frequency separation Ω and time lag τ. The function $R(\Omega,\tau)$ is called the time-frequency correlation function.

Because of the Fourier transform relationship between $T(f,t)$ and $g(t,\xi)$, one may show that (2.7) implies

$$\overline{g^*(t,\xi)g(t+\tau,\eta)} = Q(\tau,\xi)\delta(\eta-\xi) \tag{2.9}$$

where $\delta(\cdot)$ is the unit impulse function and $Q(\tau,\xi)$ is the Fourier transform of $R(\Omega,\tau)$ on the Ω variable. $Q(\tau,\xi)$ has been called the tap gain correlation function because it is proportional to the autocorrelation function of the fluctuations in the complex tap gain at delay ξ in the differential tapped delay line model interpretation of Eq. (2.2). Equation (2.9) implies that the fluctuations of the complex gains at different positions on the delay line are uncorrelated, which is the reason for the US in WSSUS.

The power spectrum of the complex gain fluctuations at a given tap delay ξ is proportional to the Fourier transform of $Q(\tau,\xi)$ with respect to τ. This power spectrum, $S(\xi,\nu)$,has been called the scattering function. It is given by

$$S(\xi,\nu) = \int Q(\tau,\xi)\, e^{-j2\pi\tau}\, d\tau \qquad (2.10)$$

The scattering function exhibits directly the delay and Doppler spreading characteristics of the channel.

To make practical use of the WSSUS model, the functions $R(\Omega,\tau)$, $Q(\tau,\xi)$, and $S(\xi,\nu)$ must be regarded as "mildly" dependent on both time origin and carrier frequency, as discussed in [2.1].

A cruder but frequently adequate description of the average fading dispersive properties of the WSSUS channel are provided by the delay and Doppler power spectra $Q(\xi)$, $P(\nu)$ and their transforms, the frequency and time autocorrelation functions $q(\Omega)$, $p(\tau)$, respectively. The latter are defined as

$$q(\Omega) = R(\Omega,0) \qquad (2.11)$$

$$p(\tau) = R(0,\tau) \qquad (2.12)$$

$q(\Omega)$ is the complex cross-correlation coefficient between two received carriers as a function of their frequency separation.

When the frequency separation is such that the cross-correlation function $q(\Omega)$ is very near the maximum value $q(0)$ for all $|\Omega| < W_{coh}$, it is clear that all transmitted frequency components within a band of frequencies of width less than W_{coh} will be received fluctuating in a highly correlated fashion. For this reason, W_{coh} is called the coherence bandwidth.

The time correlation function $p(\tau)$ is the autocorrelation function of the complex envelope of a received carrier. Clearly, one may define a coherence duration parameter T_{coh} in terms of $p(\tau)$ in the same way as W_{coh} is defined in terms of $q(\Omega)$.

The gross channel parameters W_{coh} and T_{coh} are particularly useful in predicting the onset of frequency and time-selective distortion when the WSSUS channel contains no discrete paths. Then both $q(\Omega)$ and $p(\tau)$ drop to zero as $\Omega, \tau \to \infty$, and pulses with bandwidths greater than W_{coh} or time durations greater than T_{coh} will suffer ever-increasing amounts of distortion. When there are discrete paths, $q(\Omega)$ and $p(\tau)$ can approach nonzero constants as $\Omega, \tau \to \infty$. If a single discrete path is sufficiently strong, increasing the pulse width beyond T_{coh} or the bandwidth beyond W_{coh} may produce only a small amount of additional distortion. Of course, if the specular component is very strong, W_{coh} T_{coh} may equal ∞ if they are defined as values of Ω and τ for which $q(\Omega)$ and $p(\tau)$ drop to a specific fraction of $q(0)$ and $p(0)$, respectively.

The Fourier transform of the frequency correlation function $q(\Omega)$ is the delay power spectrum $Q(\xi)$ which can be expressed in the following forms:

$$Q(\xi) = Q(0,\xi) = \int S(\xi,\nu)\, d\nu \tag{2.13}$$

This function is proportional to the intensity of the complex tap gain at delay ξ in a differential tapped delay line model of the channel. One may define a multipath or delay spread parameter as the "width" of $Q(\xi)$ where width is defined in some convenient fashion.

Two measures of width that occur frequently in applications are "total" and "rms". The total delay spread, L_{tot}, is meant to define the extent of $Q(\xi)$ for values of ξ where $Q(\xi)$ is significantly different from zero (e.g., 40 dB down from the maximum value of $Q(\xi)$). The utility of L_{tot} is that it defines the width of $g(t,\xi)$ vs. ξ. Then, by Nyquist's sampling theorem, the transfer function $T(f,t)$ vs. f must be sampled at least at a sampling "rate" of $1/L_{tot}$ samples/Hz to allow reconstruction of $T(f,t)$.

The rms delay spread, L_{rms}, is defined as twice the standard deviation of $Q(\xi)$ when it has been normalized to unit area and regarded as a probability distribution. This parameter may be shown to control the degree of frequency selectivity in a bandwidth which is some small multiple of the coherence bandwidth [2.1].

The Fourier transform of the time correlation function $p(\tau)$ is the Doppler power spectrum $P(\nu)$, which is the power spectrum of a received carrier. This spectrum may be expressed as an integration over $S(\xi,\nu)$

$$P(\nu) = \int S(\xi,\nu)\, d\xi \tag{2.14}$$

The "total" Doppler spread, B_{tot}, and rms Doppler spread, B_{rms}, parameters are defined analogous to L_{tot} and L_{rms}, respectively, and have analogous utilities.

When the product of the coherence bandwidth and time duration W_{coh}, T_{coh} of a channel exceeds the time-bandwidth product of the signaling elements used in communicating over that channel, both time and frequency-selective distortion will not be simultaneously active. Then $P(\nu)$ and $Q(\xi)$ [or, equivalently, $p(\tau)$ and $q(\Omega)$] are sufficient to describe the average multipath and Doppler spreading characteristics of the channel. In effect, for the class of waveforms considered, one may replace the actual scattering function $S(\xi,\nu)$ by the simpler scattering function

$$S_0(\xi,\nu) = P(\nu)\, Q(\xi) \tag{2.15}$$

without altering the observed average time and frequency selective distortion on the received signals. For the determination of raw (uncoded) error rates, it appears that the simplification (2.15) may be used for the channels of interest in the present study.

The reader should be reminded that to be practically meaningful, the functions $S(\xi,\nu)$, $P(\nu)$, $Q(\xi)$ must be regarded as slowly varying with time and generally dependent on carrier frequency, in addition to being dependent upon the physical location and motion of the terminals of the link.

2.1.3 Statistics

In order to be able to evaluate analytically the performance of various modulation techniques over a channel, it is necessary to have more statistical information than the channel correlation functions defined in 2.1.2. Strictly speaking, for an exact statistical characterization one needs multi-dimensional probability distributions of the system functions. Unfortunately, these have not been measured and, if they were, they would be

prohibitively complex to use. Fortunately, however, there are useful statistical models that may be used in characterizing radio links. In addition, as will be discussed in Section 3 at high SNR's the error rate behavior is only weakly dependent on the statistics of the fading and additive noise.

The detailed analytical statistical models use Gaussian processes to model channel fluctuations either directly or indirectly. The utility of the Gaussian characterization, either direct or indirect, is that the statistics can be completely specified from the correlation functions of the Gaussian processes.

Three very useful models that keep recurring are:

a) The Gaussian WSSUS channel

b) The Gaussian discrete WSSUS channel

c) The Gaussian phase-modulation discrete stationary channel

Model a) is useful for troposcatter links, model b) for HF links and ionospheric scintillation links, and model c) for LOS links.

The Gaussian WSSUS channel is a WSSUS channel in which the transmission of a carrier results in the reception of a narrowband process whose in-phase and quadrature components are stationary Gaussian processes. A special case of this channel, which is the one most often used, is the complex Gaussian [2.2], [2.3] stationary scatter channel in which the in-phase and quadrature components of a received carrier are of equal strength and satisfy certain symmetry conditions that force the average

$$\overline{T(f,t)T(f+\Omega,t+\tau)} = 0 \tag{2.16}$$

Note that the left side of (2.16) is <u>not</u> the time-frequency correlation function because the conjugate sign is missing [c.f. (2.8)].

One of the characteristics of the complex Gaussian channel is that a received carrier has an envelope which has the Rayleigh probability density function. Both theoretical considerations involving the central limit theorem and measurements of the distribution of received carrier envelopes for HF, tropospheric scatter, and strongly scintillating satellite channels frequently exhibit the Rayleigh character and in modeling such channels it has become customary to use the complex Gaussian model.

The utility of the complex Gaussian model is that the time-frequency correlation function $R(\Omega,\tau)$ or, equivalently, $Q(\tau,\xi)$ or $S(\xi,\nu)$ completely specifies the statistics of the channel and frequently makes possible the analytic computation of error rates. In any case, the Gaussian assumption allows the determination of system performance by hardware or software simulation techniques.

The Gaussian discrete WSSUS channel has the property that the fluctuations $G_k(t)$ in (2.6) have Gaussian (possibly nonzero mean) statistics. The complex Gaussian discrete WSSUS channel is of interest also, for which the moment property

$$\overline{(G_k - \overline{G_k})(G_j - \overline{G_j})} = 0 \tag{2.17}$$

applies.

The Gaussian phase-modulation discrete stationary channel is a stationary discrete channel in which $G_k(t)$ takes the form

$$G_k(t) = A_k e^{j\varphi_k(t)} \tag{2.18}$$

where A_k is constant and $\varphi_k(t)$ is a Gaussian process. Note that, in general, $G_k(t)$ has a nonzero mean, i.e.,

$$G_k(t) = A_k e^{-\sigma_\varphi^2/2} \tag{2.19}$$

where σ_φ is the rms value of the phase fluctuation.

In some applications, σ_φ is so large compared to 2π that φ is regarded as uniformly distributed, modulo 2π, and $\overline{G_k} = 0$.

The stationary statistical models described above are convenient idealizations. However, the actual radio channel characteristics are nonstationary. Thus, in the practical use of these models, a quasi-stationary approach must be used with the channel correlation functions and others defining the statistics of the Gaussian processes, allowed to vary slowly with time, carrier frequency and system geometry. From the point of view of predicting performance apriori, it is clearly desirable to have statistical information on the variation of channel correlation functions or as a minimum the variation of such gross channel

parameters of multipath and Doppler spread. Surprisingly little definitive information of this type is available and Section 2.2 summarizes some of this for the channels of interest.

The difficulty of the statistical modeling problem is further compounded by the fact that reliable and practical communication over fading dispersive channels, such as those of interest here, require the use of diversity methods. Conventional diversity communications involves the transmission of the same information over more than one channel, preferably fluctuating independently, and combining the outputs of the channels to reduce the frequency of deep fades. There are several ways to physically implement diversity channels and several ways used to combine channel outputs. The following section discusses typical diversity methods used for each of the channels of interest. Further discussions of diversity combining are presented in Section 3 where relationships between error rate and channel characteristics are discussed.

From a channel modeling point of view, diversity communications with M channels involves characterizing the joint statistics of M channels having time-variant transfer functions $\{T_\ell(f,t);\ \ell=1,2,\ \ldots\ M\}$. The assumption of complex Gaussian WSSUS channel statistics allows the complete specification of performance from channel correlation functions, e.g.,

$$\overline{T^*_\ell(f,t)T_p(f+\Omega,t+\tau)} = R_{\ell p}(\Omega,\tau) \qquad (2.20)$$

As pointed out above for the single channel, $R_{\ell p}(\Omega,\tau)$ is only a quasi-stationary correlation function and long term statistics of these are needed in performance prediction.

The difficulties of the statistical modeling and performance prediction problem are somewhat mitigated by the following observations:

1) In most cases of interest the diversity channels can be selected to have small correlation, most of the time.

2) Performance evaluations have indicated that remarkably high correlations between diversity channels can occur before significant performance loss occurs.

3) A well designed modem will not usually be performance-limited by time and frequency selective fading distortions.

4) Low error rates usually require high SNR's on fading dispersive channels.

5) At high SNR the error rate performance of a digital modem is weakly dependent on the precise statistical characters of the fading and the additive noise.

Considerable use is made of modeling simplifications arising from the above observations in the development of concepts for MQU's in the succeeding sections.

2.1.4 Canonic Models

The finite bandwidth of signals transmitted over the real channels allows certain discrete representations of the channel that simplify the representation of received signals. The reader is referred to [2.1] for the most general development of canonic model representations for time-variant linear systems. We present here only two of the canonic models, the cascade differentiator (or just differentiator) model and the tapped delay line (or just delay line) model.

2.1.4.1 The Differentiator Model

The differentiator model is particularly effective in modeling the channel when the degree of frequency selectivity is small over the bandwidth of the input pulse, i.e., when the pulse bandwidth W moderately exceed W_{coh}, the coherent bandwidth of the medium. Since the period of the highest frequency variation in $T(f,t)$ vs. f is $W_{max} = 1/L_{tot}$, the cascade differentiator model is most useful when

$$\frac{W}{W_{max}} = WL_{tot} << 1 \tag{2.21}$$

where W is the bandwidth of the input signal. A cascade differentiator model is derived in [2.1] by representing $T(f,t)$ as its Taylor series expansion in f about f=0. The resulting expansion converges fastest when the time origin is chosen so that the delay occupancy region is centered at $\xi=0$. For simplicity, we assume that the spectrum of $z(t)$ is centered at f=0. The resulting input-output relationship is

$$w(t) = \sum_{n=0}^{\infty} T_n(t) \frac{d^n z(t)}{dt^n} \tag{2.22}$$

where the time-varying complex gain $T_n(t)$ is given by

$$T_n(t) = \frac{1}{n!} \int (-\xi)^n g(t,\xi)\, d\xi \qquad (2.23)$$

In practice, only a finite number of terms of the sum in (2.22) would be used to approximate w(t). A double power series model involving expansion of T(f,t) in f and t is discussed in [2.1] and used effectively in Section 4 to determine the effects of selective fading on an estimator.

Instead of using a finite number of terms in the Taylor series expansion of T(f,t) at f=0 to represent T(f,t) for $f < W/2$, one may use other approaches for generating polynomial approximations to T(f,t) for $f < W/2$. The general form of the input-output relationship will still be (2.22) although the $T_n(t)$ will no longer be given by (2.23). Figure 2.1 interprets (2.22) as a cascade of differentiators with complex time-varying gains applied after each stage of differentiation. The outputs of the multipliers are summed to form the output w(t).

For the stationary scatter channel model, the cross correlation between the complex gains (2.23) becomes

$$\overline{T_n^*(t)T_m(t)} = \frac{(-1)^{m+n}}{n!m!} \int \xi^{m+n} Q(\xi)\, d\xi \qquad (2.24)$$

In applying (2.24) to the quasi-stationary scatter channel model, the ensemble auto- and cross-correlation coefficients in (2.24) must be assumed slowly varying in time (and mildly dependent on carrier frequency). For the complex Gaussian channel, the complex functions $T_n(t)$ are complex Gaussian processes. Note that the statistics of the complex gains are completely determined from the delay power spectrum $Q(\xi)$.

When the degree of frequency selectivity is small, the first few terms in the series (2.23) is a good approximation to the output w(t). Use of the first three terms above in (2.23) produces a channel model called the quadratically-selective fading model [2.1] which should be adequate for computing signal degradation when the signal bandwidth begins to exceed the coherence bandwidth. For LOS links, using typical bandwidths for DCS links, the differentiator model should be quite good.

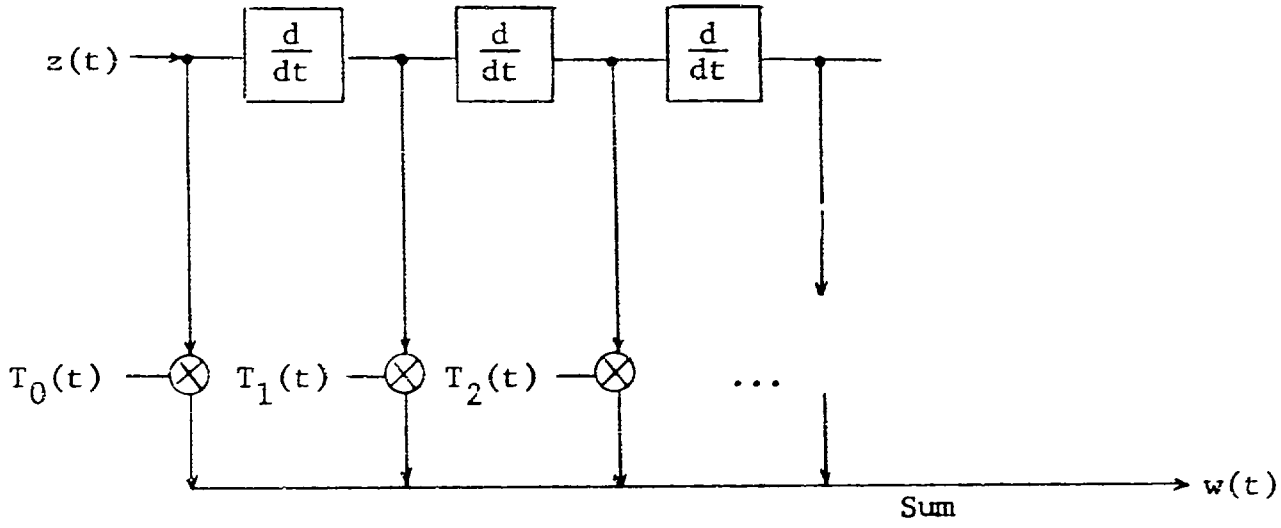

Figure 2.1 Cascade Differentiator Model

2.1.4.2 Delay Line Model

The second channel model is the one most commonly used both for analysis and the basis of channel simulation, the tapped delay line model. The derivation of this model is based upon the assumption, as in the differentiator model, that the spectrum of the input signal complex envelope $Z(f)$ is essentially confined to a finite bandwidth, say, $-W/2 < f < W/2$. Then the time-variant transfer function outside this interval clearly does not affect the output signal since only the product $Z(f)T(f,t)$ occurs in

$$w(t) = \int Z(f)T(f,t)e^{j2\pi ft}\, df \tag{2.25}$$

One may then replace $T(f,t)$ by a periodic function in f, $\hat{T}(f,t)$, which is identical to $T(f,t)$ within $-\hat{W}/2 < f < \hat{W}/2$, where $\hat{W} > W$, without changing the output complex envelope $w(t)$. However, since this modified time-variant transfer function is periodic, it has a Fourier series expansion and its Fourier transform on the frequency variable, $g(t,\xi)$, has the discrete representation

$$g(t,\xi) = \sum_{-\infty}^{\infty} g_k(t)\delta(\xi - K/\hat{W}) \tag{2.26}$$

where $g_k(t)$ are the (time-variable) Fourier coefficients in the expansion of $\hat{T}(f,t)$. In [2.1], $\hat{W}$ was chosen equal to W which leads to the two equivalent expressions for the kth tap complex gain

$$g_k(t) = \int \text{sinc}\,[W(\xi - k/W)]g(t,\xi)\, d\xi \tag{2.27}$$

$$g_k(t) = \frac{1}{W}\int_{-W/2}^{W/2} T(f,t)e^{j2\pi kf/W}\, df \tag{2.28}$$

where

$$\text{sinc}\, W\xi = \frac{\sin \pi W\xi}{\pi W\xi} \tag{2.29}$$

Equation (2.26) leads to the input-output representation

$$w(t) = \sum_{-\infty}^{\infty} g_k(t)z(t - k/\hat{W}) \tag{2.30}$$

which, as shown in Fig. 2.2, is identical to the output of a uniformly tapped delay line with taps spaced $1/\hat{W}$ seconds apart and with time variable complex tap "gain" $g_k(t)$ applied to the

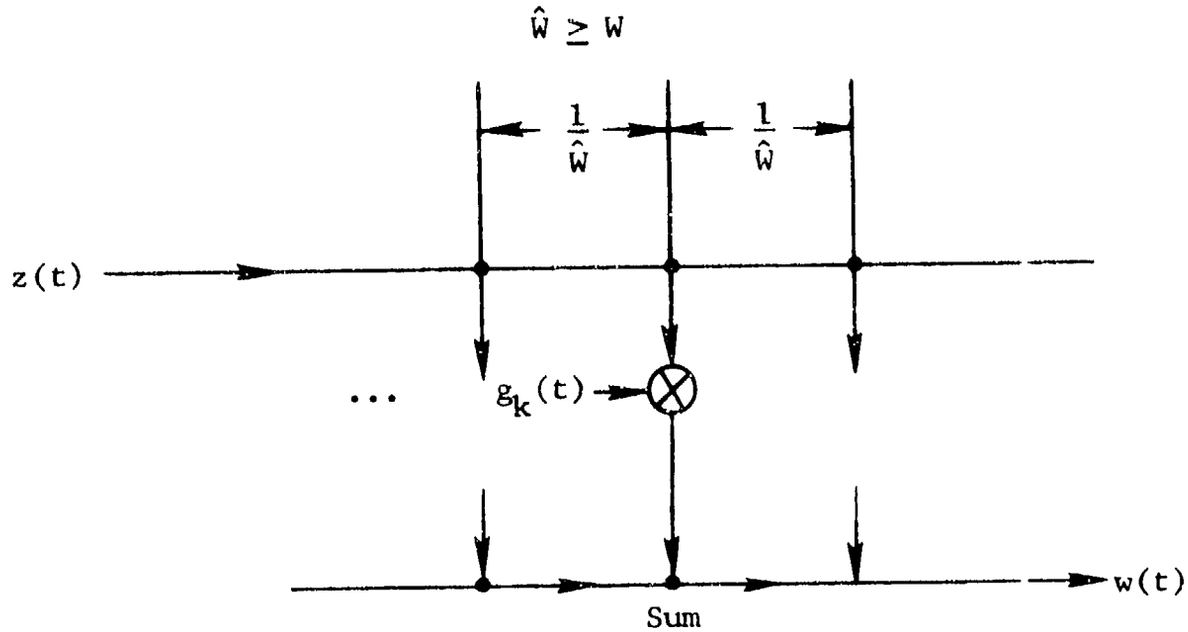

Figure 2.2 Tapped Delay Line Model

tap providing delay $k/\hat{W}$. Strictly speaking, the number of taps is infinite; however, practically speaking, an adequate approximation may be achieved with a finite number. From (2.27) we see that for $\hat{W} = W$, the k^{th} tap gain is given by samples at delays $1/W$ apart of the convolution on the delay variable ξ of the impulse response with the function $\text{sinc}[W\xi]$. The width of the former is L_{tot}. The width of the latter is infinite, strictly speaking. However, one may choose a value of α such that for $|\xi| > \alpha/W$, $\text{sinc}\, W\xi$ will be as small as desired. Because $\text{sinc}[W\xi]$ decreases so slowly with ξ, α can be a large number for any reasonable definition of width. The convolution of $\text{sinc}\, W\xi$ and $g(t,\xi)$ will be effectively nonzero for values of ξ in an interval of duration $L_{tot} + \alpha/W$. Since the taps are spaced $1/W$ apart, the number of taps needed is

$$N_W = W L_{tot} + \alpha \tag{2.31}$$

For a stationary scatter channel, it is readily found that the cross-correlation coefficients between the complex tap gains is given by

$$\overline{g_k^*(t) g_\ell(t)} = \int \text{sinc}\, W(\xi - k/W)\ \text{sinc}\, W(\xi - \ell/W)\ Q(\xi)\, d\xi \tag{2.32}$$

Note that these correlation coefficients can be determined once the delay power spectrum is specified. When $Q(\xi)$ varies little in a delay interval $1/W$, we see from (2.32) that

$$\overline{g_k^*(t) g_\ell(t)} \approx \begin{cases} Q(k/W) & ; \quad k = \ell \\ 0 & ; \quad k \neq \ell \end{cases} \tag{2.33}$$

i.e., the taps become uncorrelated with strengths proportional to samples of the delay power spectrum.

In the case of the complex Gaussian quasi-stationary scatter channel, the $\{g_k\}$ would be complex Gaussian with slowly varying strengths and correlation coefficients dependent upon the time variation of $Q(\xi)$.

2.2 Specific Channel Characteristics

The preceding section has provided a framework within which the characteristics of specific links of interest may be discussed. We consider, in order, troposcatter, LOS microwave radio relay, HF, and satellite links. For each case we present a brief discussion of the basic radio propagation phenomena, ranges of system parameters (e.g., path length, power, etc.), channel characteristics vs. system/propagation parameters, and modem techniques with error performance peculiarities appropriate to the link.

2.2.1 Troposcatter Links

The physical basis for communication beyond the horizon at UHF frequencies is reflection and scattering from inhomogeneities in the refractive index structure of the lower atmosphere (troposphere). Since the refractive index at any point in space is a function of temperature, pressure, and humidity, meteorological conditions have a direct influence on troposcatter propagation.

For sizable fractions of an hour the quasi-stationary complex Gaussian WSSUS channel model appears to be a good approximation and simulators designed on this basis have been found useful in system design.

Figure 2.3 indicates the geometry associated with a troposcatter link. The antenna beams are aligned along a great circle path. The intersection of the antenna beams, called the common volume, limits the region from which scattering takes place. If the common volume is broken up into small elemental volumes and the scattering cross section of each volume is specified as a function of spatial position, one may compute the delay power spectrum $Q(\xi)$ by summing up the power returned from all elemental volumes yielding the same path delay. This elemental volume is a thin ellipsoidal shell as indicated in Fig. 2.3. Such calculations of $Q(\xi)$ have been presented by Bello [2.4].

Movement of the scattering and reflecting elements within the common volume will cause Doppler spreading. For example, moving scatterers approaching the center of the common volume

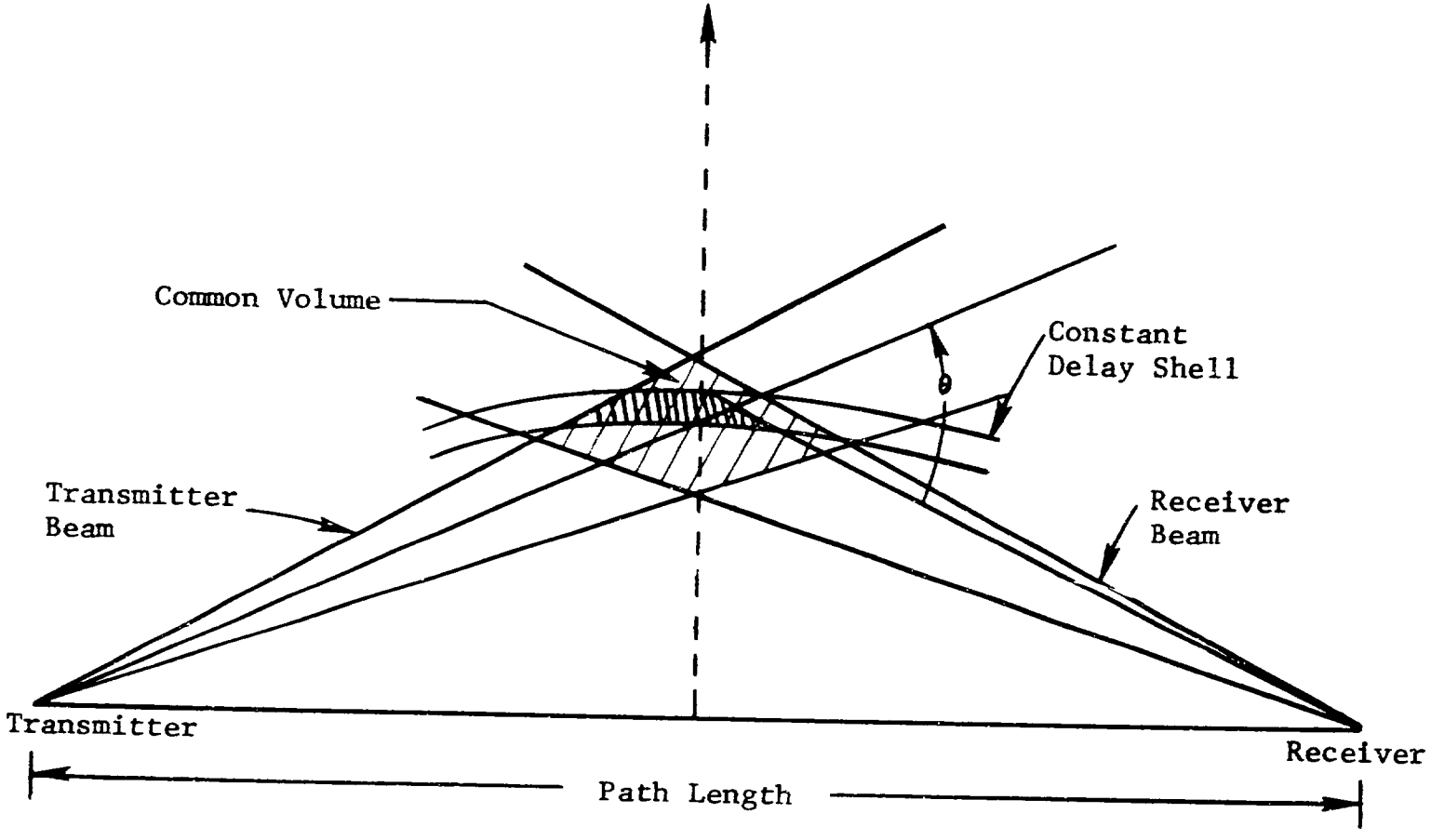

Figure 2.3 Troposcatter Link Geometry

produce a positive Doppler shift which decreases to zero as the center is reached and becomes negative as the scattering element recedes from the center of the common volume. Since there are scattering elements throughout the common volume a range of Doppler shifts or a Doppler spread, is produced.

The scattering cross section per unit volume and thus the power received is a rapidly decreasing function of the scattering angle θ (Fig. 2.3) which is the angle between the ray from transmitter to scattering volume and the ray from scattering volume to receiver.

Changes in the mean refractive index with height influence the pointing of the antenna beams. Such bending of the beams may be calculated with the aid of ray tracing techniques. From the geometry of Fig. 2.3 we see that the common volume will increase or decrease in size as the beams bend upward or downward. As a result there is a tendency for path loss, multipath spread, and Doppler spread to increase or decrease together as gross changes in the mean refractive index gradient occur with atmospheric conditions.

For a given link the Doppler spread can vary over an order of magnitude or more, due to variations in wind speed and propagation mechanisms within common volume. For a given beamwidth, the fading rate will generally increase with carrier frequency. For a 1 GHz carrier frequency and a typical set of link parameters, rms Doppler spreads varying from .1 - 2 Hz may be expected while an increase in operating frequency to 10 GHz will result in an approximate tenfold increase in this range of Doppler spreads.

There are very few measurements of multipath spread. From what has been measured, variations in multipath spread appear to be less severe* varying over a range of around 3 to 1. For path lengths and parameters of interest the predicted average rms multipath spread can vary from a very small fraction of a microsecond for the shorter paths to a substantial fraction of a microsecond at the longer paths (350 miles).

---

*An abnormal condition known as ducting occurs when there is a sufficiently strong negative gradient of mean refractive index. In such a case a guided mode of propagation exists, Doppler and multipath spread become very small and the received signal becomes very strong. We exclude this mode from our general discussions.

Path losses are high for troposcatter communications and hourly median path loss fluctuations can easily vary by 30 dB or more over a year. Thus, an attempt is made to provide sufficient power at the higher path losses, to obtain some minimum average SNR, say, 20 dB, resulting in large swings in hourly median SNR during a year.

Large transmitter powers (10 kw for the average link) large antennas (.0 ft. diameter dish for the average link), and diversity reception (four h-order typically for strategic links) are required. To obtain the required large average powers essentially cw operation is required. The only form of diversity used extensively is space-diversity. Multi-channel radio telephony is carried out by FDM/FM (frequency division multiplex and frequency modulation). Typically 60 analog voice channels may be carried by a troposcatter link. Presently, data transmission takes place through a voice channel slot or for higher data rates, a whole group (12 channels). This procedure is an inefficient mode of data transmission both from the utilization of bandwidth and power, and consideration has been given by DOD to more efficient means of high speed data transmission.

Except for the GRC-143 built by ITT, only experimental models of high speed TDM modems have been built. These modems may be classified according to whether the signaling pulses have been designed to suffer small distortion from the channel or not. Modems in the former class, with one exception, have been around 1 Mbs and use incoherent detection techniques. The measured and modeled performance of a few of these modems is presented in [2.5]. The exception is a 3 Mbs coherent FSK/PSK modem [2.6]. This modem uses synchronized time gates to eliminate portions of received pulses contaminated by intersymbol interference. After the time gates a maximum likelihood (i.e., minimum probability of error) demodulator is constructed. The 3 Mbs is achieved by transmitting a one μsec pulse having one of four frequencies and one of two phases. Time gates of 1/2 μsec duration are used provided protection against 1/2 μsec of multipath.

Subsequent to the development of the FSK/PSK modem new techniques have been proposed which use pulses that can be highly distorted by the propagation medium. The object of these systems is to obtain a performance close to that achievable by a matched filter system where the receiver is matched to the received distorted pulse and intersymbol interference has been

made negligible. Thus if a particular received pulse is $w_\ell(t)$, for the ℓth diversity channel, the error rate of such a system at the time of reception would depend upon an energy/bit to noise power density ratio of*

$$E_b/N_0 \sim \sum_{\ell=1}^{L} \int |w_\ell(t)|^2 \, dt \tag{2.34}$$

Assuming the troposcatter channel can be modeled by a tapped delay line with K independently fading paths one may show* that approximately

$$\int |w_\ell(t)|^2 \, dt \sim \sum_{k=1}^{K} |g_k^{(\ell)}|^2 \tag{2.35}$$

where $g_k^{(\ell)}$ is the value of the kth complex gain in the tapped delay line model of the ℓth diversity channel at the time of reception. Because the $\{g_k^{(\ell)}\}$ are fluctuating independently the matched filter output has the same mathematical properties as the output of a maximal ratio diversity combiner with K paths. Such diversity has gone by several names: in-band, inherent, multipath, and implicit diversity. We shall use the terminology in-band.

There are three modem techniques suggested for achieving this in-band diversity, one of which has been built and one is in development. The one which has been conceived and built by Raytheon involves the transmission of 4 PSK pulses at a duty cycle of 50% resulting in a 3 dB power loss at the transmitter. The receiver attempts to set up a filter matched to the transmitted pulse shape and thus achieve the benefits of in-band diversity.

The one presently under development by Sylvania utilizes 4 PSK transmission 100% duty cycle with an adaptive nonlinear equalizer. Data rates up to 12.6 Mbps are to be achieved. Some simulations [2.7] have indicated that this equalizer under some ideal conditions can yield a performance close to the inter-symbol interference free matched filter receiver.

---

*This point is discussed in detail in Section 5.6.

The third approach is the maximum likelihood receiver which provides the minimum error probability and thus is superior to the nonlinear equalizer.

Assuming that one or more of these can extract the in-band diversity, it is clear that the performance of the modem will vary with the multipath spread since the number of independent paths is approximately $K = WL$ where W is the bandwidth occupied and L is the multipath spread of the channel. For sufficiently small multipath spread the in-band diversity will disappear. The demodulator would be designed to handle some maximum multipath spread as determined from measurements or theoretical predictions. For multipath spreads exceeding the design value intersymbol interference will appear causing an "irreducible" error probability.

Another form of in-band diversity, which we shall call time diversity, can be achieved on troposcatter links for any modem by use of coding techniques. This class of techniques has been studied by CNR [2.8] and CNR is currently under contract [2.9] to implement and field test such techniques. The basic concept is one of interleaving bits or blocks of bits to have the coding constraints spread over a time interval encompassing several fades. This technique will improve in performance as the Doppler spread increases but will show no benefit if the Doppler spread becomes too small.

The advanced modems all use some form of channel measurement. If the Doppler spreads become too large the channel measurements will degrade primarily because of fixed processing delays in the system. Thus the phase corrections required in coherent processing will lag, causing an uncorrelated component of output to appear. This component acts like an effective additive noise and will result in an irreducible error probability.

Given a properly designed system, excessive multipath and Doppler spread that cause an irreducible error probability to dominate performance should be a rare event. However, even in the usual case where performance is limited by additive noise, it should be clear that for the in-band and time diversity systems the error rate will be determined by the amount of multipath and Doppler spread since these parameters determine the degree of in-band and time diversity.

2.2.2 LOS Microwave Relay Links

Unlike the troposcatter link, which is always a fading dispersive channel, the LOS microwave link acts as a fading dispersive channel only a fraction of the time. For a well designed over-land link the primary source of multipath fading is the existence of certain meteorological conditions which cause a sharp negative gradient in refractive index. The most common meteorological condition producing such negative gradients are temperature inversions which occur in the evening due to rapid cooling of the earth's surface from radiation and wind convection.

Analysis of propagation through a layer of sharp negative refractive index gradient based upon geometric optics reveals the existence of several ray paths from transmitter to receiver. Thus the impulse response of such a link corresponds to a discrete multipath model in contrast to the troposcatter link where a continuum of differential paths exist. While small phase fluctuations occur on these paths due to atmospheric turbulence, the major source of phase fluctuations of the paths is due to the movement of the layer which causes a time-variant change in the group delay of each multipath component. The relative amplitudes of each path show much less variation than the relative phases with layer movement.

The most recent calculations of multipath spread as a function of link parameters have been carried out by CNR [2.10] for RADC. These calculations generally agree with the limited amount of measurements available, predicting multipath spreads of up to a few nanoseconds. The rates of fading are extremely slow with characteristic time constants measured in minutes.

Under normal nonfading conditions the received SNR's are very large, e.g., 60 dB in a 14 MHz bandwidth with only 5 watts transmitter power. Thus only at the bottom of very deep (>40 dB) fades will the SNR become small enough to produce poor performance. However at the high data rates of interest, 12.6×2^n Mbs, this would involve degradation of a considerable block of data since such deep fades can last several seconds. Dual space diversity, usually with selection combining, is used to alleviate the fading problem.

Because the outages occur only during deep fades and because such fades occur very slowly by comparison to the data rates of interest, the appropriate media quality estimate of error rate performance should occur on an "instantaneous" or "frozen channel"

basis. Averages over fading conditions do not appear meaningful for LOS channels. The achievable error rate performance of the LOS digital modem should be predicted on an instant-by-instant basis particularly during the deep fades. Estimation of error rates during deep fades requires a channel model conditioned on the existence of a fade. While the multipath spread is small and one would normally expect little frequency selective fading over a typical DCS 14 MHz bandwidth, the degree of frequency selectivity has been found to be greatly enhanced during deep fades [2.10]. In [2.10], the effect of frequency-selective fading on signal distortion was analyzed using a power series channel model. An approximate calculation showed that small distortion required the satisfaction of the inequality

$$\frac{\pi}{\sqrt{2}} \nu_{max} \frac{L}{\alpha} \ll 1 \tag{2.36}$$

where ν_{max} is the peak frequency deviation of the transmitted signal (assumed constant envelope), L is the rms multipath spread, and α is the fade depth relative to average signal strength in the absence of fading. Large distortion is defined by the equality

$$\frac{\pi}{\sqrt{2}} \nu_{max} \frac{L}{\alpha} = 1 \tag{2.37}$$

Note that the rms multipath spread and the fade level α occur as the ratio L/α so that the deeper the fading, the smaller the tolerable multipath spread for a given level of signal distortion. To choose a typical example, assume an rms multipath spread of L=2 nanoseconds, ν_{max} = 5 MHz. Then it is found that intolerable distortion occurs at a level of α corresponding to a 33 dB fade, or lower. An rms multipath spread of 1 nanosecond corresponds to excessive distortion occurring at a 39 dB fade, or lower. Alternatively, one may say that the rms multipath spread must be much less than 2 and 1 nanosecond to cause negligible distortion at a 33 and 39 dB fade, respectively.

Frequency-division-multiplex (FDM) followed by frequency modulation (FM) has been used universally for voice transmission on military links. Data transmission at the present time would have to take place either by using channels prior to the FDM or else by by-passing the FDM and placing high speed baseband data into the frequency modulator. The latter technique was investigated recently [2.30] by the Defense Communication Agency. A 12.6 Mbps three-level partial-response digital baseband signal was used with frequency deviation adjusted to make the radiated

signal occupy a 99% power bandwidth of 14 MHz. Research and development work is contemplated by the USAF to produce experimental models of LOS modems which can achieve data rates at multiples of the 99% bandwidth occupancy. CNR, Inc. recently completed a study [2.10] involved with devising and evaluating such techniques for DCS links.

No consideration has been given yet to counteracting the affects of frequency selective fading with modem design, so that, as a minimum, channel quality monitoring should provide knowledge of the presence of excessive frequency selective fading. For the more typical case of flat fading an essentially continuous estimate of error rate should be sufficient.

2.2.3 HF Links

The nominal frequency range quoted for HF communications is 3 to 30 MHz. Long distance communication takes place in this frequency range via the mechanism of continuous refractive bending of the transmitted wave as it passes obliquely through ionized regions in the upper atmosphere.

The earth is surrounded by ionized regions which are approximately arranged in layers at different heights and with different approximate thicknesses. These heights and thicknesses are dependent mostly on ultraviolet and soft x-ray solar radiation and thus the pattern of their distribution and degree of ionization change daily, seasonally, and in response to the eleven-year sunspot cycle. The layer of most importance to long range communication is the F_2 layer which is the most highly ionized and highly variable layer located from 240 - 400 km height. The lowest layer, D, located from 60 - 80 km is responsible for most of the absorption of transmitted electromagnetic energy by the ionosphere. In addition to these layers unusual regions of high ionization occur near the polar caps where auroras exists.

The refractive index of an ionospheric layer is less than unity, decreases as the electron density increases, and increases as the transmission frequency increases. This causes an electromagnetic wave leaving the earth at some take-off angle (angle with respect to horizontal) to be continually refracted towards the earth as it traverses regions of continually lower refractive index (higher electron density). If the refractive index drops low enough the wave will return to the earth, providing the mechanism for HF communications. As pointed out, the refractive

index increases with increasing frequency. If the frequency of the transmitted wave is too high, the refractive index will be prevented from dropping to a sufficiently low value to allow the wave to return to earth. This maximum critical frequency of return is a function of take-off angle, decreasing as the take-off angle increases. The frequency above which waves are not refracted back to earth for a particular HF link is called the MUF (maximum usable frequency) of that link.

The following types of ray paths are discussed repeatedly in HF propagation,

1) High-angle and low-angle rays
2) Ordinary and extra-ordinary rays.

For a given path length and ionospheric layer and operation below the MUF it may be shown that two ray paths with different take-off angles exist connecting the transmitter and receiver. The lower ray path is called the low-angle ray and the upper ray path is called the high-angle or Pederson ray. When the operating frequency approaches the MUF the high and low angle rays merge. Above the MUF (assuming a single layer) no ray path exists at the given path length. The path length for which the operating frequency is the MUF is called the "skip" distance. At path lengths smaller than this no communication is possible by refraction from the layer at the same operating frequency.

The magnetic field of the earth introduces anisotropy into the ionosphere which causes each ray path to split into two magneto-ionic paths called the ordinary and extra-ordinary rays. Thus in general it is possible for a layer to have four ray paths connecting transmitter and receiver, i.e., ordinary and extra-ordinary, upper and lower rays. The two magneto-ionic waves corresponding to a transmitted linearly polarized wave have oppositely rotating circular polarization. Ionospheric absorption will cause the amplitudes of the magneto-ionic components to differ, producing elliptical polarization. In addition changes in the ionosphere will affect the magneto-ionic components differently causing the axis of the polarization ellipse to change, producing fading in a linearly polarized receiving antenna.

A lower limit on useful transmission frequency, called LUF, also exists due to D layer absorption and atmospheric noise, both of which increase as frequency is reduced. Both the MUF and LUF vary hourly in a more or less systematic way, sometimes requiring more than one change of operating frequency during the day to maintain adequate quality of communication.

Because of the large wavelengths at HF, narrow beam widths require large physical structures and are not economical. Thus at HF most transmitting antennas transmit rays at many different take-off angles (20^{o} - 30^{o} beamwidth typically) and receiving antennas correspondingly will receive waves coming in at a range of angles. This fact, coupled with the possible existence of several refracting layers and multiple reflections between layers and ground, produce a number of simultaneous paths between transmitter and receiver having different time delays. Moreover, under the influence of the sun, the intensity of ionization of these layers changes with time causing the electrical lengths of these paths to be time-variant and producing fading in the combined signal at the receiver. By operating close to the MUF it is possible to prevent many paths from reaching the receiver. However, since the MUF varies with time and not in an entirely predictable way, there is the danger that the transmission frequency may exceed the MUF for some period, causing complete interruption of communications.

The multipath spread varies with path distance, operating frequency, time of day, season, and sunspot number. R.K. Salaman [2.11] has derived (from both ray-path theory and experiments) a family of curves that allow one to estimate the multipath spread as a function of operating frequency (relative to the MUF) and path length. All paths which are 30 dB smaller than the strongest path are neglected in the calculation and he claims to have included the variations due to time of day and season (no mention is made of sunspot numbers). From Salaman's curves it may be seen that at a path length of 2000 kilometers and an operating frequency of .83 MUF, the multipath spread will be .5 ms. The maximum multipath spread of approximately 3.5 ms occurs at around .42 MUF for a path length of 2000 Km. For path lengths exceeding 600 km the multipath spread is less than 6 ms.

The dual of Salaman's curves have not been obtained for Doppler spread although a start has been made by Pickering [2.12]. Reported fading rates show sharp differences between transauroral paths and others, the former usually being an order of magnitude higher.

It may be of interest to examine Fig. 2.4 which presents one of the only probability distributions of measured rms Doppler spread that we have been able to find. This was undertaken by Stanford Research Institute for the U.S. Army as part of an experimental research program on HF channels. Power spectra were derived from measurements [2.13] made on a mid-latitude 4100 km path and a 5050 km transauroral path at 7.366 Mcs for four months (February, March, June, November 1964). They noted that the Doppler spread in June was around twice that of the other months. Most of this increased spread was attributed to the existence of many more propagation modes in that month due to the greater level of ionization remaining in the F region during the night in June. In particular for the other three months 7.366 was near the MUF while in June it was not. The multipath spread increases as the operating frequency becomes a smaller fraction of the MUF. Evidently the Doppler spread increases also. Figure 2.5 presents measured rms Doppler spread as a function of ionogram-measured time-spread for the mid-latitude path. A definite trend is exhibited. For wild guesses (these seem to be the only ones available) one may use multipath spread from Salaman's curves and the straight line trend of Fig. 2.5 to predict Doppler spread. From this trend one might estimate an rms spread in Hz equal to the rms multipath spread in ms.

The complex Gaussian model has been found useful in modeling the amplitude and phase fluctuations of received carriers. Measurements of the amplitude distributions of individual paths do not always show the Rayleigh distribution characteristic of zero-mean complex Gaussian fluctuations but rather the Ricean distribution characteristic of non-zero-mean complex Gaussian fluctuations [2.14].

Three types of noise are of importance on HF links, atmospheric noise, man-made noise, and cosmic (or galactic) noise.

Cosmic noise has the characteristics of thermal noise, i.e., Gaussian noise essentially flat over a receiver bandwidth. However since it traverses the ionosphere it may be subjected to fading by the ionosphere. From the point of view of worst case performance calculations it appears sufficient to model cosmic noise as white Gaussian noise.

The term "atmospheric noise" has been employed with somewhat different meanings in the literature depending upon the point in the receiver at which it is measured. However, no

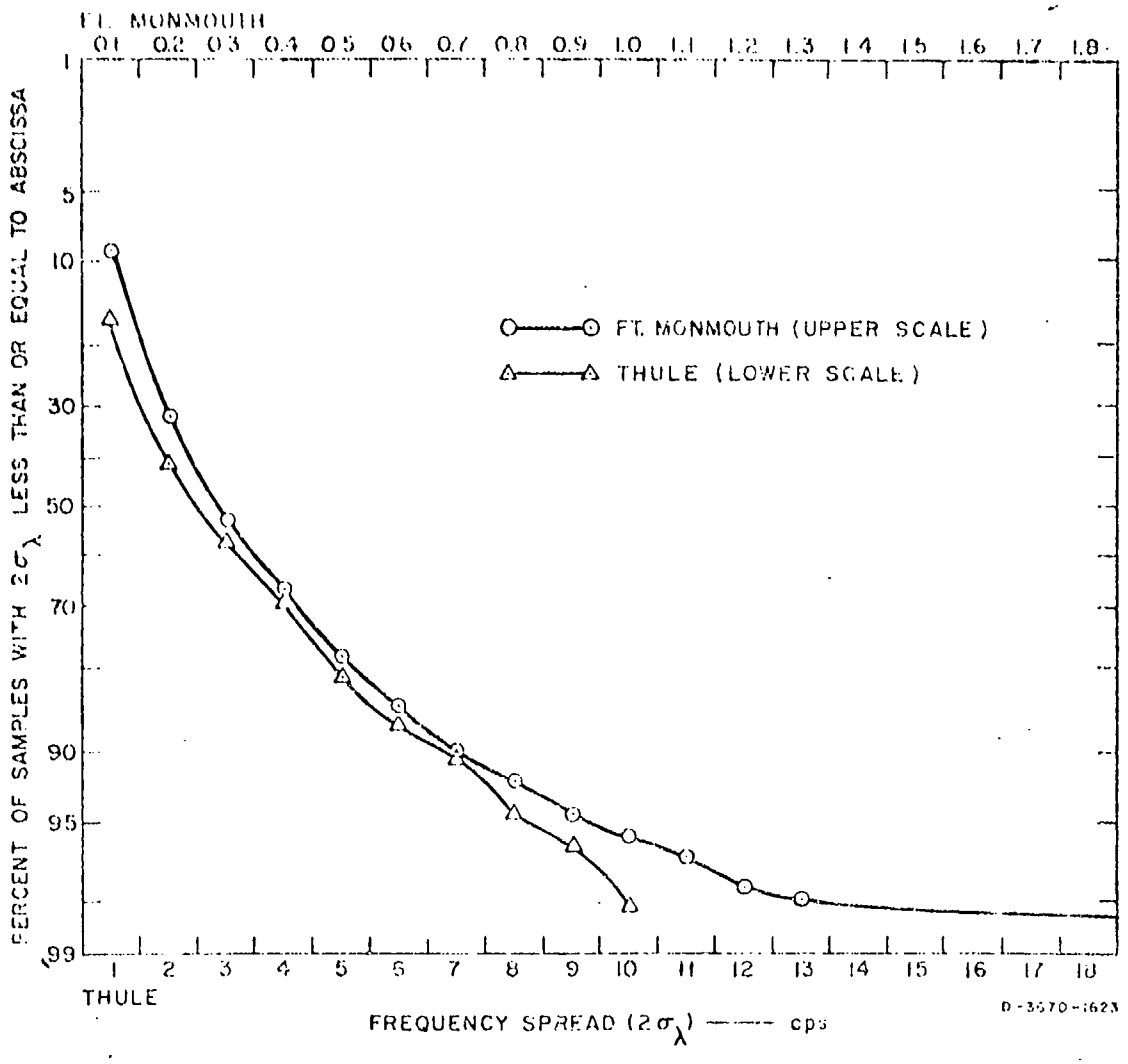

Figure 2.4 Distributions of Fort Monmouth—and Thule-to-Palo Alto Path Frequency Spread on Normal Probability Scale

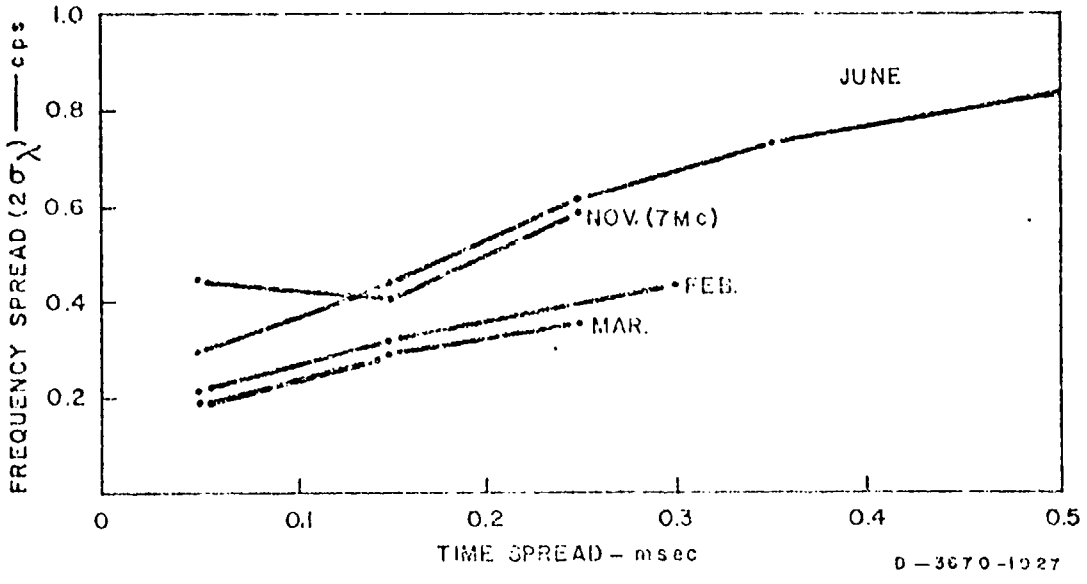

Figure 2.5 Frequency Spread as a Function of Ionogram-Measured Time Spread—Fort Monmouth-to-Palo Alto Path

ambiguity exists as to the source of atmospheric noise, namely lightning discharges. These discharges occur randomly in time and geographical location and propagate over long distance via ionospheric reflection. The collective nature of these discharges is such as to produce random pulses of electromagnetic field at a given receiving antenna. These pulses are of the "low pass" type, i.e., their perceptible spectrum extends from very low frequencies up to around 30 Mc/s. Thus it is not meaningful to talk about either the phase or envelope of the received atmospheric voltage in a hypothetical infinite bandwidth receiving antenna. However, antenna bandwidths are finite, and, more to the point, the filters used to detect HF digital signals are narrow band filters centered in the HF band. Thus in determining error rates for digital systems used over the HF ionospheric medium, one must deal with an interfering noise at the detector output which is the result of exciting a narrow band filter with randomly occurring "low pass" pulses having random amplitudes and shapes.

Measurements of atmospheric noise have dealt almost exclusively with the envelope at the output of a narrow band filter. An extensive series of such measurements carried out on a worldwide basis and over a wide frequency range has been accomplished by the National Bureau of Standards [2.15]. These measurements include both noise power and probability distributions. Although measurements were performed for a 200 c/s bandwidth, correction curves are given to allow conversion of the results to other bandwidths. It has been found [2.15] that the probability distribution of the envelope is close to the Rayleigh distribution only for the small-noise high-probability levels. However, in the high-level low-probability region there is marked departure from Rayleigh, the measured distribution having a much longer "tail." Such a distribution might have been expected apriori, the small noise levels being caused by the overlapping of a large number of low level atmospheric discharges and the large noise levels by much fewer distinct atmospheric "spikes" extending above the ambient noise level.

It has been found [2.16], [2.17] that the peak values of the large atmospheric noise spikes have a probability distribution which conforms rather well with the log-normal distribution. This fact, no doubt, is the reason why the tail of the log-normal distribution fits closely with the tail of the measured envelope probability distributions, as pointed out in [2.18].

For signal-to-noise ratios of practical interest it is primarily the spikes of noise that cause errors and thus it is primarily the tail of the noise probability distribution that is of interest. Consequently, as far as error rate computation is concerned, it appears reasonable to assume that the envelope detected noise distribution in the receivers to be analyzed can be approximated by a log-normal distribution, which has the same "tail" as the true measured probability distribution. Unfortunately, for an arbitrary receiver to be analyzed, the narrow band filters do not necessarily have the same transfer function or bandwidth as the 200 c/s filter used for noise measurements by NBS. Although NBS gives curves which allow one to take account of a change in bandwidth on the envelope probability distribution, no curves are given to allow one to determine the effect of a change in filter shape. It is necessary to make the assumption that the NBS envelope distribution curves apply to arbitrary receiver filters for lack of the correct measured distributions. However, this assumption is not likely to make final answers less useful for performance prediction than if the correct measured distributions were available since the random variations of measured distributions at a given geographic location and in a given time block will probably introduce sufficient unavoidable prediction error to obscure the foregoing approximation error.

The wide number of different sources for man-made noise and interference make it unlikely that any simple probability distribution will be meaningful. Thus in evaluating the effects of man-made noise a wide variety of possible distributions should be considered, ranging from Gaussian noise to impulse noise and including interfering communication signals.

The transmission of high speed, highly reliable digital data in a voice bandwidth is difficult because of the multipath spread (up to a few milliseconds), Doppler spread (up to a few Hz), and ambient noise and interference of HF links. Also the variability of propagation conditions require frequent changes of operating frequency to optimize transmission and, sometimes, ionospheric storms may interrupt communications. Despite these difficulties, and in the face of satellite communications, HF communications still has military significance.

Essentially linear power amplifiers are available at HF frequencies which can transmit the required average powers with signals whose peak-to-average power ratios approach those of Gaussian noise. To conserve bandwidth single-sideband transmission is used. High speed data transmission would normally take place by transmitting the data signal through a 3 kc channel usually reserved for voice. Dual frequency diversity is employed sometimes by using an adajcent 3 kc slot. A typical data rate for high speed transmission is 2400 bits/sec., implemented with subcarriers uniformly spaced in frequency with each subcarrier carrying a low data rate stream employing some form of differential phase shift keying. The parallel transmission format is necessary because of the large degree of frequency selective fading present in the 3 kc bandwidth. The low bandwidth occupancy of each subcarrier data pulse greatly minimizes frequency selective distortion. The differential-phase format is chosen over coherent phase-shift keying because the increased averaging time necessary to extract a phase reference in the latter case increases the irreducible error rate due to fast fading.

The development of advanced modem techniques have been supported by the Navy based upon the CODEM work of Chase [2.19]. These have allowed simultaneously a doubling of the data rate to 4800 bits/sec. and a reduction of the error rate as compared to conventional modems. Adaptive equalizer concepts were proposed for the HF channel [2.20] but after implementation did not perform well. Although indications are that the fading time constant is not long enough in comparison to the impulse response duration to prevent significant error from occurring in adaptive equalizer systems, the utility of adaptive channel measurement techniques for HF channels is still an open question.

The most viable approach presently available is that of Chase, referenced above. A code is employed across the data bits of all the subcarriers in the same time slot. Through use of the channel measurement decoding algorithms of Chase [2.21] a near maximum likelihood demodulation is achieved, allowing the attainment of in-band diversity. Time gates are used extensively on advanced HF modems for the elimination of intersymbol interference and crosstalk caused by multipath.

If the Doppler spread gets too large an irreducible error probability will occur in the advanced modems, all of which employ differential phase shift keying. Too small an amount of multipath spread will not allow much in-band diversity to be achieved, as in troposcatter links. Too much multipath will eventually degrade performance because the time guard bands provide a fixed amount of multipath protection.

2.2.4 Satellite Links

Normally satellite links provide reliable communications. Assuming elevation angles of the LOS link from transmitter to satellite exceeding 8^{o} the only serious propagation problem experienced is "ionospheric scintillation". For lower elevation angles, refractive anomalies in the lower atmosphere can cause problems as in LOS links. Also, if the beamwidth is wide enough surface reflection and scatter multipath can occur [2.31]. For military links we assume that a well-designed system will not suffer from the latter two propagation problems.

The words "ionospheric scintillation" refer, generally, to the phenomenon whereby the amplitude and phase of a radio signal change in a random manner after passage through the ionospheric transmission medium. The occassional fading of transionospheric signals is now known to be caused by the same phenomena earlier associated with the fluctuations in the reception of signals from radio stars; random electron density irregularities in the ionosphere, arising primarily in the F-layer of the ionosphere at a mean height of about 250 kilometers, scatter radio waves incident on them and produce interference effects through phase mixing. Due to an internal reconfiguration of the electron density irregularities and a slow east-west drift, the amplitude of a received signal can be observed to fade in time after transmission through the ionosphere. Unfortunately little data are available on the statistics of fade rate. Koster [2.22] made crude fade rate estimates for six months of the data obtained during his 1967 - 1968 observations and his results indicate an average fade rate of six per minute during the peak evening hours. Time correlation functions of VHF fading presented by Pomalaza, et al., [2.23] show correlation times ranging from one second to 4 seconds. These temporal changes in signal strength occur due to a west to east drift of ionospheric irregularities at a velocity of approximately 100 meters/second. Values of Doppler spread can be estimated from the time autocorrelation function $\rho(\tau)$ by using a Taylor's expansion and retaining terms to second order. Using the Pomalaza data it is found that a typical value for the rms Doppler spread, B, is given by

$B = 0.2$ Hz

This applies to a fixed line of sight. A moving line of sight increases the fading rate. Values up to 7.2 Hz have been observed [2.24, p. 15] for a low orbiting satellite at VHF.

Amplitude fluctuation of received signals are usually categorized in recent work according to the scintillation index, S_4, which is essentially just the standard deviation of the received power normalized to the mean received power. This parameter can be related to the specular-to-scatter power ratio, γ, which characterizes the fluctuations under the assumption of Ricean fading. The relation is given by

$$\gamma = \frac{(1 - S_4^2)^{1/2}}{1 - (1 - S_4^2)^{1/2}} \tag{2.38}$$

Once thought to be just an approximation [2.25], this relation has been shown to be exact [2.26]. Note, when $S_4=1$, that $\gamma=0$ and the fading becomes Rayleigh.

Other indices have been found useful, especially for experimental purposes. One such is

$$S.I.(\%) = \frac{P_{max} - P_{min}}{P_{max} + P_{min}} \times 100 \tag{2.39}$$

Cumulative distribution of signal amplitude measurements made using this index are illustrated in Fig. 2.6 (in decibels). Some idea of fade depths can be gained from this figure which is taken from ATS-3 data at 136 MHz [2.27].

Questions relating to the statistics of amplitude fluctuations still remain generally unresolved. Fremouw and Rino [2.28] argue for utilizing a general (non-equal means, non-equal variances) joing Gaussian distribution for the in-phase and quadrature components, and their calculations do indeed seem to indicate that the variances, σ_x^2 and σ_y^2 of the two components can be markedly unequal. Their predictions await experimental verification, however, and current engineering practice is to use the Ricean distribution. In many situations of importance, i.e., high scintillation conditions, the fading takes on more of a

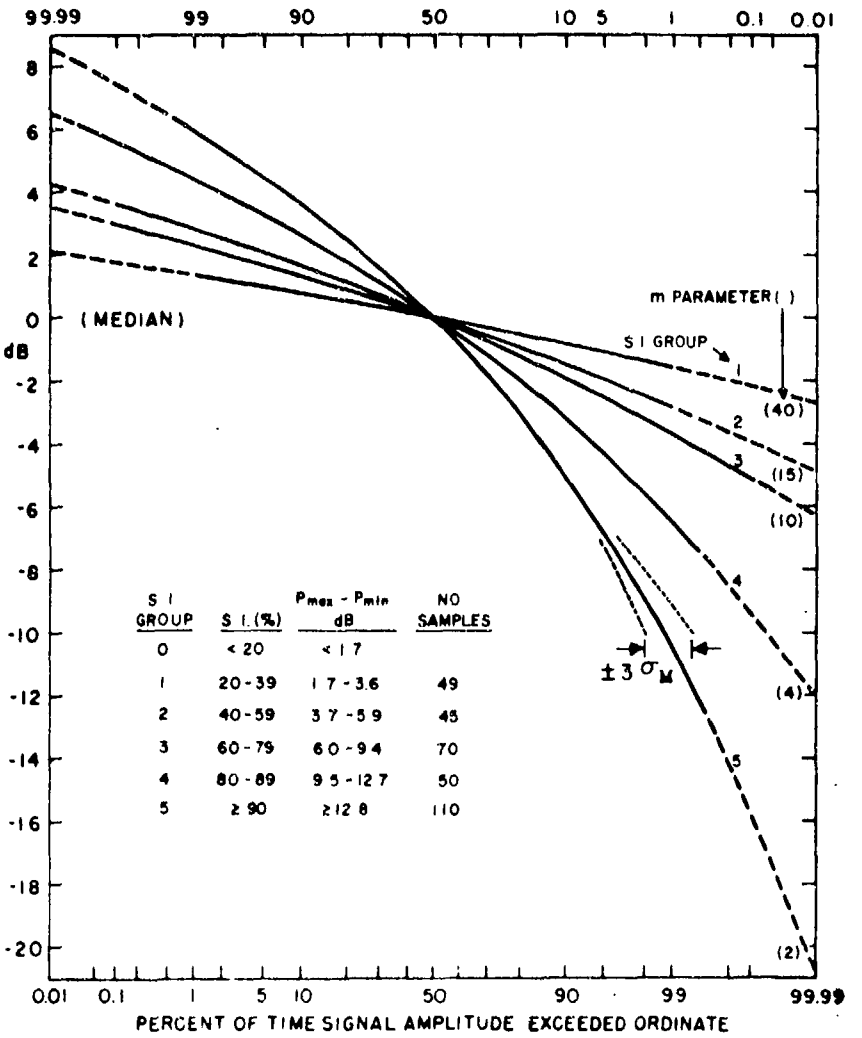

Figure 2.6 Median (Model) Distributions Obtained From The Sample Size for Each S.I. Group From ATS-3 Data Recorded at Hamilton, Massachusetts. Solid Curves Denote the Range of the Experimental Data; Dashed Curves Denote an Extension Based on the Nakagami Distribution for the Value of m in Parentheses. σ_M Equals Standard Error of the Mean.

Rayleigh character ($\gamma \rightarrow 0$) and at the lower frequencies (where scintillation is more pronounced) this may be the norm. This seems to be borne out by the curves in Fig. 2.7, where we note the proximity of the data to the S_4=1 limit; especially for the 150 MHz data.

At the higher frequencies, i.e., in excess of 1.5 GHz the effects of fading tend to be considerably reduced and are often unobservable. Nevertheless, fades as high as 6 dB peak-to-peak have been observed to occur with non-negligible frequency in the equatorial zone. Generally, though, the fading tends to be Ricean in nature with the specular-to-scatter power ratio γ remaining in excess of 6.

Multipath on the ionospheric scintillation channel has been studied to even less a degree than the previously mentioned phenomena. One can only make gross estimates of multipath spread from the limited data and theoretical work on frequency correlation. From the curves in [2.24, p. 38], one can estimate multipath spread as approximately equal to the reciprocal of the carrier frequency, but this estimate is rough in the extreme. At L-band frequencies we get a multipath spread on the order of 10^{-9}.

According to Crane [2.24] either space or time diversity can be used effectively but not frequency or polarization diversity.

For both UHF and SHF satellite links variable rate phase shift keyed modems are generally employed which interface with the radio equipment at 70 MHz, (as for tropo and LOS ground microwave relay), with data rates varying from 75 bits per second to as high as several megabits per second. While conventional and differential phase shift keying is generally employed, staggered quadraphase and minimum shift keying are some times utilized for obtaining desirable spectrum with class C operation.

Assuming that the multipath spread is sufficiently small to be neglected, the ionospheric scintillation channel acts as a single complex time-varying gain (apart from the mean path delay). Doppler spreads exceeding system design values can cause irreducible error rates to appear but for high data rates it appears unlikely that this will ever be a serious source of error. Thus a performance estimation of the digital modem in the presence of slow non-selective fading will be adequate for most cases of interest.

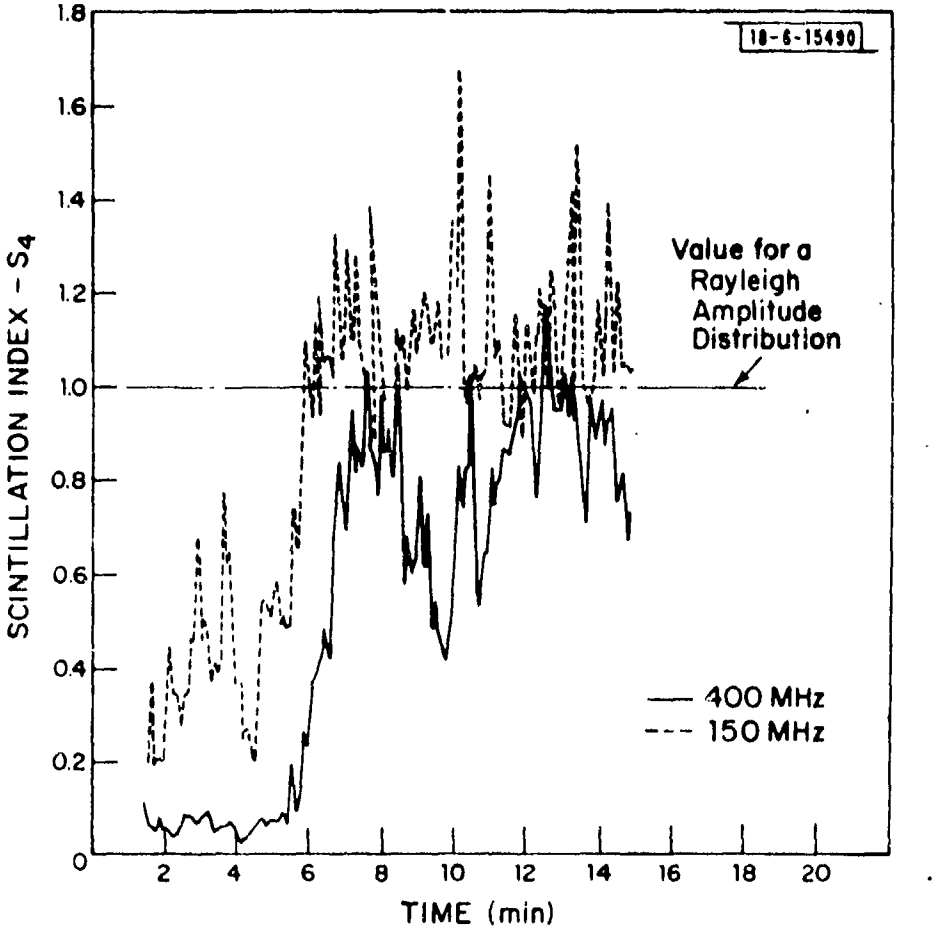

Figure 2.7 S_4 Versus Time for Pass of Object #3133 Rising at 0411 GMT on 4 August 1972 ($Kp = 8^+$).

SECTION 2

REFERENCES

[2.1] P. A. Bello, "Characterization of Random Time-Variant Linear Channels," IRE Trans. on Comm. Systems, Vol. CS-11, pp. 360-393, December 1963.

[2.2] J. L. Doob, Stochastic Processes, New York, Wiley, 1953.

[2.3] R. Arens, "Complex Processes for Envelopes of Normal Noise," IRE Trans. on Info. Theory, Vol. IT-3, pp. 204-207, September 1957.

[2.4] P. A. Bello, "Troposcatter Channel Model," IEEE Trans. on Comm. Tech., Vol. COM-17, No. 2, April 1969, pp. 130-137.

[2.5] P. A. Bello, L. Ehrman, D. S. Arnstein, "Modeling and Data Analysis-Short and Medium Range Troposcatter Tests," Technical Report RADC-TR-69-233, Rome Air Development Center, June 1969, p. 3-25, AD 862-767.

[2.6] P. A. Bello, J. W. Graham, L. Ehrman, "Troposcatter Multi-Mode FSK/PSK Modem," Technical Report RADC-TR-70-175, Rome Air Development Center, September 1970, AD 875-992.

[2.7] P. Monsen, "Digital Transmission Performance on Fading Dispersive Diversity Channels," IEE Trans. on Comm., Vol. COM-21, No. 1, January 1973, pp. 33-39.

[2.8] "Coding/Mux Overhead Study," Final Report by CNR on RADC Contract (F30602-73-C-0271).

[2.9] "Troposcatter Interleaver," (F30602-7[illegible]-C-0133), Current Contract Between CNR and RADC.

[2.10] "Line-of-Sight Technical Investigation," Final Report by CNR on RADC Contract F30602-73-C-0244.(AD006104)

[2.11] R. K. Salaman, "A New Ionospheric Multipath Reduction Factor," IRE Trans. on Comm. Systems, Vol. CS-10, June 1962.

[2.12] L. W. Pickering, "The Calculation of Ionospheric Doppler Spread on HF Communication Channels," submitted to IEEE Trans. on Comm., July 18, 1974.

[2.13] R. A. Shephered and J. B. Lomax, "Frequency Spread in Ionospheric Radio Propagation," IEEE Trans. on Comm. Tech., April 1967, pp. 268-275.

[2.14] M. Balser and W. B. Smith, "Some Statistical Properties of Pulsed Oblique HF Ionospheric Transmission," J. Res. National Bureau of Standards, Vol. 66D, pp. 721-730, November-December 1962.

[2.15] "World Distribution and Characteristics of Atmospheric Radio Noise," National Bureau of Standards Document Submitted to CCIR, February 7, 1964 and to be published as CCIR Report 322.

[2.16] F. Horner and J. Harwood, "An Investigation of Atmospheric Noise at Very Low Frequencies," Proc. IEE, (London), Vol. 103B, pp. 743-751, 1956.

[2.17] G. Foldes, "The Log-Normal Distribution and Its Applications to Atmospheric Studies," Statistical Methods in Radio Wave Propagation, W. C. Hoffman, Ed. London: Pergamon, 1960, pp. 227-232.

[2.18] P. Beckmann, "Amplitude Probability Distribution of Atmospheric Radio Noise," Radio Science, Vol. 68D, pp. 723-736, June 1964.

[2.19] D. Chase, "A Combined Coding and Modulation Approach Over Dispersive Channels," IEEE Trans. on Comm., March 1973, pp. 159-174.

[2.20] DiToro, M. J., et al., "Design and Performance of a New Adaptive Serial Data Modem on a Simulated Time-Variable Multipath HF Link," Record of the 1965 IEEE Int. Comm. Conf., Boulder, Colorado, June 7-9, 1965, pp. 769-773.

[2.21] D. Chase, "A Class of Algorithms for Decoding Block Codes With Channel Measurement Information," IEEE Trans. on Info. Theory, Vol. IT-18, January 1972.

[2.22] J. R. Koster, "Equatorial Studies of the VHF Signal Radiated by Intelstat III, F-3: 1. Ionospheric Scintillation," Progress Report 3, Dept. of Physics, University of Ghana, September 1968, (AD 681462).

[2.23] J. Pomalaza, et al., "A Progress Report on Scintillation Observations at Ancon and Jamacia Observations," Report X-520-70-398, Goddard Space Flight Center, October 1970.

[2.24] R. K. Crane, "Morphology of Ionospheric Scintillation," Tech. Note 1974-29, Lincoln Labs., 31 May 1974.

[2.25] P. D. Shaft, "On the Relationship Between Scintillation Index and Ricean Fading," IEEE Trans. on Comm., May 1974.

[2.26] L. W. Pickering, Final Report on Contract No. TSC-516-3, by CNR, Inc.

[2.27] J. Aarons, Total Electron Content and Scintillation Studies of the Ionosphere, AGARD-ograph No. 166, NATO.

[2.28] Fremouw, and Rino, "Development of a World-Wide Model for F-Layer Produced Scintillation," Stanford Research Institute Final Report, November 1971.

[2.29] J. Aarons, H. Whitney, and R. S. Allen, "Global Morphology of Ionospheric Scintillation," Proc. of the IEEE, February 1971.

[2.30] Final Report, "Pulse Code Modulation (PCM) Time-Division Multiplex (TDM) System Design Verification Test Program," AD 902148L, Defense Communication Engineering Office, February 25, 1972.

SECTION 3

CHANNEL QUALITY MONITORING

The previous section discussed the modeling of fading dispersive channels both in a general framework and specifically for the channels of interest in the present study. Critical channel parameters were identified and typical ranges of numerical values associated with these parameters given for each channel. The types of advanced digital modems being considered for each link were discussed and the gross effect of variations of channel parameters on modem performance was pointed out.

In the present section we wish to develop the rationale for concepts studied in detail in succeeding sections. Section 3.1 discusses quantitatively the relationships between digital modem error rate performance and channel characteristics and parameters. A classification of channel quality monitoring techniques is first presented in Section 3.2 to place the proposed techniques in the proper perspective. Following this, the recommended MQU (media quality unit) configuration is discussed. The major signal processing functions in the MQU are identified and the cooperating role of the MQU and other channel quality monitoring techniques in identifying degradation trends and fault isolation is discussed. Section 3.3 discusses implementation alternatives for the MQU concepts considered in the study.

3.1 Error Rates Vs. Channel Characteristics

Lack of attention to the fading dispersive character of a radio channel has frequently led in the past to modems whose performances have been greatly degraded by the time-selective (fast) and frequency selective fading properties of the channel. Such degradations become manifested in the appearance of symbol distortion, intersymbol interference, crosstalk between channels, and degraded phase references. However, for each of the radio channels of interest in the present study good designs are possible wherein the performance would be rarely determined by the time and frequency selective fading distortion. Thus in estimating the performance of a modem based upon the channel characteristics our major attention will be given to performance limited by flat-flat fading, i.e., no frequency selective and time selective distortion of symbols. This point of view is sensible because the major benefit of the MQU will be to alert the controller to the existence of degradation trends and sudden faults

occurring in the receiving equipment. The occasional outage caused by the propagation medium is worth noting so that misdirected corrective action will not be initiated. However there is probably little technical control action that would normally be taken per se during brief propagation outages. Primarily, then, one needs to detect the presence of propagation outages due to excessive multipath and Doppler spread rather than provide a precise error rate prediction during such highly disturbed conditions. Thus we first consider in 3.1.1 the error rate behavior for well designed modems under normal channel conditions, i.e., where performance is not determined by excessive time and frequency selective fading or unexpected additive disturbances. Section 3.1.2 considers performance under disturbed conditions.

3.1.1 Error Rate Estimation for Well-Designed Modems Under Normal Conditions

In considering modem performance over fading dispersive channels it must be realized that unless enormous SNR's can be achieved, diversity reception must be employed. We consider conventional or "explicit" diversity communications first in 3.1.1.1, where clearly identified diversity channels exist. The newer techniques employing "in-band" or "implicit" diversity are considered in Section 3.1.1.2.

3.1.1.1 Performance With Conventional Diversity Methods

Conventional diversity communications involves the transmission of the same digital data over more than one channel, preferably fluctuating independently, and combining the outputs of the channel to reduce the frequency of deep fades. The modem would be designed so that each diversity channel would produce decision-variables identical to those for slow non-selective fading. Thus the received signal $w(t)$ corresponding to the transmitted complex envelope $z(t)$ would be

$$w_\ell(t) = g_\ell(t)z(t) + \eta_\ell(t) \qquad (3.1)$$

where $g_\ell(t)$ is a slowly fading complex gain characterizing the ℓth diversity channel, and $\eta_\ell(t)$ is a received additive noise.

Several methods of combining diversity channels are used. The ones most commonly discussed are:

- Maximal ratio predetection
- Equal gain predetection
- Selection
- Post-detection

Predetection diversity combining is carried out prior to the filtering processes associated with digital decisions and involves adjusting the signal components of each channel so that they add in-phase. Such techniques are useful when the data signal bandwidth is much greater than the total Doppler spread of the channel, B_{tot}. Since the data signal must occupy a bandwidth no greater than the coherence bandwidth to avoid distortion we see that

$$\frac{W_{coh}}{B_{tot}} \gg 1 \tag{3.2}$$

must be valid for the use of predetection diversity combining. Of the channels studied here only the HF channel is questionable for predetection diversity combining.

For maximal ratio predetection combining and equal strength noises* on each channel the combined signal takes the form

$$w(t) = \sum_{\ell=1}^{M} g_\ell^*(t) w_\ell(t)$$

$$= \sum_{\ell=1}^{M} \{ |g_\ell(t)|^2 z(t) + g_\ell^*(t) \eta_\ell(t) \} \tag{3.3}$$

while for equal gain predetection combining

*If the noises are not of equal strength gains should be applied to each channel to make them equal prior to combining.

$$w(t) = \sum_{\ell=1}^{M} \frac{g_\ell^*(t)}{|g_\ell(t)|} w_\ell(t)$$

$$= \sum_{\ell=1}^{M} \left\{ |g_\ell| z(t) + \frac{g_\ell^*(t)}{|g_\ell(t)|} \eta_\ell(t) \right| \qquad (3.4)$$

where M is the number of diversity channels.

In the case of selection combining the channel with the largest SNR is selected and the others are not used. This selection process can take place pre- or post-detection. Thus

$$w(t) = w_m(t) \qquad (3.5)$$

where $w_m(t)$ is the received signal of the diversity channel having the maximum SNR.

Post-detection combining involves summing decision variables (sampled matched filter outputs) and cannot be expressed simply in terms of the complex envelope of received signals as in (3.2) - (3.5). For FSK we may express the post-detection diversity combined (sometimes called square-law combined) decision variable in the form

$$q_M = \sum_{\ell=1}^{M} |g_\ell + \xi_\ell|^2 - \sum_{\ell=1}^{M} |\eta_\ell|^2 \qquad (3.6)$$

where ξ_ℓ, η_ℓ are sampled output noises. For binary differentially coherent PSK the decision-variable becomes

$$q_M = \mathrm{Re} \left\{ \sum_{\ell=1}^{M} [g_\ell^* + \xi_\ell][g_\ell + \eta_\ell] \right\} \qquad (3.7)$$

In terms of decision variables for binary PSK the maximal ratio predetection, equal gain predetection, and selection combining techniques would read

$$q_M = \mathrm{Re} \left\{ \sum_{\ell=1}^{L} g_\ell^* [g_\ell + \eta_\ell \right\} \qquad (3.8)$$

$$q_M = \sum_{\ell=1}^{M} \mathrm{Re}\left\{|g_\ell| + \frac{g_\ell^*}{g_\ell}\eta_\ell\right\} \tag{3.9}$$

$$q_M = \mathrm{Re}\left\{|g_m| + \frac{g_m^*}{g_m}\eta_m\right\} \tag{3.10}$$

To develop the rationale for some of the error rate estimation procedures discussed in Section 5 it is convenient to express the error probability P_e as an average over the channel fluctuations of the conditional probability of error given a "frozen" channel. It is clear from the above formulations that for well designed modems not limited by time and frequency selective fading, the conditional error probabilities for all the combining techniques depends only on the complex amplitudes of the channels $\{g_\ell;\ \ell = 1,2, \ldots M\}$. If, in addition, as will almost always be true for the channels of interest, the noises are statistically independent with uniformly distributed phases, it is also easy to see that the conditional error probabilities depend only on the "instantaneous" SNR's on each branch, i.e.,

$$\Pr(\text{error}\,|\,\text{frozen diversity channels}) = P_c(\gamma_1,\gamma_2, \ldots \gamma_M) \tag{3.11}$$

where

$$\gamma_\ell = \frac{|g_\ell|^2}{|\eta_\ell|^2} \tag{3.12}$$

is the instantaneous SNR on the ℓth branch.

The desired error rate can then be expressed in the form

$$P_e = \int \cdots \int P_c(\gamma_1,\gamma_2, \ldots \gamma_M)W(\gamma_1,\gamma_2, \ldots \gamma_M)d\gamma_1 d\gamma_2 \cdots d\gamma_M \tag{3.13}$$

where $W(\gamma_1, \ldots \gamma_M)$ is the joint density function of the SNR's on the diversity branches.

Assuming that some unexpected interference is not limiting performance, the noises may be adequately modeled as complex Gaussian for all the channels of interest except the HF channel. For the HF channel log-normal random phase noise appears to be a good model (see calculations by Bello [3.1]). In either case one may derive expressions for the conditional error probability $P_c(\gamma_1,\gamma_2, \ldots \gamma_M)$ for any of the diversity combining techniques. For example, with differentially coherent PSK and additive Gaussian noise the conditional error probabilities become

$$P_c(\gamma_1,\gamma_2, \ldots \gamma_L) = \begin{cases} \frac{1}{2} \exp\left\{-\sum_{\ell=1}^{M} \gamma_\ell\right\} & ; \text{ maximum ratio predetection} \\ \frac{1}{2} \exp\left\{-\frac{1}{M}\left(\sum_{\ell=1}^{M} \sqrt{\gamma_\ell}\right)^2\right\} & ; \text{ equal gain predetection} \\ \frac{1}{2} \exp\{-\gamma_m\} & ; \text{ selection} \\ \frac{1}{2} \exp\left\{-\sum_{\ell=1}^{M} \gamma_\ell\right\} F_M\left(\sum_{\ell=1}^{M} \gamma_\ell\right) & ; \text{ postdetection} \end{cases} \tag{3.14}$$

where [3.2]

$$F_M(\gamma) = \sum_{j=0}^{M-1} \left(\sum_{m=j}^{M-1} C_{m-j}^{m+M-1} \left(\frac{1}{2}\right)^{m+M-1}\right) \frac{1}{j!2^j} \gamma^j \tag{3.15}$$

If the instantaneous SNR's are available one may estimate the average error probability by forming time averages of the conditional error probabilities,

$$\boxed{\hat{P}_e = \langle P_c(\gamma_1(t),\gamma_2(t), \ldots \gamma_M(t)) \rangle} \tag{3.16}$$

where $P_c(\cdot)$ would be selected appropriate to the combiner technique and modem to be monitored. This estimation technique,

called the conditional error probability approach is studied in Section 5. Note that no assumptions need be made about the fading statistics with this approach.

When the error rate is low it is well known that error counting to estimate errors requires a rapidly increasing amount of measurement time to achieve a given estimation error. As the calculations in Section 5 indicate, the same effect occurs in trying to estimate error rates by averaging conditional error rates. For low error rates in the diversity combined signal we may employ an "error amplification" technique to make the apparent error rate larger and then use an extrapolation procedure to estimate the true error rate from the amplified error rate. It is noteworthy that for high SNR's there is a simple extrapolation procedure valid for general classes of additive noise and fading statistics. The derivation is sufficiently simple to be presented here.

The joint density function for the instantaneous SNR's on the diversity channels can be expressed in terms of a normalized density function in which the average signal strengths on the diversity channels have been normalized to unity average SNR, i.e.,

$$W(\gamma_1,\gamma_2,\cdots\gamma_M) = \frac{1}{\prod_{\ell=1}^{M}\Gamma_\ell} w_M\left(\frac{\gamma_1}{\Gamma_1}, \frac{\gamma_2}{\Gamma_2}, \cdots \frac{\gamma_M}{\Gamma_M}\right) \tag{3.17}$$

where

$$\Gamma_\ell = \overline{\gamma_\ell} \tag{3.18}$$

is the average SNR of the ℓth branch. Using (3.17) in (3.18) we find that

$$P_e = \frac{1}{\prod_{\ell=1}^{M}\Gamma_\ell} \int \cdots \int P_c(\gamma_1,\gamma_2,\cdots\gamma_M) w_M\left(\frac{\gamma_1}{\Gamma_1}, \frac{\gamma_2}{\Gamma_2}, \cdots \frac{\gamma_M}{\Gamma_M}\right) d\gamma_1 d\gamma_2 \cdots d\gamma_M \tag{3.19}$$

The conditional error probability $P_c(\gamma_1, \ldots, \gamma_M)$ drops from 1/2 to small values, as $\gamma_1 \ldots \gamma_M$ increases from zero to large values (e.g., refer to (3.14) for the case of Gaussian noise). For large $\{\Gamma_\ell;\ \ell = 1, \ldots M\}$ the normalized density function will "spread out" and be flat around the origin and $P_c(\gamma_1,\gamma_2, \ldots \gamma_M)$ will look impulsive by comparison with $w_M(\gamma_1/\Gamma_1,\gamma_2/\Gamma_2, \ldots \gamma_M/\Gamma_M)$ provided that the latter is not a singular distribution. A Taylor expansion of $w_M(\gamma_1/\Gamma_1,\gamma_2/\Gamma_2, \ldots \gamma_M/\Gamma_M)$ about the origin may be used to provide an expansion of P_e in inverse powers of SNR. The first term in this series is given by

$$P_e = \frac{w_M(\underline{0}) \int P_c(\underline{\gamma})\, d\underline{\gamma}}{\prod_{\ell=1}^{M} \Gamma_\ell} \tag{3.20}$$

where we have used the vector notation

$$w_M(\underline{0}) = w_M(0,0, \ldots 0) \tag{3.21}$$

$$\int P_c(\underline{\gamma})\, d\underline{\gamma} = \int_0^\infty \cdots \int_0^\infty P_c(\gamma_1,\gamma_2, \ldots \gamma_M) d\gamma_1 d\gamma_2 \cdots d\gamma_M \tag{3.22}$$

If $w(\underline{0})$ is identically zero or very small compared to $w(\underline{\gamma})$ at nearby $\underline{\gamma}$ values one must include other terms in the series expansion. However this does not appear necessary for the troposcatter, HF, and satellite ionospheric scintillation channels. The question does not arise for LOS channels because we have already pointed out that for this channel average error rate has questionable meaning for quality monitoring for quality monitoring and that conditional error rates should be presented instead.

In the error amplification approach the instantaneous SNR on the ℓth branch is reduced by r_ℓ so that

$$\boxed{\hat{P}_e(\underline{r}) = \left\langle P_c\left(\frac{\gamma_1}{r_1}, \frac{\gamma_2}{r_2}, \ldots \frac{\gamma_M}{r_M}\right)\right\rangle} \tag{3.23}$$

is computed. Assuming that the new reduced SNR's are still high enough to use the approximate expression (3.20), we see that with sufficient averaging time

$$\hat{P}_e(\underline{r}) \rightarrow \prod_{\ell=1}^{M} \left(\frac{r_\ell}{\Gamma_\ell}\right) w_M(\underline{0}) \int P_c(\bar{\gamma})\, d\bar{\gamma}$$

$$= \prod_{\ell=1}^{M} r_\ell \cdot P_e \qquad (3.24)$$

so that as our extrapolated error rate estimate we may use

$$\boxed{\hat{P}_e = \frac{\hat{P}_e(r_1, r_2, \ldots r_M)}{\prod_{\ell=1}^{M} r_\ell}} \qquad (3.25)$$

An estimation of the set of branch SNR's $\{\Gamma_\ell\}$ can provide guidance in the selection of $\{r_\ell\}$ so that the set $\{\Gamma_\ell/r_\ell\}$ are still reasonably high SNR values but not so high that estimation error standard deviations are not acceptable.

We now consider a somewhat simpler error probability estimation procedure which we call the "threshold" method. This technique is also applicable to general classes of fading statistics and additive noise, but unlike the conditional error probability approach will not be useful at low SNR's. That is to say it will be effective for SNR's in the same range as those making the error amplification technique work.

In the "threshold" method γ_ℓ is compared against a threshold X_ℓ and an estimate is made of the probability P_X of the joint event $\{\gamma_\ell < X_\ell;\ \ell = 1,2, \ldots M\}$,

$$P_X = \int_0^{X_1} \int_0^{X_2} \cdots \int_0^{X_M} \frac{1}{\prod_{\ell=1}^{M} \Gamma_\ell} w_M\left(\frac{\gamma_1}{\Gamma_1}, \frac{\gamma_2}{\Gamma_2}, \ldots \frac{\gamma_M}{\Gamma_M}\right) d\gamma_1 d\gamma_2 \cdots d\gamma_M \qquad (3.26)$$

The average SNR's Γ are assumed measured and the thresholds $\{X_\ell\}$ are set sufficiently below $\{\Gamma_\ell\}$ so that

$$w_M\left(\frac{X_1}{\Gamma_1}, \frac{X_2}{\Gamma_2}, \ \ldots \ \frac{X_M}{\Gamma_M}\right) \approx w_M(0,0, \ \ldots \ 0) \tag{3.27}$$

Using (3.27) in (3.26) we see that

$$P_X \approx w_M(0,0, \ \ldots \ 0) \prod_{\ell=1}^{M} X_\ell/\Gamma_\ell \tag{3.28}$$

Since the product on the right-hand side of (3.27) is known we can obtain an estimate of $w_M(\underline{0})$,

$$\hat{w}_M(0,0, \ \ldots) \approx \frac{\hat{P}_X}{\prod_{\ell=1}^{M} X_\ell/\Gamma_\ell} \tag{3.29}$$

From (3.20) we see that P_e can be determined at high SNR from knowledge of $w_M(\underline{0})$, the SNR's, and the integral (3.22). But we have estimated the first two quantities and the last may be computed since the conditional error probability expression $P_c(\gamma_1,\gamma_2, \ \ldots \ \gamma_M)$ is a known function. In terms of $\hat{P}_X$, the estimated threshold probabilities, we see that our error rate estimate becomes

$$\boxed{\hat{P}_e = \hat{P}_X \frac{\int P_c(\chi) \ d\chi}{\prod_{\ell=1}^{M} X_\ell}} \tag{3.30}$$

Analysis of this procedure in Section 5 reveals that the estimator bias is less for the threshold than for the conditional error probability approach at high SNR.

If one is willing to assume that the fading statistics are known except for some average channel parameters, in some cases the averages over the fading (3.13) can be carried out to obtain explicit formulae for error probability as a function of these average parameters. Then measurement of the average parameters and their use in these formulae allow an estimation of error probability. This approach, which is called the "formula" approach, is also evaluated in Section 5 for some specific cases.

It has been pointed out in Section 2.1.3 that complex Gaussian fading statistics appear to be the best general model available. Fortunately, there exist a considerable number of evaluations of error probability assuming complex Gaussian statistics. A recent summary of such results is provided in [3.3]. To use the formula approach for error rate estimation in the case of correlated fading on the diversity channels it is necessary to measure the complex cross correlation coefficients between the diversity channels in addition to the average SNR's on each branch.

3.1.1.2 Error Rate Estimation for Advanced Modems Utilizing In-Band Diversity

The modems discussed in the previous subsection use signaling elements that are affected minimally by the intersymbol interference and signal distortion caused by frequency selective fading. As pointed out in Section 2.2 modems have been conceived and are being developed which attempt to achieve close to maximum likelihood demodulation when the bandwidth occuped by a pulse exceeds considerably the coherent bandwidth. In such a case considerable intersymbol interference and signal distortion will result but the demodulation procedure "unscrambles" the individual pulse returns and ideally achieve close to a matched filter receiver response on the individual received pulses. By estimating the performance of the matched filter receiver and applying correction factors, performance estimates of advanced modems may be obtained.

The instantaneous SNR at the matched filter output of the ℓth diversity channel is given by

$$s_\ell = \frac{\int |p_\ell(t)|^2 \, dt}{2N_0} \tag{3.31}$$

where $p_\ell(t)$ is a particular received pulse for this channel and the noise has been assumed white with real one-sided noise power density of N_0. Assuming independent noises with uniform phase distributions the conditional error probability will be a function of $\gamma_1, \gamma_2, \ldots \gamma_M$ only and the error rate can be expressed in a form identical to (3.13)

$$P_e = \int \ldots \int P_c(s_1, s_2, \ldots s_M) W_1(s_1, s_2, \ldots s_M) ds_1 ds_2 \ldots ds_M \tag{3.32}$$

where $W_1(s_1, s_2, \ldots s_M)$ is the joint density function of the matched filter output SNR's.

Techniques are proposed in Section 5 for measurement of the quantities $(s_\ell;\ \ell=1, \ldots, M)$. Thus one may estimate the error rate by the time average

$$\hat{P}_e = \langle P_c(s_1, s_2, \ldots s_M) \rangle \tag{3.33}$$

The conditional error probability expressions are formally identical to those in (3.14) with s_ℓ replacing γ_ℓ. Thus for maximal ratio combining and binary DPSK modulation,

$$P_c(s_1, s_2, \ldots s_M) = \frac{1}{2} \exp \left\{ - \sum_{\ell=1}^{M} s_\ell \right\} \tag{3.34}$$

For conventional systems not employing in-band diversity we described an error amplification approach to aid in estimation of low error rates. A corresponding procedure does not exist in a rigorous sense for the present case because the "amount" of in-band diversity is not only unknown but not even clearly definable. However, if one were willing to make such an estimate, one could generalize the error amplification approach to the present case. The same comments apply to the "threshold" and "formula" methods discussed previously, i.e., they do not apply directly.

3.1.2 Error Rate Estimation for Atypical Situations

The techniques discussed in the previous section will provide error rate predictions for a perfectly functioning receiver that can be continually compared with actual performance as determined at the demodulator output. This comparison will reveal trends in receiver degradation or sudden failures. However there will always be occasional propagation or interference conditions which will cause the error rate to increase beyond design values and it is important to detect these situations so that they will not be misinterpreted as receiver degradation. We consider in sequence the effects of excessive Doppler spread, excessive multipath spread, and interference.

3.1.2.1 Excessive Doppler Spread

If Doppler spreads become too large (i.e., fast fading) two types of nonidealities occur in data reception:

a) Pulse distortion, destruction of orthogonality relationships, and crosstalk in parallel subchannels

b) Channel measurement functions degrade.

In either case one may show that the rms Doppler spread* B is the fundamental channel parameter not only determining the onset of fast fading degradation but also frequently allowing a quantitative estimate of performance degradation. We will illustrate the importance of B by examining the effects of fast fading on performance due to channel measurement degradation. One may carry out similar calculations for a) but for the channels and modems of interest in this study the effects of b) dominate (for calculations that typify a) see [3.4]).

For conventional modems channel measurement appears primarily in the guise of providing phase references for coherent or differentially coherent detection and for predetection diversity combining. Consider for illustration purposes a DPSK modem. Let w_1, w_2 denote the complex representation of the integrate-and-dump outputs for two successive pulses. The decision variable for DPSK is

$$d = \mathrm{Re}(w_1^* w_2) \tag{3.35}$$

*It is assumed that the mean Doppler shift is tracked and compensated for with some form of AFC.

The complex outputs contain signal and noise components are

$$w_1 = \gamma_1 z_1 + n_1 \tag{3.36}$$

$$w_2 = \gamma_2 z_2 + n_2 \tag{3.37}$$

where n_1, n_2 are independent noises, γ_1 and γ_2 take on the values ± 1, and z_1, z_2 are proportional to the value of the channel complex gain at two instants separated by the bit duration Δ. That is, assuming a WSSUS channel

$$\overline{z_1^* z_2} \sim \overline{T^*(f,t)T(f,t+\Delta)} = R(0,\Delta) = p(\Delta) \tag{3.38}$$

where $R(\Omega,\tau)$ is the channels time-frequency correlation function and $p(\tau)$ is the channels time correlation function.

When Δ is less than the coherence time duration of the channel

$$\Delta < T_{coh} \tag{3.39}$$

then z_1 will differ little from z_2. If we also assume the additive noise negligible then the decision variable becomes

$$d = |z|^2 \gamma_1 \gamma_2 \tag{3.40}$$

and d will be positive if γ_1, γ_2 have the same sign and negative otherwise yielding zero error probability.

For simplicity assume that $\gamma_1 = \gamma_2 = 1$ and consider the effect of decorrelation introduced between z_1 and z_2 by excessive Doppler spread. Any two correlated random variables may be expressed in terms of a common correlated part and uncorrelated parts as follows

$$z_1 = \sqrt{p^*(\Delta)}\ z + \sqrt{1 - |p(\Delta)|}\ \mu \tag{3.41}$$

$$z_2 = \sqrt{p(\Delta)}\ z + \sqrt{1 - |p(\Delta)|}\ \nu \tag{3.42}$$

where we have normalized

$$p(0) = 1 \tag{3.43}$$

and μ, ν, z are uncorrelated with unit average magnitude squared. For complex Gaussian statistics this means that μ, ν, z are mutually independent.

Assuming that mean Doppler shift has been removed by AFC and that such mean is defined by the centroid of the Doppler power spectrum, the following Taylor expansion applies

$$p(\Delta) = 1 - \frac{\pi^2 B^2 \Delta^2}{2} + \ldots \tag{3.44}$$

where B is the rms Doppler spread. For $p(\Delta)$ near one

$$z_1 = z + \frac{\pi B \Delta}{\sqrt{2}} \mu \tag{3.45}$$

$$z_2 = z + \frac{\pi B \Delta}{\sqrt{2}} \nu \tag{3.46}$$

Use of (3.46) in (3.36) and (3.37) for $\gamma_1=\gamma_2=1$ results in

$$w_1 = z + \frac{\pi B \Delta}{\sqrt{2}} \mu + n_1 \tag{3.47}$$

$$w_2 = z + \frac{\pi B \Delta}{\sqrt{2}} \nu + n_2 \tag{3.48}$$

Assuming n_1 and n_2 complex Gaussian we see that the effect of Doppler spread is to introduce effective additive noise components that exist even when the true additive noise vanishes, i.e., an irreducible error probability is introduced. If the error probability expression for zero Doppler spread is given by $P_e(S)$ where

$$S = \frac{\overline{|z|^2}}{\overline{|n|^2}} \tag{3.49}$$

is the SNR, then we see that the error rate with non-zero Doppler spread is given by $P_e(S_{eff})$ where

$$S_{eff} = \frac{S}{1 + S(\pi B\Delta)^2/2} \tag{3.50}$$

For Doppler spread not to degrade performance at all we see that

$$(B\Delta)^2 << \frac{2}{\pi^2 S} \tag{3.51}$$

A numerical example may prove interesting. At 19 dB SNR (3.51) implies that

$$(20B\Delta)^2 << 1 \tag{3.52}$$

A value of

$$B\Delta = \frac{1}{60} \tag{3.53}$$

makes the left-hand side of (3.52) equal to 1/9.

In HF communications pulse widths from 10 to 20 milliseconds are used. For Doppler spread to have negligible effect on performance at an SNR of 19 dB (around 10^{-2} error probability with nondiversity operation) we see that for a 20 ms pulse width

$$B < 5/6 \text{ Hz} \tag{3.54}$$

For the other channels of interest the pulse widths would be orders of magnitude smaller and Doppler spread would always have negligible effect for DPSK communications. However Doppler spread could still have an undesirable effect when phase references are established for coherent detection and predetection diversity combining, because long averaging times are used to extract the phase reference, e.g., as in the use of a filtered pilot tone. The predominant effect of the averaging is the group delay suffered by the fading pilot tone. This will produce decorrelation between the complex fading on the data signal and that on the pilot tone.

Normally the noise on the pilot tone is negligible so that a different resolution from (3.47) and (3.42) is used to relate error rates with and without Doppler spread. Thus if the complex representation of the pilot tone is z and that of the complex fading on the data is w one uses the representation

$$w = \rho z + \sqrt{1 - |\rho|^2}\,\mu \tag{3.55}$$

where μ and z are uncorrelated,

$$\overline{z^* w} = \rho \tag{3.56}$$

and we have normalized

$$\overline{|z|^2} = \overline{|w|^2} = \overline{|\mu|^2} = 1 \tag{3.57}$$

As we have mentioned, the group delay of the averaging filter Δ_{gr} is the primary cause of decorrelation. Then

$$\rho \approx p(\Delta_{gr}) \approx 1 - \frac{\pi^2 B^2 \Delta_{gr}^2}{2} + \ldots \tag{3.58}$$

and assuming small decorrelation

$$w = z + \pi B \Delta_{gr} \mu \tag{3.59}$$

Normally the received signal is accompanied by noise

$$w = z + \pi B \Delta_{gr} \mu + n \tag{3.60}$$

from which we see that decorrelation is equivalent to adding a noise component. Thus it may be seen that if the error rate without decorrelation is $P_e(S)$ the error rate with decorrelation is $P_e(S_{eff})$; where

$$S_{eff} = \frac{S}{1 + S(\pi B \Delta_{gr})^2} \tag{3.61}$$

For a numerical example we note that if Doppler spread is to have negligible effect at an SNR of 16 dB

$$B\Delta_{gr} < \frac{1}{60} \tag{3.62}$$

For 8 GHz troposcatter links Doppler spreads of 20 Hz are possible although extreme. From (3.62) we see that the group delay of the channel measurement should be less than 833 μsec to have negligible degradation with such a Doppler spread.

For more complicated channel measurement schemes, such as those using decision directed operations and the implicit ones used in adaptive equalizers the same general comments apply. The product of the Doppler spread by the group delay of the measurement process must be sufficiently small.

3.1.2.2 Excessive Multipath Spread

As the multipath spread increases beyond modem design values, the following nonidealities will occur:

a) Excessive intersymbol interference

b) Pulse distortion, destruction of orthogonality, and crosstalk in parallel subchannels

c) Degradation of channel measurement functions

The major effect of these nonidealities is to produce an irreducible error rate. Unfortunately, the relationship between modem performance and channel parameters is considerably more complex than for channel measurement degradation due to excessive Doppler spread. Generally speaking, as the rms multipath spread, L, increases, all the nonidealities become successively worse so that although it is not usually possible to relate error rate uniquely to rms multipath spread, one may always use the size of L as a flag to signal the presence of atypical multipath spreads.

We consider now the kinds of average channel parameters needed to predict modem average error rate. These calculations are useful for HF and troposcatter links. They are not important for the Satellite Ionospheric Scintillation channel which has negligible multipath. Average calculations over the fading are probably not meaningful for the LOS microwave relay, as mentioned

previously. However, we do point out the essential channel parameters needed to specify the relationship between excessive frefrequency-selective fading and modem performance for the LOS channel.

Performance analyses of FSK, DPSK, and PSK modems in the presence of frequency-selective fading have been carried out by Bello [3.5] - [3.7], Bello and Nelin [3.8],[3.9], Bello and Ehrman [3.10],[3.11] and Bello and Crystal [3.12]. We draw upon these varied calculations to present a brief summary of the relationship between channel characteristics and modem performance in the presence of frequency-selective fading.

In discussing these relationships, it is necessary to distinguish the modem type according to the presence or absence of the following features:

1) Bandlimited or rectangular signaling pulses
2) Phase-continuous or discontinuous operation
3) The existence of receiver time gates
4) Conventional or "in-band" operation

When the signaling pulses do not have slowly decreasing spectral tails, as for a rectangular pulse, but has its energy well-confined to a given bandwidth W, the first few terms of the frequency power series model (see Section 2.1.4) are adequate to characterize the frequency-selective fading. Thus for the quadratically selective fading model

$$w(t) \approx T_0(t)z(t-\tau_0) + T_1(t)\dot{z}(t-\tau_0) + T_2(t)\ddot{z}(t-\tau_0) \tag{3.63}$$

where $z(t)$, $w(t)$ are the complex envelopes of the transmitted and received signal, τ_0 is a mean path delay, and $T_0(t)$, $T_1(t)$, and $T_2(t)$ are the complex zero mean slowly-changing channel coefficients. Assuming complex Gaussian channel fluctuations, the statistics of $w(t)$ given $z(t)$ will be completely determined from the correlation matrix of the coefficients. From (2.24) we see that this correlation matrix is completely determined from the first few moments of the delay power spectrum $Q(\xi)$. However, the second moment is just the centroid of $Q(\xi)$ and may be set equal to zero by explicit definition of the mean path delay τ_0 in (3.63); i.e., we set

$$\int \xi\, Q(\xi)\, d\xi = 0 \tag{3.64}$$

For convenience, we normalize

$$\int Q(\xi)\, d\xi = 1 \tag{3.65}$$

With (3.64) and (3.65), the square root of the second moment of $Q(\xi)$ equals just half our definition of rms multipath L, i.e.,

$$\sqrt{\int \xi^2 Q(\xi)\, d\xi} = \frac{L}{2} \tag{3.66}$$

The other two moments can be related to dimensionless shape parameters called the "skewness" β_3 and the "excess" β_4 in classic probability theory,

$$\beta_3 = \frac{\int \xi^3 Q(\xi)\, d\xi}{(L/2)^3} \tag{3.67}$$

$$\beta_4 = \frac{\int \xi^4 Q(\xi)\, d\xi}{(L/2)^4} \tag{3.68}$$

Theoretical calculations of L, β_3, and β_4 have been carried out in [3.11] for troposcatter links as a function of range and antenna size.

Except for the case of data transmission by the frequency-division-multiplex of parallel data subchannels on an FM carrier, data transmission analyses have been concerned with sharp, essentially rectangular, pulses. If calculations are carried out for PCM-TDM data transmission with bandlimited pulses, it will be found that the channel parameters L, β_3, β_4 (in addition to SNR, of course, are sufficient to predict error rate performance. In fact, the shape parameters β_3 and β_4 may sometimes have little effect as was found in [3.11] so that L will frequently be the dominant parameter. To summarize, for bandlimited communication

with conventional* modems, the essential average channel parameters to estimate error rates due to complex Gaussian frequency-selective fading are L, β_3 and β_4.

For the LOS radio relay channel, strictly bandlimited communications is involved because the transmission of data with high bits/sec/Hz data rate packing is of prime interest to the military. The parameters of interest are the coefficients T_0, T_1, T_2 themselves rather than L, β_3, β_4 because averages over the fading have little meaning for the LOS microwave ground link.

Whether a linear or nonlinear modulation scheme is used, T_0, T_1, T_2 will allow calculation of distortion. For example, when a frequency discriminator or phase detector is employed, one may model the output as a series expansion of linear and nonlinear distortion terms [3.13]. If the transmitted signal is phase-modulated,

$$z(t) = e^{j\varphi(t)} \tag{3.69}$$

where $\varphi(t)$ is the input phase modulation containing the data signal. In [3.13] it is shown that with small-frequency-selective distortion the output of the phase detector can be represented as

$$\varphi_{out}(t) = \varphi(t - \tau_0) + A(t)\dot{\varphi}(t - \tau_0) + B(t)\ddot{\varphi}(t - \tau_0) + C(t)\varphi^2(t - \tau_0) + \ldots \tag{3.70}$$

where

$$A(t) = \mathrm{Re}\left\{\frac{T_1 T_0^*}{|T_0|^2}\right\} \tag{3.71}$$

$$B(t) = \mathrm{Re}\left\{\frac{T_2 T_0^*}{|T_0|^2}\right\} \tag{3.72}$$

$$C(t) = \mathrm{Re}\left\{\frac{T_1 T_0^*}{|T_0|^2}\right\} \mathrm{Im}\left\{\frac{T_1 T_0^*}{|T_0|^2}\right\} - \mathrm{Im}\left\{\frac{T_2 T_0^*}{|T_0|^2}\right\} \tag{3.73}$$

*Not multipath "unscrambling".

For FM, where

$$z(t) = e^{j\int x(t)dt} \tag{3.74}$$

where x(t) is the input frequency modulation, the output of the discriminator takes the form

$$x_{out}(t) = x(t-\tau_0) + A(t)\dot{x}(t-\tau_0) + B(t)\ddot{x}(t-\tau_0)$$
$$+ 2x(t-\tau_0)\dot{x}(t-\tau_0)C(t) + \ldots. \tag{3.75}$$

where derivatives of A, B, C have been neglected because of the slow fluctuations of the channel.

In the case of rectangular pulses and conventional systems, the essential channel parameters are one-sided moments rather than two-sided moments as in the bandlimited pulse case. However, the particular moments needed depend upon whether phase-continuous operation or phase-discontinuous operation is employed [3.5],[3.9] and whether time-gating is used in the receiver [3.12]. Thus, for a four-phase QPSK modem not using time gates, it is found [3.5] that the following one-sided moments allow prediction of modem error rate:

$$m_1^+ = \int_0^\infty \xi\, Q(\xi)\, d\xi \tag{3.76}$$

$$m_1^- = \int_{-\infty}^0 \xi\, Q(\xi)\, d\xi = \int_0^\infty \xi\, Q(\xi)\, d\xi \tag{3.77}$$

$$m_2^+ = \int_0^\infty \xi^2\, Q(\xi)\, d\xi \tag{3.78}$$

$$m_2^- = \int_\infty^0 \xi^2\, Q(\xi)\, d\xi = \int_0^\infty \xi^2\, Q(-\xi)\, d\xi \tag{3.79}$$

On the other hand, for phase-continuous FSK transmission [3.9] one finds that the pertinent parameters are

$$m_2^{\pm} = \int_0^{\infty} \xi^2 \, Q(\pm\xi) \, d\xi \tag{3.80}$$

$$m_3^{\pm} = \int_0^{\infty} \xi^3 \, Q(\pm\xi) \, d\xi \tag{3.81}$$

$$m_4^{\pm} = \int_0^{\infty} \xi^4 \, Q(\pm\xi) \, d\xi \tag{3.82}$$

The expressions for error rate in terms of these parameters and SNR are rather cumbersome and will not be reproduced here.

When time gates are used as in the FSK/PSK modem conceived by Bello [3.12], the essential channel parameters are also one-sided integrals over the delay power spectrum with integration interval determined by the time gate duration.

For the case of multipath unscrambling modems which attempt to achieve the intersymbol interference-free matched filter performance, the presence of multipath spread in excess of the design values results in the demodulator "matching" to the received signal corresponding to only part of the multipath structure. The unmatched part acts like an additive noise and produces an irreducible error rate. Thus, let us assume that the impulse response $g(t,\xi)$ is divided into two parts:

$$g(t,\xi) = g_0(t,\xi) + g_1(t,\xi) \tag{3.83}$$

where

$$\overline{g_0^*(t,\eta)g_0(t,\eta+\xi)} = \begin{cases} Q(\xi)\delta(\eta-\xi) & ; \quad \xi < \xi_m \\ 0 & ; \quad \xi > \xi_m \end{cases} \tag{3.84}$$

$$\overline{g_1^*(t,\eta)g_1(t,\eta+\xi)} = \begin{cases} 0 & ; \quad \xi < \xi_m \\ \\ Q(\xi)\delta(\eta - \xi) & ; \quad \xi > \xi_m \end{cases} \tag{3.85}$$

$$\overline{g^*(t,\eta)g(t,\eta+\xi)} = Q(\xi)\delta(\eta - \xi) \tag{3.86}$$

The impulse response $g_0(t,\xi)$ corresponds to the main part of the actual impulse response contributing path delays up to ξ_m, while $g_1(t,\xi)$ is the "tail" of the impulse response corresponding to path delays in excess of ξ_m. We assume that the demodulator is capable of producing the ideal receiver for path delays up to ξ_m and ignores contributions due to other paths. The maximum likelihood demodulator takes the deceptively simple form

$$\underset{k}{\text{Min}} \int |w(t) - w^{(k)}(t)|^2 \, dt \tag{3.87}$$

where $w^{(k)}(t)$ is the received signal corresponding to the k^{th} transmitted data sequence and the received signal is constructed on the basis of the impulse response $g_0(t,\xi)$. The process $w(t)$ is the complex envelope of the received signal,

$$w(t) = w_0(t) + w_1(t) + \eta(t) \tag{3.88}$$

where

$$w_0(t) = \int z(t - \xi)g_0(t,\xi) \, d\xi \tag{3.89}$$

$$w_1(t) = \int z(t - \xi)g_1(t,\xi) \, d\xi \tag{3.90}$$

and $\eta(t)$ is an additive noise.

For any given transmitted squence, $w_1(t)$ is complex Gaussian and independent of $w_0(t)$ for a complex Gaussian WSSUS channel. When k is selected correctly,

$$w^{(k)}(t) = w_0(t) \tag{3.91}$$

and the integral in (3.87) reads

$$\int |w(t) - w^{(k)}(t)|^2 dt = \int |w_1(t) + \eta(t)|^2 dt \tag{3.92}$$

It is clear that the unmatched part of the received signal acts identically like an additive noise term producing an irreducible error rate. We note that

$$\overline{|w_0(t)|^2} = \overline{|z|^2} \int_{-\infty}^{\xi_m} Q(\xi)\, d\xi \tag{3.93}$$

$$\overline{|w_1(t)|^2} = \overline{|z|^2} \int_{\xi_m}^{\infty} Q(\xi)\, d\xi \tag{3.94}$$

If an expression for error rate as a function of SNR, Pe(S), is available in the absence of mismatch, then it may be seen that the error rate with mismatch is given by using in place of S an effective SNR

$$S_{eff} = \frac{S}{1 + S \int_{\xi_m}^{\infty} Q(\xi) ds \Big/ \int_{-\infty}^{\xi_m} Q(\xi) ds} \tag{3.95}$$

Only when $L_{tot} > \xi_m$ will no irreducible error rate occur. It is clear that for the advanced modems an integral over the delay power spectrum is required to estimate error rates.

For a final situation of interest, consider the channel measurement degradation caused by frequency-selective fading when predetection diversity combining is attempted with a complex

reference taken from the center of a band and used to demodulate a data stream offset from the center by F Hz. This situation was studied in [3.8]. Here we present a simplified analysis. This analysis parallels closely that for fast fading presented in the previous section. The predetection operation involves the formation of the product z*w where z represents the transfer function complex amplitude at the center of the band and w represents the complex amplitude of the data channel. As in (3.55), we represent

$$w = \rho z + \sqrt{1 - |\rho|^2}\ \mu \tag{3.96}$$

where μ and z are uncorrelated,

$$\overline{z^* w} = \rho \tag{3.97}$$

and we have normalized

$$\overline{|z|^2} = \overline{|\mu|^2} = \overline{|w|^2} = 1 \tag{3.98}$$

In the present case,

$$\rho = q(F) \tag{3.99}$$

where $q(\Omega)$ is the frequency correlation function of the channel

$$q(\Omega) = \overline{T^*(f,t)T(f+\Omega,t)} = \int Q(\xi)\ e^{-j2\pi\Omega\xi}\ d\xi \tag{3.100}$$

Assuming that mean path delay has been included in the definition of time origin, we find the following expansion dual to (3.58):

$$q(F) \approx 1 - \frac{\pi^2 L^2 F^2}{2} + \ldots. \tag{3.101}$$

where L is the rms multipath spread of the channel. Assuming small decorrelation

$$w = z + \pi L F \mu \tag{3.102}$$

Normally, the received signal is accompanied by noise

$$w = z + \pi L F \mu + \eta \tag{3.103}$$

from which we see that frequency-selective fading adds an effective noise component. If $P_e(S)$ is the error rate without selective fading, then the error rate with selective fading will be $P_e(S_{eff})$ where

$$S_{eff} = \frac{S}{1 + S(\pi L F)^2} \tag{3.104}$$

For a numerical example we note that if multipath spread is to have negligible effect at an SNR of 16 dB

$$L F < \frac{1}{60} \tag{3.105}$$

For a troposcatter link with an rms multipath spread of 1/3 μs, (3.105) leads to a maximum allowable separation frequency between the reference and the data of 50 kHz.

To summarize, we note that to handle the general case of error rate estimation due to frequency-selective fading, certain integrals over the delay power spectrum $Q(\xi)$ are needed. In some cases these are conventional moments, in others single-sided moments and integrated tails of $Q(\xi)$. Only in the case of channel measurement errors due to frequency-selective fading do we find direct performance prediction possible from the single rms multipath spread parameter. However, degradation will increase uniformly with this parameter and it should be possible to use it to flag atypical frequency-selective distortion.

3.1.2.3 Interference

It is assumed that under normal operating conditions, interfering signals will not be present. When they are present, it is essential (as a minimum) to flag this condition. Additional

information concerning the gross structure and specific statistical parameters of the noise would be helpful in identifying the source of noise and, if desired, estimating modem performance.

The presence of an interfering signal can be determined by an increase in the power level of the received signal when averaged over the fading. Of course, this procedure will only be effective if no changes took place in the transmitted power and if nonstationary changes in fading conditions are sufficiently small over the averaging time used to establish the power level. The former type of change would not normally be a problem since it should be monitored at the transmitter and telemetered to a central technical control facility. The latter type of changes are unavoidable and their harm depends upon the degree of nonstationarity. There will generally be an optimum averaging time to estimate power level since too long a time causes nonstationary effects to degrade performance while too short an integration time does not average out the fading fluctuations sufficiently.

The presence of interference can sometimes be recognized by the change in shape of the power spectrum if the interference is not broadband. A simple method for distinguishing between narrowband and broadband interference is to examine the centroid and rms bandwidth of the received power spectrum. A narrowband interfering signal at band center will cause the rms bandwidth of the spectrum to become smaller while a narrowband interfering signal off band center will cause a shift in the centroid of the power spectrum. Thus, the centroid and rms bandwidth are useful parameters for distinguishing between narrowband and broadband interference. Of course, if a full spectrum estimation is carried out, a variety of pattern recognition techniques could be employed for making such a distinction.

The only general study of the effect of arbitrary noise on modem error performance over fading channels has been carried out by Bello [3.1],[3.14]. It has already been proven here in Section 3.1 that the error rate is primarily dependent only on the average noise power at high SNR's for some rather general classes of fading and additive noise statistics. This suggests that reasonably tight bounds on error rate can be achieved with minimal knowledge of the statistics of the interference, as has been demonstrated in [3.1] and [3.14].

Unlike Gaussian noise, the statistics of noise at the output of a filter are not simply related to those at the input and to the filter transfer function. In fact, no general formulae exist

at the present time for relating input and output statistics when non-Gaussian noise is filtered. The only general theorem useful in this regard is the Central Limit Theorem which allows the filter output to be approximated by Gaussian noise when there are a large number of independent noise fluctuations in one time constant of the filter.

Since all receivers employ filters for discriminating against noise, it is necessary to deal with the noise components of decision variables in bounding performance if non-Gaussian noise is to be handled. One may then try to work backward from the parameters of the noise components of decision variables to those of the broadband input noise, or else assume the existence of processing operations which allow the direct estimation of decision variable noise parameters.

The decision variable noises of interest are either sampled outputs of filters or linear combinations of mark-space filter outputs. We consider the simplest case for discussion purposes, binary PSK transmission. Assuming complex Gaussian fading and predetection maximal ratio diversity combining, it is shown [3.1], [3.14] that the error rate depends only on the composite noise variable

$$U = \sum_{m=1}^{M} |\eta_m|^2 \tag{3.106}$$

where η_m is the matched filter output noise for the m^{th} diversity channel and M is the order of diversity. In particular,

$$P_e = \int_0^\infty W(U)G(U)\,dU \tag{3.107}$$

where W(U) is the density function of U and

$$G(U) = \frac{1}{2}\left[1 - e^{-U} \sum_{-(M-1)}^{(M-1)} I_r(U)\right] \tag{3.108}$$

and $I_r(U)$ is the modified Bessel function of order r. In (3.100) the signal component at the decision variable output has been normalized to unit strength so that the individual noise variables $\{\eta_m\}$ are actually instantaneous noise-to-average-signal power ratios.

In [3.14], upper and lower bounds on error probability due to additive noise were derived as a function of an SNR constraint assuming that two practically meaningful peak constraints exist for the additive noise. One of these constraints is a maximum allowable value for the ratio of peak-to-average noise power, i.e., a constraint on the maximum "crest factor" of the detected noise β. The other constraint is a maximum allowable value for the ratio of peak noise power to average signal power γ in the absence of noise. This constraint arises from the finite dynamic ranges of receivers, which cause the outputs to saturate for sufficiently high input voltages. A receiver is designed to have sufficient dynamic range to handle a specified class of input signals having certain mean and peak powers. One may thus assume that detected noises cannot exceed the design value of output signal power by more than some factor.

For moderate crest factors, the bounds are surprisingly close and, for nondiversity operation, the upper and lower bounds coincide for large SNR. For $B \leq 10$, they are only around 2 dB apart at 15 dB SNR.

Upper and lower bounds on error probability in terms of moments of the generalized noise variable U are given in [3.2] as

$$\frac{C_L}{\rho^L}\left(1 - \frac{D_L}{\rho}\right) < P_e < \frac{C_L}{\rho^L} \tag{3.109}$$

where ρ is the SNR at the matched filter output,

$$C_L = \overline{\mu^M}\,\frac{M^M}{2^{2M}M!} \tag{3.110}$$

$$D_L = \frac{\overline{\mu^{M+1}}}{\overline{\mu^M}}\left[\frac{M(2M+1)}{4(M+1)}\right] \tag{3.111}$$

in which μ is the normalized noise variable

$$\mu = \frac{U}{\overline{U}} \tag{3.112}$$

which has unit mean value. The moments in (3.111) and (3.112) can be expressed in terms of $F(\mu)$, the amplitude probability distribution of μ, as

$$\overline{\mu^m} = m \int_0^\infty \mu^{m-1} F(\mu)\, d\mu \tag{3.113}$$

where

$$F(\mu) = \Pr\left\{\frac{U}{\overline{U}} > \mu\right\} \tag{3.114}$$

As a result of (3.110), at large SNR the binary PSK error rate becomes

$$P_e \approx \frac{1}{(4\rho)^M} \frac{\overline{\mu^M}\, M^M}{M!} \tag{3.115}$$

and a single moment of the noise is required to estimate error rate. Note that since, by hypothesis,

$$\overline{\mu} = 1 \tag{3.116}$$

we find for nondiversity operation that

$$P_e \approx \frac{1}{4\rho} \tag{3.117}$$

independent of noise statistics.

The more the information measured on the noise statistics, the better the estimation of error rate. Thus one may develop a crude histogram, as suggested in [3.14], and develop tighter upper and lower bounds or else use different parameters of the noise. For example, in Section 5, upper and lower bounds are derived with the crest factor constraint replaced by a threshold exceedance probability constraint. Generally speaking, it does not appear that very precise knowledge of noise statistics is necessary to closely bound error rates for deep fading channels utilizing moderate orders of diversity.

3.2 Media Quality Unit

This subsection develops the basic signal processing structures proposed for the MQU, discusses its use in relation to the PMU to estimate receiver degradation trends and distinguish outages in the receiver from those in the media, and investigates implementation alternatives. Section 3.2.1 presents an overview of channel monitoring techniques, and Section 3.2.2 presents the rationale for the study emphasis on estimation techniques utilizing the information-bearing signal alone with pickoff of signals as close to the antenna as possible. Finally, Section 3.2.3 presents a block diagram of the MQU subsystem and a discussion of their use in channel quality monitoring.

3.2.1 An Overview of Channel Monitoring Techniques

In this section we present an overview of channel monitoring techniques to place the techniques selected for study in proper perspective. Figure 3.1 presents a breakdown of attributes for channel monitoring techniques. The first breakdown shown is according to physical location and traffic continuity.

With regard to physical location, one may consider two mutually exclusive approaches:

- Self-test units for communication subsystems built-in by manufacturer
- External test hardware applied at appropriate interfaces between communication subsystems

The use of self-test and fault indication circuits is becoming standard procedure in manufacturing communication subsystems, particularly in digital implementations, because of the complexity of large systems. Clearly, the outputs from these self-test units are of direct relevance to the quality of a channel.

The other channel quality monitoring techniques involve specially built test hardware applied to appropriate interfaces of the communication system. One may identify three classes of such techniques depending on where the interface is located:

- Techniques applied to RF interfaces
- Techniques applied to IF interfaces
- Techniques applied to baseband interfaces

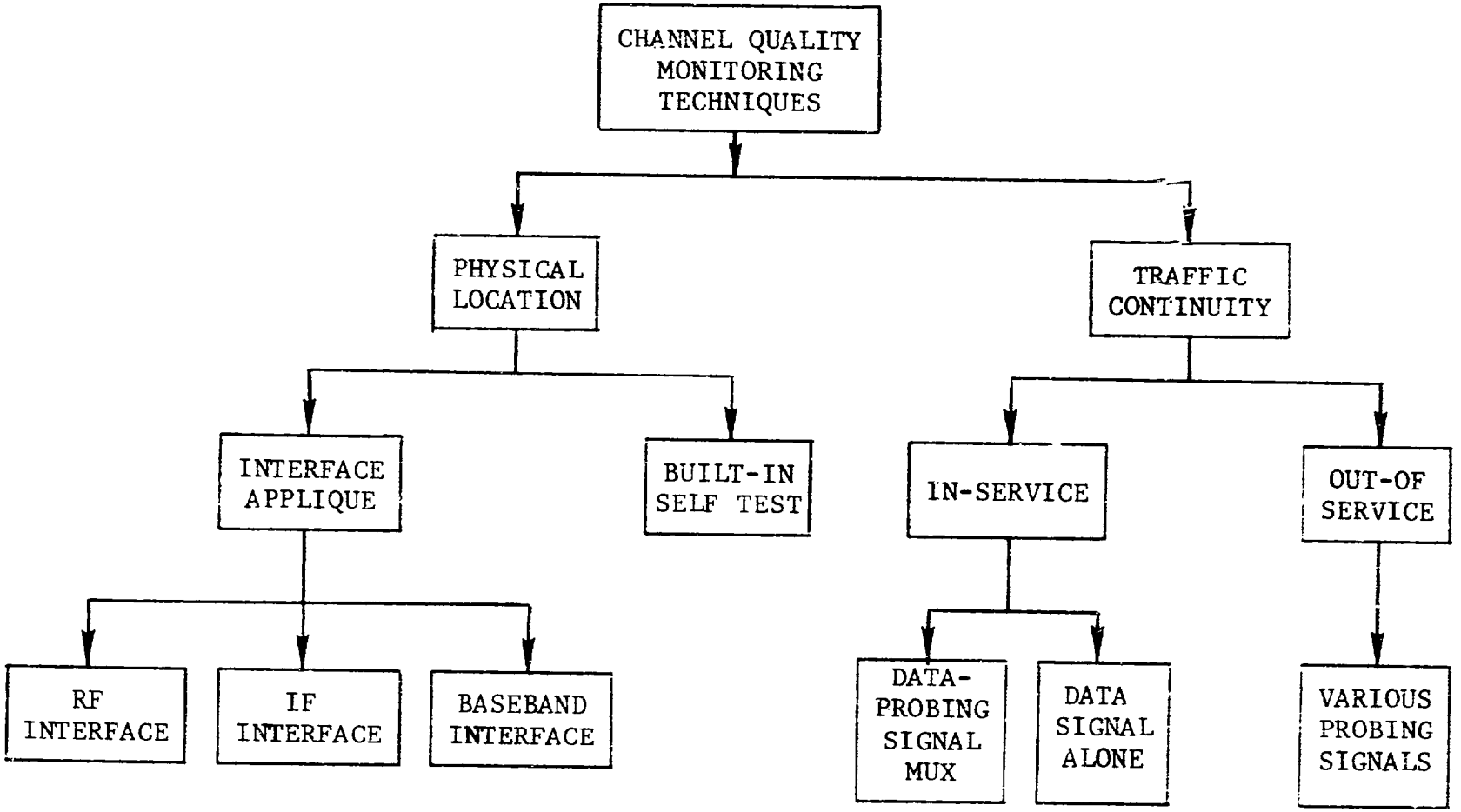

Figure 3.1 A Breakdown of Channel Quality Monitoring Techniques

As the interface is moved from the front end to the information sink in the receiver, more and more hardware is being included in the definition of a "channel". By considering the simultaneous use of monitoring techniques at each of these interfaces, it is possible to isolate faults and degradations to subsystems lying between monitored interfaces.

"Traffic continuity" is a property of a channel measurement technique which describes whether traffic can occur during monitoring or not. Thus, channel monitoring is said to occur "in-service", i.e., while data is flowing, or "out-of-service". In the latter case, traffic has to be interrupted so that channel parameters can be measured.

For out-of-service operation, channel parameter measurements other than those of additive noise require the use of special probing signals and processing techniques. A wide variety of probing signals are possible, the most typical being tones or psuedo-noise (PN) probes.

For in-service operation, probing signals may also be used but they must be multiplexed in with the data signal. Generally speaking, one may consider orthogonal (e.g., FDM, TDM) and non-orthogonal multiplex approaches. In the case of FDM, a frequency slot either in-band or out-of-band would be provided. A probing signal could be sent in this slot to be used for channel parameter measurement or else the slot could be left empty, providing the means for estimating noise characteristics. A dual approach could be used for TDM, with the received probing signal or noise being recovered by appropriate demultiplexing. A popular example of nonorthogonal multiplexing is the use of a wideband probing signal and data signal in the same band. Another possibility is the addition of very low level tones. In either case, careful consideration must be given to the mutual interference created by the nonorthogonal multiplexing.

Even without special purpose probing signals, useful channel information can be obtained by processing the received information bearing signal itself, regarded as a wideband "noise" probe which is unknown at the receiver.

3.2.2 Rationale for Study Emphasis

The use of the received information-bearing signal alone for channel measurement, when effective, has clear advantages over the other approaches: no instrumentation for generation of

probing signals, no loss in channel capacity, no multiplexing and demultiplexing equipment, and in-service operation.

Figure 3.2 presents a classification of measurement techniques which use the data signal alone. We first subdivide these techniques into two subclasses depending upon whether or not signals normally present inside the data demodulator (e.g., decision variables, binary decisions, bit synchronization, etc.) are involved in the channel measurement process. Each of these subclasses is further divided into two parts. In the case of signal processing external to the data demodulator, we subdivide into measurements at RF and IF and measurements at baseband. In the case of signal processing involving signals within the data demodulator, we subdivide into those techniques that depend on utilization of the values of digital decisions (e.g., decision-directed techniques) and those that depend only on the decision variable (e.g., integrate-and-dump outputs).

We first discuss some channel measurement techniques that utilize processing within the data demodulator. All the techniques reported in the literature are both decision-dependent and decision-variable-dependent. Thus, Epstein and Franco [3.15] (using the basic error rate formulation of incoherent and differentially coherent systems in the presence of fading multipath formulated by Bello and Nelin [3.9]) classify integrate-and-dump outputs for different triplets or quadruplets of transmitted bit sequences. This classification reveals different dependencies on noise, multipath, and signal, from which, by algebraic manipulation, one may estimate noise, multipath, and SNR for FSK and DPSK systems. Similarly, Hingorani and Chesler [3.16], in developing an error rate prediction technique based upon the error rate formulations of Bello [3.1],[3.14], show that the noise component of the decision variable may be estimated if the bit decision information is available.

These techniques and their obvious decision directed generalizations will only estimate the channel parameters if

1) there is a modest, but not high, error rate (because of the decision direction),

2) bit synchronization exists,

3) the modem has suffered no equipment failure.

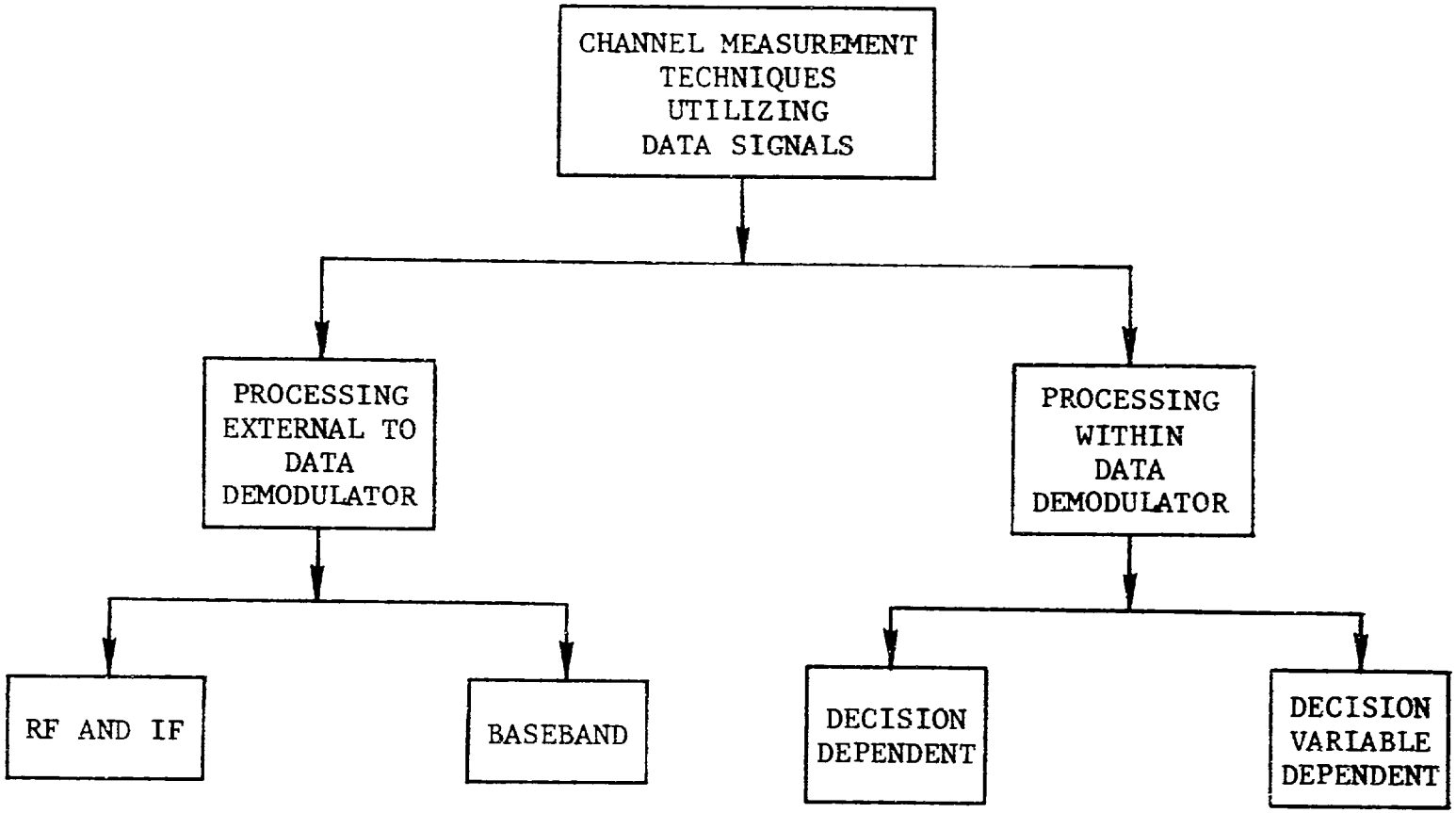

Figure 3.2 Categorization of Measurement Approaches Which Use Data Signals Alone

Since a main objective of the study is to develop techniques which will allow an assessment of receiver degradation trends and also allow a distinction to be made between propagation outages and equipment failure, the excessive dependence of the above techniques upon modem operation makes them highly undesirable for channel measurement.

If channel measurement techniques appropriate to the objectives of this study are to be utilized which depend upon variables within a modem, then these variables should at least be independent of bit synch and bit decisions. Unfortunately, there is little of a general nature that may be said about the existence of these techniques, because they would depend very intimately upon the detailed structure of the modem signal processing. For example, the FSK/PSK digital troposcatter modem designed by Bello [3.17] utilizes pilot tones. The relative amplitude fluctuations of these pilot tones can be used to estimate frequency selectivity and multipath spread. However, some modems will not use pilot tones and such an approach would be inapplicable.

For the above reasons no effort was expended upon studying channel measurement techniques that involve the data demodulator. This does not mean that effective utilization of variables in the data demodulator cannot take place in some technical control functions. In particular, raw error rate estimation by a PMU (performance monitor unit) can be carried out effectively by using data demodulator variables, as discussed by Gooding [3.18]. However, the development of performance monitoring techniques per se is not within the scope of the present study. It is assumed that an effective PMU exists.

In considering measurement techniques external to the data demodulator, we have pointed out that processing can occur after the demodulator, at baseband, or before the data demodulator at RF or IF. One may readily dispose of baseband processing as being an important source of channel measurement for the present effort. Note that much of the receiver instrumentation has been traversed by the time this point has been reached, so that channel and receiver degradations are very much intermixed in their effect on the reconstructed digital sequence. At this point the only parameter than can be available for discrimination between channel and receiver degradations is the distribution of detected errors. While some gross distinctions can probably be made between error patterns induced by bad channel conditions and those induced by equipment malfunction, it is also clear that considerable confusion is possible.

In view of the above, we have concentrated our efforts primarily on the use of the received signal alone for channel measurement. Moreover, in developing ooncepts for channel measurement utilizing the data signal, we have confined our attention to techniques which examine received signals at RF and IF interfaces. In essence, the data signal is regarded as a random probing signal with known statistical characteristics at transmission.

3.2.3 Proposed System Configuration

Drawing upon the results of the previous sections, a signal processing structure has been conceived for establishing receiver degradation trends and discriminating between media and receiver-induced performance degradation. This structure is sketched out in Figure 3.3 for the most complex case, the quadruple diversity troposcatter channel. For the other channels, some simplifications of this structure are possible; e.g., for the LOS channel, no average error rate estimation and no gross (i.e., average) channel parameter estimation would be carried out.

Examination of Figure 3.3 reveals that two basic subsystems, labeled MQU (media quality unit) and PMU (performance monitor unit), are used to eventually reach conclusions with regard to degradation trends, cause of outage, and the existence of intermittent faults. The PMU estimates the actual raw error rate of the digital signal passed forward to decryption, decoding, and demultiplexing operations. The effective design and operation of this unit is a subject outside the scope of the present study, where it is merely assumed that such a unit exists. The primary purpose of the MQU, which is the focus of the present study, is to provide error rate estimates for a hypothetical nondegraded receiver based upon information concerning the media characteristics. A comparison of the MQU and PMU average and short-term error rate estimates then allows an estimation of receiver degradation trends, performance margins, and intermittent faults. Of course, it also allows an identification of abrupt outages caused by receiver malfunction. A secondary purpose of the MQU is to provide an indication and identification of the rare outages caused by excessive Doppler spread (i.e., fast fading), multipath spread (i.e., frequency-selective distortion), and interference.

The inputs to the MQU come from appropriate pickoffs at RF or IF for each of the diversity receivers. As pointed out previously, the pickoff should be as close to the antenna as feasible to avoid confusing receiver degradation from channel impairments. AGC (automatic gain control) complicates some channel measurement

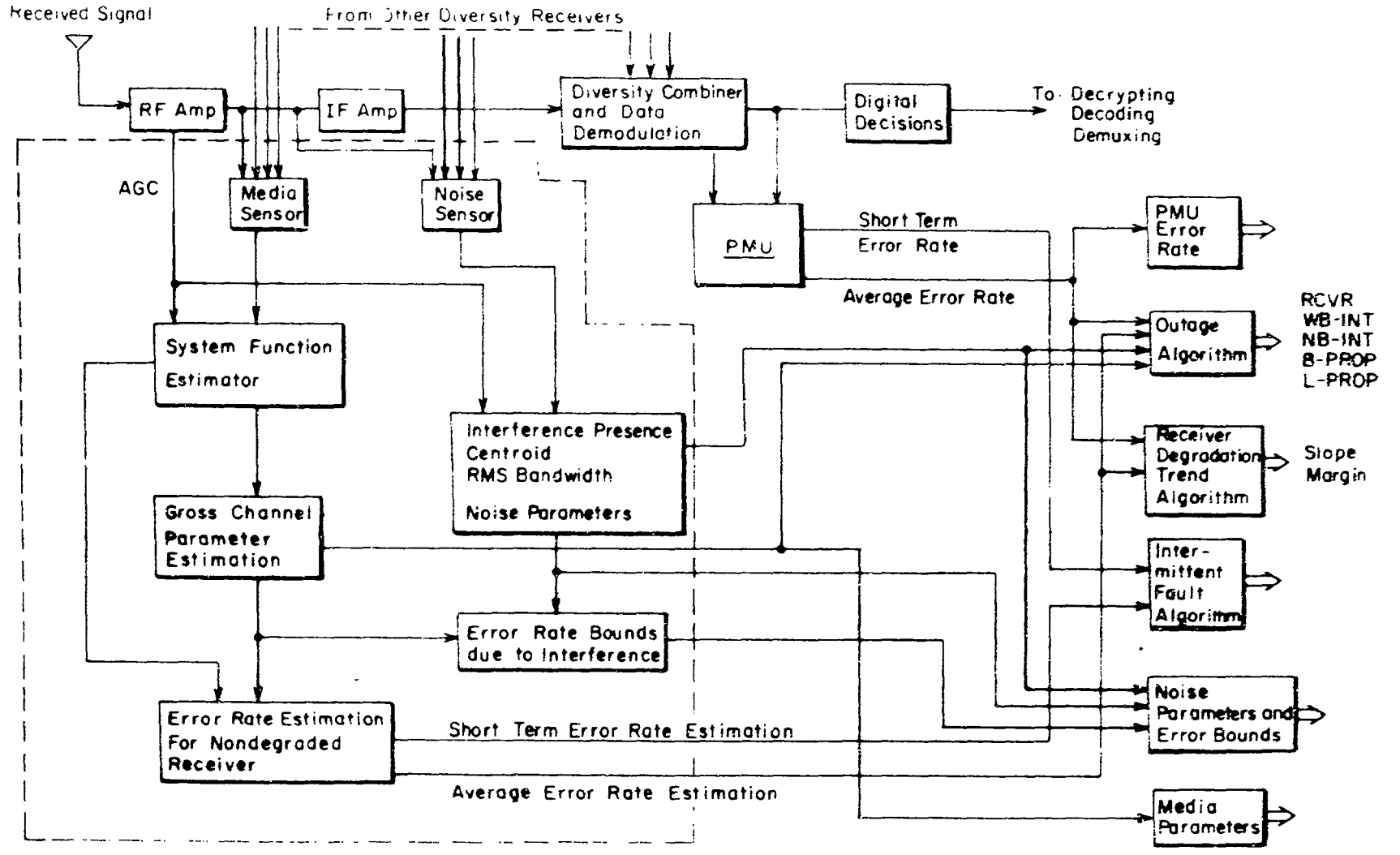

Figure 3.3 Proposed Signal Processing Structure for Establishing Receiver Degradation Trends and Discriminating Between Media and Receiver Induced Degradation

functions by providing a variable gain not existing in the media itself. To account for such gains, it is assumed that those AGC voltages affecting the signal level used as input to the MQU are also picked off and that gain vs. AGC calibration curves are stored in the MQU where they are periodically updated.

The picked-off signals are filtered and brought to baseband in the media and noise sensors in preparation for further processing in the MQU. If the received information-bearing signal alone is to be used for channel measurements, the output of the system function estimator would be estimates of the squared magnitude of the transfer functions for the diversity channels at one or more frequencies within the signal bandwidth. A detailed analysis of the use of short-term power measurements to achieve estimates of the squared magnitude of the channel transfer function is presented in Section 4. Figure 3.4 shows a possible signal processing structure for one diversity channel and one frequency location within the diversity channel. Obvious time-multiplexed serial and/or parallel processing arrangements may be used to handle all diversity channels and all frequency samples required. The bandwidth of h(t) is selected small enough so that little frequency selectivity occurs over its passband. The time constant of k(t) is much longer than that of h(t) to average out the data noise fluctuations but short enough not to average over the fading. With specified shapes for h(t),k(t), it is shown in Section 4 that it is possible to optimize the bandwidth of the predetection filter h(t) and the time constant of the postdetection filter k(t) so as to minimize the combined effects of data noise, noise, frequency-selective fading and time-selective fading.

If special probing signals are used, the sensor system function estimator processing shown in Figure 3.4 would have to be replaced by an appropriate probe demodulator, such as the correlation processor shown in Figure 6.1 of Section 6. However, the remainder of the structure shown in Figure 3.3 would stay the same. For purposes of discussion, we assume that only the information-bearing signal is used to obtain channel information and that the squared magnitude of the diversity channel transfer functions are determined at selected frequencies by a structure like that shown in Figure 3.4.

With the aid of noise power measurements and removal of AGC gain fluctuations one may scale the squared-magnitude transfer function measurements so that they will represent instantaneous SNR's for each diversity branch. As discussed in Section 3.1

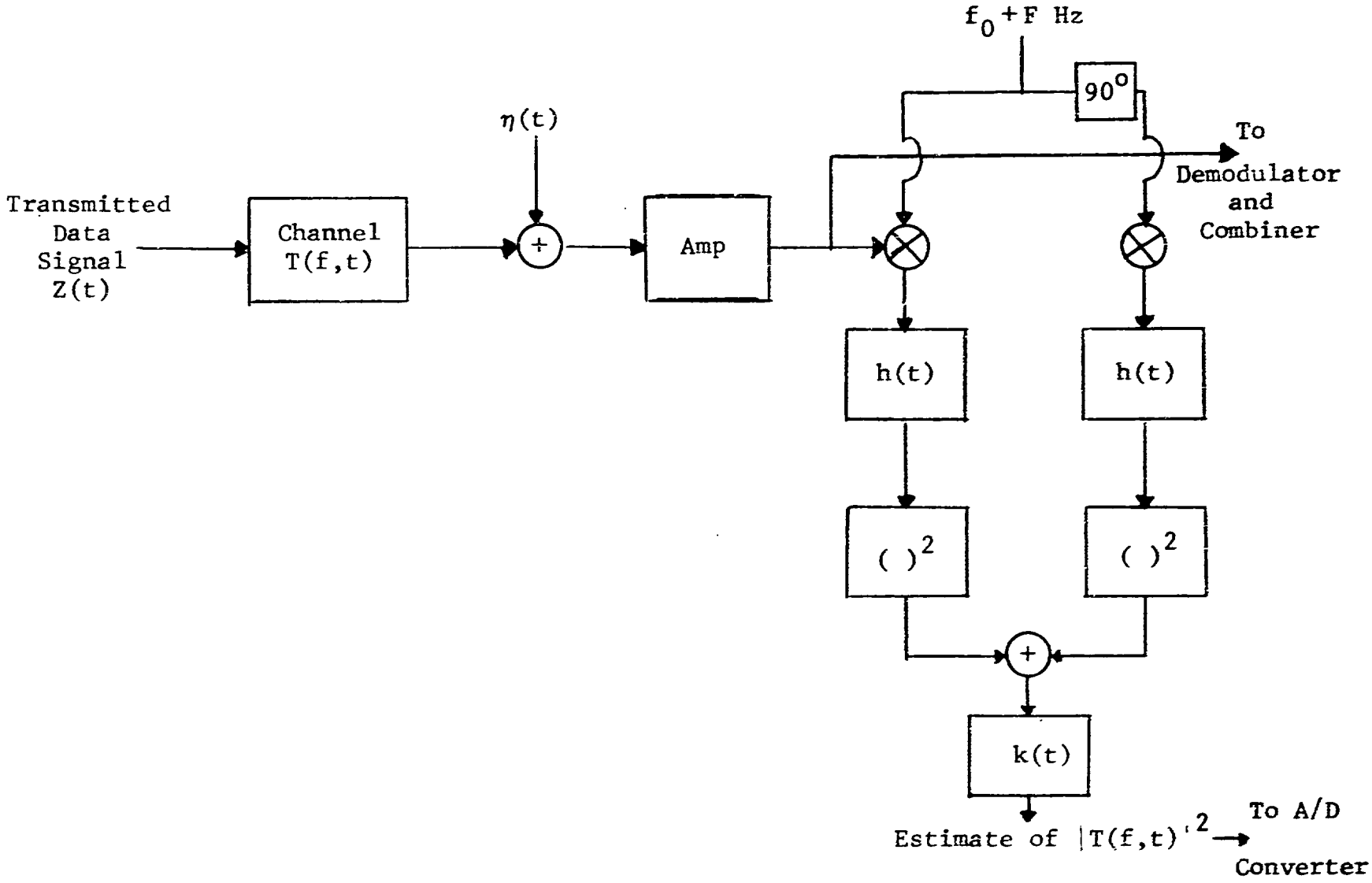

Figure 3.4 Estimator of the Magnitude Squared of the Channel Transfer Function for One Diversity Channel

and analyzed in Section 5, one may use these instantaneous SNR's in appropriate algorithms to estimate the average and short-term error rate for a nondegraded receiver. Multipath and Doppler spread can also be estimated from the squared magnitude of the diversity channels' transfer functions, as discussed and analyzed in Section 4. These parameters can be used to flag outages due to excessive multipath and Doppler spread. However, as discussed in Section 3.1, only with special probing signals which yield estimates of the complex transfer function and/or impulse response can enough information be obtained to estimate error rates due to excessive multipath.

The noise sensor would utilize out-of-band noise or time-multiplexed signal-free slots to estimate noise parameters (see Section 4.5) for determining bounds on error rate (see Section 5) when an interfering signal has been flagged by the interference-present detector. The latter detector compares the measured average received power on each diversity channel for two adjacent time intervals, looking for significant changes in power level (see Section 4.4.3). Additional information on interference-presence is available from the narrowband interference detector which uses changes in the centroid or rms bandwidth of the received signal as a detection criterion (see Section 4.4.2 for an analysis). If noise slots are available adjacent to the signal band, they also can provide information concerning the presence of an interfering signal.

Under normal conditions, excessive multipath and Doppler spread or interference will not be present. When this is the case, the average and short-term error rates estimated by the MQU are compared with those measured for the receiver by the PMU. A steady and increasing departure of these error rates will indicate the presence of a degradation trend in the receiver. A comparison of short-term error rates will allow a determination of whether the receiver degradation is due to an intermittent receiver fault.

When an outage occurs, the measurements shown in Figure 3.3 should allow it to be categorized into one of the following:

- Receiver outage
- Wideband interference
- Narrowband interference
- Propagation, due to excessive Doppler spread (B)
- Propagation, due to excessive multipath spread (L)

Because of the slowness of fading on the links of interest, it is clear that a considerable amount of the signal processing indicated in Figure 3.3 can be carried out by small computers. However, the sensor uses analog processing and, except for HF channels, the short-term power measurement used to estimate the squared-magnitude transfer functions would have to be implemented with hardware. Some general implementation considerations are presented in the following section.

3.3 Implementation Considerations

This section discusses implementation of the MQU assuming the information-bearing signal alone is used to derive channel information. It focuses on the hardware and computation requirements and shows how these depend upon the media parameters. In accordance with both the emphasis of the work statement and the current trends in technology, the implementation discussed is as digital as is reasonably possible, and the digital processing is done by programmed hardware (computer) whenever possible.

Our goal in this section is to delineate the implementation problems of potential media quality units and to show the division between analog, hardwired digital, and programmed digital hardware for each case. Estimation of the magnitude squared of the channel transfer functions is the major calculation, and it dominates the system.

Consider the system diagram shown in Figure 3.3. Given the RF or IF input signals, the MQU computes an estimate of the magnitude squared of the channel transfer function and, from this estimate, calculates other desired channel parameters and error rate estimates. In what follows we discuss first estimation of the magnitude squared of the channel transfer function and then discuss the remaining computation burdens given that the magnitude squared of the channel transfer function has already been computed.

3.3.1 Estimation of the Magnitude Squared of the Channel Transfer Function

Figure 3.4 shows the estimation of the squared-magnitude transfer function in block diagram form. Figure 3.5 displays a maximally digital implementation of this estimator. The signals are mixed down from IF or RF, passed through an analog lowpass filter to prevent aliasing, and then converted to digital samples. All further filtering is then performed digitally either in

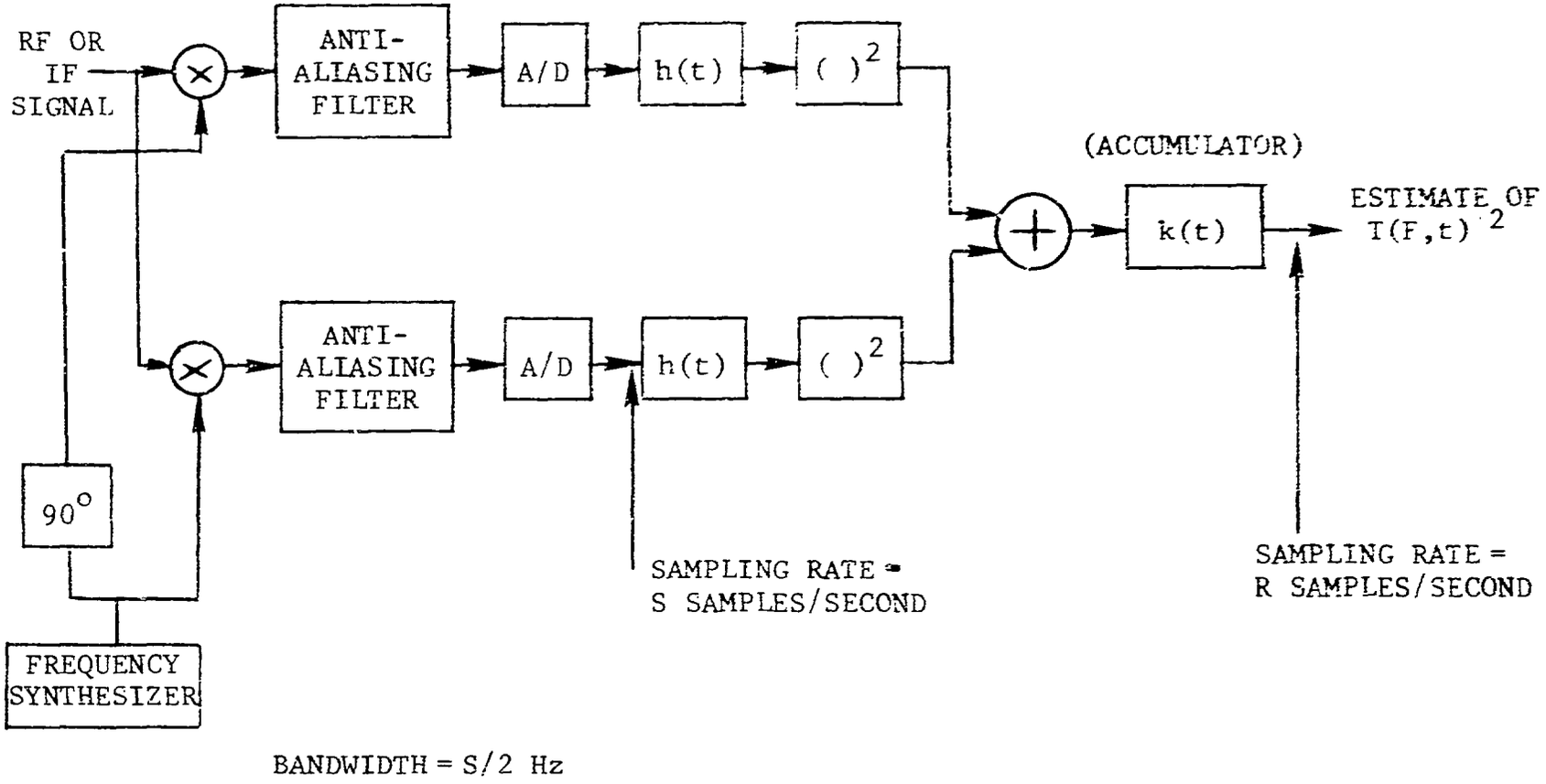

Figure 3.5 Maximally Digital Implementation of Estimator of the Magnitude Squared of the Channel Transfer Function

hardwired logic or a computer, depending upon the data rate. (As an aside, notice that this design is not necessarily the maximally possible digital form for the HF channel. Because of the low IF and narrow bandwidths involved, it would probably be technically possible to do the anti-aliasing filtering and sampling at IF.)

The essential parameters of this system are the bandwidth of the filters h(t) and the duration of the integrating filter k(t). The bandwidth of the predetection filter h(t) determines the minimum sampling rate S, and thus determines the anti-aliasing filters.

Table 3-1 presents optimum predetection filter bandwidths from Section 4 together with calculated minimum sampling rates corresponding to a sampling frequency of twice the filter bandwidth. Since h(t) is only a two-pole lowpass filter and W_{opt} is the 6-dB bandwidth, this sampling rate is only approximate. However, for the purposes of the present discussion they will be close enough to give a good idea of the implementation problems.

These sampling rates determine the implementation technique used. Consider first HF, and count only multiplication operations. A second-order filter for h(t) would require two multiplications per sample. Squaring the output of h(t) requires one more multiplication per sample. Allowing for dual diversity and both an in-phase and quadrature signal path filter required, a total of $12 \times 300 = 3600$ multiplications are required each second.to implement the h(t) filters. However, the measurement of rms multipath spread requires that $|T(f,t)|^2$ be estimated for at least two frequencies within a diversity channel. Thus, we arrive at $2 \times 3600 = 7200$ multiplications per second. Similarly, using the sampling rates given above and maximal diversity as indicated, we obtain Table 3-2.

The filters for the HF channel can easily be accommodated in a modern minicomputer or future microprocessor. At 7200 multiplications per second, there are about 139 microseconds available for each multiply. But current minicomputers perform a multiplication in 5 to 20 microseconds. Thus, for an HF channel, the h(t) filters would occupy less than 20% of minicomputers' available processing time.

The tropo channel and LOS (30-dB fade) parameters are comparable. The required sampling rate on one signal path is 173 and 226 kilo samples per second, or about 5.8 and 4.3 microseconds

TABLE 3-1

OPTIMUM BANDWIDTHS FOR h(t)

Channel	W_{opt}† (Hz)	Minimum Sampling Rate (samples/second)
HF	1.5×10^2	300
LOS*	8.64×10^4	173,000
Tropo	1.14×10^5	226,000
Satellite, Ionospheric Scintillation (1.6 GHz)	10.1×10^6	20.2 million

*Filter parameters optimized for measurements at a fade depth of 30 dB.

†It is assumed that the transmitted signal bandwidth exceeds W_{opt}. Otherwise the predetection filter bandwidth would be set equal to that of the transmitted signal bandwidth.

TABLE 3-2

COMPUTATION REQUIRED FOR $\hat{h}(t)$ FILTER

Channel	Maximal Diversity	Multiplications/second for $\hat{h}(t)$
HF	2	$2 \times 3 \times 4 \times 300 = 7200$
LOS	2	$2 \times 3 \times 4 \times 1.73 \times 10^5 = 4.16 \times 10^6$
Tropo	4	$2 \times 3 \times 8 \times 2.26 \times 10^5 = 1.68 \times 10^7$
Satellite, Ionospheric Scintillation	2	$3 \times 4 \times 20.2 \times 10^6 = 2.4 \times 10^8$ *

*Multipath spread measurement is probably not of interest for this channel

per conversion. This is well within the range of today's inexpensive 12-bit A/D converters. However, the complete multiplexing of A/D's for diversity operation would yield too high a conversion rate and some parallel processing would have to be used.

The arithmetic burden of 4 to 10 million multiplies per second is too great to load onto a processor and further hardwired digital filters arranged for parallel processing would have to be implemented at these data rates.

The high sampling rates of the optimized 1-GHz ionospheric scintillation channel mandate an analog implementation.

The above discussion was predicated upon values of W_{opt} equal to the optimal bandwidths of the h(t) filter to minimize the estimator variance. The sampling rate and computation burden are a linear function of this bandwidth. One possible design alternative,which is applicable to all except the HF channel, is to decrease the bandwidth of h(t), degrading performance to some still satisfactory level, but simplifying implementation.

A block diagram of a maximally analog implementation of the estimator is shown in Figure 3.4. Notice how few extra analog components are required compared to the maximally digital implementation. Analog filters are needed for h(t) but the anti-aliasing filters have disappeared. Thus the circuit has actually simplified.

Next comes a squaring circuit which can be implemented at the frequency bands of interest by an analog multiplier module. Finally there is a summing junction followed by an integrate-and-dump to implement the filter with impulse response k(t). The output of the integrate-and-dump is A/D-converted and fed to the digital processor. Table 3-3 tabulates values of optimum integration time T_{opt} for a rectangular impulse response filter derived in Section 4. If a sample is taken from the filter with impulse response k(t) after each integrate-and-dump on each diversity path, the sampling rates shown in Table 3-3 are obtained.

The entry for the tropo channel is not unusual for strategic links but it is low for tactical links since it is based upon an rms Doppler spread of 1 Hz. A more representative value for tactical links is an rms Doppler spread of 20 Hz. With quadruple diversity the total sampling rate might be as high as 1300 samples per second. Even this worst case is still slow compared to the rates of current technology A/D converters and computer interfaces.

TABLE 3-3

SAMPLING RATES

Channel	Diversity	T_{opt} (s)	Sampling Rate (samples/s)
HF	2	0.53	3.7
LOS*	2	0.49	4.1
Tropo	4	0.059	67.8
Satellite, Ionospheric Scintillation	2	0.088	22.7

*30-dB fade measurement estimation

Comparing the digital and analog implementations of the estimator of $|T(f,t)|^2$, the following conclusions can be drawn:

1) Except for the HF channel, the filters with impulse response h(t) should probably be analog filters and could replace the anti-aliasing filters if the design is carried out carefully.

2) If all the digital processing is to be done in a computer, then a maximally analog implementation of the estimator of $|T(f,t)|^2$ is probably best. This conclusion is based upon today's components and prices.

3) Hardwired digital filters could be used to implement both the squaring operation and the post-detection filters except in the satellite channel. However, this digital processing does not significantly simplify the design.

3.3.2 Estimation of RMS Doppler Spread and RMS Multipath Spread

Three techniques will be presented in this report in Section 4 for calculation of $\hat{B}$, an estimate of B, the rms Doppler spread of the channel. These are called the level-crossing method, the differentiation method, and the correlation method. Each of these techniques takes, as given, the estimates of the magnitude squared of the channel transfer function, and uses these estimates to calculate $\hat{B}$. The best in performance is the level-crossing technique. The major part of the computation burden of the level-crossing technique is the calculation of a square root which might be regarded as equivalent to a few, say three, multiplications. This square root must be calculated for each sampled value of the estimate of squared magnitude of the channel transfer function $|\tilde{T}(F,t)|^2$. Other calculations are required, of course, but the square root is the dominant computation.* The differentiation method provides slightly poorer performance but requires only two multiplications per sample. One of these multiplications is involved in estimating the mean value of $|\tilde{T}(F,t)|^2$, and is common to the differentiation method of measurement of multipath spread. The correlation technique also requires two multiplications for each value of $|\tilde{T}(F,t)|^2$ and has far poorer performance.

*However, note that one may change the algorithm, if desired, to a level crossing applied to $|\tilde{T}(F,t)|^2$ instead of $\sqrt{|\tilde{T}(F,t)|^2}$.

Since the differentiation technique provides almost equivalent performance but with a reduction in computation burden, it seems to be the method of choice unless the level-crossing algorithm is changed to apply to a squared envelope.

Three techniques also exist for estimating the multipath spread on the channel. These techniques are exactly the time-frequency duals of the techniques for estimation of the Doppler spread. However, estimating the multipath spread creates a new problem, as mentioned above, since all methods require estimates of $|T(F,t)|^2$ at more than one value of F. But to do this essentially requires new copies of the circuitry for estimating $|T(F,t)|^2$. The level-crossing technique requires these estimates at many values of F, while both the correlation technique and the differentiation method require estimates at just two values. The correlation method needs one multiplication for each sampling instant as does the differentiation method.

If the formulas for these two techniques are inspected, they will show two multiplications are required, but one of them is also required in estimating the Doppler spread and has already been counted.

3.3.3 Estimation of RMS Bandwidth and Frequency Centroid of Received Signal

As discussed in Section 4, an estimate of the frequency centroid is

$$\hat{\bar{f}} = \frac{\langle x\dot{y} - y\dot{x} \rangle}{\langle x^2 + y^2 \rangle} \tag{3.118}$$

where x is the in-phase and y is the quadrature component of the received signal. The triangular brackets indicate time averages, and these time averages should be over a long enough period to average out the effect of fading on the channel. One technique for implementing this estimator is shown in Figure 3.6. An analog filter is used to differentiate x(t) and y(t). All four signals are sampled at the same instant and the samples held and fed through a multiplexer into an A/D converter. The A/D output is then fed directly into the computer.

Given samples of x, $\dot{x}$, y, $\dot{y}$, it is easy to compute $\hat{\bar{f}}$. Four multiplications are required for each sample taken. Similarly, the estimator of the rms bandwidth is a function of x, $\dot{x}$, y, $\dot{y}$.

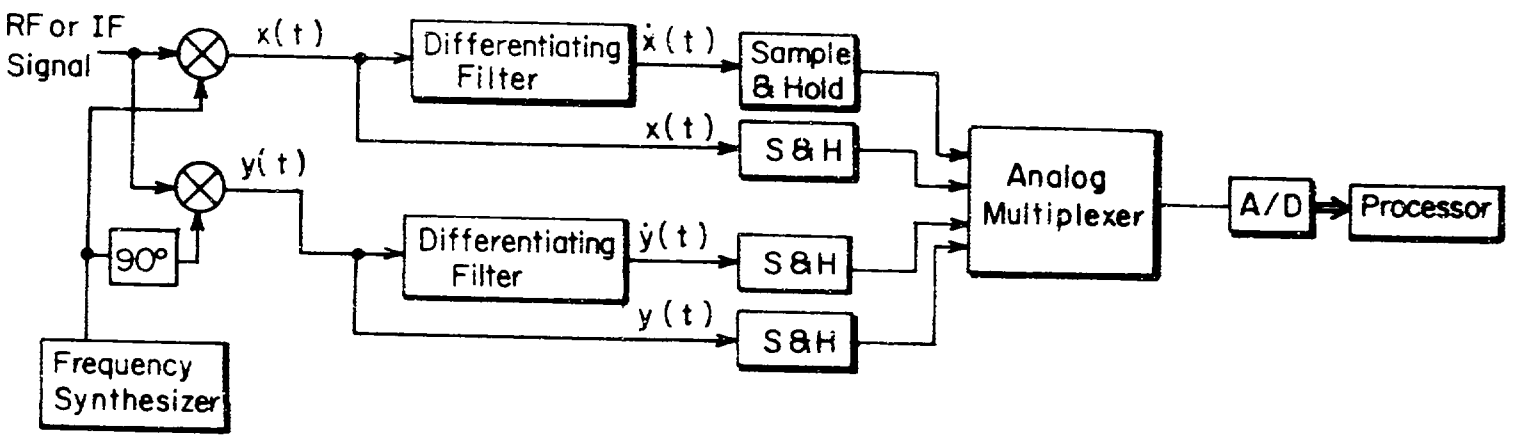

Figure 3.6 Generation of Samples of x, $\dot{x}$, y, $\dot{y}$

Two more multiplications are required for each sample point, in addition to the multiplications used in calculating $\bar{f}$, giving a total computation burden of six multiplications per sample.

3.3.4 Calculation of Estimated P_e

The calculation of the estimate of P_e poses a smaller computation burden in the worst case than might be expected from the complexity of the functions involved [see Eq. (3.14)]. This is due to the diversity combining which reduces the number of data points that need to be processed. An estimate of $|T(F,t)|^2$ can be combined with an estimate of noise to get an estimate of instantaneous signal-to-noise ratio. The estimated instantaneous signal-to-noise ratios on each diversity branch can then be operated on by a function to estimate the conditional probability of error.

The function used would depend upon the specific communications system design but typically would be either an error function or an exponential function. In either case, a rapid yet sufficiently accurate program can be written to calculate the function. For the sake of argument, we shall assume that calculating this function is equivalent to six multiplies. This would allow using several comparison operations to select an approximation formula valid for the value of the argument and then evaluating a fourth-order polynomial approximation. The averaging of the conditional error rate to compute average error rates involves the use of accumulators.

3.3.5 Total Computation Burden

Table 3-4 displays the computation needed for each subtask and the total for the specific case of the tropo channel with quadruple diversity, which is a worst case. Notice that a high sampling rate is being used corresponding to fast fading. Consider several points from this table:

1) The computation burden is essentially a linear function of both the order of diversity and the Doppler bandwidth.

2) The estimation of $\bar{f}$ and B imposes half the computation burden. It would be unnecessary to calculate these quantities on all diversity paths if it were assumed that an interference would be received by all diversity branches. Also, this

TABLE 3-4

TOTAL COMPUTATION BURDEN FOR TROPO
(Assuming Use of 500 Samples/Second of $|T(F,t)|^2$
and Quadruple Diversity)

Subtask	Computation Burden	Form	Comments
Estimation of $\|T(F,t)\|^2$	I/O only		This function is performed in hardware, before the computer
Estimation of average SNR	2,000 multiplies/second	1 x 4 x 100	This operation is used in the differentiation method of multipath and Doppler spread measurement
Estimation of Doppler spread	2,000 multiplies/second	1 x 4 x 500	Differentiation technique
Estimation of multipath spread	2,000 multiplies/second	1 x 4 x 500	Differentiation technique
Estimation of total power, $\overline{f,B}$	12,000 multiplies/second	6 x 4 x 500	Sampling rate used is 500 samples/second
Calculation of $\hat{P}_e$	3,000 multiplies/second	6 x 500	
TOTAL	21,000 multiplies/second		

computation is fairly simple and can be easily implemented in digital hardware.

3) Twenty-one thousand multiplies per second corresponds to just under 50 microseconds per multiply. Modern minicomputers, such as the Data General Nova Series or the PDP-11, with hardware multiply/divide have multiplication times in the range from 5 to 20 microseconds. Thus it appears that a safety factor of about 2.5 is available.

An important warning should be inserted here. This discussion of computation burden has focused on multiplications alone and on multiplications that must be done at the input data rate. This focus was chosen because these multiplications are probably more than half of the total computation load. But a safety factor must be allowed on top of the estimates in the table. Before attempting to implement these techniques, the burden of other operations, expecially input/output control, should be examined to insure that the processor chosen can handle the task.

REFERENCES FOR SECTION 3

[3.1] P. A. Bello, "Error Probabilities Due to Atmospheric Noise and Flat Fading in HF Ionsopheric Communication Systems," IEEE Trans. on Comm. Tech. (September 1965).

[3.2] J. Omura and T. Kailath, "Some Useful Probability Distributions," Stanford Electronics Laboratories, Report 7050-6 p. 13, formula 6 (September 1965).

[3.3] S. Stein, Communication Systems and Techniques, Part III, McGraw Hill (1966).

[3.4] P. A. Bello and B. D. Nelin, "The Influence of Fading Spectrum on the Binary Error Probabilities of Incoherent and Differentially-Coherent Matched Filter Receivers," IRE Trans. on Comm. Systems, Vol. CS-10, No. 2, pp. 160-168 (June 1962).

[3.5] P. A. Bello, "Comparative Evaluation of High Speed Digital Data Transmission Techniques over the Troposcatter Channel," ADCOM Research Report No. 16 (30 September 1964).

[3.6] P. A. Bello, "Selective Fading Limitations of the Kathryn Modem and Some System Design Considerations, IEEE Trans. on Comm. Tech., Vol. COM-13, No. 3, pp. 320-333 (September 1965).

[3.7] P. A. Bello, "Some Signal Design Considerations for HF PSK Modems," ADCOM Research Report No. 10 (30 September 1964).

[3.8] P. A. Bello and B. D. Nelin, "Predetection Diversity Combining with Selectively Fading Channels," IRE Trans. on Comm. Systems, Vol. CS-10, No. 1, pp. 32-42 (March 1962).

[3.9] P. A. Bello and B. D. Nelin, "The Effect of Frequency-Selective Fading on the Binary Error Probabilities of Incoherent and Differentially-Coherent Matched Filter Receivers," IEEE Trans. on Comm. Systems, Vol. CS-11, No. 2, pp. 170-186 (June 1963).

[3.10] P. A. Bello and L. Ehrman, "Performance of an Energy Detection FSK Digital Modem for Troposcatter Links," IEEE Trans. on Comm. Tech.,Vol. COM-17, No. 3, pp. 368-379 (June 1969).

[3.11] P. A. Bello and L. Ehrman, "Error Rates in Diversity FDM-FM Digital Troposcatter Transmission," IEEE Trans. on Comm. Tech., Vol. COM-17, No. 2, pp. 183-191 (April 1969).

[3.12] P. A. Bello and T. Crystal, "A Class of Efficient High-Speed Digital Modems for Troposcatter Links," IEEE Trans. on Comm. Tech., Vol. COM-17, No. 2, pp. 162-183 (April 1969).

[3.13] P. A. Bello and B. D. Nelin, "The Effect of Frequency-Selective Fading on Intermodulation Distortion and Subcarrier Phase Stability in Frequency Modulation Systems," IEEE Trans. on Comm. Systems, pp. 87-101 (March 1964).

[3.14] P. A. Bello, "Bounds on the Error Rate of FSK and PSK Receivers due to Non-Gaussian Noise in Fading Channels," IEEE Trans. on Information Theory, Vol. IT-12, No. 3, pp. 315-326 (July 1966).

[3.15] M. Epstein and A. G. Franco, "Medium Disturbance Sensing Techniques for FSK Modulation," IEEE Trans. on Comm. Tech., pp. 76-80 (February 1970).

Also, A. G. Franco, et al., "Adaptive Communication Techniques," Communications and Systems, Inc., Report C&S 68-10, Contract F30602-68-C-0017 for Rome Air Development Center (November 1968). (AD854654)

[3.16] G. D. Hingorani and D. A. Chesler, "A Performance Monitoring Technique for Arbitrary Noise Statistics," IEEE Trans. on Comm. Tech., pp. 430-435 (June 1968).

[3.17] J. W. Graham and P. A. Bello, "A High-Speed TDM Coherent FSK/PSK Digital Data Modem for Troposcatter Links," Record of the IEEE Inter. Conf. on Comm., pp 20-18 - 20-24 (1971).

[3.18] D. J. Gooding, "Performance Monitor Techniques for Digital Receivers Based on Extrapolation of Error Rate," IEEE Trans. on Comm. Tech., pp. 380-387 (June 1968).

SECTION 4

CHANNEL MEASUREMENT TECHNIQUES UTILIZING THE RECEIVED INFORMATION-BEARING SIGNAL ALONE

The proposed MQU incorporates a number of channel measurement functions as discussed in Section 3.2.3 and illustrated in Figure 3.3. This section is devoted to a detailed analysis of various measurement techniques designed to carry out the necessary measurement functions. Expressions are derived for estimation errors and biases as a function of measurement time and bandwidth, multipath and Doppler spread, including the effects of additive noise and data noise.

Section 4.1 is devoted to a consideration of the measurement of the squared magnitude of the transfer function of a channel, $|T(f,t)|^2$, via short-term power measurement in a bandwidth of the order of the coherence bandwidth of the channel. Optimum values of predetection and postdetection bandwidths are shown to exist and are evaluated for specific filter shapes. Numerical evaluations of performance are carried out for the HF, LOS, Troposcatter, and Satellite Ionospheric Scintillation channels.

Section 4.2 considers the estimation of the time-frequency correlation function of the squared-magnitude channel transfer function. This correlation function can be used to estimate channel parameters. The variance and bias of the estimator are evaluated as a function of errors in the estimation of $|T(f,t)|^2$ and as a function of averaging time. As far as average channel correlation functions and channel parameters are concerned, results are given for HF, Troposcatter, and Satellite Ionospheric Scintillation but not for LOS channels. As pointed out several times in previous sections, the LOS channel fading, when it occurs, is very slow and outages occur only during deep fades. The averaging time required to estimate hypothesized channel parameters, such as Doppler spread, with any reliability would greatly exceed the duration of time during which fading itself would occur. Thus, only the $|T(f,t)|^2$ measurement analyzed in Section 4.1 is of interest.

Techniques are proposed and analyzed in Section 4.3 for the measurement of the gross channel parameters of Doppler spread, multipath spread, SNR, and diversity branch correlation coefficient. Three different techniques are examined for Doppler and multipath spread measurement, called the Differentiation, Correlation, and Level-crossing techniques. These techniques assume that complex Gaussian fading is a satisfactory model of the fading.

The problem of detecting the pres[illegible] of an interfering signal by in-band processing alone is trea[illegible]n Section 4.4. Two basic procedures are analyzed. In one p[illegible]e, the centroid and rms bandwidth of the power spectrum of the [illegible]ived signal are examined to see if they have changed significantly from their a priori known values. This procedure is effective in the measurement of the presence of a narrowband interference. In the other procedure, an attempt is made to detect a sudden change in received power level. The effectiveness of this procedure is analyzed considering the influence of channel nonstationarities which could be confused with a change in power level.

Section 4.5 considers the problem of measuring certain noise parameters assuming that the condition "noise alone" exists eith[illegible] due to a service interrupt or the existence of idle time and/or frequency slots provided for that purpose. The noise parameters considered are average noise power, peak noise power, and a threshold exceedance probability. These parameters were analyzed because they are used in Section 5 to estimate upper and lower bounds on error rate.

4.1 System Function Measurements

4.1.1 Introduction

A transmitted data signal may be regarded as a random probing signal which upon reception carries information concerning the characteristics of the channel. In this section we analyze the effectiveness of short-term power spectral estimation of a received IF data signal as a means of estimating the squared magnitude of the channel transfer function. This section develops expressions for the RMS fractional error of this estimation technique as a function of processing bandwidth and time, channel parameters, and the structure of the data signal.

4.1.2 System Model

The system to be analyzed is shown in Figure 4.1, where complex representations of signals and linear operations are used. The transmitted data signal is shown as input to a channel with time-variant transfer function $T(f,t)$ and with additive noise $\eta(t)$. The receiver filters and translates the received signal to some intermediate frequency, say f_0 Hz, and hence to demodulators and diversity combiners.

As shown in Figure 4.1, the IF signal is picked-off as input to the squared-magnitude transfer function estimator. The estimation process is as follows. The received IF data signal is mixed to baseband with a locally generated quadrature pair of sinusoids at $f_0 + F$ Hz and the resulting pair of baseband outputs are filtered, squared and summed. The summer output represents the instantaneous power in that portion of the data signal of spectrum located at $f_0 + F$ Hz and within a bandwidth equal to that of the low pass filters. A finite time averager operates upon the summer output, providing a short term spectral estimate of the input data signal power spectrum at the frequency $f_0 + F$.

The received signal complex envelope is given by the two equivalent forms

$$r(t) = \int z(t - \xi)g(t,\xi)d\xi + \eta(t) \qquad (4.1)$$

$$r(t) = \int Z(f)T(f,t)\, e^{j2\pi ft}\, df + \eta(t) \qquad (4.2)$$

where $g(t,\xi)$ is the time variant impulse response related to $T(f,t)$ by the frequency transform pair

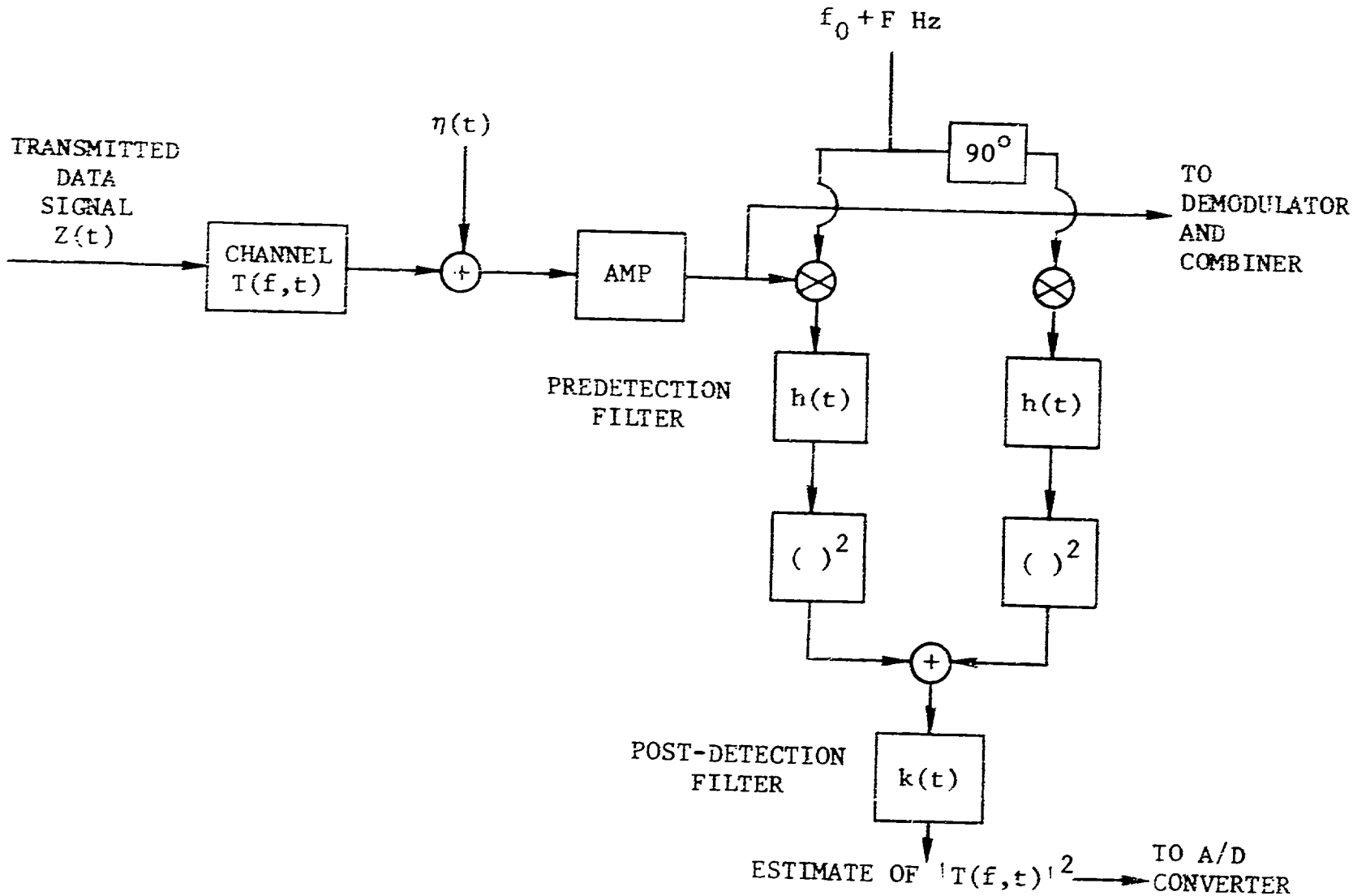

Figure 4.1 Block Diagram of System to be Analyzed

$$g(t,\xi) = \int T(f,t)\, e^{j2\pi f\xi}\, df \tag{4.3}$$

$$T(f,t) = \int g(t,\xi)\, e^{-j2\pi f\xi}\, d\xi \tag{4.4}$$

$\eta(t)$ is a white additive noise (complex envelope) with autocorrelation function

$$\overline{\eta^*(t)\eta(t+\tau)} = 2N_0\delta(\tau) \tag{4.5}$$

where N_0 is the one-sided power density of the real noise.

The operation of the channel estimator prior to the squaring and averaging operation is given by the function $\mu(t)$,

$$\mu(t) = r(t)\, e^{-j2\pi Ft} \otimes h(t) \tag{4.6}$$

and the output of the system $\nu(t)$ is given by

$$\nu(t) = |\mu(t)|^2 \otimes k(t) \tag{4.7}$$

where k(t) is the impulse response of a low-pass filter that is used to average the signal power fluctuations passed by h(t).

4.1.3 Flat-Flat Fading Analysis

We consider first the case wherein the channel is fading slowly relative to the time constant of the output averaging filter k(t) and in addition there is negligible frequency selectivity over the bandwidth of the low-pass filter h(t).

The filter h(t) may be assumed to have a time constant very much smaller than the fading correlation time. In addition, the channel multipath spread is assumed to be much smaller than the fading correlation time of the channel. As a result, the cascade of channel filtering, frequency-shifting, and low-pass filtering may be inverted with little error. Thus, let

$$r(t) = w(t) + \eta(t) \tag{4.8}$$

where

$$w(t) = \int z(t-\xi)g(t,\xi)\, d\xi \tag{4.9}$$

is the complex envelope of received signal in the absence of additive noise. Note that

$$w(t)\, e^{-j2\pi Ft} = \int Z(f)T(f,t)\, e^{j2\pi(f-F)t}\, df$$

$$= \int Z(f+F)T(f+F,t)\, e^{j2\pi ft}\, df \qquad (4.10)$$

or, alternatively,

$$w(t)\, e^{-j2\pi Ft} = \int z(t-\xi)\, e^{-j2\pi F(t-\xi)}\, e^{-j2\pi F\xi}\, g(t,\xi)\, d\xi \qquad (4.11)$$

The cascade inversion discussed above takes the form

$$w(t)\, e^{-j2\pi Ft} \otimes h(t) = \int y(t-\xi)\, e^{-j2\pi F\xi}\, g(t,\xi)\, d\xi$$

$$= \int Y(f)T(f+F,t)\, e^{j2\pi ft}\, df \qquad (4.12)$$

where

$$y(t) = h(t) \otimes z(t)\, e^{-j2\pi Ft}$$

$$Y(f) = \int_{-\infty}^{\infty} y(t)\, e^{-j2\pi ft}\, dt \qquad (4.13)$$

Physically, the inversion amounts to passing a frequency shifted data signal through a low-pass filter and then transmitting this filtered signal through a frequency-shifted channel. Figure 4.2(a) shows the correct sequence of operations involved in producing the average output $\nu(t)$ from the signal input $z(t)$ and noise input $\eta(t)$. Figure 4.2(b) shows the inverted sequence which will yield an output $\nu(t)$ essentially identical to that of 4.2(a). We use 4.2(b) because the analysis is simplified.

The bandwidth of $y(t)$ is controlled by the bandwidth of $h(t)$. We assume in this section that there is negligible frequency selectivity over the bandwidth of $h(t)$. Then $T(f+F,t)$ in (4.12) will be negligibly different from $T(F,t)$ for values of f at which $Y(f)$ has significant values. Using the approximation

$$T(f+F,t) \approx T(F,t) \qquad (4.14)$$

in (4.12), (4.6) - (4.10), we readily find that

$$\mu(t) \approx T(F,t)\, y(t) + n(t) \qquad (4.15)$$

where

$$n(t) = \eta(t) \otimes h(t) \qquad (4.16)$$

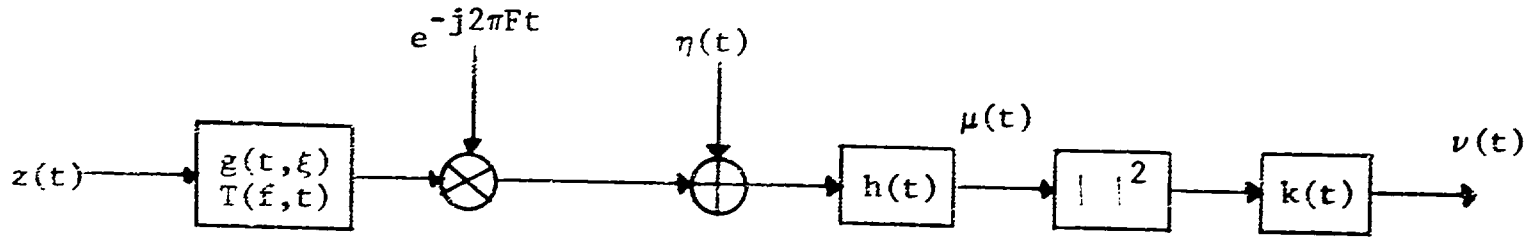

(a)

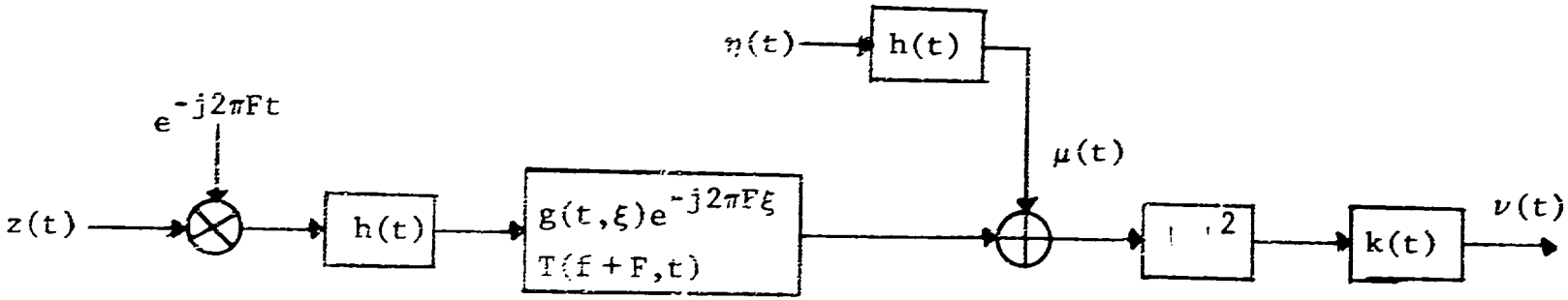

(b)

Figure 4.2 Illustration of Cascade Inversion

The estimate of $|T(F,t)|^2$ is then given by

$$\nu(t) = |T(F,t)\, y(t) + n(t)|^2 \otimes k(t) \tag{4.17}$$

Two assumptions, which may be expected to be generally valid for this study, greatly simplify the statistical analysis of $\nu(t)$:

1) There are very many data pulses during a time interval of the order of the time constant of $\nu(t)$.

2) The time constant of $k(t)$ is very much larger than the time constant of $h(t)$.

The first assumption allows (via the central limit theorem) the real and imaginary parts of $y(t)$ to be approximated by Gaussian processes. The last assumption allows $\nu(t)$ (again via central limit theorem arguments) to be approximated by a quasi-stationary Gaussian process with a slowly varying mean and variance dependent upon $|T(F,t)|$.

We now develop expressions for the mean and variance of the output $\nu(t)$. The ensemble mean value of $\nu(t)$ averaged over the noise and data signal only is given by

$$\begin{aligned}\overline{\nu(t)} &= \int \overline{|T(F,t-\xi)\, y(t-\xi) + n(t-\xi)|^2}\; k(\xi)\, d\xi \\ &= \overline{|y(t)|^2} \int |T(F,t-\xi)|^2\, k(\xi)\, d\xi \\ &\quad + \overline{|n(t)|^2} \int k(\xi)\, d\xi \end{aligned} \tag{4.18}$$

where we have used the fact that $n(t)$ and $y(t)$ are independent. Assuming that the $T(F,t)$ changes little during a time interval equal to the duration of $k(\xi)$,

$$|T(F,t)|^2 \otimes k(t) \approx |T(F,t)|^2\, K(0) \tag{4.19}$$

where

$$K(0) = \int k(t)\, dt \tag{4.20}$$

is the dc response of the averaging filter. It follows from (4.18) and (4.19) that

$$\overline{\nu(t)} \approx \left(\overline{|y|^2}\; |T(F,t)|^2 + \overline{|n|^2} \right) K(0) \tag{4.21}$$

Thus the mean value of our estimator is biased. However, this bias is known or can be estimated and may be subtracted from the estimate.

The mean-square value of $\nu(t)$ (averaged over noise and data) is given by

$$\overline{|\nu(t)|^2} = \overline{\left| \int |\mu(t-\xi)|^2 \, k(\xi) \, d\xi \right|^2}$$

$$= \iint \overline{|\mu(t-\xi)|^2 \, |\mu(t-\eta)|^2} \, k(\xi) \, k(\eta) \, d\xi \, d\eta \qquad (4.22)$$

Writing out the average inside the double integral and using the subscript 1 to denote the argument $t - \xi$ and the subscript 2 to to denote the argument $t - \eta$,

$$\overline{|\mu_1|^2 \, |\mu_2|^2} = \overline{|T_1 y_1 + n_1|^2 \, |T_2 y_2 + n_2|^2}$$

$$= \overline{\left(|T_1|^2 |y_1|^2 + T_1 y_1 n_1^* + T_1^* y_1^* n_1 + |n_1|^2 \right)}$$

$$\times \overline{\left(|T_2|^2 |y_2|^2 + T_2 y_2 n_2^* + T_2^* y_2^* n_1 + |n_2|^2 \right)} \qquad (4.23)$$

Taking advantage of the fact that odd order moments of Gaussian processes are zero and that for a complex Gaussian process [4.1] - [4.4]

$$\overline{n(t) \, n(t+\tau)} = 0 \qquad (4.24)$$

we find

$$\overline{|\mu_1|^2 \, |\mu_2|^2} = |T|^4 \, \overline{|y_1|^2 \, |y_2|^2} + |T|^2 \, \overline{y_1^* y_2} \; \overline{n_1 n_2^*} + |T|^2 \, \overline{y_1 y_2^*} \; \overline{n_1^* n_2}$$

$$+ |T|^2 \, \overline{|y_1|^2} \, \overline{|n_2|^2} + |T|^2 \, \overline{|y_2|^2} \, \overline{|n_1|^2} + \overline{|n_1|^2 \, |n_2|^2}$$

(4.25)

In (4.25) we have dropped subscripts on T because T(f,t) is essentially constant as far as the filter k(t) is concerned. Defining the correlation functions

$$\overline{|y_1|^2 |y_2|^2} = C(\xi - \eta) \tag{4.26}$$

$$\overline{y_1^* y_2} = R_y(\xi - \eta) \tag{4.27}$$

$$\overline{n_1^* n_2} = R_n(\xi - \eta) \tag{4.28}$$

$$\overline{|n_1|^2 |n_2|^2} = C_n(\xi - \eta) \tag{4.29}$$

we find that

$$\begin{aligned}\overline{|\nu(t)|^2} \approx\ & |T(F,t)|^4 \int C(\tau) R_k(\tau)\, d\tau \\ & + |T(F,t)|^2\, 2\,\mathrm{Re}\left\{\int R_y(\tau) R_n^*(\tau) R_k(\tau)\, d\tau\right\} \\ & + 2|T(F,t)|^2\, \overline{|y|^2}\ \overline{|n|^2}\ |K(0)|^2 \\ & + \int C_n(\tau) R_k(\tau)\, d\tau\end{aligned} \tag{4.30}$$

where we have used the double-to-single integral transformation

$$\iint A(\xi - \eta)\, k(\xi)\, k(\eta)\, d\xi\, d\eta = \int A(\tau) R_k(\tau)\, d\tau \tag{4.31}$$

in which we have defined the autocorrelation function of the averaging filter impulse response

$$R_k(\tau) = \int k(\xi)\, k(\xi + \tau)\, d\xi \tag{4.32}$$

We consider now the correlation functions (4.26) and (4.29). The noise n(t) is a complex Gaussian process. For such a process [4.1] - [4.4]

$$\overline{|n_1|^2\,|n_2|^2} = \left|\overline{n_1^* n_2}\right|^2 + \overline{|n|^2}^2$$

$$= |R_n(\xi - \eta)|^2 + \overline{|n|^2}^2 \qquad (4.33)$$

Except for special cases which can be avoided by judicious choice of the frequency F [4.23], the filtered data signal y(t) will be closely characterizable as a complex Gaussian process. For the purposes of the present analysis, we assume that y(t) is complex Gaussian. Then [4.1] - (4.4]

$$\overline{|y_1|^2\,|y_2|^2} = |R_y(\xi - \eta)|^2 + \overline{|y|^2}^2 \qquad (4.34)$$

Using (4.33) and (4.34) in (4.30), we find that

$$\begin{aligned}\overline{|\nu(t)|^2} &= |T(f,t)|^4\,|K(0)|^2\,\overline{|y|^2}^2 \\ &+ |T(f,t)|^4 \int |R_y(\tau)|^2 R_k(\tau)\,d\tau \\ &+ |T(f,t)|^2\, 2\,\mathrm{Re}\left\{\int R_y(\tau)\,R_n^*(\tau)\,R_k(\tau)\,d\tau\right\} \\ &+ 2|T(f,t)|^2\,\overline{|y|^2}^2\,\overline{|n|^2}^2\,|K(0)|^2 \\ &+ \overline{|n|^2}^2\,|K(0)|^2 + \int |R_n(\tau)|^2 R_k(\tau)\,d\tau \qquad (4.35)\end{aligned}$$

It follows that the variance of the fluctuations at the low pass filter output are given by

$$\begin{aligned}\overline{|\nu(t)|^2} - |\overline{\nu(t)}|^2 &= |T(f,t)|^4 \int |R_y(\tau)|^2 R_k(\tau)\,d\tau \\ &+ |T(f,t)|^2\, 2\,\mathrm{Re}\left\{\int R_y(\tau)\,R_n^*(\tau)\,R_k(\tau)\,d\tau\right\} \\ &+ \int |R_n(\tau)|^2 R_k(\tau)\,d\tau \qquad (4.36)\end{aligned}$$

The expression (4.36) may be simplified by noting that $R_y(\tau)$ and $R_n(\tau)$ are "impulsive" by comparison with $R_k(\tau)$ because

the time constant of k(t) is much larger than that of h(t). Thus

$$\int |R_y(\tau)|^2 R_k(\tau)\, d\tau \approx R_k(0) \int |R_y(\tau)|^2 \, d\tau$$
$$= R_k(0) \int P_y^2(f)\, df \qquad (4.37)$$

$$\int R_y(\tau) R_n^*(\tau) R_k(\tau)\, d\tau \approx R_k(0) \int R_y(\tau) R_n^*(\tau)\, d\tau$$
$$= R_k(0) \int P_y(f) P_n(f)\, df \qquad (4.38)$$

$$\int |R_n(\tau)|^2 R_k(\tau)\, d\tau \approx R_k(0) \int |R_n(\tau)|^2 \, d\tau$$
$$= R_k(0) \int P_n^2(f)\, df \qquad (4.39)$$

where we have used Parsevals theorem and $P_y(f), P_n(f)$ are the power spectra of y(t) and n(t). Since

$$y(t) = h(t) \otimes z(t)\, e^{-j2\pi Ft} \qquad (4.40)$$

It follows that

$$P_y(f) = |H(f)|^2 P_z(f - F) \qquad (4.41)$$

where $P_z(f)$ is the power spectrum of the data signal and H(f) is the transfer function corresponding to h(t). Assuming that $P_z(f)$ varies little over a frequency interval of the order of the bandwidth of h(t)

$$P_y(f) \approx P_z(F)\ |H(f)|^2 \qquad (4.42)$$

Since

$$n(t) = h(t) \otimes \eta(t) \qquad (4.43)$$

where $\eta(t)$ is complex Gaussian white noise of (two-sided) spectral density $2N_0$ (N_0 is the one-sided spectral density of the real noise), we have

$$P_n(f) = 2N_0 |H(f)|^2 \qquad (4.44)$$

Using (4.42), (4.44) in (4.37)-(4.39) we find

$$\overline{|\nu(t)|^2} - |\overline{\nu(t)}|^2 = \left(|T(f,t)|^2 P_z(F) + 2N_0\right)^2 R_k(0) \int |H(f)|^4 \, df \tag{4.45}$$

Examining (4.21) we note that

$$\overline{|y|^2} = \int P_y(f) \, df = P_z(f) \int |H(f)|^2 \, df \tag{4.46}$$

$$\overline{|n|^2} = \int P_n(f) \, df = 2N_0 \int |H(f)|^2 \, df \tag{4.47}$$

so that

$$\boxed{\overline{\nu(t)} = \left(|T(f,t)|^2 P_z(F) + 2N_0\right) \int |H(f)|^2 \, df \cdot K(0)} \tag{4.48}$$

Thus the standard deviation of the fluctuations of the estimator normalized to the mean value of the output is given by

$$\frac{\sqrt{\overline{|\nu(t)|^2} - \overline{\nu(t)}^2}}{\overline{\nu(t)}} \equiv \epsilon = \frac{\sqrt{R_k(0) \int |H(f)|^4 \, df}}{K(0) \int |H(f)|^2 \, df} \tag{4.49}$$

which depends upon the characteristics of the two filters alone.

The noise bandwidth of the averaging filter is defined as

$$W_0 = \frac{\int |K(f)|^2 \, df}{K^2(0)} \tag{4.50}$$

Since

$$R_k(0) = \int k^2(t) \, dt = \int |K(f)|^2 \, df \tag{4.51}$$

we see that

$$\epsilon = \sqrt{W_0} \, \frac{\sqrt{\int |H(f)|^4 \, df}}{\int |H(f)|^2 \, df} \tag{4.52}$$

The other ratio in (4.52) depending on H(f) can be interpreted as the square root of a time constant. Note that if the autocorrelation function of h(t) is defined as

$$R_h(\tau) = \int h(t)\, h(t+\tau)\, dt \tag{4.53}$$

then

$$\int |H(f)|^4\, df = \int R_h^2(\tau)\, d\tau \tag{4.54}$$

$$\int |H(f)|^2\, df = R_h(0) \tag{4.55}$$

A duration for the autocorrelation function of h(t), T_0 may clearly be defined as

$$T_0 = \frac{\int R_h^2(\tau)\, d\tau}{R_h^2(0)} \tag{4.56}$$

so that

$$\boxed{\epsilon = \sqrt{W_0 T_0}} \tag{4.57}$$

It might appear that by choosing W_0 and T_0 small enough, one may make ϵ as small as desired. Unfortunately, W_0 and T_0 cannot be made small without eventually violating certain basic assumptions of the derivations. In particular, if W_0 is made too small, the estimate of $|T(f,t)|^2$ will become distorted, i.e., time-selective distortion effects will appear. On the other hand, if T_0 is made too small, the bandwidth of h(t) will be wide enough to be affected by frequency-selective fading.

The question arises as to how small W_0 and T_0 can be made before the distortion terms become comparable to the fluctations due to additive noise and finite sample size. This question is taken up in the next section.

4.1.4 Time and Frequency Selectivity Analysis

In Section 4.1.3 a technique for estimating the squared magnitude of the channel transfer function was analyzed assuming a flat-flat fading channel. This section extends the analysis to include the effects of time and frequency selectivity. An expression for the rms measurement error is derived for this case.

In order for the estimator to work properly, the averaging time must be long enough to average out data fluctuations and short enough not to filter channel fluctuations. Also, the predetection bandwidth must be large enough to provide sensitivity against additive noise and small enough so that only a small amount of frequency selectivity exists within its band. Optimization of the predetection filter bandwidth and the averaging filter duration is performed.

The estimator to be discussed was described in Section 4.1.2 and a functional block diagram after cascade inversion is given by Figure 4.2(b). The quantity $T(f,t)$ is the channel transfer function, $Z(t)$ is the modulated data signal, and $\eta(t)$ is the additive noise. The filters $h(t)$ and $k(t)$ are, respectively, the predetection filter and the averaging filter of the estimator.

We would like to estimate the magnitude squared of the channel transfer function at a frequency F and a time instant t'; that is, we would like to estimate $|T(F,t')|^2$. From Figure 4.2(b) the translated and lowpass filtered data signal is

$$x(t) = \int_{-\infty}^{\infty} H(f)\, Z(f+F)\, T(f+F,t)\, e^{j2\pi ft}\, df \tag{4.58}$$

and including the filtered additive noise

$$\mu(t) = x(t) + n(t) \tag{4.59}$$

where

$$n(t) = h(t) \otimes \eta(t) \tag{4.60}$$

The magnitude squared of Eq. (4.59) is given by

$$|\mu(t)|^2 = |x(t)|^2 + |n(t)|^2 + 2\,\mathrm{Re}\,\{x^*(t)\, n(t)\} \tag{4.61}$$

From Eq. (4.58) we have

$$\overline{|x(t)|^2} = \int_{-\infty}^{\infty} H^*(f)\, H(\ell)\, \overline{Z^*(f+F)\, Z(\ell+F)}\, T^*(f+F,t)\, T(\ell+F,t) \cdot e^{j2\pi t(\ell-f)}\, df\, d\ell \tag{4.62}$$

The overbar denotes ensemble average with respect to the data sequence. With $Z(t)$ a wide sense stationary random process, we have by duality (see Ref. [4.5])

$$\overline{Z^*(f+F)\,Z(\ell+F)} = P_Z(f+F)\,\delta(\ell - f) \tag{4.63}$$

where $P_Z(f)$ is the power spectrum of the data signal. Combining Eqs. (4.62) and (4.63) gives

$$\overline{|x(t)|^2} = \int_{-\infty}^{\infty} |H(f)|^2\, |T(f+F,t)|^2\, P_Z(f+F)\, df \tag{4.64}$$

Assuming that $P_Z(f)$ varies little over the bandwidth of $H(f)$,

$$|x(t)|^2 = P_Z(F) \int_{-\infty}^{\infty} |H(f)|^2\, |T(f+F,t)|^2\, df \tag{4.65}$$

The response of $k(t)$ to an input of $|\mu(t)|^2$ can be separated into a signal term, a distortion term caused by the time and frequency selectivity of the channel, a noise term and various cross terms. The effects upon the output of the estimator by the distortion and the ambient noise are each small compared to the signal. Therefore, the cross terms of the distortion and the noise are negligible compared to the individual effect of either. Hence, these cross terms will be neglected in the analysis. The effects of the noise upon the estimation error were discussed in Section 4.1.3. Here we will consider the effects of the distortion caused by time and frequency selectivity upon the estimation of the magnitude-squared of the channel transfer function.

If $k(\cdot)$ has duration T, and it is desired to know $|T(F,t')|$, then we should sample the output of $k(t)$ at $t = t' + \Delta$, where Δ is approximately equal to T/2. That is, the averaging filter should average over an interval centered at the time at which we would like to estimate the channel. Defining the output of $k(t)$ to a noiseless input as

$$q(t) = \overline{|x(t)|^2} \otimes k(t) \tag{4.66}$$

then we can represent $q(t+\Delta)$ by

$$q(t+\Delta) = d(t+\Delta) + S(t) \tag{4.67}$$

where $d(t+\Delta)$ is the distortion introduced into the estimator by the time and frequency selectivity and $S(t)$ is the desired distortionless output. The output of $k(t)$ is given by [see Eqs. (4.65) - (4.67)]

$$q(t) = P_Z(F) \int_{-\infty}^{\infty} |H(f)|^2 \left[|T(f+F,t)|^2 \otimes k(t)\right] df \tag{4.68}$$

With no selectivity $|T(f+F,t)|^2$ is constant over a time interval greater than the duration of k(t) and over a frequency band greater than the bandwidth of H(f). Therefore, we can express S(t) as

$$S(t) = |T(F,t)|^2 \, P_z(f) \tag{4.69}$$

where we have defined

$$H_n \triangleq \int_{-\infty}^{\infty} f^n |H(f)|^2 \, df \quad ; \quad H_0 = 1 \tag{4.70}$$

$$\int_{-\infty}^{\infty} k(t) \, dt = 1 \tag{4.71}$$

Combining Eqs. (4.65) - (4.67) and (4.69) yields

$$d(t+\Delta) = P_Z(F)\left[\int_{-\infty}^{\infty}\int_{-\infty}^{\infty} |H(f)|^2 \, |T(f+F,t+\Delta-\tau)|^2 \, k(\tau) \, d\tau \, df - |T(F,t)|^2\right] \tag{4.72}$$

Letting $\xi = \tau - \Delta$ gives

$$d(t+\Delta) = P_Z(F)\left[\int_{-\infty}^{\infty}\int_{-\infty}^{\infty} |H(f)|^2 \, |T(f+F,t-\xi)|^2 \, k(\xi+\Delta) \, d\xi \, df - |T(F,t)|^2\right] \tag{4.73}$$

When the degree of time and frequency selective fading is small over the time duration of the averaging filter and over a range of frequencies of the order of the bandwidth of h(t), then the distortion term can be represented as a series by expressing the transfer function of the channel by the following power series (see Ref. [4.6]).

$$T(g,t-\xi) = e^{-j2\pi[g\xi_0 - \nu_0 t + \nu_0 \xi]} \sum_m \sum_n T_{mn}(F,t)[2\pi j]^{m+n}[g-F]^m(-\xi)^n \tag{4.74}$$

where ξ_0, ν_0 are the mean path delay and Doppler shift of the channel and the coefficients $T_{mn}(F,t)$ are given by

$$T_{mn}(F,t) = \frac{1}{m!n!(2\pi j)^{m+n}} \left[\frac{\partial^{m+n} T_{00}(f,t)}{\partial f^m \partial t^n} \right]_{f=F} \tag{4.75}$$

The function $T_{00}(f,t)$ is the transfer function of a channel which differs from the original channel only in having zero mean path delay and Doppler shift. Letting $g = f + F$ in Eq. (4.74) and substituting into Eq. (4.73) gives

$$d(t+\Delta) = P_Z(F) \left[\int_{-\infty}^{\infty} \int_{-\infty}^{\infty} |H(f)|^2 k(\xi+\Delta) \left| \sum_m \sum_n T_{mn}(F,t) [2\pi j]^{m+n} f^m (-\xi)^n \right|^2 d\xi \, df \right.$$
$$\left. - |T(F,t)|^2 \right] \tag{4.76}$$

Expanding Eq. (4.76) and retaining up to second order terms gives

$$\begin{aligned} \frac{d(t+\Delta)}{P_Z(f)} = {} & 4\pi^2 K_2 |T_{01}(F,t)|^2 + 4\pi^2 H_2 |T_{10}(F,t)|^2 \\ & - 4\pi K_1 \mathrm{Re}\{T_{00}^*(F,t)\, T_{01}(F,t) j\} \\ & + 4\pi H_1 \mathrm{Re}\{T_{00}^*(F,t)\, T_{10}(F,t) j\} \\ & + 8\pi^2 H_1 K_1 \mathrm{Re}\{T_{00}^*(F,t)\, T_{11}(F,t)\} \\ & - 8\pi^2 K_2 \mathrm{Re}\{T_{00}^*(F,t)\, T_{02}(F,t)\} \\ & - 8\pi^2 H_2 \mathrm{Re}\{T_{00}^*(F,t)\, T_{20}(F,t)\} \\ & - 8\pi^2 H_1 K_1 \mathrm{Re}\{T_{01}^*(F,t)\, T_{10}(F,t)\} \end{aligned} \tag{4.77}$$

where

$$K_n = \int_{-\infty}^{\infty} \tau^n k(\tau+\Delta)\, d\tau \quad ; \quad k_0 = 1 \tag{4.78}$$

With $H_1 = 0$ and Δ given by $\Delta = \int_{-\infty}^{\infty} \tau k(\tau)\, d\tau$, then we can express $d(t+\Delta)$ as

$$\frac{d(t+\Delta)}{P_z(f)} = 4\pi^2 K_2 |T_{01}(F,t)|^2 + 4\pi^2 H_2 |T_{10}(F,t)|^2 - 8\pi^2 K_2 \mathrm{Re}\{T^*_{00}(F,t)\, T_{02}(F,t)\} - 8\pi^2 H_2 \mathrm{Re}\{T^*_{00}(F,t)\, T_{20}(F,t)\} \quad (4.79)$$

We would like to determine the effect of the distortion $d(t+\Delta)$ upon the estimation of $|T(F,t')|^2$. This is accomplished by first separating $d(t+\Delta)$ into two parts, one correlated with $S(t)$ and one uncorrelated with $S(t)$. Therefore,

$$d(t+\Delta) = \alpha S(t) + U(t) \quad (4.80)$$

where $U(t)$ is uncorrelated with $S(t)$. From Eq. (4.80) it follows that

$$\alpha = \frac{E\{S(t)d(t+\Delta)\} - E\{S(t)\}\, E\{d(t+\Delta)\}}{\sigma_S^2} \quad (4.81)$$

$$\sigma_U^2 = \sigma_d^2 - \frac{[E\{S(t)d(t+\Delta)\} - E\{S(t)\}\, E\{d(t+\Delta)\}]^2}{\sigma_S^2} \quad (4.82)$$

where $E\{\cdot\}$ denotes ensemble averaging over the random parameters of the channel and σ_U^2, σ_d^2, and σ_S^2 are the variances of $U(t)$, $d(t+\Delta)$ and $S(t)$, respectively.

For a complex Gaussian wide-sense stationary uncorrelated scattering (WSSUS) channel the moments of the coefficients in the power series expansion are given by

$$E\{T^*_{mn}(F,t)\, T_{\ell p}(F,t)\} = \frac{1}{m!\, n!\, \ell!\, p!} W(m+\ell, n+p) \quad (4.83)$$

where $W(a,b)$ is defined by

$$W(a,b) \triangleq \int_{-\infty}^{\infty}\int_{-\infty}^{\infty} (-\xi)^a \nu^b S(\xi+\xi_0, \nu+\nu_0)\, d\xi\, d\nu \quad (4.84)$$

$$W(0,0) = 1$$

and $S(\xi+\xi_0, \nu+\nu_0)$ is the scattering function of the channel. Using Eq. (4.83), the following moments needed to evaluate α and σ_U^2 are found to be given by

$$E\{S(t)\} = P_z(F)$$

$$\sigma_S^2 = P_z^2(F)$$

$$E\{d(t+\Delta)\} = 0$$

$$E\{d(t+\Delta)S(t)\} = -4\pi^2\left[K_2W(0,2) + H_2W(2,0)\right]P_z(F)$$

$$\sigma_d^2 = 16\pi^4\left\{\frac{3}{2}K_2^2W^2(0,2) + \frac{3}{2}H_2^2W^2(2,0) + H_2K_2[W(0,2)W(2,0) + W(2,2)] + \frac{1}{2}K_2^2W(0,4) + \frac{1}{2}H_2^2W(4,0)\right\}P_z^2(F) \qquad (4.85)$$

Substituting Eq. (4.85) into (4.81) and (4.82) gives

$$\alpha = -4\pi^2\left[K_2W(0,2) + H_2W(2,0)\right]$$

$$\sigma_U^2 = 8\pi^2\left\{\left[K_2W(0,2) - H_2W(2,0)\right]^2 + K_2^2W(0,4) + H_2^2W(4,0) + 2K_2H_2W(2,2)\right\}P_z^2(F) \qquad (4.86)$$

Furthermore, the mean of U(t) is easily found to be given by

$$E\{U(t)\} = -\alpha P_z(F) \qquad (4.87)$$

To simplify the expressions for α and σ_U^2, we define an rms Doppler spread parameter B and an rms multipath spread parameter L by

$$B \triangleq 2\sqrt{\frac{W(0,2)}{W(0,0)}}$$

$$L \triangleq 2\sqrt{\frac{W(2,0)}{W(0,0)}} \qquad (4.88)$$

where the mean path delay and Doppler shift used in Eq. (4.84) to define W(a,b) are given by

$$\xi_0 = \frac{\int_{-\infty}^{\infty}\int_{-\infty}^{\infty} \xi\, S(\xi,\nu)\, d\xi\, d\nu}{\int_{-\infty}^{\infty}\int_{-\infty}^{\infty} S(\xi,\nu)\, d\xi\, d\nu}$$

$$\nu_0 = \frac{\int_{-\infty}^{\infty}\int_{-\infty}^{\infty} \nu\, S(\xi,\nu)\, d\xi\, d\nu}{\int_{-\infty}^{\infty}\int_{-\infty}^{\infty} S(\xi,\nu)\, d\xi\, d\nu} \tag{4.89}$$

Using the above definitions of ξ_0 and ν_0 result in Eq. (4.88) defining rms Doppler and multipath spreads that have frequently occurred in the literature [4.6]. To simplify the expressions, normalized filter parameters will be defined as

$$K \triangleq \pi^2 \frac{K_2}{K(0)} = \pi^2 \frac{\int_{-\infty}^{\infty} \tau^2 k(\tau+\Delta)\, d\tau}{\int_{-\infty}^{\infty} k(t)\, dt}$$

$$H \triangleq \pi^2 \frac{H_2}{H_0} = \pi^2 \frac{\int_{-\infty}^{\infty} f^2\, |H(f)|^2\, df}{\int_{-\infty}^{\infty} |H(f)|^2\, df} \tag{4.90}$$

With B, L, H, and K defined as above, it immediately follows that

$$\alpha = -HL^2 \cdot KB^2 \tag{4.91}$$

From (4.67) and (4.80), we have

$$q(t+\Delta) = (1+\alpha)\, S(t) + U(t) \tag{4.92}$$

where the reader is reminded that U(t) is uncorrelated with S(t). Since, in the absence of noise, we would like to use $q(t+\Delta)$ as an estimate of $|T_{00}(F,t)|^2$, then the mean of $q(t+\Delta)$ conditional on $|T_{00}(F,t)|^2$ is given by

$$E\left\{q(t+\Delta)\,|T_{00}(F,t)\right\} = P_z(f)\left\{|T_{00}(F,t)|^2 + (HL^2+KB^2)\left[1 - |T_{00}(F,t)|^2\right]\right\} \tag{4.93}$$

Therefore, due to the selectivity of the channel, the estimate of $|T_{00}(F,t)|^2$ is biased. Furthermore, since $W(0,0) = 1 = E\left\{|T_{00}(F,t)|^2\right\}$ and $HL^2+KB^2 \geq 0$, then a positive bias exists when $|T_{00}(F,t)|^2$ is less than its mean and a negative bias exists when $|T_{00}(F,t)|^2$ is greater than its mean. Frequently the bias will not present a problem for one of the following reasons: first, the bias is small; secondly, the bias can be estimated and corrected; lastly, for the estimation of some parameters, the bias will have a self-cancelling effect. An example of the last reason would be the estimation of a parameter proportional to $W(0,0)$, in which case use of $q(t+\Delta)$ would result in an unbiased estimate.

Since S(t) and U(t) are uncorrelated, the variance of $q(t+\Delta)$ conditional upon $|T_{00}(F,t)|^2$ is equal to σ_U^2. Thus, the overall effect of the selectivity of the channel on the estimation of the magnitude squared of the channel transfer function is to produce a biased estimate and to bring about an uncorrelated disturbance. Substituting the previously defined filter and channel parameters, then the variance of the estimate due to the channel selectivity is

$$\frac{\sigma_U^2}{P_z^2(F)} = \frac{1}{2}\left(KB^2 - HL^2\right)^2 + 8\left[K^2W(0,4) + H^2W(4,0) + 2HKW(2,2)\right] \tag{4.94}$$

It is convenient to define the shape factors

$$A_1 = \frac{W(0,4)W(0,0)}{W^2(0,2)}$$

$$A_2 = \frac{W(4,0)W(0,0)}{W^2(2,0)}$$

$$A_3 = \frac{W(2,2)W(0,0)}{W(2,0)W(0,2)} \tag{4.95}$$

in carrying out specific calculations. Combining (4.94) and (4.95) gives

$$\sigma_U^2 = \frac{P_z^2(f)}{2}\left[(1+A_1)K^2B^4 + (1+A_2)H^2L^4 + 2(A_3-1)HKB^2L^2\right] \tag{4.96}$$

The estimate of the magnitude squared of the channel transfer function can be related to its actual value by considering the errors due to both the noise and the channel selectivity. From (4.21) and (4.49), the variance of the estimate due to noise and data can be expressed as

$$\sigma_{\nu(t)}^2 = (W_0T_0)\ P_z^2(f)\left[|T_{00}(F,t)|^2 + \frac{2N_0}{P_z(f)}\right]^2 \tag{4.97}$$

Assuming the error due to the noise and data to be uncorrelated with that due to the channel selectivity, then the variance of the estimate due to noise, data, and the selectivity of the channel is

$$\sigma_U^2 + \sigma_{\nu(t)}^2 = W_0T_0\ |T_{00}(F,t)|^4\ P_z^2(f) + 4W_0T_0N_0\ |T_{00}(F,t)|^2\ P_z(f)$$
$$+ 4W_0T_0N_0^2 + \frac{P_z^2(f)}{2}\left[(1+A_1)K^2B^4 + (1+A_2)H^2L^4\right.$$
$$\left. + 2(A_3-1)HKB^2L^2\right] \tag{4.98}$$

With the predetection filter bandwidth and averaging filter duration properly chosen, the middle two terms will be negligible for all values of $|T_{00}(F,t)|^2$. Therefore, the variance of the estimate can be closely approximated by

$$\frac{\sigma_U^2 + \sigma_{\nu(t)}^2}{P_z^2(f)} = W_0 T_0 |T_{00}(F,t)|^4 + \frac{1}{2}\left[(1+A_1)K^2B^4 + (1+A_2)H^2L^4 + 2(A_3 - 1)H K B^2 L^2\right] \quad (4.99)$$

Defining

$$\boxed{\begin{aligned} \epsilon_S^2 &\triangleq \frac{1}{2}\left[(1+A_1)K^2B^4 + (1+A_2)H^2L^4 + 2(A_3 - 1)H K B^2 L^2\right] \\ \delta^2 &\triangleq \frac{\sigma_U^2 + \sigma_{\nu(t)}^2}{P_z^2(f)} \end{aligned}} \quad (4.100)$$

then we can write

$$\delta^2 = \epsilon^2 |T_{00}(F,t)|^4 + \epsilon_S^2 \quad (4.101)$$

where δ^2 is the variance of the estimate of the magnitude squared of the channel transfer function and $\epsilon = W_0 T_0$. Assuming that the biases in the estimates can be corrected, then we can write

$$|\hat{T}(F,t)|^2 = (1+\delta_1)\ |T(F,t)|^2 + \delta_2 \quad (4.102)$$

where $|\hat{T}(F,t)|^2$ is the unbiased estimate of $|T(F,t)|^2$ and

$$\overline{\delta_1} = \overline{\delta_2} = 0$$

$$\overline{\delta_1^2} = \epsilon^2 \quad ; \quad \delta_2^2 = \epsilon_S^2 \quad (4.103)$$

The biases are given in terms of the rms multipath and Doppler spreads and the average SNR of the received signal. Fortunately, it may be shown that, except for the HF channel, these particular three parameters can always be estimated well enough without bias correction* so that good estimates of the biases may be formed. For the HF channel, the mean SNR can be estimated well and, as discussed in Section 5, can be used to predict average error rate by the "formula" method. Error performance with diversity operation cannot be estimated under all conditions without special probing signals in the case of HF channels. Thus, Eq. (4.102) is the form of the estimate that will be used to evaluate the effectiveness of gross channel parameter and error rate estimation techniques. An rms fractional error can be defined as

$$\epsilon_p \triangleq \frac{\sqrt{\{E\,\delta^2\}}}{E\{|T(F,t)|^2\}} = \sqrt{E(\delta^2)} = \sqrt{2\epsilon^2 + \epsilon_S^2} \qquad (4.104)$$

In the next section, the bandwidth of the predetection filter and the duration of the averaging filter will be evaluated such that ϵ_p is minimized.

4.1.5 Application of Magnitude-Squared Channel Transfer Function Measurement to Tropo, HF, LOS, and Satellite Channels

In this section, we will evaluate the rms fractional error for estimating the magnitude-squared channel transfer function for Troposcatter, HF, LOS, and Satellite channels. For analysis purposes and to determine bandwidths and integration times for the various systems, forms for the filters h(t) and k(t) will be assumed. The predetection filter h(t) will be assumed to be a synchronously tuned double pole filter with 6 dB bandwidth of W Hz, and the averaging filter k(t) is assumed to have a rectangular impulse response with duration of T seconds; that is,

$$h(\tau) = \pi^2 W^2 \tau\, e^{-\pi W \tau}$$

$$k(\tau) = \begin{cases} 1, & 0 \le \tau \le T \\ 0, & \text{otherwise} \end{cases} \qquad (4.105)$$

*See Appendix A.

With the above functional forms for the filters, the filter parameters required to evaluate the rms fractional error given by Eq. (4.104) are:

$$W_0 = \frac{1}{T}$$

$$T_0 = \frac{5}{2\pi W}$$

$$H = \frac{\pi^2 W^2}{4}$$

$$K = \frac{\pi^2 T^2}{12} \tag{4.106}$$

Using the expressions for ϵ and ϵ_s given by (4.57) and (4.100), and the above filter parameters gives for the rms fractional error

$$\epsilon_p = \left\{ \frac{5}{\pi WT} + \frac{\pi^4}{32} \left[\left(\frac{B^2T^2}{3} - W^2L^2 \right)^2 + A_1 \frac{B^4T^4}{9} + A_2 W^4 L^4 + 2A_3 \frac{B^2T^2W^2L^2}{3} \right] \right\}^{1/2} \tag{4.107}$$

Recalling the definitions of A_1, A_2, and A_3 as given by (4.95) and noting that $A_3 \leq \sqrt{A_1 A_2}$, then ϵ_p can be upper bounded by letting $A_3 = \sqrt{A_1 A_2}$. Since in general information concerning A_3 is not available, we will use this upper bound. Setting $A_3 = \sqrt{A_1 A_2}$ in (4.107) gives

$$\epsilon_p \approx \left\{ \frac{5}{\pi WT} + \frac{\pi^4}{32} \left[\left(\frac{B^2T^2}{3} - W^2L^2 \right)^2 + \left(\sqrt{A_1}\, \frac{B^2T^2}{3} + \sqrt{A_2}\, W^2L^2 \right)^2 \right] \right\}^{1/2} \tag{4.108}$$

For a given B, L, A_1 and A_2, we would like to find the values of W and T such that ϵ_p is minimized. This minimization is easier to perform if the following definitions are made:

$$X = \frac{\pi BT}{2[18]^{1/4}} \tag{4.109}$$

$$Y = \frac{\pi WL}{[32]^{1/4}} \tag{4.110}$$

$$C = \frac{5\pi BL}{4.76} \tag{4.111}$$

Substituting the above definitions into (4.108) and squaring gives

$$\epsilon_p^2 = \frac{C}{XY} + (1+A_1)X^4 + (1+A_2)Y^4 + 2(\sqrt{A_1A_2} - 1)X^2Y^2 \qquad (4.112)$$

The procedure to find the X and Y that minimizes ϵ_p^2 (and thus minimizes ϵ_p) is to take the partial of ϵ_p^2 with respect to X and set to zero, then take the partial of ϵ_p^2 with respect to Y and set to zero. The solution of these simultaneous equations is an extremum.

Taking the partial of ϵ_p^2 with respect to X, setting to zero, and multiplying by X gives

$$4(1+A_1)X^4 = \frac{C}{YX} - 4(\sqrt{A_1A_2} - 1)X^2Y^2 \qquad (4.113)$$

Similarly, taking the partial of ϵ_p^2 with respect to Y, setting to zero, and multiplying by Y gives

$$4(1+A_2)Y^4 = \frac{C}{YX} - 4(\sqrt{A_1A_2} - 1)X^2Y^2 \qquad (4.114)$$

Combining (4.113) and (4.114) gives

$$X = \left[\frac{1 + A_2}{1 + A_1}\right]^{1/4} Y \qquad (4.115)$$

Using (4.115) to solve for X and Y, the W and T that minimize ϵ_p^2 are given by

$$W_{opt} = \frac{1}{\pi L}\left\{\frac{40\pi BL/\sqrt{3}}{(1+A_2)\left[\frac{1+A_2}{1+A_1}\right]^{1/4} + (\sqrt{A_1A_2} - 1)\left[\frac{1+A_1}{1+A_2}\right]^{3/4}}\right\}^{1/6} \qquad (4.116)$$

$$T_{opt} = \frac{1}{\pi B}\left\{\frac{360\,\pi\,B\,L\sqrt{3}}{(1+A_1)\left[\frac{1+A_1}{1+A_2}\right]^{1/4} + (\sqrt{A_1A_2}-1)\left[\frac{1+A_1}{1+A_2}\right]^{3/4}}\right\}^{1/6} \quad (4.117)$$

To evaluate the rms fractional error for the channels of interest, it is necessary to determine A_1 and A_2. For the HF and LOS channels, a two-path channel model will be used.[2]

For a two-path channel the scattering function is given by

$$S(\xi,\nu) = P_1\delta(\xi - M_1)\delta(\nu - D_1) + P_2\delta(\xi - M_2)\delta(\nu - D_2) \quad (4.118)$$

where P_i, M_i and D_i are, respectively, the power, time delay, and Doppler shift of the i'th path, i = 1,2. With P_1 and P_2 normalized such that

$$P_1 + P_2 = 1 \quad (4.119)$$

then the mean time delay and Doppler shift are given by

$$\bar{M} = P_1M_1 + P_2M_2$$

$$\bar{D} = P_1D_1 + P_2D_2 \quad (4.120)$$

The moments of the scattering function defined by

$$W(a,b) = \int_{-\infty}^{\infty}\int_{-\infty}^{\infty} (\xi - \bar{M})^a\ (\nu - \bar{D})^b\ S(\xi,\nu)\ d\xi\ d\nu \quad (4.121)$$

were found to be

$$W(0,0) = P_1 + P_2 = 1 \quad (4.122)$$

$$W(2,0) = P_1P_2(M_1 - M_2)^2 \quad (4.123)$$

$$W(0,2) = P_1P_2(D_1 - D_2)^2 \quad (4.124)$$

$$W(2,2) = P_1P_2\left(P_1^2 + P_2^2 - P_1P_2\right)(D_1 - D_2)^2(M_1 - M_2)^2 \quad (4.125)$$

$$W(4,0) = P_1P_2\left(P_1^2 + P_2^2 - P_1P_2\right)(M_1 - M_2)^4 \quad (4.126)$$

$$W(0,4) = P_1 P_2 \left(P_1^2 + P_2^2 - P_1 P_2\right)\left(D_1 - D_2\right)^4 \tag{4.127}$$

From the definitions of rms Doppler and multipath, Eqs. (4.92) and (4.93), it follows that

$$L = 2\sqrt{P_1 P_2 (M_1 - M_2)^2} \tag{4.128}$$

and

$$B = 2\sqrt{P_1 P_2 (D_1 - D_2)^2} \tag{4.129}$$

Substituting the scattering function moments given above into (4.95), it follows that

$$A_1 = A_2 = A_3 = \frac{P_1^2 + P_2^2 - P_1 P_2}{P_1 P_2} \tag{4.130}$$

Therefore, for the two-path model, $A_3 = \sqrt{A_1 A_2}$. For $A_1 = A_2$, (4.116) and (4.117) reduce to

$$W_{opt} = \frac{1}{\pi L}\left\{\frac{20\ \pi B L}{\sqrt{3}\ A_1}\right\}^{1/6} \tag{4.131}$$

$$T_{opt} = \frac{1}{\pi B}\left\{\frac{180\ \sqrt{3}\ \pi B L}{A_1}\right\}^{1/6} \tag{4.132}$$

Figure 4.3 presents the performance of the magnitude-squared channel transfer function estimator for typical HF and LOS channels. For the HF channel, the filter parameters were evaluated from Eqs. (4.131) and (4.132) using the design parameters given in Table 4-1. For the LOS channel, a conditional rms fractional error is shown in Figure 4.3; this error is given by*

$$\epsilon_C = \epsilon^2 + \frac{\epsilon_S^2}{F_L^2} \tag{4.133}$$

where F_L is the fade level.

*See Appendix C for derivation of conditional rms fractional error for LOS channels.

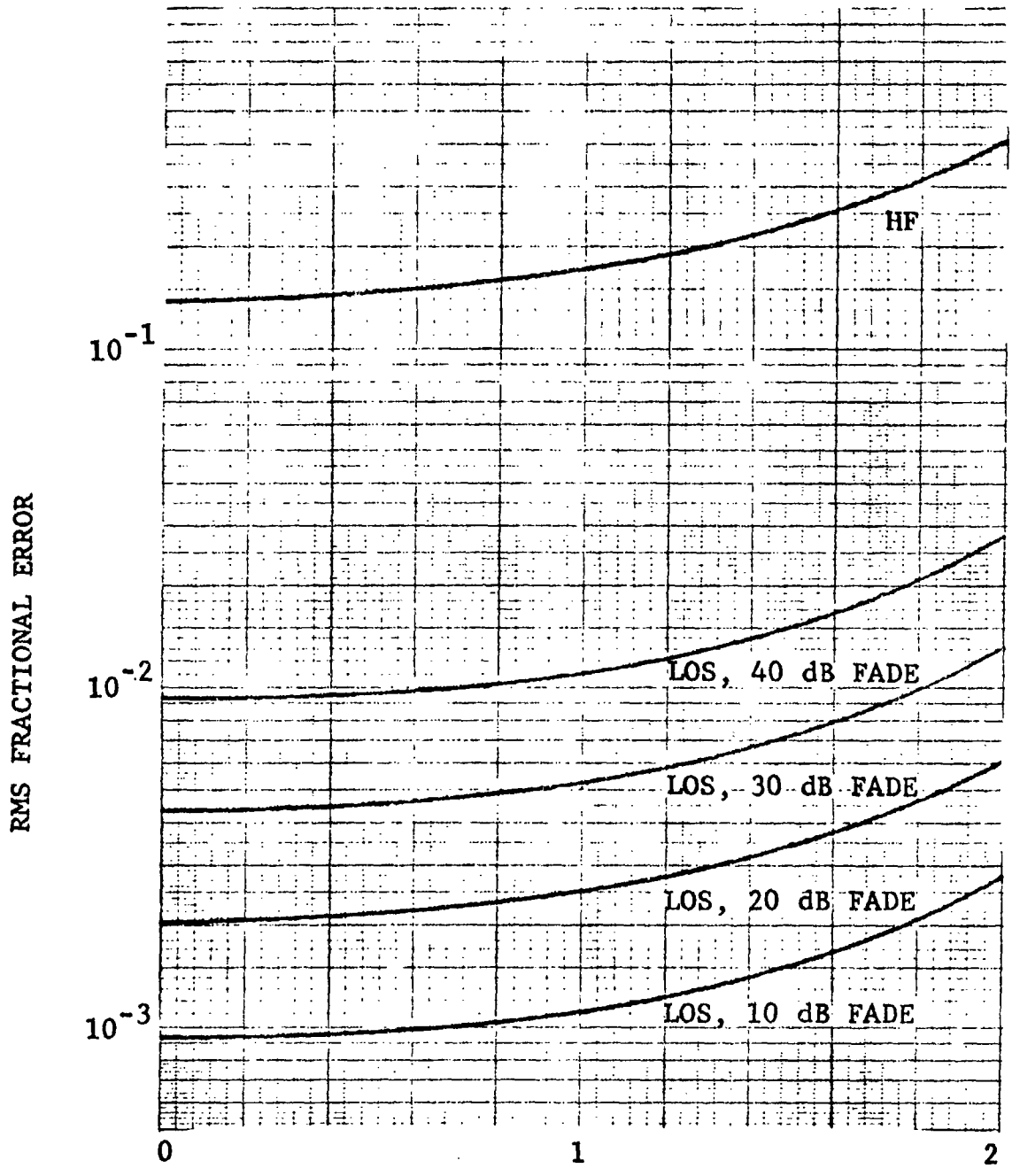

Figure 4.3 Performance of Magnitude-Squared Channel Transfer Function Estimator for HF and LOS Channels

TABLE 4-1

DESIGN PARAMETERS FOR HF AND LOS CHANNELS

	L_D (s)	B_D (Hz)	$\lvert M_1 - M_2 \rvert_D$ (s)	$\lvert D_1 - D_2 \rvert_D$ (Hz)
HF	10^{-3}	0.5	1.06×10^{-3}	0.53
LOS	10^{-8}	0.003	1.06×10^{-8}	0.0032

A fractional path difference is used to illustrate the estimator performance. A fractional path difference of 2 implies that both the Doppler and multipath differences are twice their design values.

It was found by example that the rms fractional error is relatively insensitive to variations in P_1. Also, the rms fractional error for the HF channel is large ($\epsilon_p \approx 0.2$ at $B = 0.6$ Hz, $L = 1.2$ ms). Use of estimators of the magnitude squared of the channel transfer function requires careful examination for HF channels. For HF channels removal of the bias given by (4.93) cannot be performed effectively due to poor rms Doppler and multipath spread estimation using bias uncorrected estimates of $|T(f,t)|^2$.* It appears that mean SNR is the only gross channel parameter that can be effectively estimated for HF channels using the estimator of Figure 4.1. For the LOS channel, the error is so small that it will be negligible compared to errors introduced by analog processing.

For troposcatter links, the two-path channel model does not accurately represent the physical channel. From Ref. [4.7], a value of A_2 approximately equal to 7 is typical for many long range troposcatter channels. Furthermore, since information concerning the Doppler power spectrum for troposcatter channels is not available, we will use for the examples two values of A_1: $A_1 = 3$ (Gaussian Doppler power spectrum) and $A_1 = 7$. The performance of the magnitude-squared channel transfer function estimator is presented in Figure 4.4. The filter parameters were found from (4.116) and (4.117) with design Doppler and multipath spreads of $B = 1$ Hz, $L = 0.3\,\mu$s, and estimation of the magnitude squared of the channel transfer function for troposcatter channels should provide useful channel information.

A satellite channel subject to ionospheric scintillation will be the final channel for which the magnitude-squared channel transfer function estimator will be evaluated. For this channel an rms Doppler spread of 0.1 - 0.2 Hz appears reasonable [4.9], [4.10], while the multipath spread is negligible. The modeling of a scintillating satellite channel to include scattering function moments has not been considered in the literature. Thus, we will make some ad hoc assumptions. Two channel models will be assumed: first, an rms multipath spread of 10^{-9} seconds and $A_1 = A_2 = 7$ will be used; second, an rms multipath spread of 10^{-9} 10^{-9} seconds and $A_1 = A_2 = 3$ will be used. The performance of the estimator is presented in Figure 4.4. The estimator performance is quite good ($\epsilon_p \approx 0.0016$ for $B = 0.2$ Hz, $L = 10^{-9}$ s). Since the

*See Appendix A and Section 1.

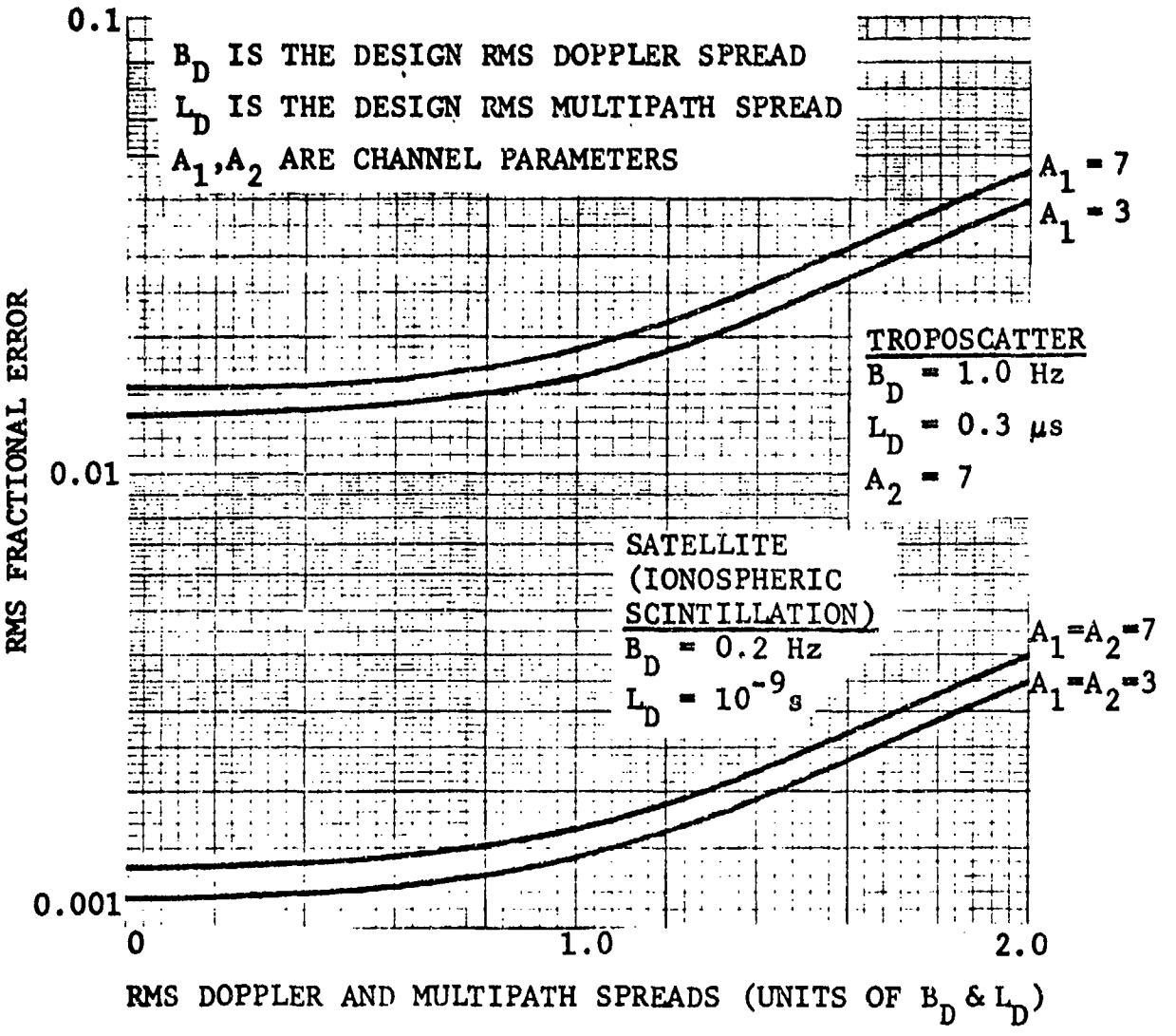

Figure 4.4 Performance of Magnitude-Squared Channel Transfer Function Estimator for Satellite and Troposcatter Channels

performance is relatively insensitive to variations in A_1 and A_2, it is expected that a better channel model will not significantly alter the filter parameters or the estimator performance.

The magnitude-squared channel transfer function estimator performance for the four channels considered is summarized in Table 4-2. These channel and filter parameters, as well as the estimator performance variables, will be used in future sections to evaluate various estimation techniques.

In some cases, it may be practical from a cost standpoint to use one estimator to estimate the magnitude squared of the channel transfer function at many frequencies or on several diversity branches. Therefore, it may become necessary to use a duration of the averaging filter that is much less than the optimum given by (4.118). If the averaging filter duration, T, is so small as to make the effect of the time selectivity negligible, then the rms fractional error can be closely approximated by

$$\epsilon_p = \left(\frac{5}{\pi WT} + \frac{\pi^4}{32} (1+A_2) W^4 L^4 \right)^{1/2} \tag{4.134}$$

The value of W that minimizes ϵ_p is given by

$$W = \frac{1}{\pi L} \left(\frac{40\ L}{T(1+A_2)} \right)^{1/5} \tag{4.135}$$

Similarly, if the bandwidth of the predetection filter must be chosen so as to result in the frequency selectivity of the channel having negligible effect on the channel transfer function squared magnitude estimator, then the rms fractional error is given by

$$\epsilon_p = \left(\frac{5}{\pi WT} + \frac{\pi^4}{32} (1+A_2) \frac{T^4 B^4}{9} \right)^{1/2} \tag{4.136}$$

TABLE 4-2

RMS FRACTIONAL ERROR IN ESTIMATING SQUARED MAGNITUDE OF CHANNEL TRANSFER FUNCTION USING RECEIVED INFORMATION-BEARING SIGNAL ALONE

Channel	Filter Bandwidth* (Hz)	Filter Time Constant** (s)	RMS Multipath Spread (s)	RMS Doppler Spread (Hz)	RMS Fractional Error†
LOS, 10 dB Fade	3.43×10^{5}	2.27	10^{-8} ††	0.003	1.09×10^{-3}
LOS, 20 dB Fade	1.82×10^{5}	1.06	10^{-8}	0.003	2.49×10^{-3}
LOS, 30 dB Fade	8.64×10^{4}	0.49	10^{-8}	0.003	5.04×10^{-3}
LOS, 40 dB Fade	3.93×10^{4}	0.227	10^{-8}	0.003	1.09×10^{-2}
Troposcatter	1.14×10^{5}	0.059	0.3×10^{-6}	1.0	1.9×10^{-2}
Satellite Iono. Scintillation (1 GHz)	10.1×10^{6}	0.088	10^{-9}	0.2	1.6×10^{-3}
HF Not Transauroral	1.5×10^{2}	0.53	10^{-3} ††	0.5	1.7×10^{-1}

* Optimum predetection filter - 6 dB bandwidth - double tuned filter.

** Optimum postdetection filter integration time for rectangular impulse response.

† For the LOS channel, the rms error is conditioned on and normalized to the signal at the fade depth. For the other channels, the rms error is normalized to the average value of the squared magnitude of the channel transfer function.

†† Two path channel models assumed for computational purposes.

and the value of T that minimizes ϵ_p is

$$T = \frac{1}{\pi B}\left\{\frac{360\ B}{W(1+A_1)}\right\}^{1/5} \qquad (4.137)$$

In this section we have determined expressions for W and T that minimize $\epsilon_p^2 = 2\epsilon^2 + \epsilon_S^2$. In Appendix C, expressions for W and T that minimize the rms error conditioned upon the fade level are determined. This is a valid criterion for choosing the estimator filter parameters for LOS channels. For some applications of the magnitude-squared channel transfer function estimator (e.g., see Section 5.1), the effect of the estimation error due to the channel selectivity is greater than that due to the data and noise. For these cases, it seems appropriate to minimize $C_1\epsilon^2 + C_2\epsilon_S^2$. The filter parameters that minimize $C_1\epsilon^2 + C_2\epsilon_S^2$ can be found by employing the minimization technique outlined above. In fact, the above expressions can be used with the design multipath and Doppler spread parameters appropriately scaled.

4.2 Channel Correlation Function Measurement

4.2.1 Introduction

In this section we address the problem of using estimates of the magnitude-squared channel transfer function to estimate the time-frequency envelope correlation function. Estimates of the magnitude-squared channel transfer function are formed by sampling the output of the estimator analyzed in Section 4.1. The time-frequency envelope correlation function is defined as

$$R_2(\Omega,\tau) \triangleq E\left\{|T(f,t)|^2\ |T(f+\Omega,t+\tau)|^2\right\} \qquad (4.138)$$

where T(f,t) is the time-varying transfer function of the channel. A complex Gaussian WSSUS channel will be assumed. This assumption allows us to draw upon the theory of complex Gaussian random processes; in particular, it will enable us to evaluate the higher order moments necessary to determine the convergence of the estimation technique. The justification for modeling a fading channel as a complex Gaussian WSSUS channel is discussed in Section 2.

The time-frequency envelope correlation function contains information concerning the channel. For example, the rms Doppler and multipath spreads can be estimated from $R_2(\Omega,\tau)$. The estimation of these gross channel parameters is discussed further in Section 4.3.

4.2.2 Estimator Description

A functional block diagram of the time-frequency envelope correlation function is given in Figure 4.5. The estimation procedure is as follows. The data signal is transmitted over the channel, picked off at RF (or IF) in the receiver, and sent to magnitude-squared channel transfer function estimators of the type analyzed in Section 4.1. The biases of these estimates are removed, resulting in unbiased estimates of $|T(F,t_p)|^2$ and $|T(F+\Omega,t_p+\tau)|^2$. An estimate of $R_2(\Omega,\tau)$ is formed by implementing (4.138) from samples of the above estimates.

Therefore, the estimate of $R_2(\Omega,\tau)$ is given by

$$\hat{R}_2(\Omega,\tau) = \frac{1}{K}\sum_{p=1}^{K} |\tilde{T}(F,t_p)|^2 \; |\tilde{T}(F+\Omega,t_p+\tau)|^2 \qquad (4.139)$$

The bias and rate of convergence of this estimate will be determined in Section 4.2.3. From Section 4.1, the estimates of $|T(f,t)|^2$ can be represented by

$$|\tilde{T}(F,t_p)|^2 = |T(F,t_p)|^2 \; (1+\delta_{1p}) + \delta_{2p}$$

$$|\tilde{T}(F+\Omega,t_p+\tau)|^2 = |T(F+\Omega,t_p+\tau)|^2(1+\epsilon_{1p}) + \epsilon_{2p} \qquad (4.140)$$

where it will be assumed that

$$E\{\delta_{1p}\} = E\{\delta_{2p}\} = E\{\epsilon_{1p}\} = E\{\epsilon_{2p}\} = 0$$

$$E\{\delta_{1p}\delta_{1q}\} = E\{\epsilon_{1p}\epsilon_{1q}\} = \begin{cases} \epsilon^2 & , \text{ if } p=q \\ 0 & , \text{ otherwise} \end{cases}$$

$$E\{\delta_{2p}\delta_{2q}\} = E\{\epsilon_{2p}\epsilon_{2q}\} = \begin{cases} \epsilon_S^2 & , \text{ if } p=q \\ 0 & , \text{ otherwise} \end{cases} \qquad (4.141)$$

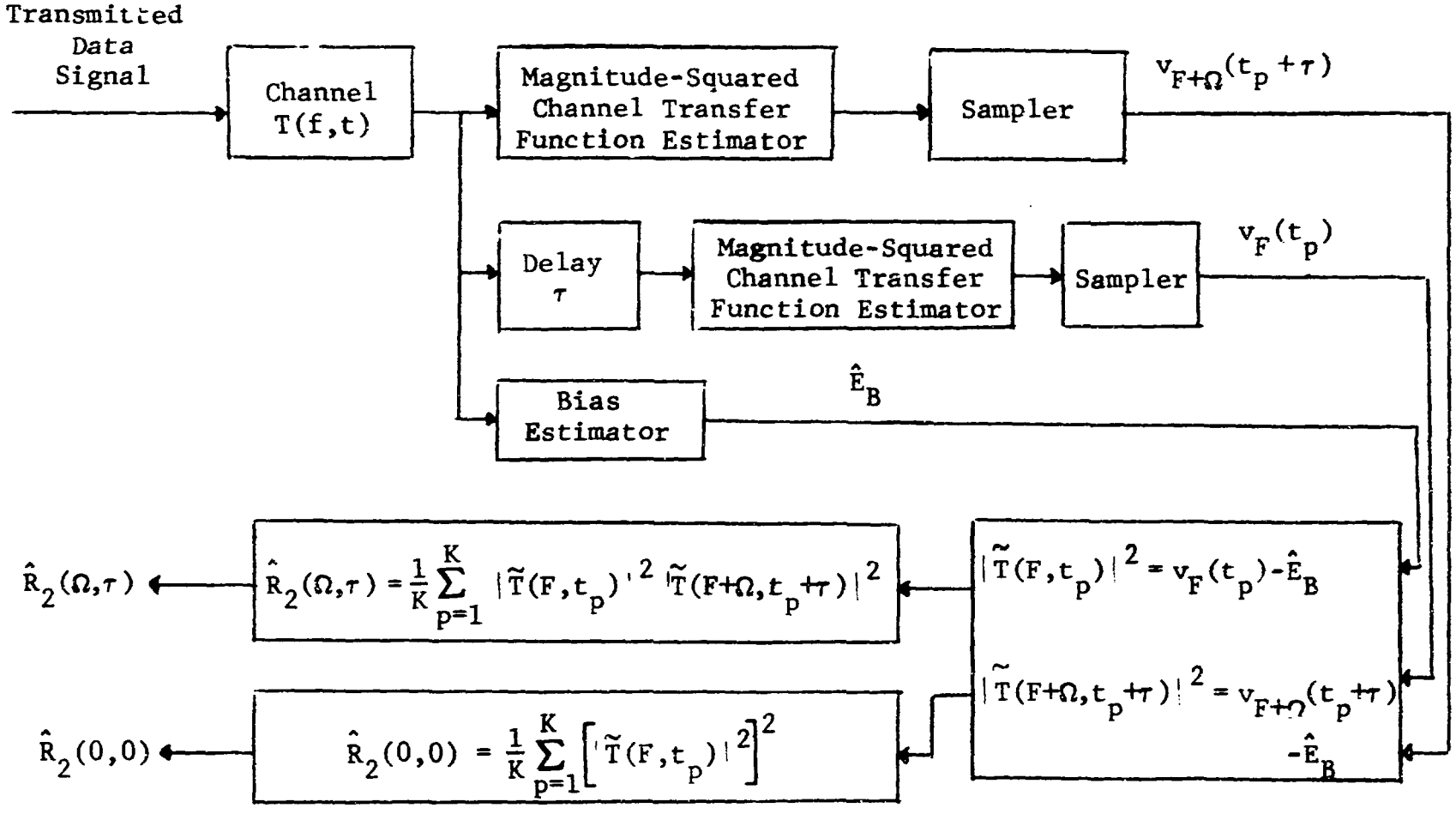

Figure 4.5 Time-Frequency Envelope Correlation Function Estimator

$$E\{\delta_{ip}\epsilon_{jp}\} = 0$$

$$E\{\delta_{ip}\delta_{jq}\} = 0 \quad , \quad \text{if } i \neq j \quad \text{or} \quad p \neq q$$

$$E\{\epsilon_{ip}\epsilon_{jq}\} = 0 \quad , \quad \text{if } i \neq j \quad \text{or} \quad p \neq q$$

and where ϵ and ϵ_S are given by (4.57) and (4.100). For the purpose of numerical evaluation of the performance of the estimator, the values of ϵ and ϵ_S given in Table 4-2 will be used. The assumption that the errors are uncorrelated is justified since the sources of these errors (noise, data, and channel selectivity) should be independent from one sample of $|\tilde{T}(f,t)|^2$ to the next.

For analysis purposes, it will be assumed that the samples are spaced far enough apart as to be considered to be independent realizations of a random process.

4.2.3 Convergence of Estimation Technique

In this section the convergence of the estimates discussed in the previous section will be determined. When it is desired to estimate $R_2(\Omega,\tau)$ at $\Omega = 0$ and $\tau = 0$, then the estimate of $R_2(0,0)$ reduces to

$$\hat{R}_2(0,0) = \frac{1}{K}\sum_{p=1}^{K}\left[|\tilde{T}(F,t_p)|^2\right]^2 \tag{4.142}$$

Substituting the expression for the estimate of the magnitude squared of the channel transfer function, as given by (4.140), into (4.142) and taking ensemble averages give

$$E\{\hat{R}_2(0,0)\} = \frac{1}{K}\sum_{p=1}^{K} E\left\{\left[|T(F,t_p)|^2(1+\delta_{1p}) + \delta_{2p}\right]^2\right\} \tag{4.143}$$

First averaging over the error terms yields

$$E\{\hat{R}_2(0,0)|T(F,t_p)\} = \frac{1}{K}\sum_{p=1}^{K}\left[|T(F,t_p)|^4(1+\epsilon^2) + \frac{R_2(0,0)}{2}\epsilon_S^2\right] \tag{4.144}$$

where we have made use of the moment theorem for complex Gaussian processes and the definitions of $R_2(0,0)$ and $W(0,0)$ to obtain

$$R_2(0,0) = 2W^2(0,0) = 2 \tag{4.145}$$

Averaging (4.144) over the channel fluctuations gives

$$\boxed{E\left\{\hat{R}_2(0,0)\right\} = 2\left[1 + \frac{\epsilon_S^2}{2} + \epsilon^2\right]} \tag{4.146}$$

Therefore, the estimate is biased. Recalling the definition of the rms fractional error for estimating the magnitude squared of the channel transfer function ϵ_p, we note [see (4.104)] that minimization of ϵ_p will result in the bias in the above estimate also being a minimum. For the channels considered in Section 4.1, the bias in the estimate will be small (less than 2%); however, for some estimators, a bias of 2% may not be tolerable. For example, the estimation of rms Doppler and multipath spreads using the correlation technique can produce a large bias from the small bias in estimating $R_2(0,0)$.

The second moment of $\hat{R}_2(0,0)$ is found by substituting (4.140) in (4.142), squaring and averaging. Performing these operations gives

$$E\left\{\hat{R}_2^2(0,0)\right\} = \frac{1}{K^2}\sum_{p=1}^{K}\sum_{q=1}^{K} E\left\{\left[|T(F,t_p)|^2(1+\delta_{1p}) + \delta_{2p}\right]^2 \left[|T(F,t_q)|^2(1+\delta_{1q}) + \delta_{2q}\right]^2\right\} \tag{4.147}$$

With the samples of $|T(f,t)|^2$ spaced far enough apart such that they can be considered to be independent realizations of a random process, it follows that

$$E\left\{\hat{R}_2^2(0,0)\right\} = \frac{1}{K^2}\sum_{p=1}^{K} E\left\{\left[|T(F,t_p)|^2(1+\delta_{1p}) + \delta_{2p}\right]^4\right\} + \frac{K-1}{K} E^2\left\{\hat{R}_2(0,0)\right\} \tag{4.148}$$

Using (4.141) to evaluate the error moments and the moment theorem of complex Gaussian processes to evaluate the moments of $T(F,t_p)$ results in

$$E\left\{\hat{R}_2^2(0,0)\right\} = \frac{R_2^2(0,0)}{K}\left[5 + 34\,\epsilon^2 + 2\,\epsilon^2\right] + E^2\left\{\hat{R}_2(0,0)\right\} \tag{4.149}$$

where higher than second-order moments of the error terms were considered to be negligible. From (4.149) it immediately follows that the variance of the estimate of $R_2(0,0)$ is given by

$$\sigma^2_{\hat{R}_2(0,0)} = \frac{R_2^2(0,0)}{K}\left[5 + 34\,\epsilon^2 + 2\,\epsilon_S^2\right] \tag{4.150}$$

and the rms fractional error is given by

$$\boxed{\frac{\sigma_{\hat{R}_2(0,0)}}{R_2(0,0)} = \left[\frac{5 + 34\epsilon^2 + 2\epsilon_S^2}{K}\right]^{1/2}} \tag{4.151}$$

For the channels considered in Section 4.1, $34\epsilon^2 + 2\epsilon_S^2 \ll 5$. Therefore, the rate of convergence is not appreciably affected by the errors in estimating the magnitude squared of the channel transfer function. The rate of convergence is dependent upon the time required to obtain K independent samples of $|T(f,t)|^2$. As a rule of thumb, there are approximately BT_c independent samples (where B is the rms Doppler spread of the channel) of $|T(F,t)|^2$ in a T_c second interval. This rule of thumb should yield slightly pessimistic indication of the time required to estimate parameters.

Using the above-mentioned rule of thumb, the convergence of the $R_2(0,0)$ estimator is presented in Figure 4.6, where the channel and magnitude-squared channel transfer function estimator parameters are given by Table 4.2 of Section 4.1.5.

For the case when $\tau \neq 0$ or $\Omega \neq 0$, the estimate of $R_2(\Omega,\tau)$ is given by (4.139). Substituting (4.140) into (4.139) gives

$$\hat{R}_2(\Omega,\tau) = \frac{1}{K}\sum_{p=1}^{K}\left[|T(F,t_p)|^2(1+\delta_{1p}) + \delta_{2p}\right]\left[|T(F+\Omega,t_p+\tau)|^2 (1+\epsilon_{1p}) + \epsilon_{2p}\right] \tag{4.152}$$

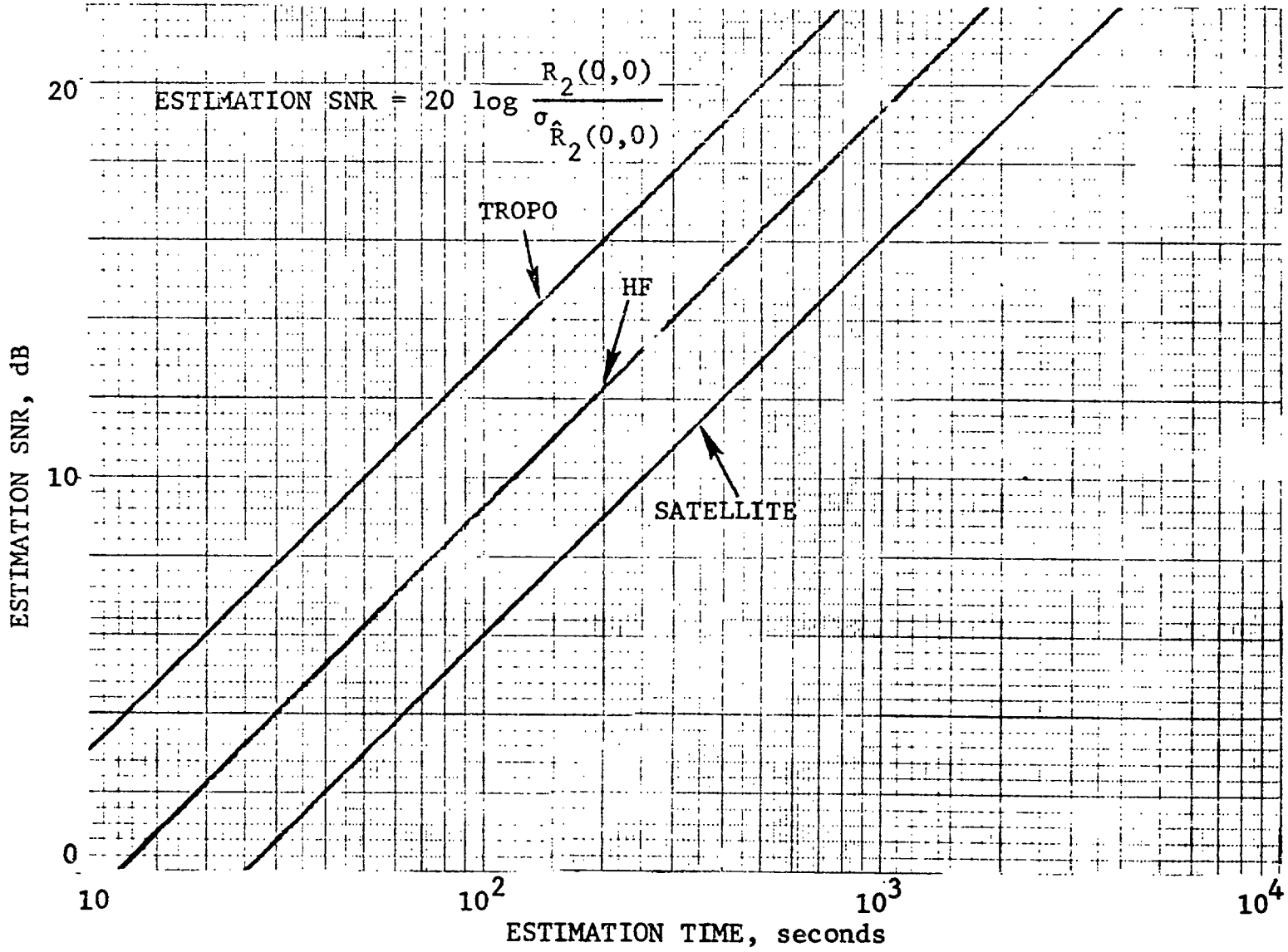

Figure 4.6 Estimation of $R_2(0,0)$

Averaging over the error terms gives

$$E\{\hat{R}_2(\Omega,\tau)|T(f,t)\} = \frac{1}{K}\sum_{r=1}^{K}|T(F,t_p)|^2|T(F+\Omega,t_p+\tau)|^2 \tag{4.153}$$

and averaging over the channel fluctuations

$$\boxed{E\{\hat{R}_2(\Omega,\tau)\} = R_2(\Omega,\tau)} \tag{4.154}$$

Therefore, (4.139) is an unbiased estimate of $R_2(\Omega,\tau)$. It should be mentioned that when Ω and τ are very small with respect to the correlation bandwidth and time, then the assumption of uncorrelated errors in estimating $|T(f,t)|^2$ may be violated. However, the bias for estimating $R_2(\Omega,\tau)$ will be bounded by the bias for estimating $R_2(0,0)$ as given in (4.146). Using the moment theorem for complex Gaussian processes, we can write

$$E\{\hat{R}_2(\Omega,\tau)\} = \frac{R_2(0,0)}{2}\left(1+\rho^2_{\Omega,\tau}\right) = 1+\rho^2_{\Omega,\tau} \tag{4.155}$$

where $\rho^2_{\Omega,\tau}$ is the channel envelope correlation coefficient defined by

$$\rho^2_{\Omega,\tau} \triangleq \frac{|E\{T^*(f,t)\ T(f+\Omega),t+\tau)\}|^2}{E^2\{|T(f,t)|^2\}} \tag{4.156}$$

With the samples of the transfer function spaced such that $|T(F,t_p)|^2$ can be considered to be independent of $|T(F,t_q)|^2$ and $|T(F+\Omega,t_q+\tau)|^2$ if $p \neq q$, then by substituting (4.140) into (4.139), squaring and averaging, we obtain

$$E\{\hat{R}_2^2(\Omega,\tau)\} = \frac{1}{K^2}\sum_{p=1}^{K} E\left\{\left[|T(F,t_p)|^2(1+\delta_{1p})+\delta_{2r}\right]^2 \left[|T(F+\Omega,t_p+\tau)|^2(1+\epsilon_{1p})+\epsilon_{2p}\right]^2\right\} + \frac{K-1}{K}E^2\{\hat{R}_2(\Omega,\tau)\} \tag{4.157}$$

Using the moment theorem for complex Gaussian processes to evaluate the moments of the channel transfer function, it follows that the variance of the estimate is

$$\sigma^2_{\hat{R}_2(\Omega,\tau)} = \frac{1}{K}\left[3 + 14\rho^2_{\Omega,\tau} + 3\rho^4_{\Omega,\tau} + 8\epsilon^2\left(1 + 4\rho^2_{\Omega,\tau} + \rho^4_{\Omega,\tau}\right) + 4\epsilon_S^2\right] \tag{4.158}$$

The rms fractional error for estimating $R_2(\Omega,\tau)$ is given by

$$\frac{\sigma_{\hat{R}_2(\Omega,\tau)}}{R_2(\Omega,\tau)} = \left\{\frac{1}{K}\left[\frac{3 + 14\rho^2_{\Omega,\tau} + 3\rho^4_{\Omega,\tau} + 8\epsilon^2\left(1 + 4\rho^2_{\Omega,\tau} + \rho^4_{\Omega,\tau}\right) + 4\epsilon_S^2}{1 + 2\rho^2_{\Omega,\tau} + \rho^4_{\Omega,\tau}}\right]\right\}^{\frac{1}{2}} \tag{4.159}$$

Again, as in the case of estimating $R_2(0,0)$, the rate of convergence is primarily dependent upon the rms Doppler spread of the channel. The performance of the $R_2(\Omega,\tau)$ estimator is presented in Figure 4.7. It should be noted from (4.159) that the rms errors in estimating the magnitude squared of the channel transfer function (ϵ and ϵ_S) have a negligible effect upon the convergence of the $R_2(\Omega,\tau)$ estimator.

4.2.4 Correlation of Estimation Errors

To evaluate some gross channel parameters, it is necessary to determine the correlation between the error in estimating $R_2(0,0)$ and the error in estimating $R_2(\Omega,\tau)$. For example, in estimating the rms Doppler spread using the correlation technique (Section 4.3), an estimate of $R_2(\Omega,\tau)/R_2(0,0)$ is required. To determine the convergence of the estimate of this ratio, the correlation between the error in estimating each of these quantities must be found.

Defining the error in estimating $R_2(\Omega,\tau)$ as

$$\epsilon(\Omega,\tau) \triangleq \hat{R}_2(\Omega,\tau) - E\left\{\hat{R}_2(\Omega,\tau)\right\} \tag{4.160}$$

then we would like to evaluate

$$E\left\{\epsilon(\Omega,\tau)\epsilon(0,0)\right\} = E\left\{\hat{R}_2(\Omega,\tau)\hat{R}_2(0,0)\right\} - E\left\{\hat{R}_2(\Omega,\tau)\right\}E\left\{\hat{R}_2(0,0)\right\} \tag{4.161}$$

Substituting $\hat{R}_2(0,0)$ and $\hat{R}_2(\Omega,\tau)$ as given by (4.142) and (4.139), respectively, into $(4.160)^2$ and performing the indicated averages results in

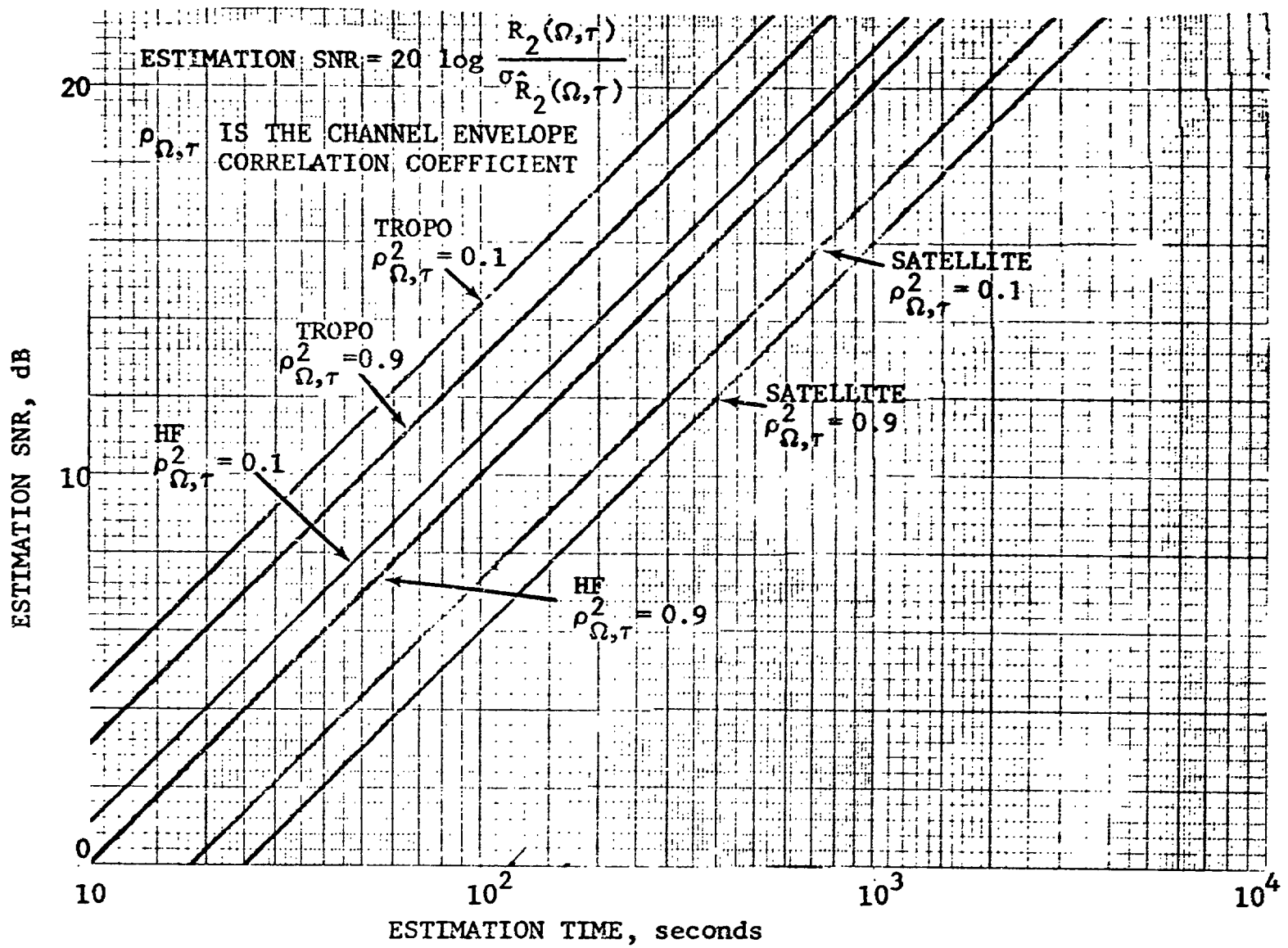

Figure 4.7 Estimation of $R_2(\Omega,\tau)$

$$E\left\{\epsilon(\Omega,\tau)\epsilon(0,0)\right\} = \frac{R_2^2(0,0)}{2}\left[1+4\rho_{\Omega,\tau}^2+\epsilon^2\left(4+13\rho_{\Omega,\tau}^2\right)+\frac{\epsilon_S^2}{2}\left(1+\rho_{\Omega,\tau}^2\right)\right] \tag{4.162}$$

where we have assumed the same statistical properties for the samples of the magnitude squared of the channel transfer function and the errors in estimating these quantities as those assumed in the previous section.

An error correlation coefficient can be defined by

$$\rho_\epsilon(\Omega,\tau) \triangleq \frac{E\left\{\epsilon(\Omega,\tau)\epsilon(0,0)\right\}}{\sigma_{\hat{R}_2(0,0)}\,\sigma_{\hat{R}_2(\Omega,\tau)}} \tag{4.163}$$

The error correlation coefficient is plotted in Fig. 4.8 for the channels considered in Section 4.1. We note from this figure that the error in estimating $R_2(0,0)$ is highly correlated with the error in estimating $R_2(\Omega,\tau)$. Therefore, in estimating the ratio of $R_2(\Omega,\tau)$ to $R_2(0,0)$ the estimates of each of these quantities will have a tendency to fluctuate together.

4.3 Gross Channel Parameter Measurement

4.3.1 Introduction

In this section the problem of estimating gross channel parameters from the estimates of the magnitude squared of the channel transfer function are considered. The gross channel parameters that will be estimated are: the rms Doppler spread, the rms multipath spread, and the mean signal-to-noise ratio. The estimates of these parameters will be used in Section 5 for error rate estimation.

4.3.2 Doppler Spread Measurement Techniques

In this section we address the problem of implementing and evaluating possible techniques for estimating the rms Doppler spread of the channel from estimates of the magnitude squared of the channel transfer function. The estimation techniques to be considered are the differentiation, correlation, and level crossing techniques. The mathematical basis for these techniques can be found in Ref [4.11] - [4.15].

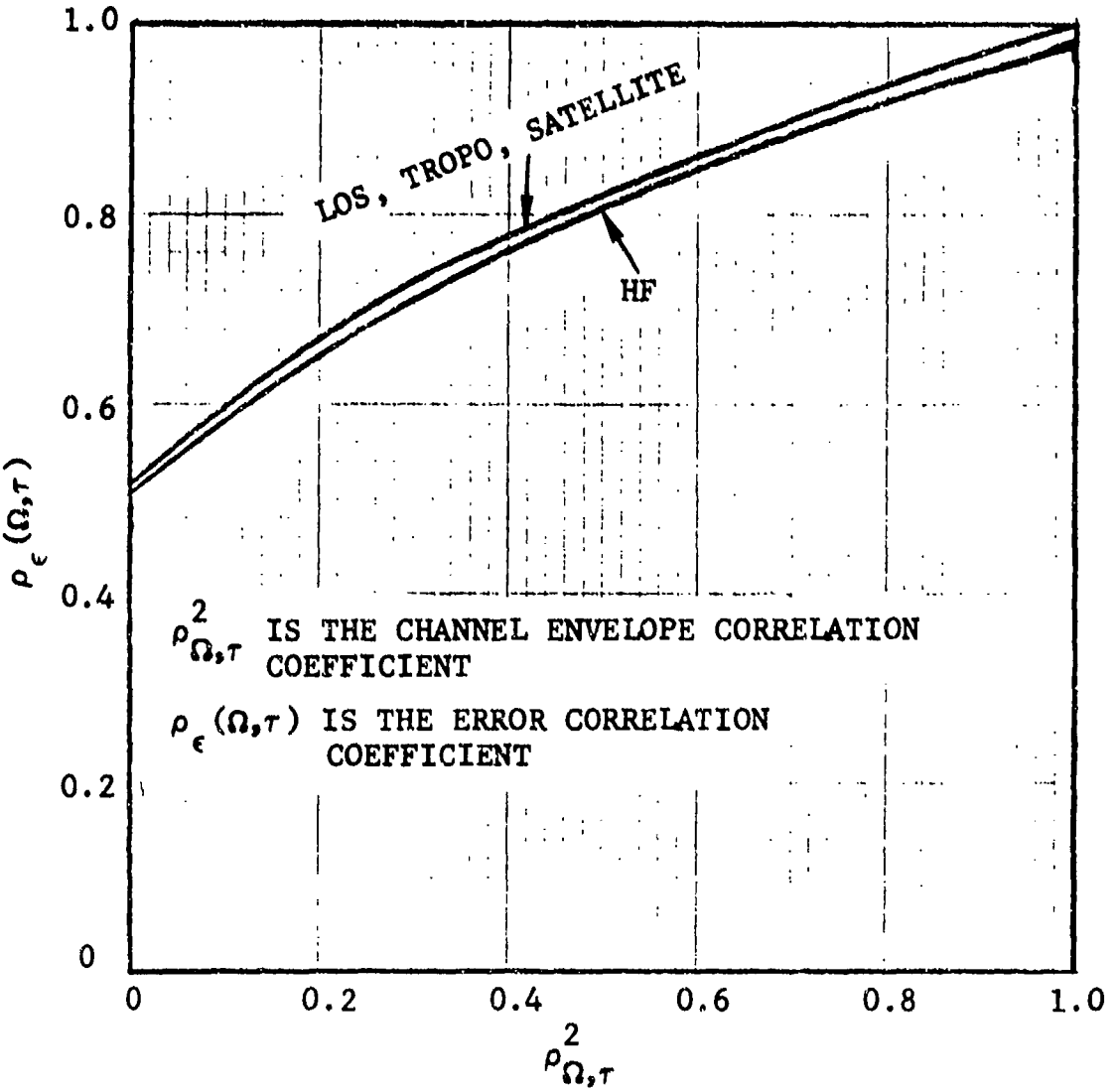

Figure 4.8 Correlation of the Errors in Estimating $R_2(0,0)$ and $R_2(\Omega,\tau)$

The rms Doppler spread parameter B is a measure of the dispersion in Doppler shifts suffered by a process in passing through a channel. This is entirely equivalent to the spectral width of a received carrier. If the power spectrum of a received carrier when referenced to the transmitted carrier frequency is denoted by P(f), then

$$P(f) = \int p(\tau)\, e^{-j2\pi f\tau}\, d\tau \tag{4.164}$$

where

$$p(\tau) = E\{T^*(f,t)T(f,t+\tau)\}$$

is the time correlation function of the channel.

The rms Doppler spread is defined to be

$$B \triangleq 2\left[\frac{\int (f-\bar{f})^2 P(f)\, df}{\int P(f)\, df}\right]^{1/2} \tag{4.165}$$

where

$$\bar{f} = \frac{\int f\, P(f)\, df}{\int P(f)\, df}$$

is the centroid of the power spectrum or the mean Doppler shift.

4.3.2.1 Differentiation Technique

In Reference [4.11], it is demonstrated that if e(t) is some nonlinear function of the envelope of the received carrier, the rms Doppler spread is given by

$$B = \frac{1}{\pi\alpha}\sqrt{\frac{\langle [\dot{e}(t)]^2 \rangle}{\langle [e(t)]^2 \rangle}} \tag{4.166}$$

where α is a constant dependent upon the nonlinear device and $\langle \cdot \rangle$ denotes time averages. Thus if we describe this nonlinear device by the function $F(\cdot)$

$$e(t) = F\left[|T(f,t)|^2\right] \tag{4.167}$$

it is shown in Ref. [4.11] that

$$\alpha = \sqrt{\frac{2\int_0^\infty r\, e^{-r}[dF(r)/dr]^2\, dr}{\int_0^\infty e^{-r} F^2(r)\, dr}} \tag{4.168}$$

In the case of a linear envelope detector $\alpha = \frac{1}{\sqrt{2}}$ and for a square law detector $\alpha = 1$. For analysis purposes, we will consider a scheme for implementing Eq. (4.161) for a square law detector. This scheme is functionally represented by Figure 4.9. Note that for convenience we will estimate B^2 instead of B.

The performance of the Doppler spread estimator of Figure 4.9 is as follows. The data signal is transmitted over the channel, picked off at RF (or IF) in the receiver, and sent to the magnitude-squared channel transfer function estimator analyzed in Section 4.1. The output of the estimator is sampled, delayed and sampled, and then combined with a noise power estimate to yield estimates of the magnitude squared of the channel transfer function at two times with separation Δt. These samples are used to approximate the derivative by a finite difference expression. The time average is approximated by averaging samples taken over a large time interval.

Therefore, the estimate of B^2 is given by

$$\widehat{B^2} = \frac{1}{\pi^2} \frac{\frac{1}{K(\Delta t)^2} \sum_{p=1}^{K} \left[|\tilde{T}(f,t_p+\Delta t)|^2 - |\tilde{T}(f,t_p)|^2 \right]^2}{\frac{1}{K} \sum_{p=1}^{K} |\tilde{T}(f,t_p)|^{2\,2}} \tag{4.169}$$

Defining

$$T_1 \triangleq \frac{1}{K} \sum_{p=1}^{K} \left[|\tilde{T}(f,t_p+\Delta t)|^2 - |\tilde{T}(f,t_p)|^2 \right]^2$$

$$T_2 \triangleq \frac{1}{K} \sum_{p=1}^{K} \left[|\tilde{T}(f,t_p)|^2 \right]^2 \tag{4.170}$$

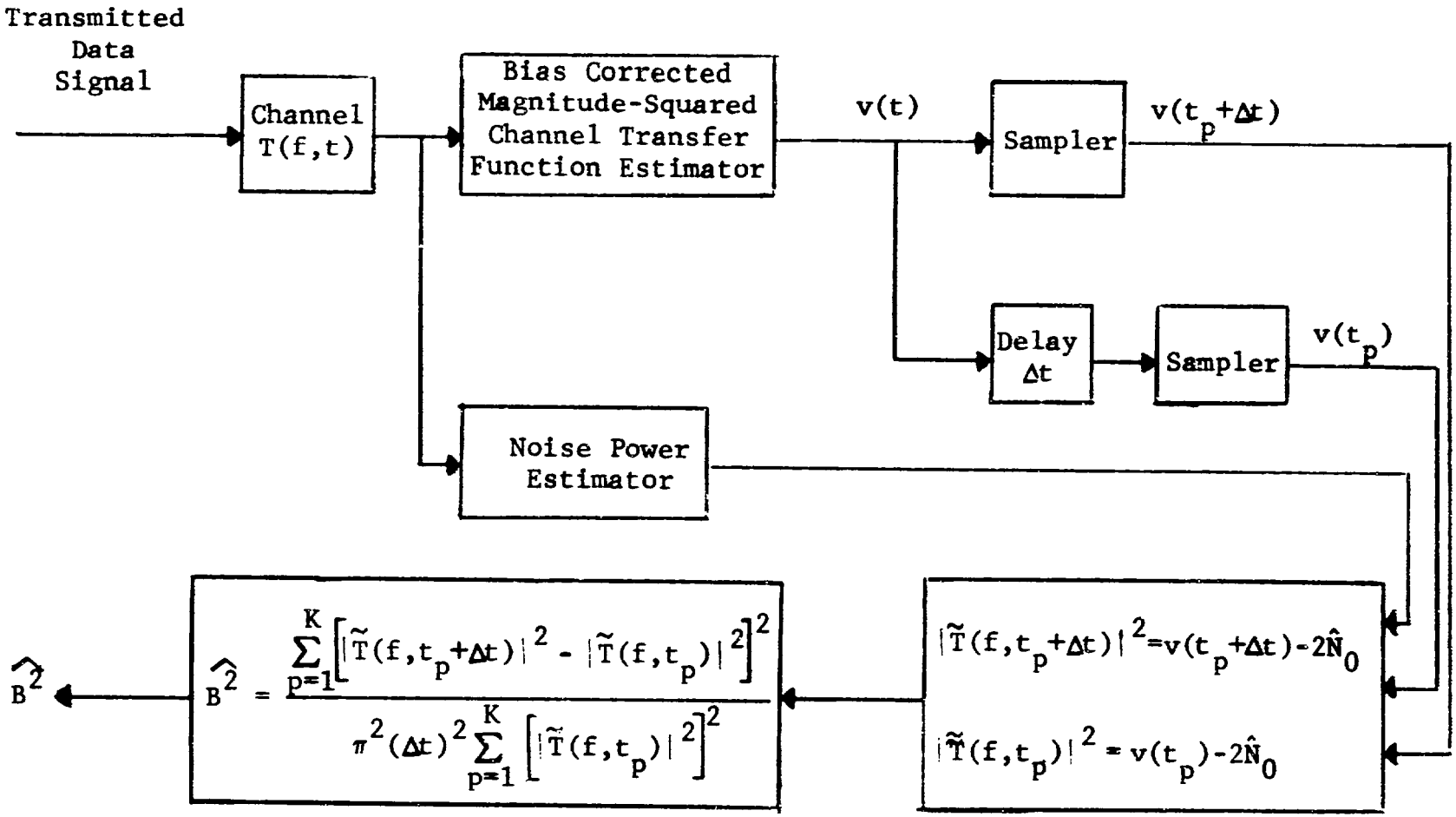

Figure 4.9 Doppler Spread Estimator Utilizing Differentiation Technique

then

$$\widehat{B^2} = \frac{1}{\pi^2(\Delta t)^2}\frac{T_1}{T_2} \tag{4.171}$$

The estimates T_1 and T_2 are random variables with means $E\{T_1\}$, $E\{T_2\}$ and variances $\sigma^2_{T_1}$, $\sigma^2_{T_2}$. We can represent the random variables T_1 and T_2 by

$$\begin{aligned} T_1 &= E\{T_1\} + \alpha \\ T_2 &= E\{T_2\} + \beta \end{aligned} \tag{4.172}$$

where

$$E\{\alpha\} = E\{\beta\} = 0$$

$$\begin{aligned} \sigma^2_\alpha &= \sigma^2_{T_1} \\ \sigma^2_\beta &= \sigma^2_{T_2} \end{aligned}$$

Substituting (4.168) into (4.167) gives

$$\widehat{B^2} = \frac{E\{T_1\}}{\pi^2(\Delta t)^2 E\{T_2\}}\frac{\left(1 + \frac{\alpha}{E\{T_1\}}\right)}{\left(1 + \frac{\beta}{E\{T_2\}}\right)} \tag{4.173}$$

Assuming that the number of samples K is large, then we can closely approximate B^2 by first- and second-order terms of α and β; this gives

$$\widehat{B^2} = \frac{E\{T_1\}}{\pi^2(\Delta t)^2 E\{T_2\}}\left[1 + \frac{\alpha}{E\{T_1\}} - \frac{\beta}{E\{T_2\}} - \frac{\alpha\beta}{E\{T_1\}E\{T_2\}} + \frac{\beta^2}{\left(E\{T_2\}\right)^2}\right] \tag{4.174}$$

The mean and variance of B^2 can be found from (4.169) to be given by

$$E\{\hat{B^2}\} = \frac{E\{T_1\}}{\pi^2(\Delta t)^2 E\{T_2\}}\left[1 + \frac{\sigma_{T_2}^2}{\left(E\{T_2\}\right)^2} - \frac{E\{\alpha\beta\}}{E\{T_1\}E\{T_2\}}\right]$$

$$\sigma^2_{\hat{B^2}} = \frac{E^2\{T_1\}}{\pi^4(\Delta t)^2\left(E\{T_2\}\right)^2}\left[\frac{\sigma_{T_1}^2}{\left(E\{T_1\}\right)^2} + \frac{\sigma_{T_2}^2}{E\{T_2\}^2} - \frac{2E\{\alpha\beta\}}{E\{T_1\}E\{T_2\}}\right] \qquad (4.175)$$

where higher than second-order moments of α and β are considered negligible. Since, from (4.167) we have

$$E\{\alpha\beta\} = E\{T_1T_2\} - E\{T_1\}E\{T_2\} \qquad (4.176)$$

Then to evaluate the effectiveness of the differentiation technique will require the evaluation of $E\{T_1\}$, $E\{T_2\}$, $\sigma_{T_1}^2$, $\sigma_{T_2}^2$, and $E\{T_1T_2\}$.

To evaluate the above moments of T_1 and T_2, we will use the bias corrected* representation for the estimates of the magnitude squared of the channel transfer function that was derived in Section 4.1. This representation allows us to express [see (4.102)]

$$|\tilde{T}(F,t_p)|^2 = |T(F,t_p)|^2(1+\delta_{1p}) + \delta_{2p}$$

$$|\tilde{T}(F,t_p+\Delta t)|^2 = |T(F,t_p+\Delta t)|^2(1+\epsilon_{1p}) + \epsilon_{2p} \qquad (4.177)$$

where

$$E\{\delta_{1p}\} = E\{\delta_{2p}\} = E\{\epsilon_{1p}\} = E\{\epsilon_{2p}\} = 0$$

$$E\{\delta_{1p}^2\} = E\{\epsilon_{1p}^2\} = \epsilon^2$$

$$E\{\delta_{2p}^2\} = E\{\epsilon_{2p}^2\} = \epsilon_S^2$$

*Estimation of B^2 using bias uncorrected estimates of $|T(F,t_p)|^2$ is considered in Appendix A.

and where ϵ and ϵ_S^2 are given by (4.57) and (4.100), respectively. Substituting the above estimates into (4.170) gives

$$T_1 = \frac{1}{K}\sum_{p=1}^{K} \left[|T(F,t_p+\Delta t)|^2(1+\epsilon_{1p}) + \epsilon_{2p} - |T(F,t_p)|^2(1+\delta_{1p}) - \delta_{2p} \right]^2 \tag{4.178}$$

Performing an ensemble average of T_1 over the error terms will yield the expected value of T_1 conditioned upon $T(f,t)$; this conditional expectation can be found to be given by

$$\begin{aligned} E\{T_1|T(f,t)\} = \frac{1}{K}\sum_{p=1}^{K} \Big[& |T(F,t_p)|^4(1+\epsilon^2) + \epsilon_S^2 R_2(0,0) \\ & - 2|T(F,t_p)|^2|T(F,t_p+\Delta t)|^2 \\ & + |T(F,t_p+\Delta t)|^4(1+\epsilon^2) \Big] \end{aligned} \tag{4.179}$$

where we have assumed that Δt is large enough such that the errors in magnitude-squared transfer functions are uncorrelated. Averaging (4.179) over the channel fluctuations and using the moment theorem for complex Gaussian processes gives

$$E\{T_1\} = R_2(0,0)\left(1 - \rho_{0,\Delta t}^2 + 2\epsilon^2 + \epsilon_S^2\right) \tag{4.180}$$

where $\rho_{0,\Delta t}^2$ is the envelope correlation coefficient of the channel defined by (4.156).

Assuming that the samples of $|T(F,t)|^2$ are spaced so that independent estimates of the derivative are formed, then the second moment of T_1 is given by

$$\begin{aligned} E\{T_1^2\} = \frac{1}{K^2}\sum_{p=1}^{K} E\Big\{ \Big[& |T(F,t_p+\Delta t)|^2(1+\epsilon_{1p}) + \epsilon_{2p} \\ & - |T(F,t_p)|^2(1+\delta_{1p}) - \delta_{2p} \Big]^4 \Big\} \\ & + \frac{K-1}{K} E^2\{T_1\} \end{aligned} \tag{4.181}$$

Averaging over the channel fluctuations and the errors and subtracting the mean squared, then the variance of T_1 is given by

$$\sigma^2_{T_1} = \frac{R_2^2(0,0)}{K}\left\{5\left(1-\rho^2_{0,\Delta t}\right)^2 + \epsilon^2\left[44\left(1-\rho^2_{0,\Delta t}\right) - 12\,\rho^2_{0,\Delta t}\left(1-\rho^2_{0,\Delta t}\right)\right] + 4\,\epsilon_S^2\left(1-\rho^2_{0,\Delta t}\right)\right\} \tag{4.182}$$

where higher than second-order error terms were considered negligible.

To evaluate $E\{T_2\}$ and $\sigma^2_{T_2}$ all that is necessary is to compare the definition of T_2 given by (4.170) with $\hat{R}_2(0,0)$ given by (4.142). Thus, the mean and variance of T_2 are given by (4.146) and (4.150), respectively.

In order to evaluate $E\{T_1T_2\}$, we use the expressions for T_1 and T_2 given by (4.170) and the expressions for the estimates of the magnitude squared of the channel transfer function as given by (4.177). From these expressions, it follows that

$$\begin{aligned} E\{T_1T_2\} = \frac{1}{K^2}\sum_{p=1}^{K} E\Big\{&\Big[|T(F,t_p+\Delta t)|^2(1+\epsilon_{1p}) + \epsilon_{2p} \\ &- |T(F,t_p)|^2(1+\delta_{1p}) - \delta_{2p}\Big]^2 \\ &\cdot\Big[|T(F,t_p)|^2(1+\delta_{1p}) + \delta_{2p}\Big]^2\Big\} \\ &+ \frac{K-1}{K}\,E\{T_1\}\,E\{T_2\} \end{aligned} \tag{4.183}$$

Performing the above ensemble averages gives

$$E\{T_1T_2\} = \frac{R_2^2(0,0)}{K}\left[4 - 5\rho^2_{0,\Delta t} + \rho^4_{0,\Delta t} + \epsilon^2\left(29 - 19\rho^2_{0,\Delta t} + 2\rho^4_{0,\Delta t}\right) + \epsilon_S^2\left(2.5 - 1.5\rho^2_{0,\Delta t}\right)\right] + \frac{K-1}{K}\,E\{T_1\}E\{T_2\} \tag{4.184}$$

where higher second-order moments of the errors are considered to be negligible. Substituting (4.184) into (4.176) and using the expressions for $E\{T_1\}$ and $E\{T_2\}$, then we can write

$$E\{\alpha\beta\} = \frac{R_2^2(0,0)}{K}\left[3 - 4\rho_{0,\Delta t}^2 + \rho_{0,\Delta t}^4 + \epsilon^2\left(26 - 18\rho_{0,\Delta t}^2 + 2\rho_{0,\Delta t}^4\right) + \epsilon_S^2\left(1 - \rho_{0,\Delta t}^2\right)\right] \quad (4.185)$$

Recalling from (4.175) the expression for the mean of $\hat{B^2}$ and substituting for $E\{T_1\}$, $E\{T_2\}$, σ_{T_2} and $E\{\alpha\beta\}$ gives

$$E\left\{\hat{B^2}\right\} = \frac{1 - \rho_{0,\Delta t}^2 + 2\epsilon^2 + \epsilon_S^2}{\pi^2 (\Delta t)^2\left(1 + \epsilon^2 + \frac{\epsilon_S^2}{2}\right)} \quad (4.186)$$

where terms that decrease as $\frac{1}{K}$ have been considered negligible with respect to 1.

From (4.164), we note that $P(f)$ and $p(\tau)$ are Fourier transform pairs and, thus, $p(\tau)$ can be expressed as

$$p(\tau) = \int P(f)\, e^{j2\pi f\tau}\, df \quad (4.187)$$

For small τ, we can approximate $p(\tau)$ by expanding $p(\tau)$ into a Taylor series and retaining the first three terms. This gives

$$p(\tau) \approx p(0) + j2\pi\tau\bar{f} - \frac{(2\pi\tau)^2}{2}\int f^2 P(f)\, df \quad (4.188)$$

where $\bar{f}$ is the mean Doppler shift given by (4.165). It immediately follows that

$$|p(\tau)|^2 \approx p^2(0) - (2\pi\tau)^2\left[\int f^2 P(f) df - \bar{f}^2\right] \quad (4.189)$$

Recalling the definition of B given by (4.165), then

$$\frac{|p(\tau)|^2}{p^2(0)} \approx 1 - \pi^2 B^2 \tau^2 \quad (4.190)$$

where this approximation is valid for $\pi^2 B^2 \tau^2 \ll 1$.

From the definition of $\rho^2_{0,\Delta t}$ as given by (4.156) and the definition of $p(\tau)$ given by (4.164), it follows that

$$\rho^2_{0,\Delta t} = \frac{|p(\Delta t)|^2}{p^2(0)} \tag{4.191}$$

From the above, we can express $\rho^2_{0,\Delta t}$ approximately as

$$\rho^2_{0,\Delta t} \approx 1 - \pi^2 B^2 (\Delta t)^2 \tag{4.192}$$

Combining (4.186) and (4.192), we can write

$$\boxed{E\left\{\hat{B^2}\right\} = \frac{B^2}{1+\epsilon_p^2/2} + \frac{\epsilon_p^2}{\pi^2(\Delta t)^2\left(1+\epsilon_p^2/2\right)}} \tag{4.193}$$

where from (4.104), $\epsilon_p^2 = 2\epsilon^2 + \epsilon_S^2$. Recalling that ϵ_p is the rms fractional error for estimating the magnitude squared of the channel transfer function and for the channels considered $\epsilon_p^2/2 \ll 1$, then the fractional bias is given by

$$\frac{E\left\{B^2\right\} - B^2}{B^2} = \frac{\epsilon_p^2}{\pi^2 B^2 (\Delta t)^2} \tag{4.194}$$

For the bias to be negligible, we must have $\epsilon_p^2 \ll \pi^2 B^2 (\Delta t)^2$ and for the approximations given by (4.192) to be valid, $\pi^2 B^2 (\Delta t)^2 \ll 1$ must be satisfied. For the error in estimating the magnitude squared of the channel transfer function due to noise and data to be uncorrelated (as was assumed in the derivation), Δt must be greater than the duration of the averaging filter $k(t)$ of Figure 4.1. It appears that for the HF channel it may not be possible to properly select Δt to insure an acceptable bias in estimating Doppler spread. The tropo and satellite channels should present no problem in selecting Δt due to ϵ_p being small. For the last two channels, selecting Δt such that $\pi B \Delta t \approx 0.1$ should yield good performance.

From Section 4.1 we noted that the filter parameters of the magnitude-squared channel transfer function were chosen so as to

minimize ϵ_p for a pair of design rms Doppler and multipath spreads. If the design Doppler spread was "near" to the value being estimated, then the bias would be near a minimum. Therefore, a performance gain can be realized by utilizing a multiplicity of rms Doppler spread estimators, each designed for a range of Doppler spreads.

To determine the rate of convergence of the estimator of Figure 4.9, the variance of B^2 must be evaluated. Substituting expressions for $\sigma^2_{T_1}$, $\sigma^2_{T_2}$, $E\{\alpha\beta\}$, $E\{T_1\}$, and $E\{T_2\}$ into the expression for $\sigma^2_{\hat{B}^2}$ given by (4.175) will yield the required variance. For the cases that the errors in estimating the magnitude squared of the channel transfer function have only a minor effect upon the estimator convergence, the variance of the estimator is approximately given by

$$\boxed{\sigma^2_{\hat{B}^2} = \frac{6\,\overline{\hat{B}^2}^2}{K}} \tag{4.195}$$

For $\overline{\hat{B}^2} \approx B^2$, then the rms fractional error for estimating B^2 is approximately given by

$$\frac{\sigma_{\hat{B}^2}}{B^2} \approx \sqrt{\frac{6}{K}} \tag{4.196}$$

and, thus, approximately 600 independent samples of $|T(f,t)|^2$ are required to reduce the rms fractional error to 0.1.

4.3.2.2 Correlation Technique

The second rms Doppler spread estimation technique to be evaluated is the correlation technique. Figure 4.10 is a functional block diagram of the estimator that will be analyzed in this section. The estimation procedure is as follows. The data signal is transmitted over the channel, picked off at IF (or RF) in the receiver, and sent to the time-frequency envelope correlation function estimator that was analyzed in Section 4.2. The outputs of this estimator are then used to form an estimate of B^2 by

$$\hat{B}^2 = \frac{2}{\pi^2\tau^2}\left(1 - \frac{\hat{R}_2(0,\tau)}{\hat{R}_2(0,0)}\right) \tag{4.197}$$

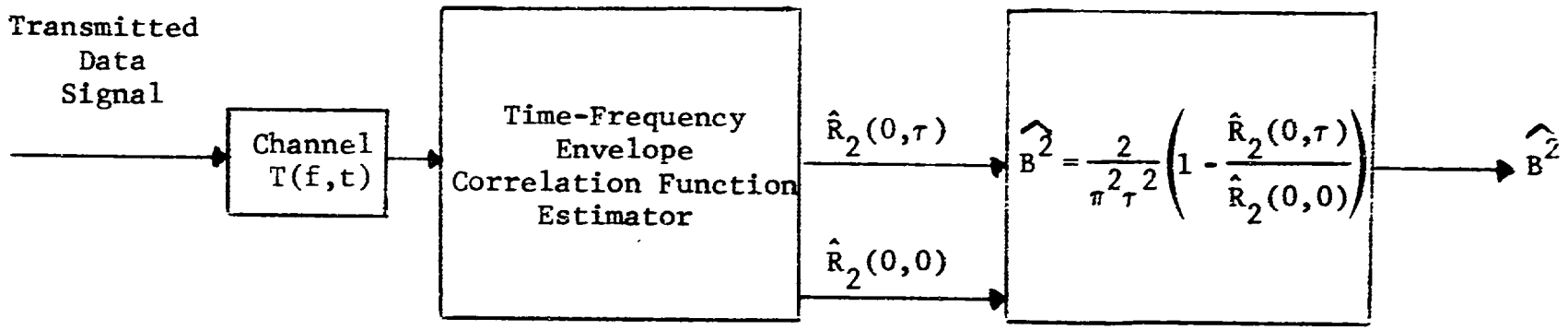

Figure 4.10 Doppler Spread Estimator Utilizing Correlation Technique

From Section 4.2, the estimates $\hat{R}_2(0,\tau)$ and $\hat{R}_2(0,0)$ can be represented by

$$\hat{R}_2(0,\tau) = E\{\hat{R}_2(0,\tau)\} + \epsilon_\tau$$

$$\hat{R}_2(0,0) = E\{\hat{R}_2(0,0)\} + \epsilon_0 \tag{4.198}$$

where from Section 4.2, we found

$$E\{\epsilon_0\} = E\{\epsilon_\tau\} = 0$$

$$\sigma^2_{\epsilon_\tau} = \frac{R_2^2(0,0)}{K}\left[\frac{3}{4} + \frac{7}{2}\rho^2_{0,\tau} + \frac{3}{4}\rho^4_{0,\tau} + \epsilon^2\left(2 + 8\rho^2_{0,\tau} + 2\rho^4_{0,\tau}\right) + 2\epsilon_S^2\right]$$

$$\sigma^2_{\epsilon_0} = \frac{R_2^2(0,0)}{K}\left[5 + 34\epsilon^2 + 2\epsilon_S^2\right]$$

$$E\{\epsilon_0\epsilon_\tau\} = \frac{R_2(0,0)}{K}\left[1 + 4\rho^2_{0,\tau} + \epsilon^2\left(4 + 13\rho^2_{0,\tau}\right) + \epsilon_S^2\left(\frac{1}{2} + \frac{1}{2}\rho^2_{0,\tau}\right)\right]$$

$$E\{\hat{R}_2(0,\tau)\} = \frac{R_2(0,0)}{2}\left(1 + \rho^2_{0,\tau}\right)$$

$$E\{R_2(0,0)\} = R_2(0,0)\left(1 + \epsilon_p^2/2\right) \tag{4.199}$$

Substituting (4.198) into (4.197) gives

$$\hat{B^2} = \frac{2}{\pi^2\tau^2}\left[1 - \frac{E\{\hat{R}_2(0,\tau)\}\left(1 + \dfrac{\epsilon_\tau}{E\{\hat{R}_2(0,\tau)\}}\right)}{E\{\hat{R}_2(0,0)\}\left(1 + \dfrac{\epsilon_0}{E\{\hat{R}_2(0,0)\}}\right)}\right] \tag{4.200}$$

For a large number of samples K, we can closely approximate the above estimate in terms of the first- and second-order terms of ϵ_0 and ϵ_τ; doing this we obtain

$$\widehat{B^2} = \frac{2}{\pi^2\tau^2}\left[1 - \frac{E\{\hat{R}_2(0,\tau)\}}{E\{\hat{R}_2(0,0)\}}\left(1 + \frac{\epsilon_\tau}{E\{\hat{R}_2(0,\tau)\}} - \frac{\epsilon_0}{E\{\hat{R}_2(0,0)\}} + \frac{\epsilon_0^2}{E^2\{\hat{R}_2(0,0)\}} - \frac{\epsilon_0\epsilon_\tau}{E\{\hat{R}_2(0,0)\}E\{\hat{R}_2(0,\tau)\}}\right)\right] \tag{4.201}$$

The mean and variance of B^2 are found from the above to be given by

$$E\{\widehat{B^2}\} = \frac{2}{\pi^2\tau^2}\left[1 - \frac{E\{\hat{R}_2(0,\tau)\}}{E\{\hat{R}_2(0,0)\}}\left(1 + \frac{\sigma^2_{\epsilon_0}}{E^2\{\hat{R}_2(0,0)\}} - \frac{E\{\epsilon_0\epsilon_\tau\}}{E\{\hat{R}_2(0,0)\}E\{\hat{R}_2(0,\tau)\}}\right)\right]$$

$$\sigma^2_{\widehat{B^2}} = \frac{4}{\pi^4\tau^4}\frac{E^2\{\hat{R}_2(0,\tau)\}}{E^2\{\hat{R}_2(0,0)\}}\left[\frac{\sigma^2_{\epsilon_0}}{E^2\{\hat{R}_2(0,0)\}} + \frac{\sigma^2_{\epsilon_\tau}}{E^2\{\hat{R}_2(0,\tau)\}} - \frac{2E\{\epsilon_0\epsilon_\tau\}}{E\{\hat{R}_2(0,0)\}E\{\hat{R}_2(0,\tau)\}}\right] \tag{4.202}$$

Substituting the moments of ϵ_0 and ϵ_τ as given by (4.199) into (4.202) gives, for the mean value of the B^2 estimate

$$E\left\{\hat{B^2}\right\} = \frac{2}{\pi^2\tau^2}\left[1 - \frac{1+\rho_{0,\tau}^2}{2+\epsilon_p^2}\right] \tag{4.203}$$

where the terms that fall off as $\frac{1}{K}$ were considered to be negligible. Performing simple algebraic manipulations gives

$$\boxed{E\left\{\hat{B^2}\right\} = \frac{1-\rho_{0,\tau}^2+\epsilon_p^2}{\pi^2\tau^2\left(1+\epsilon_p^2/2\right)}} \tag{4.204}$$

Comparing (4.186) with (4.204), and recalling that $\epsilon_p^2 = 2\epsilon^2 + \epsilon_s^2$, we note that the biases for the correlation and differentiation techniques are identical if $\tau = \Delta t$ (thus, the same comments apply to selecting τ as mentioned in selecting Δt).

From (4.199) and (4.202), the variance of the estimator given by Figure 4.10 can be evaluated. For the case that the errors in estimating the magnitude squared of the channel transfer function have a negligible effect upon the convergence of the rms Doppler spread estimator, we can write

$$\sigma^2_{\hat{B^2}} \approx \frac{4\left(1-\rho_{0,\tau}^2\right)\left(1+2\rho_{0,\tau}^2\right)}{\pi^4\tau^4 K} \tag{4.205}$$

Using (4.192) to approximate $1-\rho_{0,\tau}^2$ by $\pi^2B^2\tau^2$ and approximating $1+2\rho_{0,\tau}^2$ by 3 gives

$$\boxed{\sigma^2_{\hat{B^2}} \approx \frac{12B^2}{\pi^2\tau^2 K}} \tag{4.206}$$

and the rms fractional error for estimating B^2 is

$$\frac{\sigma_{\hat{B^2}}}{B^2} = \sqrt{\frac{12}{\pi^2B^2\tau^2K}} \tag{4.207}$$

For Eq. (4.192) to closely approximate $\rho^2_{0,\tau}$, and, thus, for the bias to be small, we must have $\pi^2 B^2 \tau^2 \ll 1$. Therefore, comparing the rms fractional error for the differentiation technique as given by (4.196) with (4.207), it is clear that the performance of the differentiation technique is far superior to that of the correlation technique.

4.3.2.3 Level Crossing Technique

The characterization of T(f,t) as a complex Gaussian process allows the estimation of gross channel parameters from properties of these processes. Fading rates have been determined previously [4.16] in fading channels by measuring the average number of times per second that the envelope of a carrier crosses a specified level. The theoretical basis for this approach is due to Rice [4.17] who has shown that, for a narrowband Gaussian process, the number of times per second that the envelope crosses a level R is simply related to an rms bandwidth measure.

From Ref. [4.17], the expected number of times per second that the envelope of a Ricean random process crosses a level R is given by (using Rice's notation)

$$N_R = \left(\frac{b_2}{2\pi}\right)^{1/2} \frac{R}{b_0} I_0\left(\frac{RQ}{b_0}\right) \exp\left[-\frac{R^2+Q^2}{2\,b_0}\right] \tag{4.208}$$

where

$$b_n = (2\pi)^n \int_0^\infty W_s(f)\ (f-\bar{f})^n\ df$$

$W_s(f)$ is the spectrum of the narrowband process centered at $\bar{f}$.

Q is the amplitude of the specular component, if any.

Making the change of variables:

$$\beta = \frac{R}{b_0^{1/2}}$$

$$a = \frac{Q}{b^{1/2}} \tag{4.209}$$

and defining the number of positive (or negative) crossings of the normalized level β by N_β, it follows that

$$N_\beta = \left(\frac{b_2}{2\pi b_0}\right)^{1/2} \beta\, I_0(a\beta)\, e^{-(\beta^2+a^2)/2} \tag{4.210}$$

From the definition of the rms Doppler spread given by (4.165) and the definition of b_n given above, we have

$$B = \frac{1}{\pi}\left[\frac{b_2}{b_0}\right]^{1/2} \tag{4.211}$$

Substituting (4.211) into (4.210) and considering the case of pure scatter ($a = 0$), it follows that

$$N_\beta = \sqrt{\frac{\pi}{2}}\, B\, \beta\, e^{-\frac{\beta^2}{2}} \tag{4.212}$$

Noting for the pure scatter case that β is Rayleigh distributed with median level $\sqrt{2\,\ell n\, 2}$, then the average number of times per second that $|T(F,t)|$ fades below its median level is related to the rms Doppler spread by

$$N_{med} = \frac{B}{2}\sqrt{\pi\,\ell n\, 2} \tag{4.213}$$

Solving for B, we have

$$B = \frac{2\,N_{med}}{\sqrt{\pi\,\ell n\, 2}} \tag{4.214}$$

Equation (4.214) is the relationship between B and the fade rate that will be implemented to form an estimate of B. Figure 4.11 is a functional block diagram of the rms Doppler spread estimator that will be analyzed in this section. The estimation procedure is as follows. The data signal is transmitted over the channel, picked off at IF (or RF) and sent a magnitude-squared channel transfer function of the type analyzed in Section 4.1. The output of this estimator is sampled and combined with a noise power estimate to form estimates of the magnitude of the channel transfer function.

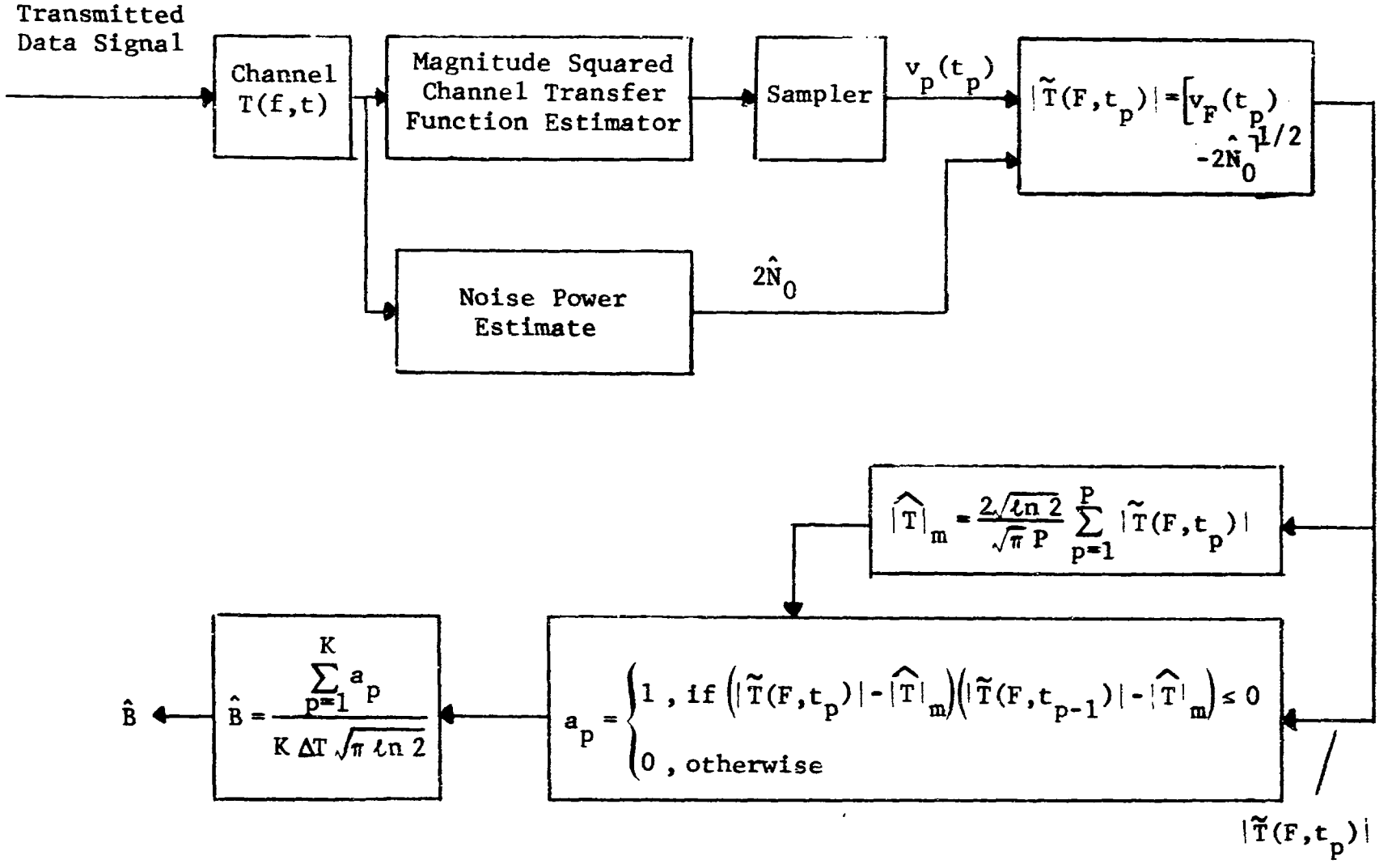

Figure 4.11 Doppler Spread Estimator Utilizing the Level Crossing Technique

These estimates are used to form an estimate of the median of the transfer function magnitude. The median level is estimated by estimating the mean and, then using the relation between the mean and the median of a Rayleigh random variable. Once the median is estimated, it is used to predict level crossing by counting the number of adjacent samples on different sides of the median estimate. These predicted crossings are then used to estimate the rms Doppler spread, where $K \cdot \Delta T$ is the total time over which crossings are counted.

The first problem encountered in implementing the level crossing technique to estimate the rms Doppler spread is that of evaluating the effect of errors in estimating the median level. From (4.212) the fractional error in counting crossing due to errors in setting the level is

$$\frac{N_{\beta+\alpha} - N_{\beta}}{N_{\beta}} = \frac{\alpha(1 - \beta^2)}{\beta} \tag{4.215}$$

where only first-order terms of α were retained. For the median level $\beta = \sqrt{2 \ell n 2}$, we have

$$\frac{N_{\beta+\alpha} - N_{\beta}}{N_{\beta}} = - 0.33 \alpha \tag{4.216}$$

If the median level is estimated over a long enough time interval, then $|\alpha|$ will be small and the fractional error in counting level crossings due to inaccurate level settings will be negligible.

To obtain good estimates of the rate of level crossings, the samples must be close enough together such that the probability of multiple crossings in an interval is at an acceptably low level. Furthermore, the samples must be far enough apart such that the magnitude of the channel transfer function changes appreciably and the additional crossings due to the errors in estimating the channel transfer function magnitude do not significantly alter the estimate of B. Both of these effects will result in biases. We would like to choose the sampling rate such that these effects are negligible. However, if the rms fractional error in estimating the magnitude squared of the channel transfer function is large, it may not be possible to select the sampling rate such that both of the above effects are negligible.

With ΔT the spacing between samples, then to evaluate the probability of multiple crossings in an interval, it is necessary

to find the probability of a fade in a ΔT interval. We will assume that the probability of three crossings in an interval is very small with respect to two crossings in an interval. With $P(\Delta T)$ the probability of two crossings of the median in a ΔT interval and $C(0,\Delta T)$ the event of at least one crossing in the interval, then

$$P(\Delta T) = \text{Prob.}\left\{2 \text{ crossings in } (0,\Delta T) \mid C(0,\Delta T)\right\} \cdot P\left\{C(0,\Delta T)\right\} \qquad (4.217)$$

where $P\left\{C(0,\Delta T)\right\}$ is the probability of at least one crossing in $(0,\Delta T)$. With $\bar{t}$ the average length of a fade below a level R, then from [4.18]

$$\bar{t} = \frac{\sqrt{2}}{R\pi^{1/2}B}\left(e^{R^2/2} - 1\right) \qquad (4.218)$$

The average length of a fade below (and also above) the median level is found from (4.218) with $R = \sqrt{2\ell n 2}$. This gives

$$\bar{t} = \frac{1}{\sqrt{\pi\ell n 2}\ B} \qquad (4.219)$$

With ΔT small, the probability of one crossing in $(0,\Delta T)$ is approximately equal to $P\{C(0,\Delta T)\}$. With $\bar{t}$ the average time between median crossings, the $P\{C(0,\Delta T)\}$ can be closely approximated by

$$P\{C(0,\Delta T)\} = \frac{\Delta T}{\bar{t}} \qquad (4.220)$$

To evaluate $P(\Delta T)$ using (4.217), we must find the probability of two crossings in $(0,\Delta T)$ given that there was at least one crossing. In [4.18], it is shown in Table III that for a Gaussian power spectrum that the probability density function for fade intervals is approximately given (for $\tau \ll \bar{t}$) by

$$f(\tau) = \frac{2\tau}{\bar{t}^2} \quad , \quad \text{for } \tau \ll \bar{t} \qquad (4.221)$$

With the up excursion intervals distributed as given by (4.221) for $\tau \ll \bar{t}$, we can then write

$$\text{Prob.}\left\{2 \text{ crossings in } (0,\Delta T) \mid C(0,\Delta T)\right\} = \int_0^{\Delta T}\int_x^{\Delta T} \frac{1}{\Delta T}\,\frac{2\tau}{\bar{t}^2}\,d\tau\,dx \qquad (4.222)$$

Evaluating the above integrals gives

$$\text{Prob.}\left\{2 \text{ crossings in } (0,\Delta T) \mid C(0,\Delta T)\right\} = \frac{2(\Delta T)^2}{3\bar{t}^2} \qquad (4.223)$$

Substituting (4.220) and (4.223) into (4.217) gives for the probability of two crossings in a ΔT interval

$$P(\Delta T) = \frac{2(\Delta T)^3}{3\bar{t}^3} \qquad (4.224)$$

With the number of intervals equal to K, the expected number of crossings is

$$N_C = \frac{K\,\Delta T}{\bar{t}} \qquad (4.225)$$

and, from (4.224), the expected number of crossings not counted is

$$N_C' = \frac{K\,4(\Delta T)^3}{3\,\bar{t}^3} \qquad (4.226)$$

Using (4.219), (4.225), and (4.226), the fraction of crossings not counted is

$$\frac{N_C'}{N_C} = \frac{4(\Delta T)^2 \pi B^2 \ln 2}{3} \qquad (4\ 227)$$

Since these crossings are not counted, the estimate of the rms Doppler spread will be negatively biased due to multiple crossings in the ΔT intervals.

Evaluation of the bias due to additional level crossings introduced by the errors in estimating the channel transfer function magnitude has not been performed due to the difficulties imposed by the processing of the estimator and the inherent complexities involved in level crossing problems. However, from Sections 4.3.2.1 and 4.3.2.2, we might reasonably expect that the bias due to these effects can be represented by

$$\epsilon_B = \frac{C\,\epsilon_P}{\pi(\Delta T)} \tag{4.228}$$

where ϵ_P is the rms fractional error in estimating the magnitude squared of the channel transfer function and C is some positive constant. Therefore, the mean value of the rms Doppler spread estimate is approximately given by

$$\boxed{E\{\hat{B}\} \approx B\left[1 - \frac{4(\Delta T)^2 \pi B^2 \ln 2}{3} + \frac{C\,\epsilon_P}{\pi B \Delta T}\right]} \tag{4.229}$$

From (4.229) we note that the biases can be safely neglected only when $\epsilon_P \ll \pi B (\Delta T)$ and $\pi^2 B^2 (\Delta T)^2 \ll 1$ are simultaneously satisfied.

Direct determination of the convergence rate for the rms Doppler spread estimate does not appear to be mathematically tractable. However, we can approximate the rate of convergence by making assumptions that should yield useful results. We will assume that the times between crossings are independent and identically distributed. From Ref. [4.16], the distribution function for the intervals can be assumed to lie between the distributions

$$F_1(u) = 1 = e^{-u}$$

$$F_2(u) = 1 - \frac{2}{u} I_1\left(\frac{2}{\pi u^2}\right) e^{-\frac{2}{\pi u^2}} \tag{4.230}$$

where a normalized interval has been defined by $u = \tau/\bar{\tau}$. Rice [4.16] derived the above distributions as limiting forms of the fade interval distribution as the level goes to ∞ and 0, respectively. These limiting forms hold for any power spectrum.

For the two distributions given by (4.230), the variance of the interval between crossings can be found to be given by

$$\sigma_1^2 = \bar{t}^2$$

$$\sigma_2^2 = \left(\frac{32}{3\pi} - 1\right) \bar{t}^2 \qquad (4.231)$$

From the theory of renewal processes [4.19], the mean and variance of the number of crossings in an interval of length t are given by

$$E\{N_t\} = \frac{t}{\bar{t}}$$

$$\mathrm{Var}\{N_t\} = \frac{\sigma^2 t}{\bar{t}^3} \qquad (4.232)$$

where σ^2 is the variance of the intervals between crossings.

From (4.231), it follows that an rms fractional error in estimating crossing rates can be defined by

$$\frac{\mathrm{Var}^{1/2}\{N_t\}}{E\{N_t\}} = \frac{\sigma}{[\bar{t}\, t]^{1/2}} \qquad (4.233)$$

For the interval distributions given by (4.230), it follows from (4.219) and (4.231) that

$$\boxed{\frac{\mathrm{Var}^{1/2}\{N_t\}}{E\{N_t\}} = \frac{1}{[B\, t]^{1/2}\, [\pi\, \ell n\, 2]^{1/4}}} \qquad (4.234)$$

for $F_1(u)$ and

$$\boxed{\frac{\mathrm{Var}^{1/2}\{N_t\}}{E\{N_t\}} = \left[\frac{\frac{32}{3\pi} - 1}{B\, t\, [\pi\, \ell n\, 2]^{1/2}}\right]^{1/2}} \qquad (4.235)$$

for $F_2(u)$. Note that the above fractional errors differ by about the $\sqrt{2}$. The interval length t equals $K\,\Delta T$ since K is the number of intervals and ΔT is the length of each interval. The rms fractional error decreases quite rapidly for the two interval distributions given by (4.230).

Since the estimate of the rms Doppler spread is proportional to the number of crossings, the rms fractional error for estimating B is given by (4.234) for $F_1(u)$ and (4.235) for $F_2(u)$.

4.3.2.4 Summary

In this section, three techniques were analyzed for their ability to estimate the rms Doppler spread. The convergence of the differentiation technique was shown to be much faster than that of the correlation technique. Therefore, since the biases for these two techniques was shown to be the same, the differentiation technique is clearly the superior of the two.

Comparison of the differentiation and level crossing techniques requires that the number of independent samples of $|T(f,t)|^2$, K, be related to Bt. As a rule of thumb, we can take K independent samples of $|T(f,t)|^2$ in a K/B interval; thus, we can assume $K \approx Bt$. Also, recalling that for the differentiation technique B^2 was estimated while the level crossing technique estimated B, then (4.196) can be roughly compared to (4.234) or (4.235). The result of this comparison is that the techniques converge at approximately the same rate. Therefore, to estimate the rms Doppler spread, either the differentiation or level crossing technique should be employed.

Using the above rule of thumb, the rms Doppler spread estimators were evaluated for the case where the errors in estimating the magnitude squared of the channel transfer function have negligible effect upon the estimator convergence. The performance of the three rms Doppler spread estimation techniques are presented in Figure 4.12.

4.3.3 Multipath Spread Measurement Techniques

In this section, we address the problem of implementing and evaluating possible techniques for estimating the rms multipath spread of the channel from estimates of the magnitude squared of the channel transfer function. The estimation techniques to be considered are the differentiation, correlation, and level crossing techniques. These techniques were considered in Section 4.3.2 in connection with estimating the channel rms Doppler spread. The mathematical basis for these techniques can be found in Refs. [4.11] - [4.15].

The rms multipath spread parameter L is a measure of the dispersion in path delays suffered by a process in passing through the channel. This is entirely equivalent to the "width" of the impulse response of the channel. Since the delay power spectrum describes the distribution of power in the various path delays, the rms multipath spread is given by

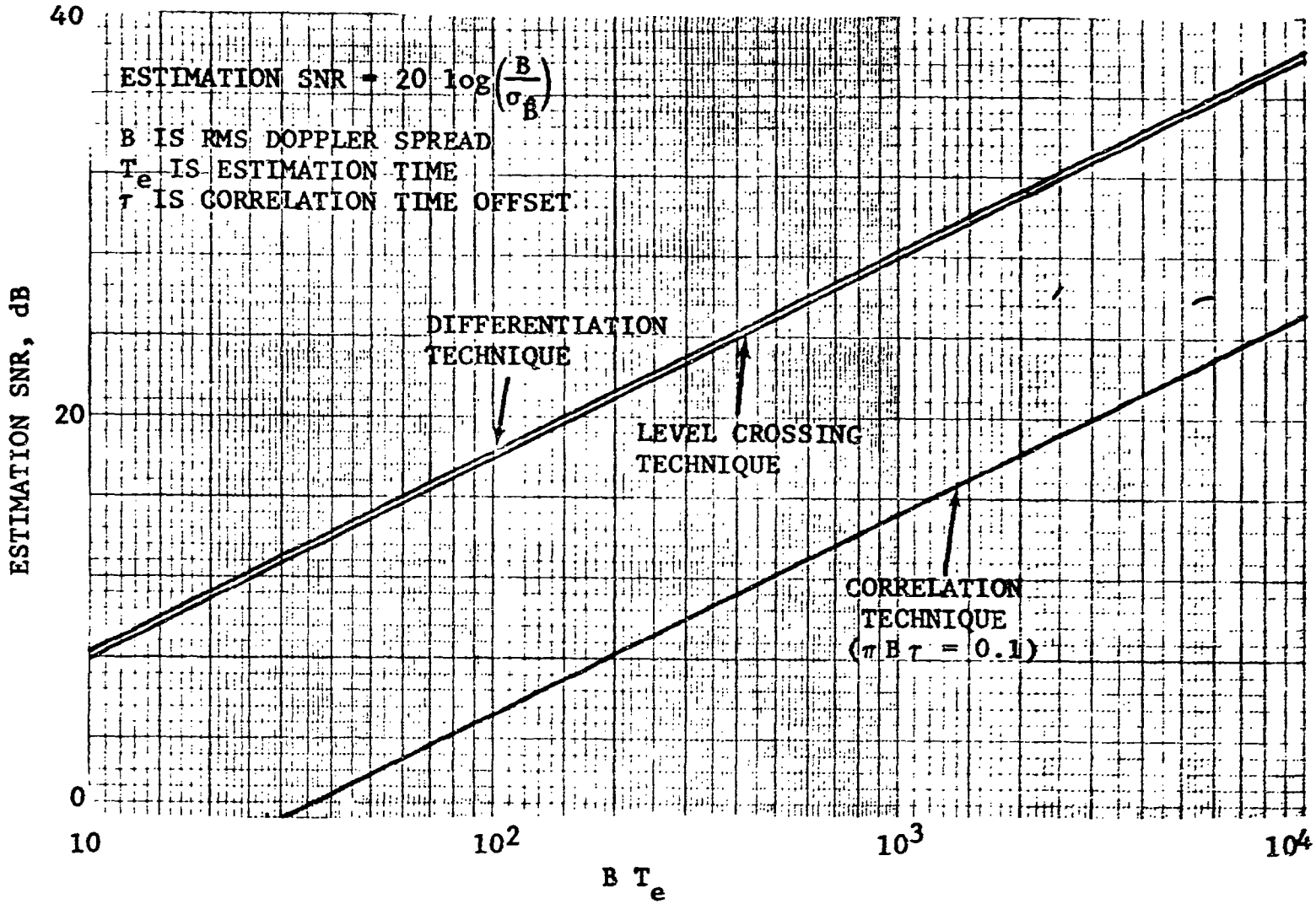

Figure 4.12 Estimation of RMS Doppler Spread

$$L \triangleq 2\left[\frac{\int(\xi - \bar{\xi})^2\, Q(\xi)\, d\xi}{\int Q(\xi)\, d\xi}\right]^{1/2} \tag{4.236}$$

where

$$\bar{\xi} = \frac{\int \xi\, Q(\xi)\, d\xi}{\int Q(\xi)\, d\xi}$$

is the "centroid" of the delay power spectrum or the "mean" path delay.

4.3.3.1 Differentiation Technique

A technique analogous to the differentiation technique for estimating the rms Doppler spread (Section 4.3.2.1) can be used to estimate the rms multipath spread. From Ref. [4.11], if E(f) is defined by

$$E(f) = F\left[|T(f,t)|^2\right] \tag{4.237}$$

then

$$L = \frac{1}{\pi\alpha}\left[\frac{\left\{[dE(f)/df]^2\right\}}{\left\{[E(f)]^2\right\}}\right]^{1/2} \tag{4.238}$$

where $\{\cdot\}$ denotes frequency average and α is given by (4.168). For the case of a linear envelope detector $\alpha = \frac{1}{\sqrt{2}}$ and for a square law detector $\alpha = 1$. For analysis purposes, Eq. (4.238) will be implemented for a square law detector and L^2 instead of L will be estimated. Figure 4.13 is the rms multipath spread estimator which utilizes the differentiation technique. This estimator is the dual of the rms Doppler spread estimator of Figure 4.9.

The performance of the rms multipath spread estimator is as follows. The data signal is transmitted over the channel, picked off at RF (or IF) in the receiver, and sent to two magnitude-squared channel transfer function estimators. The output of the estimators are combined with a noise power estimate to yield estimates of the magnitude squared of the channel transfer function at two frequencies with separation ΔF. ΔF should be selected in a manner dual to the selection of Δt of Section 4.3.2.1.

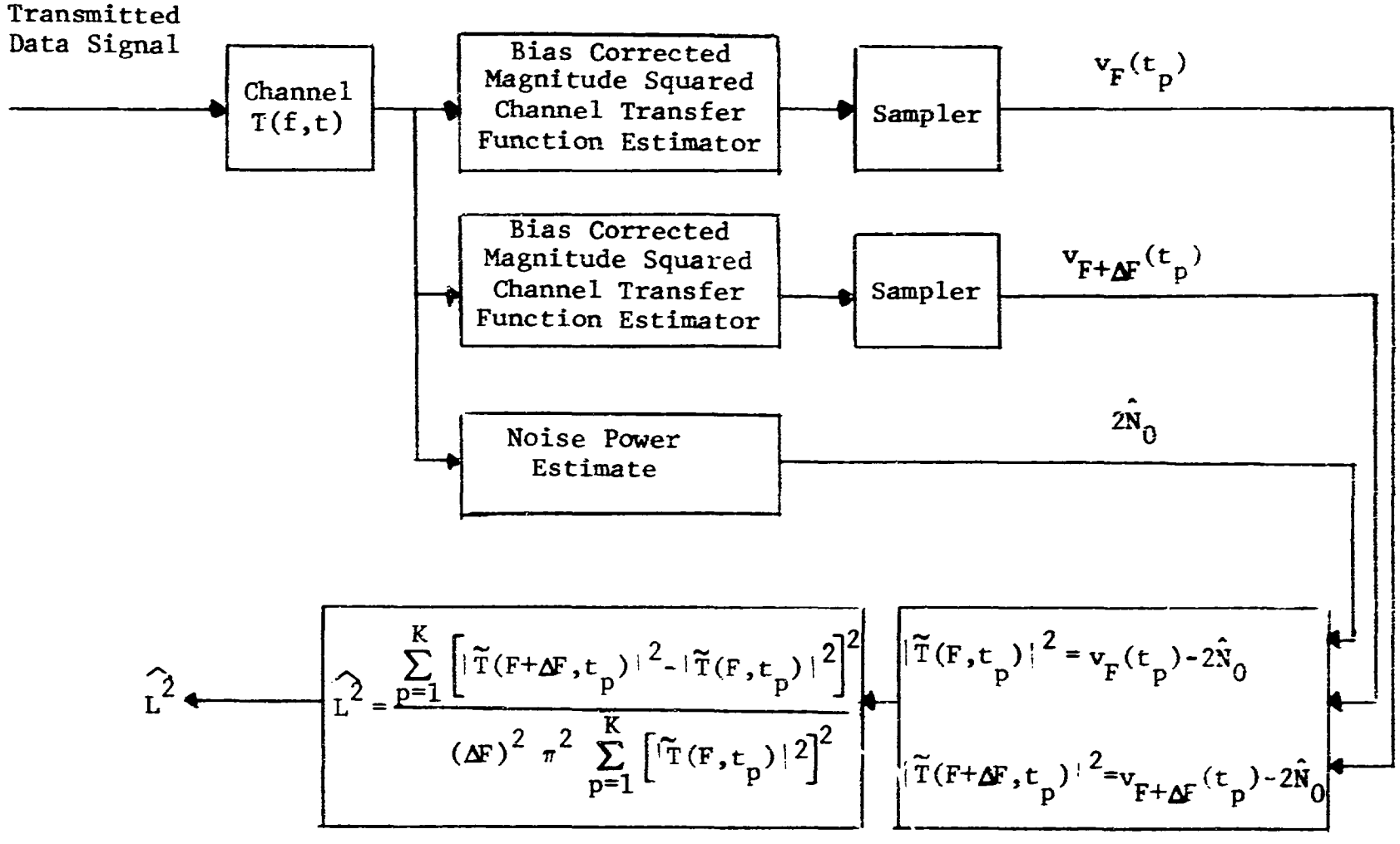

Figure 4.13 Multipath Spread Estimator Utilizing Differentiation Technique

The estimate of L^2 is given by

$$\hat{L}^2 = \frac{1}{\pi^2} \frac{\frac{1}{K(\Delta F)^2} \sum_{p=1}^{K} \left[|\tilde{T}(F+\Delta F, t_p)|^2 - |\tilde{T}(F,t_p)|^2 \right]^2}{\frac{1}{K} \sum_{p=1}^{K} \left[|\tilde{T}(F,t_p)|^2 \right]^2} \tag{4.239}$$

The mean and variance of $\hat{L}^2$ can be found in the same manner as the mean and variance of $\hat{B}^2$ were found in Section 4.3.2.1.* Doing this yields

$$E\{\hat{L}^2\} = \frac{L^2}{1+\epsilon_p^2/2} + \frac{\epsilon_p^2}{\pi^2(\Delta F)^2}$$

$$\sigma^2_{\hat{L}^2} = \frac{6\,\overline{\hat{L}^2}^2}{K} \tag{4.240}$$

which are the expressions analogous to (4.173) and (4.175). For $E\{L^2\} \approx L^2$, the rms fractional error for estimating L^2 is

$$\frac{\sigma_{\hat{L}^2}}{L^2} \approx \sqrt{\frac{6}{K}} \tag{4.241}$$

and, as in Section 4.3.2.1, approximately 600 independent samples of $|T(f,t)|^2$ are required to reduce the rms fractional error to 0.1.

4.3.3.2 Correlation Technique

The second rms multipath spread estimator implements the correlation technique derived in Refs. [4.11] - [4.14]. This technique is the dual of the rms Doppler spread estimation technique analyzed in Section 4.3.2.2. Figure 4.14 is a block diagram of the estimator that will be considered in this section. The data is transmitted over the channel, picked of at RF (or IF)

*Appendix A considers the estimation of L^2 using the differentiation technique from bias uncorrected estimates of $|T(F,t_p)|^2$.

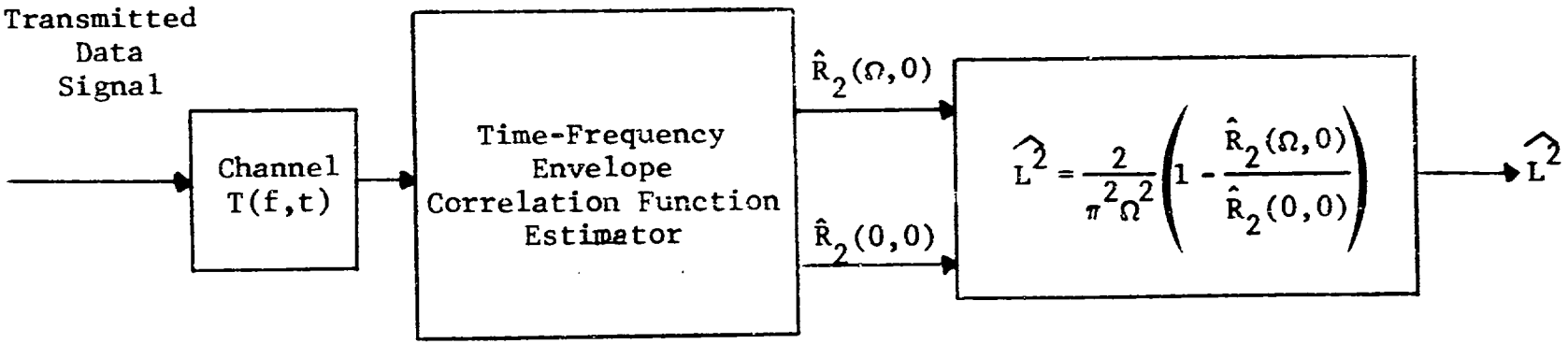

Figure 4.14 Multipath Spread Estimator Utilizing Correlation Technique

in the receiver, and sent to a time-frequency envelope correlation function of the type analyzed in Section 4.1. The outputs of this estimator are used to form an estimate of L^2 by

$$\hat{L^2} = \frac{2}{\pi^2\Omega^2}\left[1 - \frac{\hat{R}_2(\Omega,0)}{\hat{R}_2(0,0)}\right] \tag{4.242}$$

The evaluation of the mean and variance of the above estimate can be found in a manner similar to that used to find the mean and variance of $\hat{B^2}$ in Section 4.3.2.2. Due to the similarity of the derivations, only the results will be presented. Therefore, the mean and variance of $\hat{L^2}$ as given by (4.242) can be closely approximated by

$$E\{\hat{L^2}\} = \frac{L^2}{1+\epsilon_p^2/2} + \frac{\epsilon_p^2}{\pi^2\Omega^2}$$

$$\sigma^2_{\hat{L^2}} \approx \frac{12\,L^2}{\pi^2\Omega^2 K} \tag{4.243}$$

where K is the number of independent samples of the magnitude squared of the channel transfer function. The rms fractional error is

$$\frac{\sigma_{\hat{L^2}}}{L^2} = \sqrt{\frac{12}{\pi^2 L^2 \Omega^2 K}} \tag{4.244}$$

Thus, as in the case of estimating the rms Doppler spread, the correlation technique converges much slower than the differentiation technique.

4.3.3.3 Level Crossing Technique

The level crossing technique used in Section 4.3.2.3 to estimate the rms Doppler spread can also be applied to the problem of estimating the rms multipath spread. We will estimate the rms multipath spread from the number of frequencies per Hz that

the magnitude of the channel transfer function crosses its median level. That is, an expression dual to (4.214) can be used to express L as

$$L = \frac{2 M_{med}}{\sqrt{\pi \ell n 2}} \tag{4.245}$$

where M_{med} is the expected number of frequencies per Hz that $|T(f,t)|$ fades below its median level.

Figure 4.15 is the estimator that will be considered. The performance of the estimator is as follows. The data signal is transmitted over the channel, picked off at RF (or IF) in the receiver and sent to a bank of J+1 magnitude-squared channel transfer function estimators. The output of these estimators is sampled and combined with a noise power estimate to form estimates of the magnitude of the channel transfer function at J+1 frequencies with a separation of ΔF between adjacent estimates. These estimates are used to estimate the median level crossings in a $J\Delta F$ band at the p^{th} time instant. The estimate of rms multipath spread is formed by summing the number of median level crossings and dividing by the total frequency band over which this estimate was formed.

The mean value of the rms multipath spread estimate can be found to be the dual of (4.229) and is approximately given by

$$E\{\hat{L}\} = L\left[1 - \frac{4(\Delta F)^2 \pi L^2 \ell n 2}{3} + \frac{C \epsilon_p}{\pi L \Delta F}\right] \tag{4.246}$$

Assuming that the time samples are spaced far enough apart such that the number of crossings at the sampling times are independent, then the rms fractional error in counting crossings can be found from the dual expressions of (4.234) and (4.235) to be given by

$$\frac{Var^{1/2}\{M_{KJ\Delta F}\}}{E\{M_{KJ\Delta F}\}} = \left[\frac{1}{L K J(\Delta F)[\pi \ell n 2]^{1/2}}\right]^{1/2} \tag{4.247}$$

for $F_1(u)$, where u is now the normalized frequency band.

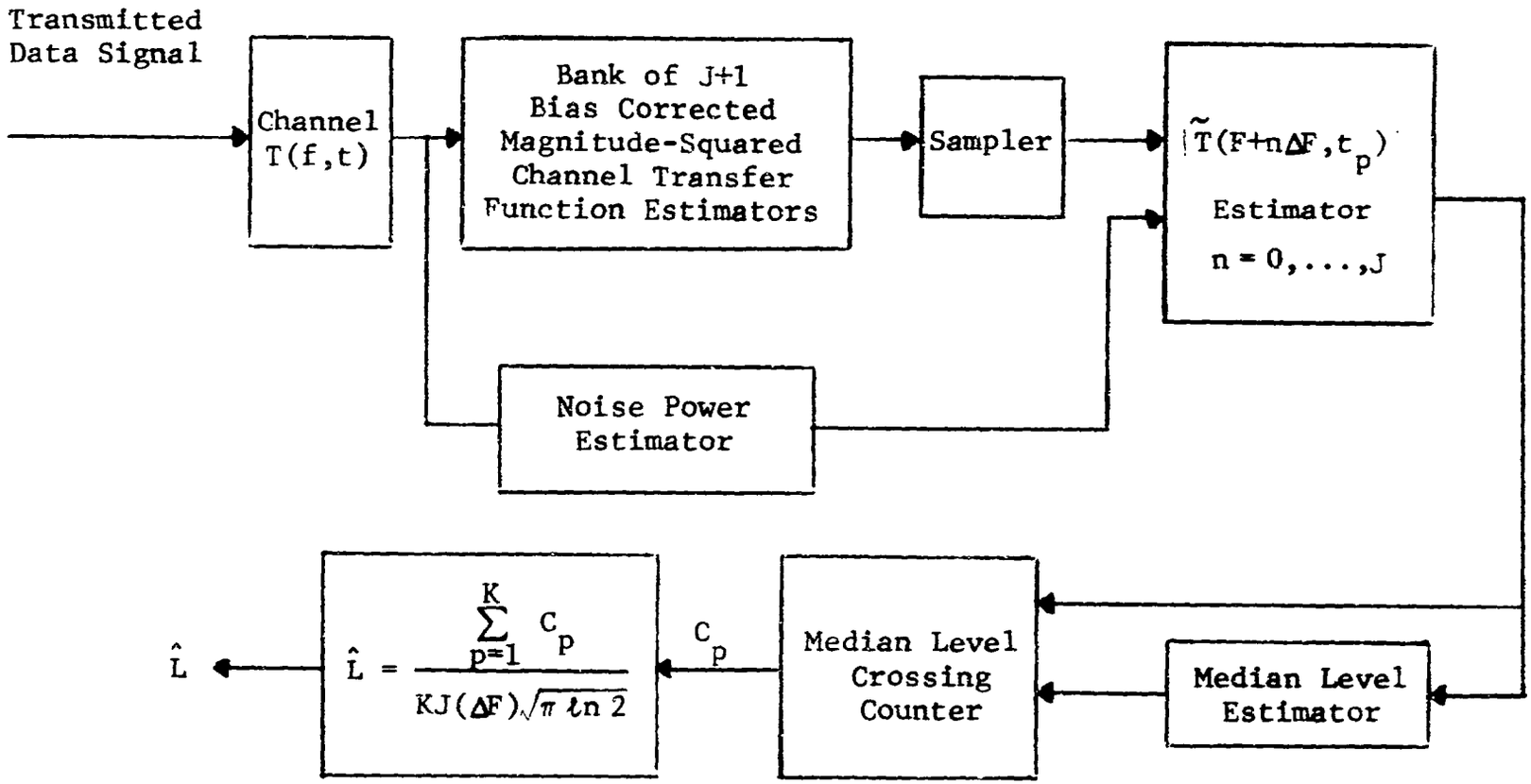

Figure 4.15 Multipath Spread Estimator Utilizing the Level Crossing Technique

$$\frac{\mathrm{Var}^{1/2}\{M_{KJ\Delta F}\}}{E\{M_{JK\Delta F}\}} = \left[\frac{\frac{32}{3\pi} - 1}{LKJ(\Delta F)[\pi \ln 2]^{1/2}}\right]^{1/2} \qquad (4.248)$$

for $F_2(u)$. $F_1(u)$ and $F_2(u)$ are given in (4.230).

4.3.3.4 Summary

The rms multipath spread can be estimated using the same techniques as were used in Section 4.3.2 to estimate the rms Doppler spread. Furthermore, the bias and variance expressions for estimating rms multipath spread are the duals of the corresponding results for Doppler spread. Hence, the same conclusions regarding the effectiveness of the various estimation techniques will hold. In particular, the differentiation technique is superior to the correlation technique. Also, the level crossing technique and the differentiation technique performance are approximately equivalent. Therefore, to estimate rms multipath spread, either the differentiation or level crossing technique should be employed.

4.3.4 SNR Measurement

One of the most important parameters used to estimate error rate is the mean signal-to-noise ratio. In this section we will address the problem of estimating the mean signal-to-noise ratio from estimates of the magnitude squared of the channel transfer function and an estimate of the noise power. Figure 4.16 is a block diagram of the mean SNR estimator that will be analyzed in this section.

The estimator performance is as follows. The data signal is transmitted over the channel, picked off at RF (or IF) in the receiver, and sent to a magnitude-squared channel transfer function estimator of the type analyzed in Section 4.1. The estimator output is then combined with a noise power estimate to form an estimate of the instantaneous SNR, which are then averaged to form an estimate of the mean SNR.

Since the (properly normalized) received signal power in a small band centered at F and in a short interval centered at t_p is proportional to $|T(F,t_p)|^2$, then the instantaneous signal-to-noise ratio at F is proportional to $|T(F,t_p)|^2$; that is,

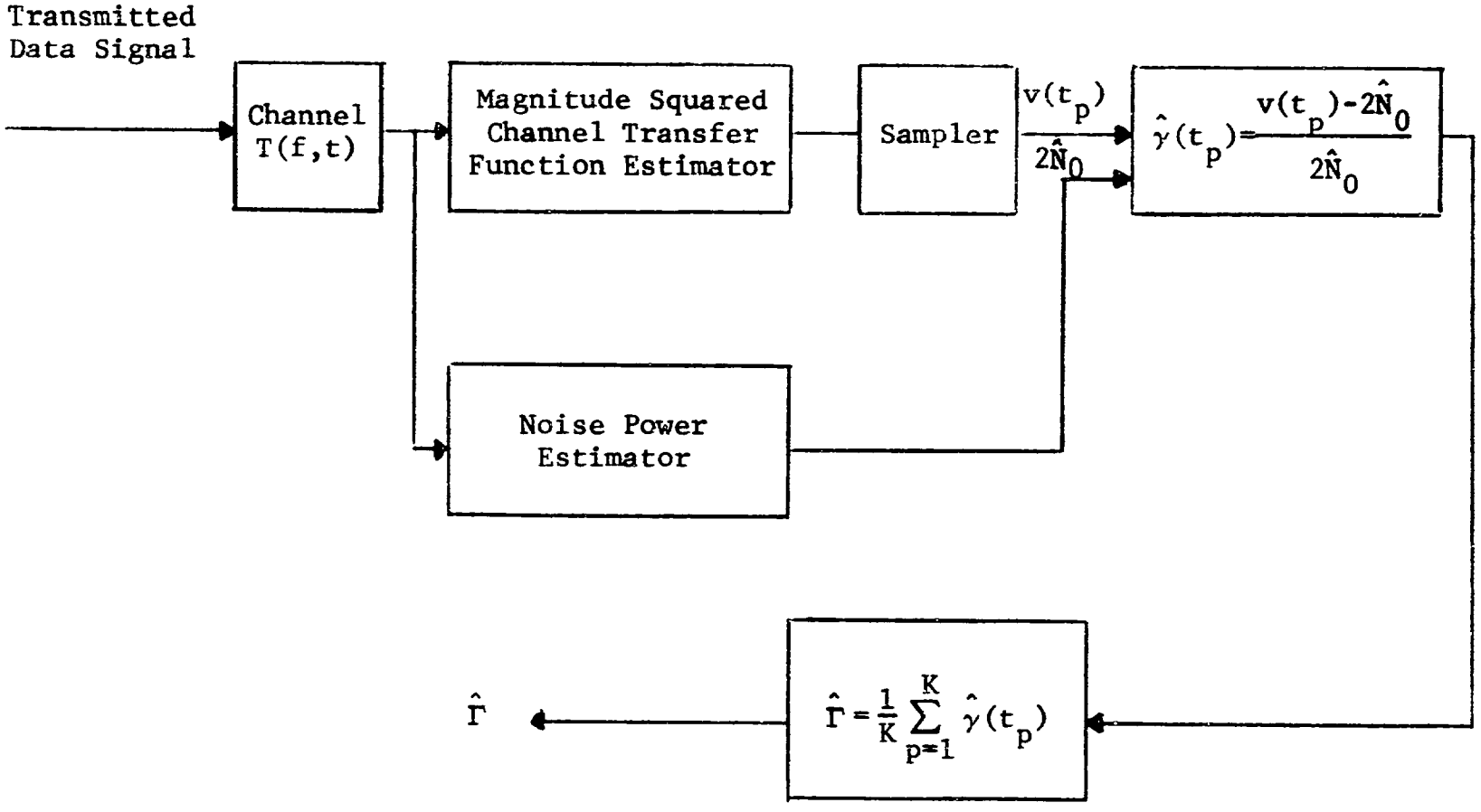

Figure 4.16 Mean Signal-to-Noise Ratio Estimator

$$\gamma(t_p) \propto \frac{|T(F,t_p)|^2}{2N_0} \tag{4.249}$$

where N_0 is the one-sided spectral density of the real noise. Assuming that we can estimate N_0 much more accurately than $|T(F,t_p)|^2$, then from (4.102) and including the bias due to additive noise, we can express the estimate of the instantaneous signal-to-noise ratio by

$$\hat{\gamma}(t_p) = (1+\delta_1)\,\gamma(t_p) + \delta_2 \tag{4.250}$$

where $\gamma(t_p)$ is the actual instantaneous SNR and δ_1 and δ_2 are estimation errors independent of $\gamma(t_p)$ with

$$\overline{\delta}_1 = \overline{\delta}_2 = 0$$
$$\overline{\delta_1^2} = \epsilon^2$$
$$\overline{\delta_2^2} = \epsilon_S^2\,\Gamma^2$$

where Γ is the mean SNR of the channel; that is,

$$\Gamma = E\{\gamma(t)\} \tag{4.251}$$

A zero mean complex Gaussian WSSUS channel will be assumed. This assumption implies that $\gamma(t)$ has a one-sided exponential as its first-order probability density function and that $|T(f,t)|$ is Rayleigh distributed.

From Figure 4.16, the estimate of the mean SNR is given by

$$\hat{\Gamma} = \frac{1}{K}\sum_{p=1}^{K} \hat{\gamma}(t_p) \tag{4.252}$$

Substituting (4.250) into (4.251) and averaging over the errors and channel fluctuations gives for the mean value of the mean SNR estimate

$$\boxed{E\{\hat{\Gamma}\} = \Gamma} \tag{4.253}$$

Hence, the estimate is unbiased. The second moment of the estimate is found by substituting (4.250) into (4.252), squaring and averaging gives

$$E\{\hat{\Gamma}^2\} = \frac{\Gamma^2}{K}\left[2 + 2\epsilon^2 + \epsilon_S^2 + \frac{1}{K}\sum_{\substack{p=1 \\ p\neq q}}^{K}\sum_{q=1}^{K}\left(1+\rho_{pq}^2\right)\right] \tag{4.254}$$

where the errors were assumed to be uncorrelated from sample to sample and where we have defined

$$\rho_{pq} \triangleq \frac{\left|E\{T^*(F,t_p)T(F,t_q)\}\right|}{E\{|T(F,t)|^2\}}$$

as the magnitude of the normalized channel correlation function.

From (4.253) and (4.254), the variance of $\hat{\Gamma}$ is given by

$$\sigma_{\hat{\Gamma}}^2 = \frac{\Gamma^2}{K}\left[1 + 2\epsilon^2 + \epsilon_S^2 + \frac{1}{K}\sum_{\substack{p=1 \\ p\neq q}}^{K}\sum_{q=1}^{K}\rho_{pq}^2\right] \tag{4.255}$$

For stationary channel and equally spaced samples, ρ_{pq} can be expressed as $\rho(m)$ where $m = |p - q|$. Therefore, for stationary scatter channels, the double sum can be reduced to a single sum. Furthermore, if terms that fall off as $1/K^2$ are negligible, we can write

$$\boxed{\sigma_{\hat{\Gamma}}^2 = \frac{\Gamma^2}{K}\left[1 + 2\epsilon^2 + \epsilon_S^2 + 2\sum_{m=1}^{K-1}\rho^2(m)\right]} \tag{4.256}$$

Recalling from (4.104) that $\epsilon_p^2 = 2\epsilon^2 + \epsilon_S^2$, then minimizing the rms fractional error in estimating the magnitude squared of the channel transfer function will result in the most rapid convergence for the estimator given by Figure 4.16. For the channels considered in Section 4.1, the SNR estimator performance is presented in Figure 4.17. The channel parameters given in Table 4.2 of Section 4.1.5 and a Gaussian channel correlation function were used in this figure.

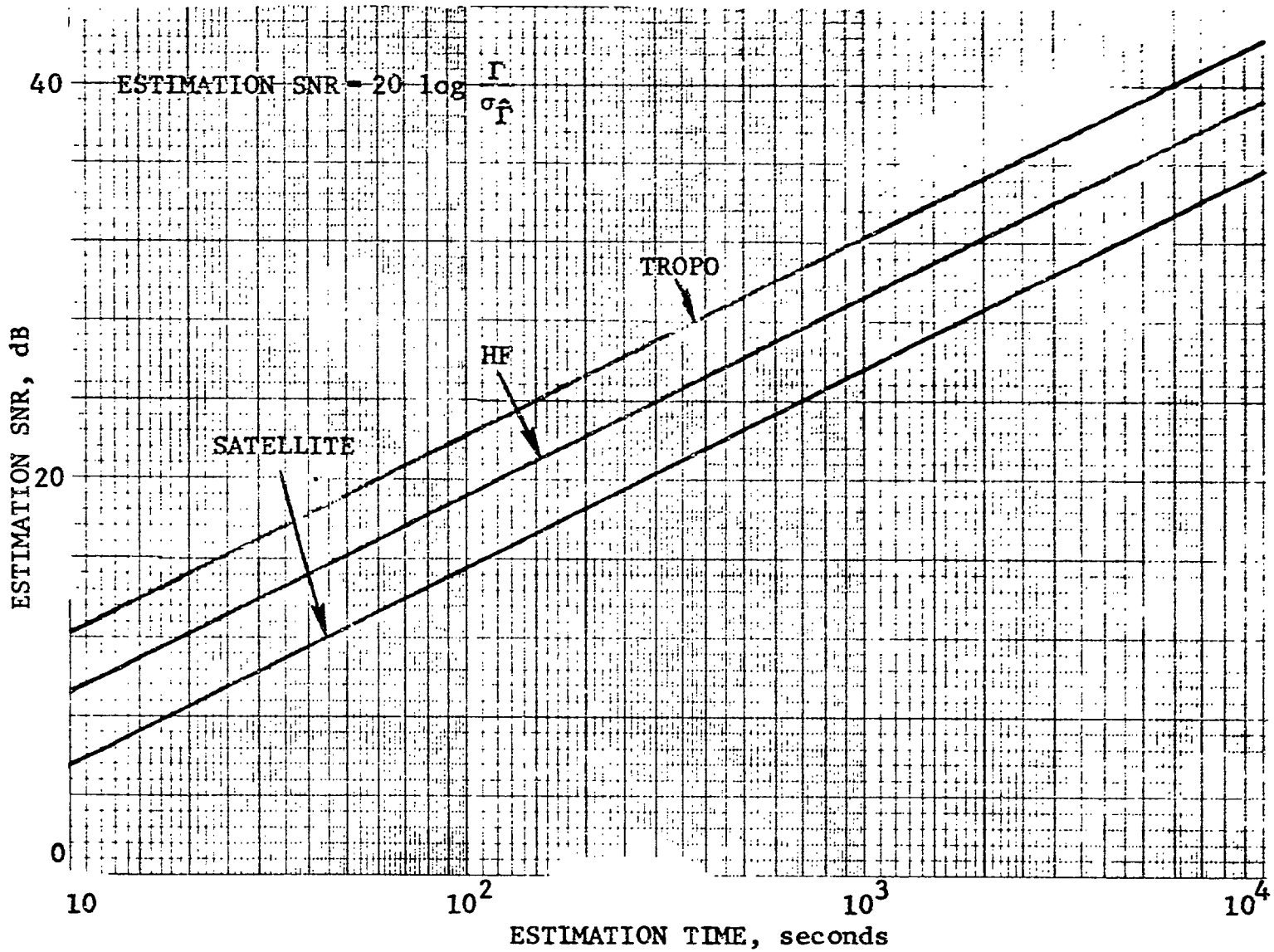

Figure 4.17 Performance of Mean SNR Estimator

4.3.5 Diversity Branch Correlation Measurement

4.3.5.1 Introduction

A common assumption in evaluating a system employing some type of diversity operation is that the diversity branches fade independently. However, in many systems, physical limitations (e.g., size, frequency) may not allow the branches to fade independently and, thus, the full diversity gain is not realized. In Section 5.3, the effect of dependent fading on diversity branches will be evaluated for its effect upon the error rate. It is frequently possible to express the degradation due to dependent fading in terms of their joint envelope correlation coefficient. It is this parameter that will be estimated.

4.3.5.2 Estimator Description

Figure 4.18 is a block diagram of the branch envelope correlation coefficient estimator that will be analyzed. The estimator performance is as follows. The data signal is transmitted over both diversity channels, picked off at RF (or IF) in the receivers and sent to magnitude-squared channel transfer function estimators of the type analyzed in Section 4.1. Using the output of these estimators to form estimates of the first and second moments of the magnitude-squared channel transfer function, then the branch envelope correlation coefficient can be estimated.

The branch envelope correlation coefficient is defined (for any general diversity technique) by

$$\rho_{kj} \triangleq \frac{E\{|x_j|^2|x_k|^2\} - E\{|x_j|^2\}E\{|x_k|^2\}}{\left\{\left[E\{|x_j|^4\} - E^2\{|x_j|^2\}\right]\left[E\{|x_k|^4\} - E^2\{|x_k|^2\}\right]\right\}^{1/2}} \quad (4.257)$$

where $x_j = T_j(f,t)$

$x_k = T_k(f,t)$

are the time-varying transfer functions of the diversity channels. For a zero mean complex Gaussian WSSUS channel, the expectations of (4.257) can be simplified by using the moment theorem for complex Gaussian processes [4.1] - [4.4]. Taking these moments gives

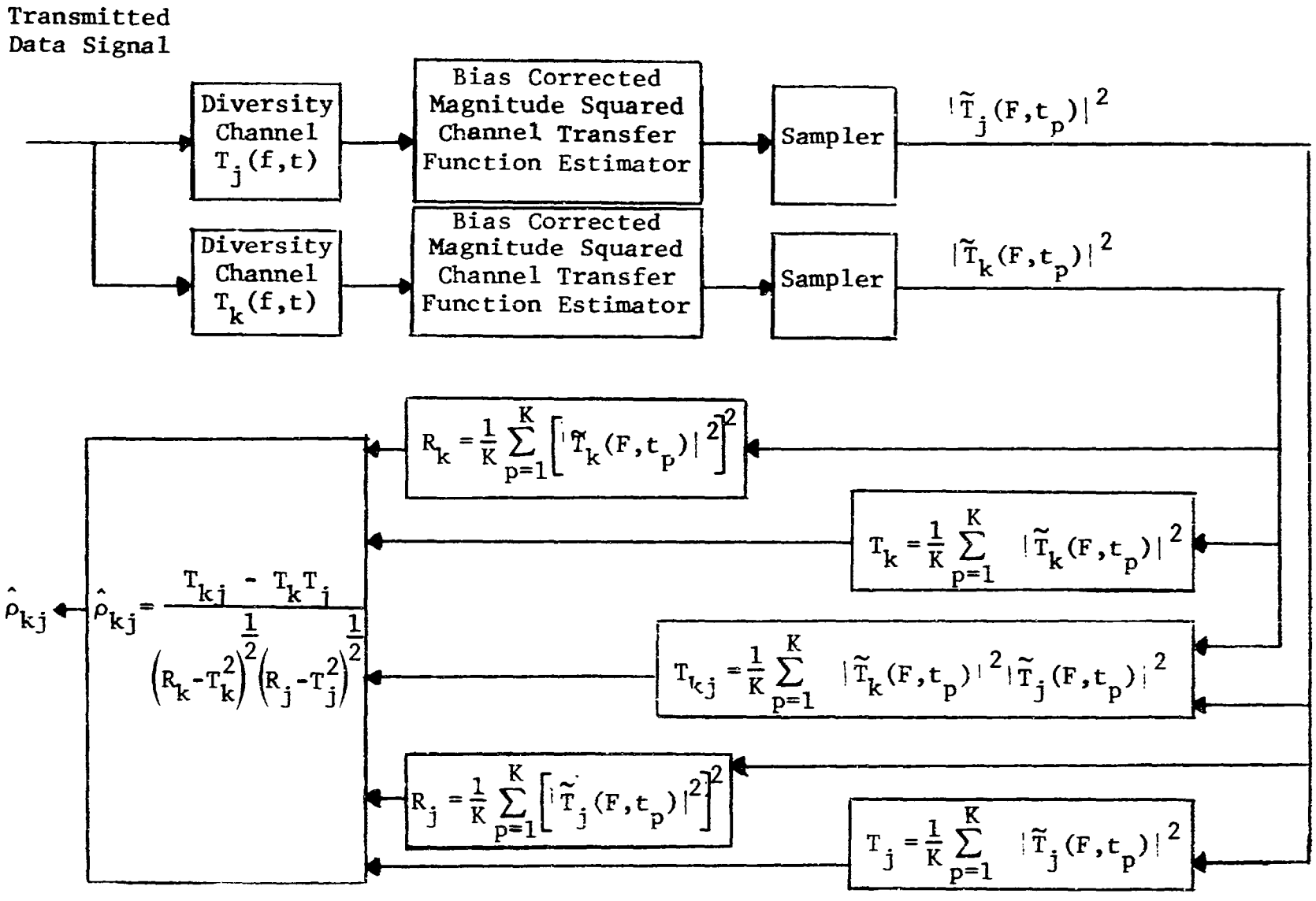

Figure 4.18 Branch Envelope Correlation Coefficient Estimator

$$\rho_{kj} = \frac{E\{|x_j|^2 |x_k|^2\}}{E\{|x_j|^2\} E\{|x_k|^2\}} - 1 \tag{4.258}$$

Defining a complex branch correlation coefficient by

$$G_{kj} = \frac{E\{x_j^* x_k\}}{\left[E\{|x_j|^2\}\ E\{|x_k|^2\}\right]^{1/2}} \tag{4.259}$$

and using the moment theorem for complex Gaussian process, it follows that

$$\rho_{kj} = |G_{kj}|^2 \tag{4.260}$$

The estimator given by Figure 4.18 is a numerical implementation of (4.257). However, evaluation of the estimator from (4.257) is very cumbersome and, therefore, we will evaluate the performance of Figure 4.18 using a numerical implementation of (4.258). This should give a slightly pessimistic evaluation of the estimator performance. Therefore, we will estimate ρ_{kj} by

$$\hat{\rho}_{kj} = \frac{T_{kj}}{T_k T_j} - 1 \tag{4.261}$$

where

$$T_{kj} = \frac{1}{K} \sum_{p=1}^{K} |\tilde{T}_k(F,t_p)|^2\ |\tilde{T}_j(F,t_p)|^2$$

$$T_j = \frac{1}{K} \sum_{p=1}^{K} |\tilde{T}_j(F,t_p)|^2$$

$$T_k = \frac{1}{K} \sum_{p=1}^{K} |\tilde{T}_k(F,t_p)|^2$$

Defining α and β such that

$$T_{kj} = E\{T_{kj}\} + \alpha$$

$$T_j T_k = E\{T_k T_j\} + \beta \tag{4.262}$$

it follows that

$$\hat{\rho}_{kj} = \frac{E\{T_{kj}\} + \alpha}{E\{T_k T_j\} + \beta} - 1$$

or

$$\hat{\rho}_{kj} = \frac{E\{T_{kj}\}\left(1 + \dfrac{\alpha}{E\{T_{kj}\}}\right)}{E\{T_k T_j\}\left(1 + \dfrac{\beta}{E\{T_k T_j\}}\right)} - 1 \tag{4.263}$$

With K large so that $\hat{\rho}_{kj}$ can be accurately expressed in terms of the first-order terms of α and β, then

$$\hat{\rho}_{kj} = \frac{E\{T_{kj}\}}{E\{T_k T_j\}}\left(1 + \frac{\alpha}{E\{T_{kj}\}} - \frac{\beta}{E\{T_k T_j\}}\right) - 1 \tag{4.264}$$

The mean of $\hat{\rho}_{kj}$ is given by

$$E\{\hat{\rho}_{kj}\} = \frac{E\{T_{kj}\}}{E\{T_k T_j\}} - 1 \tag{4.265}$$

and the variance of $\hat{\rho}_{kj}$ is given by

$$\sigma^2_{\hat{\rho}_{kj}} = \frac{E^2\{T_{kj}\}}{E^2\{T_k T_j\}}\left[\frac{E\{\alpha^2\}}{E^2\{T_{kj}\}} + \frac{E\{\beta^2\}}{E^2\{T_k T_j\}} - \frac{2E\{\alpha\beta\}}{E\{T_{kj}\}E\{T_k T_j\}}\right] \tag{4.266}$$

The moments required to evaluate the mean and variance of $\hat{\rho}_{kj}$ can be found by using (4.102) to express the estimates of the magnitude squared of the channel transfer function and averaging over the errors and channel fluctuations. We will assume for analysis purposes that the samples of the magnitude-squared channel transfer function estimates are spaced far enough apart that independent realizations are obtained. With these conditions, the mean of $\hat{\rho}_{kj}$* can be found to be

$$E\{\hat{\rho}_{kj}\} = \rho_{kj}\left(\frac{1 - \frac{1}{K}}{1 + \frac{\rho_{kj}}{K}}\right) \tag{4.267}$$

Therefore, the estimate of the branch envelope correlation coefficient is asymptotically unbiased. Assuming that the errors in estimating the magnitude squared of the channel transfer function have little effect upon the convergence of the estimator given by Figure 4.18, then the variance of $\hat{\rho}_{kj}$ is approximately given by

$$\sigma^2_{\hat{\rho}_{kj}} = \frac{1}{K}\left(3 + 6\rho_{kj} + \rho^2_{kj} + 6\rho^3_{kj}\right) \tag{4.268}$$

where terms that fall off faster than 1/K were considered negligible.

In Section 5.3, the estimate of the branch envelope correlation coefficient will be used to evaluate the effect of correlated fading of the diversity branches. In that section, the effects of the error in estimating ρ_{kj} will be assessed.

4.4 Interference Detection Measurement

4.4.1 Introduction

In this section we explore some techniques whereby the presence of interference can be detected through observation of various parameters of the total received signal. In Section 4.4.2 we first deal with a scheme that depends on observation of the rms bandwidth and frequency centroid of the total received signal. It is argued that this detector can operate reliably under a wide range of interference conditions. In Section 4.4.3 we describe a scheme that depends on power measurements achieved by estimators similar to that shown earlier in Figure 4.1. This scheme utilizes

*Appendix C considers in some detail the mean of $\hat{\rho}_{kj}$ from bias corrected and bias uncorrected estimates of $|T(F,t_p)|^2$.

a comparison of power measurements taken at one time under suspected interference conditions with power measurements taken at an earlier time under supposedly interference-free conditions. Unfortunately, such a scheme can be degraded seriously by channel non-stationarity. This question is explored in Section 4.4.3, but is difficult to resolve because of the lack of extensive data on channel non-stationarity.

4.4.2 Detection of Narrowband Interference by Using Measurements of Centroid and RMS Bandwidth of Received Signal

4.4.2.1 Preliminary Comments

The presence of narrowband interference may be indicated by measurable changes in the rms bandwidth and centroid of a received signal. It is a reasonable intuitive notion, when the data is totally swamped out by the narrowband interference, that the rms bandwidth of the received signal will be equal to that of the interference, and its centroid will be equal to the frequency offset (difference between interference and data carrier frequencies) of the interference.

Optimal procedures for detecting the presence of narrowband interference can be based on observations of both f_R, the frequency centroid of the total received signal, and B_R, its rms bandwidth. Decision-theoretic concepts have been applied to the development of a detection technique utilizing estimates of these quantities. The effectiveness of any such scheme must depend, of course, on the reliability of the estimates, and this is discussed below at some length.

The detection schemes which are discussed and evaluated in this report are suboptimal in the sense that there are idealized detectors, not necessarily implementable, that can do better. Nevertheless, the calculated detector operating characteristics for the detection schemes discussed here show good performance. Their relation to the optimal detectors is given detailed discussion.

We proceed with the analysis by first discussing, in Section 4.2.2, the characterization of narrowband interference and its effect on the rms bandwidth and frequency centroid of the total received signal. The dependence of these quantities on the bandwidth of the interference and its power is clearly illustrated.

The statistical properties of the measurements of rms bandwidth and frequency centroid are discussed in Section 4.4.2.3. In addition, central-limit theorem arguments are invoked which indicate that the observation variables may be approximated by Gaussian random variables.

In Section 4.4.2.4, the results of the previous section are applied to first evaluate the performance of a detector which uses only the rms bandwidth observation. In the class of detectors using only the bandwidth observation, this detector is found to be near-optimal. (The departure from optimality is found to be negligible.) The performance of another, more reasonable, detector that uses measurements of rms bandwidth and centroid is also presented in Section 4.4.2.4. This detector, because of its simplistic decision rule, is clearly sub-optimal. Even so, its performance is clearly superior to that of the detector which uses a single observation variable, and indicates that good performance can be achieved.

Results and possibilities for more sophisticated detection schemes are summarized and discussed in Section 4.4.2.5.

4.4.2.2 Characterization of Narrowband Interference and its Effect on Bandwidth and Centroid of Total Output Signal

Before discussing the means of detecting narrowband interference, it is first necessary to characterize the narrowband interference and the way in which it affects the received signal. That is the topic of this section. A discussion of the statistical properties of the observation variables used in the detection process is deferred until Section 4.4.2.3, and the detection schemes themselves are discussed in Section 4.4.2.4.

In the following analysis, the effect of other additive disturbances, e.g., wideband noise, is not considered; the level of receiver noise can be determined by out-of-band sampling or calculated from knowledge of the receiver characteristics, and its effect on measurement bias, etc., can be compensated for. The sole additive influence considered below is the narrowband interference we are attempting to detect.

We first note that the channel output, in the absence of interference, is given by

$$\mathrm{Re}\left\{w(t)\ e^{j2\pi f_0 t}\right\} \tag{4.269}$$

where $w(t)$ is the complex envelope of the data passed by the channel and f_0 is the carrier frequency. The additive interference on a nearby carrier frequency, f_1, has the representation

$$\mathrm{Re}\left\{i(t)\ e^{j2\pi f_1 t}\right\} \tag{4.270}$$

This can be written as

$$\mathrm{Re}\left\{i(t)\ e^{j2\pi f_\Delta t}\ e^{j2\pi f_0 t}\right\} \qquad f_\Delta = f_1 - f_0 \qquad (4.271)$$

which is now in the form of (4.269). Thus, we need only deal with with complex envelopes

(1) Signal Complex Envelope:

$$w(t) = \int g(t,\xi)\ x(t-\xi)\ d\xi \qquad (4.272)$$

where x(t) represents the data complex envelope

(2) Narrowband Interference Complex Envelope:

$$I(t) = i(t)\ e^{j2\pi f_\Delta t} \qquad (4.273)$$

Assuming wide-sense stationarity, we have for the correlation functions

$$R_w(\tau) = \overline{w^*(t)\ w(t+\tau)} \qquad (4.274)$$

$$R_i(\tau) = \overline{i^*(t)\ i(t+\tau)} \qquad (4.275)$$

$$R_I(\tau) = R_i(\tau)\ e^{j2\pi f_\Delta \tau} \qquad (4.276)$$

and denote the respective power spectra $P_w(f)$, $P_i(f)$ and $P_I(f)$. The narrowband interference power spectra are related by

$$P_I(f) = P_i(f - f_\Delta) \qquad (4.277)$$

The power spectrum of the output is

$$P_R(f) = P_w(f) + P_i(f - f_\Delta) \qquad (4.278)$$

as illustrated in Figure 4.19.

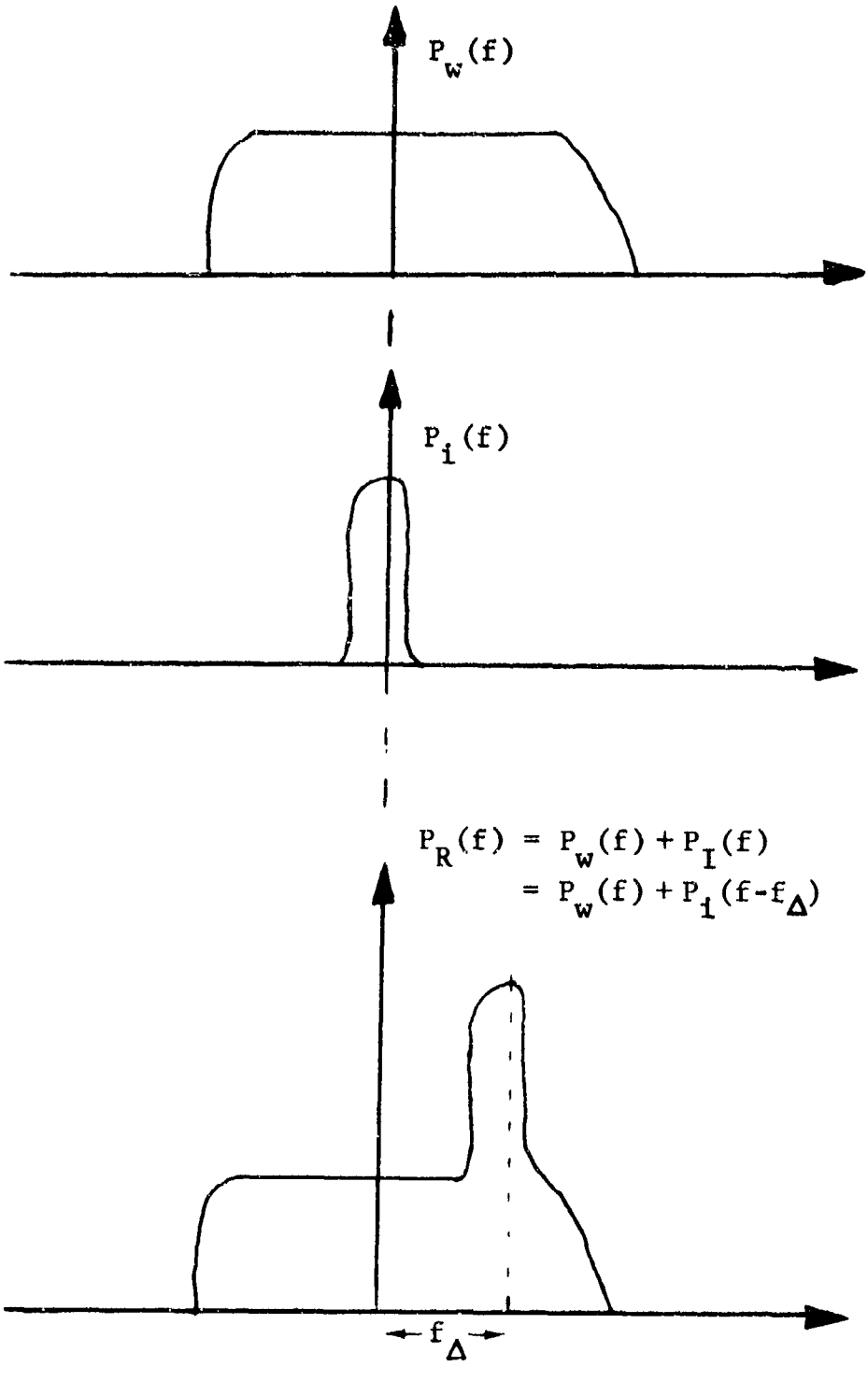

Figure 4.19 Power Spectra for Received Signal, Narrowband Interference, and Total Output Signal

We now define the bandwidth parameters:

$$B_R^2 = \frac{4\int (f - f_R)^2 P_R(t)df}{\int P_R(f)df} \qquad f_R = \frac{\int f\, P_R(f)df}{\int P_R(f)df} \tag{4.279}$$

$$B_w^2 = \frac{4\int (f - f_w)^2 P_w(f)df}{\int P_w(f)df} \qquad f_w = \frac{\int f\, P_w(f)df}{\int P_w(f)df} \tag{4.280}$$

$$B_i^2 = \frac{4\int (f - f_i)^2 P_i(f)df}{\int P_i(f)df} \qquad f_i = \frac{\int f\, P_i(f)df}{\int P_i(f)df} \tag{4.281}$$

$$B_I^2 = \frac{4\int (f - f_I)^2 P_I(f)df}{\int P_I(f)df} \qquad f_I = \frac{\int f\, P_I(f)df}{\int P_I(f)df}$$

$$= \frac{\int f\, P_i(f - f_\Delta)df}{\int P_I(f)df} \tag{4.282}$$

To simplify notation, we define

$$P_R = \int P_R(f)df \qquad P_w = \int P_w(f)df$$

$$P_i = \int P_i(f)df \qquad P_I = \int P_I(f)df = P_i \tag{4.283}$$

and the fractional power ratios

$$p_w = \frac{P_w}{P_i + P_w} \qquad p_i = \frac{P_i}{P_i + P_w} \tag{4.284}$$

We now proceed to calculate f_R, the centroid of the total received signal, and B_R, its rms bandwidth. From (4.278), (4.279), (4.280), and (4.282), it is easy to show that

$$f_R = f_w p_w + f_I p_I \tag{4.285}$$

which has been written in terms of the fractional power ratios defined in (4.284). An expression for the rms bandwidth can be obtained from (4.278) and (4.279). We have

$$\frac{B_R^2 P_R}{4} = \int (f - f_R)^2 P_w(f)df + \int (f - f_R)^2 P_i(f - f_\Delta)df \tag{4.286}$$

To simplify the analysis, we assume that $f_w = 0$ and $f_i = 0$. This is just an assumption of symmetric power distribution of signal and narrowband interference about their own respective carrier frequencies. [See (4.270).] The retention of non-zero values for f_w and f_i would only serve to obscure the issues at this point. From (4.285) we have

$$f_R = f_I p_I \tag{4.287}$$

and, since $f_i = 0$, we have from (4.282)

$$\begin{aligned} f_I &= \int f\, P_i(f - f_\Delta)df / P_i \\ &= \int (f + f_\Delta)\, P_i(f)df / P_i \\ &= f_\Delta \end{aligned} \tag{4.288}$$

Hence

$$f_R = p_i f_\Delta \tag{4.289}$$

and by substituting this expression in (4.286), it is easy to show that

$$B_R^2 = \frac{4 \int f^2 \left[P_w(f) + P_i(f - f_\Delta)\right]df}{P_R} - 4(f_\Delta p_i)^2 \tag{4.290}$$

which can be interpreted as a second central moment about zero, modified by a term that depends on the frequency offset, f_Δ, of the narrowband noise.

We can gain some insight into this expression by considering the case of extremely narrowband interference, i.e., the case when $P_i(f - f_\Delta)$ is impulsive. We then have

$$\frac{B_R^2}{4} = \frac{B_w^2}{4} \cdot p_w + f_\Delta^2 p_i(1 - p_i) \tag{4.291}$$

or

$$\frac{B_R^2}{4} = (1 - p_i)\left[\frac{B_w^2}{4} + f_\Delta^2 p_i\right] \tag{4.292}$$

Now, in the absence of a frequency offset (i.e., when $f_\Delta = 0$) we would have

$$\frac{B_R^2}{4} = (1 - p_i)\,\frac{B_w^2}{4} \tag{4.293}$$

an intuitively satisfying expression in that the rms bandwidth B_R^2 decreases as interference power increases, and is B_w when $p_i = 0$. Because of the offset (4.292) does not exhibit this nice behavior. In fact, by differentiating with respect to p_i, it is easy to show that an increase in p_i causes a decrease in B_R only when

$$f_\Delta^2 < \frac{1}{(1 - 2p_i)}\,\frac{B_w^2}{4} \tag{4.294}$$

For very small p_i this is just a requirement that the frequency offset be less than one half the rms bandwidth. Unfortunately, for such values, the dependence of (4.293) on p_i is weak enough so that decision procedures depending on observations of B_R according to (4.293) would be of little value.

Returning now to the general case in (4.290), we note first that

$$\int f^2 P_i(f - f_\Delta)\, df = \frac{B_i^2}{4} + f_\Delta^2 P_i \tag{4.295}$$

and dropping the subscript on the p_i we have

$$B_R^2 = B_w^2(1 - p) + B_i^2 p + 4f_\Delta^2 p(1 - p) \tag{4.296}$$

$$p = \frac{P_i}{P_i + P_w} \tag{4.297}$$

An increase in the interference parameter, p, results in an rms bandwidth decrease only when the condition

$$B_i^2 + 4f_\Delta^2(1 - 2p) < B_w^2 \tag{4.298}$$

holds.

Clearly, then, there are values of p and f_Δ for which any decision scheme depending on only observations of rms bandwidth will be deficient. This topic is discussed in more detail in Section 4.4.2.4.

4.4.2.3 Statistical Properties of the Measurements

4.4.2.3.1 Introduction

Procedures which utilize measurements of rms bandwidth and centroid to detect the presence of narrowband interference give rise to errors which must necessarily depend on the accuracy with which the measurements are obtained. In this section we discuss the means for estimating the rms bandwidth and centroid, and the corresponding estimation errors. There are a variety of ways in which such estimates can be obtained. In this report we do not intend to indicate which of these methods is best but only to indicate, through our somewhat arbitrary choice of two particular estimation procedures, the kind of results that can be obtained in practice.

4.4.2.3.2 RMS Bandwidth Estimate

From the definitions in (4.279) - (4.282) we rewrite the rms bandwidth for the total received signal and drop the subscript R.

$$\frac{B^2}{4} = \frac{\int (f - \bar{f})^2 P(f)\, df}{\int P(f)\, df} \tag{4.299}$$

Utilizing the correlation function of the received signal,

$$R(\tau) = \int P(f)\, e^{j2\pi f\tau}\, df \tag{4.300}$$

and expanding the exponential, we have

$$\rho(\tau) \triangleq \frac{R(\tau)}{R(0)} \approx 1 + j2\pi\bar{f}\tau - \frac{(2\pi\tau)^2}{2}\,\overline{f^2} \tag{4.301}$$

where

$$\overline{f^2} = \frac{\int f^2 P(f)\, df}{\int P(f)\, df} \tag{4.302}$$

and is related to B^2 through

$$\frac{B^2}{4} = \overline{f^2} - \bar{f}^2 \tag{4.303}$$

From (4.301) we can calculate $|\rho(\tau)|^2$, and retaining terms of the same order of smallness as retained in (4.301), we have

$$|\rho(\tau)|^2 \approx 1 - (\pi\tau)^2 B^2 \tag{4.304}$$

Approximating the square root of this expression in the same way, we obtain

$$B^2 \approx \frac{2}{(\pi\tau)^2}\,[1 - |\rho(\tau)|] \tag{4.305}$$

It is on this expression that we will base our estimate of the received signal rms bandwidth, i.e.,

$$\widehat{B^2} \cong \frac{2}{(\pi\tau)^2}\left[1 - \widehat{|\rho(\tau)|}\right] \tag{4.306}$$

where the caret denotes the estimate of the quantity it covers as it will in the sequel. Hence, the statistical properties of the rms bandwidth estimate depend in direct fashion on the correlation function estimate. Though this estimate is mildly biased at small values of τ (by virtue of the fact that it is an approximation), it will be assumed here that the τ is chosen small enough so that the bias can be neglected. This question is discussed at greater length in Section 4.4.2.3.4.

For a given observation $\hat{B^2}$, the (fractional estimation error is given by

$$\epsilon_B = \frac{\hat{B^2} - B^2}{B^2} = -\frac{2}{B^2(\pi^2\tau^2)}\left(\widehat{|\rho(\tau)|} - |\rho(\tau)|\right) \tag{4.307}$$

For an estimate $\widehat{|\rho(\tau)|}$ we use

$$\widehat{|\rho(\tau)|} = \frac{\widehat{|R(\tau)|}}{\widehat{|R(0)|}} = \frac{|R(\tau)|(1+\epsilon(\tau))}{|R(0)|(1+\epsilon(0))} \tag{4.308}$$

where

$$\epsilon(\tau) = \frac{\widehat{|R(\tau)|} - |R(\tau)|}{|R(\tau)|} \tag{4.309}$$

and

$$\epsilon(0) = \frac{\widehat{|R(0)|} - |R(0)|}{|R(0)|} \tag{4.310}$$

represent the fractional errors in estimating the correlation function at time offset τ and zero, respectively. For small values of $\epsilon(\tau)$ and $\epsilon(0)$ we have

$$\epsilon_B \approx -\frac{2}{B^2\pi^2\tau^2}\left[\frac{|R(\tau)|}{|R(0)|}\left\{\epsilon(\tau) - \epsilon(0)\right\}\right] \tag{4.311}$$

Since our eventual goal is to calculate $\overline{|\epsilon_B|^2}$, we need only deal with the variance of the error difference, i.e., we must calculate

$$\overline{|\epsilon(0) - \epsilon(\tau)|^2} = \overline{|\epsilon(0)|^2} + \overline{|\epsilon(\tau)|^2} - 2\,\overline{\epsilon(0)\epsilon(\tau)} \tag{4.312}$$

We note from (4.312) that $\hat{R}(\tau)$ and $\hat{R}(0)$, if processed in an independent manner, give rise to no contribution from the cross-product terms at the right of (4.312). This assumption, though not strictly justified, has, at most, the effect of placing an upper bound on $\overline{|\epsilon_B|^2}$. Since the performance of the detector, eventually discussed in Section 4.4.2.4, tends to deteriorate as ϵ_B increases, setting $\overline{\epsilon(0)\epsilon(\tau)} = 0$ in (4.312) will not lead to higher predictions of detector performance than will be achieved in practice. Our main interest here is in demonstrating the feasibility of the detection schemes; hence we concentrate on determining the value of

$$\overline{|\epsilon(0) - \epsilon(\tau)|^2} = \overline{|\epsilon(0)|^2} + \overline{|\epsilon(\tau)|^2} \tag{4.313}$$

Along the same lines, we note from (4.309) and (4.310) that

$$\epsilon(\tau) \le \frac{|\hat{R}(\tau) - R(\tau)|}{|R(\tau)|} \tag{4.314}$$

and

$$\epsilon(0) \le \frac{|\hat{R}(0) - R(0)|}{|R(0)|} \tag{4.315}$$

so that, now, (4.313) reduces to

$$\overline{|\epsilon(0) - \epsilon(\tau)|^2} \le \frac{\overline{|\hat{R}(0) - R(0)|^2}}{|R(0)|^2} + \frac{\overline{|\hat{R}(\tau) - R(\tau)|^2}}{|R(\tau)|^2} \tag{4.316}$$

We recall from (4.272) that the total received signal is given by

$$z(t) = w(t) + I(t) \tag{4.317}$$

where

$$w(t) = \int g(t,\xi)\, x(t-\xi)\, d\xi \tag{4.318}$$

is the channel passed data [x(t) represents the data and $g(t,\xi)$ the time-varying impulse response of the channel, and I(t) is the complex envelope of the narrowband interference].

The estimate for the correlation function of the total received signal is given by

$$R(t,s) = \overline{z(t)z(s)} = \frac{1}{T}\int_{-\frac{T}{2}}^{+\frac{T}{2}} z^*(t)\, z(s)\, dt\, ds \tag{4.319}$$

which, under the assumption of wide-sense stationarity, depends, of course, only on the difference t-s.

To compute (4.316), we must first find the value of

$$\overline{|\hat{R}(\tau) - R(\tau)|^2} = \overline{|\hat{R}(\tau)|^2} - |R(\tau)|^2 \tag{4.320}$$

where

$$\overline{|\hat{R}(\tau)|^2} = \frac{1}{T^2}\int_{-\frac{T}{2}}^{+\frac{T}{2}}\int_{-\frac{T}{2}}^{+\frac{T}{2}} \overline{z(t)z^*(s)z^*(t+\tau)z(s+\tau)}\, dt\, ds \tag{4.321}$$

We first note that

$$R(\tau) = R_w(\tau) + R_I(\tau) \tag{4.322}$$

where $R_w(\tau)$ and $R_I(\tau)$, the correlation functions of channel-passed data and narrowband interference, respectively, were defined in (4.274) - (4.276). The simple form of (4.322) results from the independence of the narrowband interference and data. This same independence simplifies things when we substitute (4.317) into (4.321); we are left with only eight nonzero terms. We have

$$\overline{z(t)z^*(s)z^*(t+\tau)z(s+\tau)} = \overline{w(t)w^*(s)w^*(t+\tau)w(s+\tau)}$$
$$+ \overline{w(t)w^*(s)I^*(t+\tau)I(s+\tau)}$$
$$+ \overline{w(t)I^*(s)w^*(t+\tau)I(s+\tau)}$$
$$+ \overline{w(t)I^*(s)I^*(t+\tau)w(s+\tau)}$$
$$+ \overline{I(t)w^*(s)w^*(t+\tau)I(s+\tau)}$$
$$+ \overline{I(t)w^*(s)I^*(t+\tau)w(s+\tau)}$$
$$+ \overline{I(t)I^*(s)w((t+\tau)w(s+\tau)}$$
$$+ \overline{I(t)I^*(s)I^*(t+\tau)I(s+\tau)} \qquad (4.323)$$

To find the moment required in the leading term of this sum, we will first calculate the expected value (averaging over the ensemble of channel impulse responses) conditional on the data, and then average over the data. Because of our assumption that the channel and data are both complex Gaussian random processes, the separate averaging operations will each take the form $\overline{V_1^*V_2^*V_3V_4}$ where, because the V_i are jointly Gaussian complex random variables, we can use the relation

$$\overline{V_1^*V_2^*V_3V_4} = \overline{V_1^*V_3}\ \overline{V_2^*V_4} + \overline{V_2^*V_3}\ \overline{V_1^*V_4} \qquad (4.324)$$

We will also make use of the result

$$\overline{V_1V_2} = 0 \qquad (4.325)$$

Thus, substituting from (4.318) and averaging over the channel, we obtain

$$\overline{w^*(s)w^*(t+\tau)w(t)w(s+\tau)\,|\,x(t)} = \int_{-\frac{T}{2}}^{+\frac{T}{2}}\iiint \overline{g^*(s,\xi)g^*(t+\tau,\eta)g(t,\xi')g(s+\tau,\eta')}$$
$$\cdot\, x^*(s-\xi)x^*(t+\tau-\eta)x(t-\xi')$$
$$\cdot\, x(s+\tau-\eta')\,d\xi\,d\eta\,d\xi'\,d\eta' \qquad (4.326)$$

We recall, for the wide-sense stationary uncorrelated scattering channel (WSSUS), that

$$\overline{g^*(s,\xi)g(t,\eta)} = Q(t-s,\xi)\,\delta(\xi-\eta) \tag{4.327}$$

By applying (4.324) and (4.327) to (4.326), and then, averaging over the data, we obtain

$$\begin{aligned}\overline{w^*(s)w^*(t+\tau)w(t)w(s+\tau)\,|\,x(t)} = &\int_{-\frac{T}{2}}^{+\frac{T}{2}}\!\!\int Q(t-s,\xi)Q(s-t,\eta)\,M_{X1}\,d\xi\,d\eta \\ &+\int_{-\frac{T}{2}}^{+\frac{T}{2}}\!\!\int Q(-\tau,\eta)Q(\tau,\xi)\,M_{X2}\,d\xi\,d\eta\end{aligned} \tag{4.328}$$

where

$$M_{X1} = \overline{x^*(s-\xi)x^*(t+\tau-\eta)x(t-\xi)x(s+\tau-\eta)}$$

$$M_{X2} = \overline{x^*(s-\xi)x^*(t+\tau-\eta)x(t-\eta)x(s+\tau-\xi)} \tag{4.329}$$

If we assume that the frequency selective fading is negligible, we can make the substitution

$$Q(\tau,\xi) = p(\tau)\,\delta(\xi) \tag{4.330}$$

After applying (4.324) to the data moments, we obtain

$$\overline{w^*(s)w^*(t+\tau)w(t)w(s+\tau)} = \left(|p(\tau)|^2 + |p(t-s)|^2\right)\left(|R_x(t-s)|^2 + |R_x(\tau)|^2\right) \tag{4.331}$$

To determine the contribution that this term makes to the integral in (4.331), we make use of the relation

$$\frac{1}{T^2}\int_{-\frac{T}{2}}^{+\frac{T}{2}}\int f(t_1 - t_2)dt_1\,dt_2 = \frac{1}{T}\int_{-T}^{+T}\left(1 - \frac{|\tau|}{T}\right) f(\tau)\,d\tau$$

$$\approx \frac{1}{T}\int_{-T}^{+T} f(y)\,dy \qquad (4.332)$$

where the approximation holds well for large T. We obtain

$$\frac{1}{T^2}\int_{-\frac{T}{2}}^{+\frac{T}{2}}\int_{-\frac{T}{2}}^{+\frac{T}{2}} \overline{w(t)w^*(s)w(t+\tau)w(s+\tau)}\,dt\,ds = \frac{|p(\tau)|^2}{T}\int_{-T}^{+T} |R_x(y)|^2$$

$$+ |p(\tau)|^2|R_x(\tau)|^2$$

$$+ \frac{1}{T}\int_{-T}^{+T} |p(y)|^2|R_x(y)|^2\,dy$$

$$+ \frac{|R_x(\tau)|^2}{T}\int_{-T}^{+T} |p(y)|^2\,dy$$

(4.333)

The other terms in (4.333) are calculated in more direct fashion; two of them are zero because of (4.325). For the five remaining terms, we obtain the sum

$$S_5 = \frac{1}{T}\int_{-T}^{+T} p(y)R_x(y)R_I(-y)\,dy + R_x(-\tau)p(-\tau)R_I(\tau) + R_x(\tau)p(\tau)R_I(-\tau)$$

$$+ \frac{1}{T}\int_{-T}^{+T} p(y)R_x(y)R_I(-y)\,dy + |R_I(\tau)|^2 + \frac{1}{T}\int_{-T}^{+T} |R_I(y)|^2\,dy \qquad (4.334)$$

We note that the true correlation function has magnitude-squared value given by

$$|R(\tau)|^2 = |p(\tau)|^2|R_x(\tau)|^2 + p(-\tau)R_x(-\tau)R_I(\tau) + p(\tau)R_x(\tau)R_I(-\tau) + |R_I(\tau)|^2 \tag{4.335}$$

From (4.320), (4.333) and (4.334) we obtain

$$\overline{|\hat{R}(\tau) - R(\tau)|^2} = \frac{|p(\tau)|^2}{T}\int_{-T}^{+T}|R_x(y)|^2\,dy + \frac{1}{T}\int_{-T}^{+T}|p(y)|^2|R_x(y)|^2\,dy + \frac{|R_x(\tau)|^2}{T}\int_{-T}^{+T}|p(y)|^2\,dy + \frac{2}{T}\int_{-T}^{+T}p(y)R_x(y)R_I(-y)\,dy \tag{4.336}$$

If the time offset, τ, is small, it seems reasonable to expect that both terms on the right hand side of (4.316) are approximately equal. By replacing the τ term with a $\tau = 0$ term, we at worst obtain an upper bound. Utilizing this replacement, and noting that $R_x(\tau)$ is impulsive with respect to both $p(\tau)$ and $R_I(\tau)$, we obtain for the mean-squared error of our bandwidth estimate [defined in (4.307)] the approximate result

$$\overline{|\epsilon_B|^2} = \frac{8}{B^4\pi^4\tau^4}\cdot\frac{1}{|R(0)|^2}\cdot\left[\frac{2|p(0)|^2}{T}\int_{-T}^{+T}|R_x(y)|^2\,dy + \frac{|R_x(0)|^2}{T}\int_{-T}^{+T}|p(y)|^2\,dy + \frac{2p(0)R_I(0)}{T}\int_{-T}^{+T}R_x(y)\,dy\right] \tag{4.337}$$

This expression takes on greater physical meaning when expressed in terms of the channel Doppler spread, B_c, and the rms bandwidth of the data, B_x. This can be accomplished most directly by using specific forms for the correlation functions of the channel and data. Specifically, we assume

$$R_x(\tau) = R_x(0)\, e^{-\frac{\pi^2 B_x^2 \tau^2}{2}} \tag{4.338}$$

and

$$p(\tau) = p(0)\, e^{-\frac{\pi^2 B_x^2 \tau^2}{2}} \tag{4.339}$$

By Fourier transforming, it is easy to verify that B_x and B_c in these expressions satisfy the definition for rms bandwidth given at the beginning of this section. Substituting in (4.337) and integrating, we obtain the result

$$\overline{|\epsilon_B|^2} = \frac{8}{B^4\pi^4\tau^4}\left(\frac{1}{|R(0)|^2}\right)\left\{\frac{2}{\sqrt{\pi}}\,\frac{p^2(0)R_x^2(0)}{B_x T_0} + \frac{1}{\sqrt{\pi}}\,\frac{p^2(0)R_x^2(0)}{B_c T_0} + 2\sqrt{\frac{2}{\pi}}\,\frac{p(0)R_x(0)R_I(0)}{B_x T_0}\right\} \tag{4.340}$$

We recall that B and B_x represent the rms bandwidth of the total received signal, respectively; $p(0) = |T(f,t)|^2$ (where $T(f,t)$ is the time-varying channel transfer function); B_c is the channel Doppler spread; τ is the time offset for the correlation function measurements; $R(0)$, $R_x(0)$ and $R_I(0)$ represent the powers in the total received signal, data, and interference, respectively; and T_0 is the processing (integration) time.

Physically, $\overline{|\epsilon_B|^2}$ represents the scatter of the rms bandwidth measurement $\widehat{B^2}$ about its true value B^2; we will make extensive use of this expression in evaluating detector performance in Section 4.4.2.4.

4.4.2.3.3 Centroid Estimate

The discussion in Section 4.4.2.2 and 4.4.2.3.1 clearly indicate the need for a centroid measurement to determine the presence of narrowband interference. In this section, we discuss the centroid estimate and its statistical properties. A knowledge of these properties is required for the detector performance evaluation covered in Section 4.4.2.4.

From the Fourier transform relation between the received signal correlation function and its power spectrum,

$$R(\tau) = \int P(f)\, e^{j2\pi f\tau}\, df \tag{4.341}$$

and the definition of the centroid,

$$\bar{f} \triangleq \frac{\int f\, P(f)\, df}{\int P(f)\, df} \tag{4.342}$$

we obtain, after differentiating (4.341) with respect to τ, the result

$$\bar{f} = \frac{-j}{2\pi} \frac{R'(0)}{R(0)} \tag{4.343}$$

Clearly, for $\bar{f}$ to have physical meaning, $R'(0)$ must be purely imaginary, i.e.,

$$R'(0) = j\, \mathrm{Im}\left(R'(0)\right) \tag{4.344}$$

and

$$\bar{f} = \frac{1}{2\pi}\, \mathrm{Im}\left\{\frac{R'(0)}{R(0)}\right\} \tag{4.345}$$

As our estimate, we use

$$\hat{\bar{f}} = \frac{1}{2\pi}\, \mathrm{Im}\left(\frac{\hat{R}'(0)}{\hat{R}(0)}\right) \tag{4.346}$$

Hence, the errors in estimating $\bar{f}$ arise in a natural way from the errors in estimating the correlation function and its derivative at $\tau = 0$.

There is a small bias to the estimate in (4.346) that disappears rapidly as the processing time increases; hence we need only compute the variance σ_f, where

$$\sigma_f \triangleq \overline{(\Delta f)^2} \tag{4.347}$$

and

$$\Delta f \triangleq \hat{\bar{f}} - \bar{f}$$

$$= \frac{1}{2\pi} \operatorname{Im}\left\{\frac{\hat{R}'(0)}{\hat{R}(0)} - \frac{R'(0)}{R(0)}\right\} \tag{4.348}$$

With exactly the same arguments used to obtain (4.311) we here obtain

$$\Delta f = \frac{1}{2\pi} \operatorname{Im}\left\{\frac{R'(0)}{R(0)} (\epsilon_1 - \epsilon_0)\right\} \tag{4.349}$$

where, now

$$\epsilon_0 \triangleq \frac{\hat{R}(0) - R(0)}{R(0)} \tag{4.350}$$

and

$$\epsilon_1 \triangleq \frac{\hat{R}'(0) - R'(0)}{R'(0)} \tag{4.351}$$

Once again approximating the variance (here $\overline{|\Delta f|^2}$) with its upper bound, we obtain

$$|\Delta f|^2 = \frac{|R'(0)|^2}{4\pi^2 R^2(0)} |\epsilon_1 - \epsilon_0|^2 \tag{4.352}$$

which, at worst, will give us a mildly pessimistic prediction of detector performance. The major difficulties in calculating the value of $\overline{|\Delta f|^2}$ will arise in the calculation of

$$\overline{|\epsilon_1 - \epsilon_0|^2} = \overline{|\epsilon_0|^2} + \overline{|\epsilon_1|^2} - \overline{2\,\mathrm{Re}(\epsilon_0 \epsilon_1)} \tag{4.353}$$

In this expression $|\epsilon_0|^2$ is known immediately from (4.336) evaluated at $\tau = 0$. In fact, defining

$$M_R = \overline{|\hat{R}(0) - R(0)|^2} \tag{4.354}$$

we have immediately, from the bracketed term in (4.338) the result

$$M_R = \frac{1}{T}\left\{\left(\frac{2}{\sqrt{\pi}}\right)\frac{1}{B_x} + \frac{1}{(\sqrt{\pi}\ell)}\frac{1}{B_c}\right\} p^2(0)\, R_x^2(0)$$

$$+ \frac{1}{T}\left(2\sqrt{\frac{2}{\pi}}\right)\frac{1}{B_x}\, p(0)\, R_x(0)\, R_i(0) \tag{4.355}$$

It remains to calculate $\overline{|\epsilon_1|^2}$ and the cross term $\overline{\epsilon_0 \epsilon_1}$. Dealing first with $\overline{|\epsilon_1|^2}$, we calculate

$$M_R' \triangleq \overline{|\hat{R}'(0) - R'(0)|^2}$$

$$= \overline{|\hat{R}'(0)|^2} - |R'(0)|^2 \tag{4.356}$$

We note first that

$$\overline{z^*(t)\, \dot{z}(s)} = R'(s - t) \tag{4.357}$$

Thus, we use

$$\hat{R}'(0) = \frac{1}{T}\int_{-\frac{T}{2}}^{+\frac{T}{2}} z^*(t)\, \dot{z}(t)\, dt \tag{4.358}$$

so

$$|\hat{R}'(0)|^2 = \frac{1}{T^2} \iint_{-\frac{T}{2}}^{+\frac{T}{2}} \overline{z^*(t)\, z^*(s)\, \dot{z}(t)\, z(s)}\; dt\, ds \qquad (4.359)$$

We note from Section 4.4.2.3.2 that the same results obtained by performing averages conditional on the data would have been obtained by applying the fourth moment relation in (4.324) to a direct, unconditional average, over the total received signal. The same is true in (4.359) for the integrand, M_z'. We obtain

$$M_z' = \overline{z^*(t)\, \dot{z}(t)}\;\; \overline{\dot{z}^*(s)\, z(s)} + \overline{\dot{z}^*(s)\, \dot{z}(t)}\;\; \overline{z^*(t)\, z(s)} \qquad (4.360)$$

Moments of the type in (4.360) can be easily evaluated by using the general formula

$$\overline{\frac{d^n z^*(t)}{d\, t^n}\, \frac{d\, w^m(s)}{d\, s^m}} = \frac{\partial^{n+m}}{\partial t^n\, \partial\, s^m} R_{zw}(t,s)$$

$$= (-1)^n\, R_{zw}^{(n+m)}\, (s - t) \qquad (4.361)$$

From (4.360)

$$M_z' = -\, R'(0)\, R'(0) \;-\; R''(t - s)\, R(s - t)$$

and we can see from (4.356) and the fact that $R'(0)$ is purely imaginary that

$$M_R' = -\, \frac{1}{T^2} \iint_{-\frac{T}{2}}^{+\frac{T}{2}} R''(t - s)\, R(s - t)\, dt\, ds \qquad (4.362)$$

or

$$M_R' = \frac{1}{T^2} \int_{-\frac{T}{2}}^{+\frac{T}{2}} \int \overline{\dot{z}^*(s)\,\dot{z}(t)}\ \ \overline{z^*(t)\,z(s)}\ dt\,ds \qquad (4.3\cdot\cdot)$$

a form that is simpler for the calculations since we need only evaluate $\overline{\dot{z}^*(s)\,\dot{z}(t)}$ and $\overline{z^*(t)\,z(s)}$. Recall $z(t)$ represents the total received signal

$$z(t) = w(t) + I(t) \qquad (4.364)$$

where $I(t)$ is the interference and $w(t)$ represents the channel passed data

$$w(t) = \int g(t,\xi)\ x(t-\xi)\,d\xi \qquad (4.365)$$

Because of the independence of the data and interference, we have

$$\overline{\dot{z}^*(s)\,\dot{z}(t)} = \overline{\dot{w}^*(s)\,\dot{w}(t)} + \overline{\dot{I}^*(s)\,\dot{I}(t)}$$

and

$$\overline{z^*(t)\,z(s)} = \overline{w^*(t)\,w(s)} + \overline{I^*(t)\,I(s)} \qquad (4.366)$$

The interference moments cause no difficulty. The data moments $\overline{w^*(t)\,w(s)}$ and $\overline{\dot{w}^*(s)\,\dot{w}(t)}$ are evaluated by utilizing (4.365). First, averaging over the data, we have

$$\overline{w^*(t)\,w(s)} = \int\int \overline{g^*(t,\xi)\,g(s,\eta)}\ \ x^*(t-\xi)\,x(s-\eta)\,d\xi\,d\eta$$

$$= \int\int Q(s-t,\xi)\,\delta(\xi-\eta)\,x^*(t-\xi)\,x(s-\eta)\,d\xi\,d\eta \qquad (4.367)$$

for the WSSUS channel. Now, neglecting frequency selective fading, as in Section 4.1, we obtain the result

$$\overline{w^*(t)\, w(s)} = \int Q(s-t,\xi)\, \overline{x^*(t-\xi)\, x(s-\xi)}\, dz$$

$$= p(s-t)\, R_x(s-t) \tag{4.368}$$

By differentiating (4.365), we have for the correlation function of the derivatives

$$\overline{\dot{w}^*(s)\, \dot{w}(t)} = \sum_{i=1}^{4} W_i$$

$$W_1 = \int\int \dot{g}^*(s,\xi)\, \dot{g}(t,\eta)\, x^*(s-\xi)\, x(t-\eta)\, d\xi\, d\eta$$

$$W_2 = \int\int \dot{g}^*(s,\xi)\, g(t,\eta)\, x^*(s-\xi)\, \dot{x}(t-\eta)\, d\xi\, d\eta$$

$$W_3 = \int\int g^*(s,\xi)\, \dot{g}(t,\eta)\, \dot{x}^*(s-\xi)\, x(t-\eta)\, d\xi\, d\eta$$

$$W_4 = \int\int g^*(s,\xi)\, g(t,\eta)\, \dot{x}^*(s-\xi)\, \dot{x}(t-\eta)\, d\xi\, d\eta \tag{4.369}$$

By making use of (4.361) and first evaluating the channel moments and then averaging over the data $x(t)$, we obtain

$$\begin{aligned} \overline{\dot{w}^*(s)\, \dot{w}(t)} &= -\, p''(t-s)\, R_x(t-s) \\ &= -\, 2p'(t-s)\, R_x'(t-s) \\ &= -\, p(t-s)\, R_x''(t-s) \end{aligned} \tag{4.370}$$

where

$$p^{(n)}(t-s) = \int Q^{(n)}(t-s,\xi)\, d\xi \tag{4.371}$$

Hence,

$$\overline{\dot{z}^*(s)\, \dot{z}(t)} = \overline{\dot{w}^*(s)\, \dot{w}(t)} - R_I''(t-s) \tag{4.372}$$

and

$$z^*(s)\, z(t) = p(s-t)\, R_x(s-t) + R_I(s-t) \tag{4.373}$$

Recall, from (4.363) that M_R', the quantity we are after, is given by

$$M_R' = \frac{1}{T^2} \int_{-\frac{T}{2}}^{+\frac{T}{2}} \int_{-\frac{T}{2}}^{+\frac{T}{2}} I(t,s)\, dt\, ds \tag{4.374}$$

where $I(t,s)$ is the product of (4.372) and (4.373).

Hence, after using the double-to-single integral transformation (4.332), we have M_R' as the sum of eight integrals:

$$\begin{aligned} M_R' = {} & \frac{1}{T} \int_{-T}^{+T} p(-y)p''(y)|R_x(y)|^2\, dy + \frac{2}{T} \int_{-T}^{+T} p(-y)p'(y)R_x(-y)R_x'(y)\, dy \\ & + \frac{1}{T} \int_{-T}^{+T} |p(y)|^2 R_x(-y)R_x''(y)\, dy + \frac{1}{T} \int_{-T}^{+T} p''(y)R_x(y)R_I(-y)\, dy \\ & + \frac{2}{T} \int_{-T}^{+T} p'(y)R_x'(y)R_I(-y)\, dy + \frac{1}{T} \int_{-T}^{+T} p(y)R_x''(y)R_I(-y)\, dy \\ & + \frac{1}{T} \int_{-T}^{+T} p(-y)R_I''(y)R_x(-y)\, dy + \frac{1}{T} \int_{-T}^{+T} R_I(-y)R_I''(y)\, dy \end{aligned} \tag{4.375}$$

The integrals in (4.375) can be calculated with the aid of the relations

$$\begin{aligned} \int f(y)R_x(y)\, dy &\approx f(0) \int R_x(y)\, dy \\ \int f(y)R_x'(y)\, dy &\approx -f'(0) \int R_x(y)\, dy \\ \int f(y)R_x''(y)\, dy &\approx f''(0) \int R_x(y)\, dy \end{aligned} \tag{4.376}$$

These impulsive relations derive from the fact that the data is wideband with respect to the interference and the temporal dependence of the channel. To facilitate matters, we introduce the specific forms for the correlation functions introduced earlier in (4.338) and (4.339). For the correlation function of the interference [see (4.276)] we use

$$R_I(\tau) = R_i(\tau)\, e^{j2\pi f_\Delta \tau} \tag{4.377}$$

and

$$R_i(\tau) = R_i(0)\, e^{-\frac{\pi^2 B_i^2 \tau^2}{2}}$$

where B_i represents the rms bandwidth of the interference.

Substituting all of these expressions in (4.375) we obtain, after extensive use of (4.376) and combining terms, the result

$$M_R' = \frac{1}{T}\left[\frac{\pi^2}{2\sqrt{\pi}}\right]\left\{B_x\, p^2(0)\, R_x^2(0) + B_i\, R_i^2(0)\right\}$$

$$+ \frac{1}{T}\left[2\pi^2\sqrt{\frac{2}{\pi}}\right]\left\{\frac{B_i^2}{B_x} - \frac{4f_\Delta^2}{B_x}\right\} p(0)\, R_x(0)\, R_i(0)$$

$$+\left[\frac{1}{T}\,\frac{\pi^2}{\sqrt{\pi}}\right]\left\{\frac{4f_\Delta^2}{B_i}\right\} R_i^2(0) \tag{4.378}$$

The cross product term in (4.353) will be neglected. In fact, it can be argued that this term is equal to zero if the measurements are taken properly. If the imaginary part of the correlation function estimate and the real part of the derivative estimate are both discarded, then ϵ_0 and ϵ_1 are, respectively, real and imaginary and their product is imaginary. Hence, the last term in (4.353) vanishes.

Now, combining (4.343), (4.352), (4.355), and (4.378), and neglecting the terms in (4.378) that are small due to the fact that we are dealing with narrowband interference (B_i small), we obtain the result

$$\overline{|\Delta f|^2} = \bar{f}^2\left[\frac{1}{R^2(0)}\right]\cdot\frac{1}{\sqrt{\pi}}\left[\frac{p^2(0)R_x^2(0)}{B_c T_0}\right] + \frac{1}{T}\left[\frac{1}{8\sqrt{\pi}}\right]\frac{B_x p^2(0)R_x^2(0)}{R^2(0)}$$

$$- \frac{1}{T}\left[\frac{1}{2\sqrt{\frac{2}{\pi}}}\right]\left[\frac{4\Gamma_\Delta^2}{B_x}\right]\frac{p(0)R_x(0)R_i(0)}{R^2(0)} + \frac{1}{T}\left[\frac{1}{4\sqrt{\pi}}\right]\left[\frac{4\Gamma_\Delta^2}{B_i}\right]\frac{R_i^2(0)}{R^2(0)} \tag{4.379}$$

The importance of this quantity will be discussed subsequently.

4.4.2.3.4 Probability Density Functions for the Observation Variables

The calculations described in Sections 4.4.2.3.2 and 4.4.2.3.3 provide the variances and means for the observations of B^2 and $\bar{f}$. It is helpful for evaluating the performance of interference detection schemes to have probability density functions (pdf's) available. In the calculations presented below, the pdf's used for $\hat{B^2}$ and $\hat{\bar{f}}$ are those for Gaussian random variables. These assumed forms seem reasonable if one writes a Riemann sum for the two integrals representing the integrals (4.319) and (4.358) from which the estimates for the correlation function and its derivative are formed, and then applies Central Limit Theorem arguments to the resulting sums. Even in the absence of strict Gaussian behavior for the observation variables it is clear that the performance presented below should not differ greatly from the actual performance that could be achieved in practice. The fact that the variances decrease with increasing T, gives a firm base to the notion that performance should be enhanced greatly at large integration times.

For the probability density function of $\hat{B^2}$, conditioned on each of the hypotheses, H_j, we have

$$p_{\hat{B^2}/H_j}(x) = \frac{1}{\sigma_j\sqrt{2\pi}}\, e^{-\frac{(x-B_j^2)}{2\sigma_j}} \tag{4.380}$$

Here, B_j refers to the true value of rms bandwidth under the appropriate hypothesis and σ_j is given by

$$\sigma_j^2 = B_j^4 \overline{|\epsilon_{B_j}|^2} \tag{4.381}$$

where $\overline{|\epsilon_{B_j}|^2}$ is the value of (4.340) under the appropriate hypothesis. Since the time offset, τ, appearing in the estimate (4.306) must be specified, we choose the value τ according to the restriction

$$2\pi B_x \tau = 0.6 \tag{4.382}$$

This somewhat arbitrary choice is in keeping with the approximation used in (4.301), and is used subsequently in the numerical calculations of (4.340).

Similarly, we have for the pdf of the frequency centroid

$$p_{\hat{\bar{f}}/H_j}(y) = \frac{1}{\Sigma_j\sqrt{2\pi}} e^{-\frac{(y-\Sigma_j)^2}{\partial\Sigma_j^2}} \tag{4.383}$$

where Σ_j is (4.379) evaluated under the appropriate hypothesis.

A final approximation for the numerical calculations presented in Section 4.4.2.4.2.2 is that the rms bandwidth and centroid estimates are independent, i.e., the joint pdf for the two observation variables can be factored into the two pdf's given above. This assumption is reasonable in view of the way the two measurements are processed, one measurement emphasizing the correlation function and the other its derivative. As can be seen in Section 4.4.2.4.2.2, the effects of dependence of the two random variables would tend to cancel, decreasing in a like manner the probability of a false alarm error and the probability of detection. In any event, the performance curves presented below would not be modified significantly by the dependence of the observations, since their independence could be totally guaranteed by processing over separate time intervals and thus having the effect, at worst, of doubling the processing time.

The detection schemes and their performance are presented below in Section 4.4.2.4.

4.4.2.4 Detection Schemes

4.4.2.4.1 Near-Optimal Detection Using RMS Bandwidth Measurements

4.4.2.4.1.1 Problem Formulation (Detector 1)

It is clear from the arguments of the last section that the interference detection problem can be treated as a hypothesis testing problem. The two hypotheses to be are simply

H_0: no narrowband interference present

H_1: narrowband interference present

An observation (estimate), $\hat{B}^2$, of the rms bandwidth of the total received signal may, under certain conditions, serve usefully as an indicator of the presence of narrowband interference. For such a purpose its usefulness depends, of course, on the reliability of the bandwidth estimate and, hence, through the probability density functions discussed in the previous section, on the measurement time and physical properties of the total received signal.

In this section we document the effectiveness of the rms bandwidth estimate as an indicator of narrowband interference, and point out its shortcomings. Though near-optimal use is made of the bandwidth estimate, it will be demonstrated in the next section that suboptimal use of both rms bandwidth and frequency centroid measurements can give superior performance.

It is known [4.20] for general problems of this type that the optimal detection scheme is a likelihood test. Here we use a near-optimal* scheme and test against a single threshold. Symbolically, we have

---

*A detailed analysis of the problem discussed here indicates that the decision space (real time) is partitioned into three regions. Only extremely small (perhaps negative) values of the observation variable would ever fall in the extreme left region. Realizations this small are of extremely small probability, and neglect of the third region gives a negligible departure for optimality.

$$\hat{B}^2 \underset{H_1}{\overset{H_0}{\gtrless}} x_{th} \tag{4.384}$$

If the rms bandwidth observation exceeds the threshold, we decide that there is no interference present; a realization below the threshold is interpreted as being due to the presence of narrowband interference, and the decision is H_1.

An important point related to this decision rule is that the rule itself, i.e., the threshold, must not depend on B_i^2 or f_Δ or on any other parameters of the inteference to be detected. The detector performance, of course, depends on all these parameters. In particular, it depends on B_i^2, the rms bandwidth of the interference, on f_Δ, its frequency offset, and on p_i, the fraction of total received power appearing as interference [see (4.284)].

Performance of the interference detector will be plotted as a detector operating characteristic (DOC). This is a plot of detection probability versus the probability of a false alarm error. A false alarm error occurs when $\hat{B}^2$ in (4.384) falls below the threshold even though there is not interference (H_0 is true). Its probability is denoted P_F and is given by

$$P_F = \int_{-\infty}^{x_{th}} p_{\hat{B}^2/H_0}(x)\, dx \tag{4.385}$$

where the integrand is just the pdf of the observation variable conditioned on the event H_0.

Detection occurs when $\hat{B}^2 < x_{th}$ and H_1 is true. This event has probability

$$P_D = \int_{-\infty}^{x_{th}} p_{\hat{B}^2/H_1}(x)\, dx \tag{4.386}$$

We note, once P_F is specified, that x_{th} in (4.385) depends only on statistical properties of the observation variable conditioned on the event H_0. Hence, the decision rule does not depend on the interference. On the other hand, the detection probability in (4.386) clearly depends on interference properties as discussed above.

The performance of a detector making near-optimal use of the rms bandwidth estimate (Detector 1) is documented in the next section.

4.4.2.4.1.2 Numerical Results (Detector 1)

Utilizing the probability functions described in Section 4.4.2.3.4 and the variance calculation in Section 4.4.2.3.2, a typical performance curve for detector 1 (utilizing single observation of rms bandwidth) is shown in Figure 4.20. The detector operating characteristic is plotted for $p = 0.3$, $f_\Delta = 0.4$, and B_cT_0 ranging from 200 to 1000 (B_c is the channel Doppler spread).* It is not surprising that performance improves with increasing B_cT_0 and also improves as p increases (dependence not shown here). Comparison with other curves we have calculated, however, indicates that the ability of detector 1 to detect narrowband interference at $f_\Delta = 0.4$ is considerably inferior to that achieved when attempting to detect interference that is closer to the center of the data band. This deterioration in performance as f_Δ increases is a clear consequence of the way in which the rms bandwidth changes in the presence of narrowband interference (see Section 4.4.2.2). In fact, for certain values of p and f_Δ, detector 1 is rendered almost completely useless.

4.4.2.4.2 Suboptimal Detection Using RMS Bandwidth and Centroid Measurements

4.4.2.4.2.1 Problem Formulation (Detector 2)

Detector 1, discussed in the previous section, is clearly deficient at high values of frequency offset, f_Δ. This is because the narrowband interference, when not in a spectral location near the carrier frequency, does not necessarily cause a pronounced reduction in the rms bandwidth of the received signal. This is clear from examination of (4.298). This situation can be remedied in a satisfactory way by also using estimates of the frequency centroid, $\bar{f}$, in conjunction with the threshold test

*B_cT_0 can be thought of as representing the average number of channel fades over which the received signal is processed to obtain the estimates of rms bandwidth and centroid. For a fading channel with $B_c = 1$ Hz, e.g., tropo and HF channel, B_cT_0 is just the processing time in seconds.

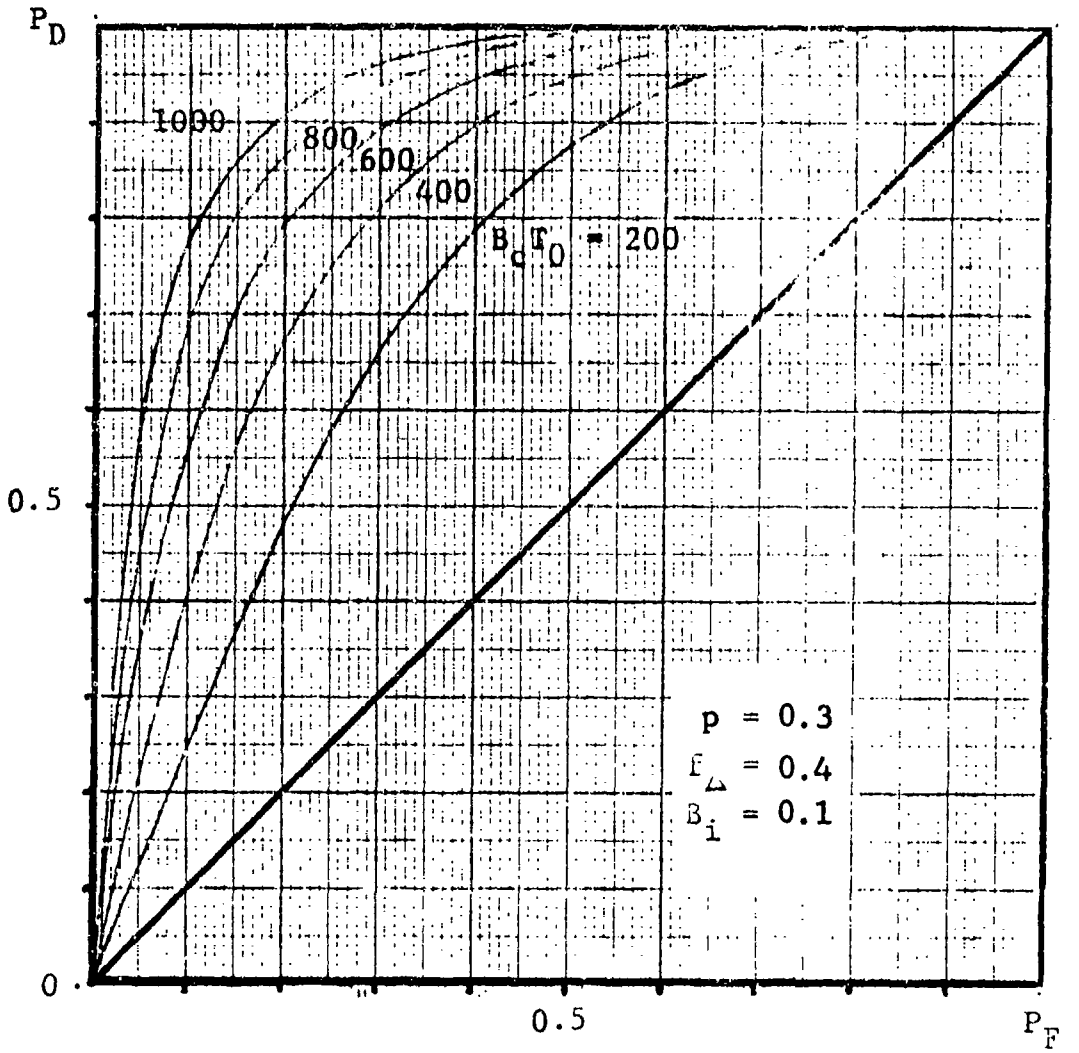

$$B_i = \frac{\text{rms bandwidth of interference}}{\text{rms bandwidth of data}}$$

$$p = \frac{\text{interference power}}{\text{total power in received signal}}$$

$$f_\Delta = \frac{\text{difference in carrier frequencies of interference and data}}{\text{rms bandwidth of data}}$$

B_c = channel Doppler spread

T_0 = integration time used to process

Figure 4.20 Detector 1 Operating Characteristic

$$\text{Decide} \quad H_1 \quad \text{if } \hat{B}^2 < x_{th}$$
$$\text{or if } |\hat{\bar{f}}| > y_{th}$$
$$\text{Decide} \quad H_0 \quad \text{otherwise} \tag{4.387}$$

The operation of this detector is illustrated in Figure 4.21.

This decision rule is based on the intuitive notion that narrowband interference that does not make itself evident through an increase in the rms bandwidth will (if this situation exists because of a high frequency offset, f_Δ) make itself evident through an increase in the frequency centroid, $\bar{f}$. The rule has the effect of partitioning the two-dimensional plane, determined by the realizations $\hat{B}^2$ and $\hat{\bar{f}}$ (x and y) into two connected regions R_0 and R_1. R_0 is the small rectangular region $x > x_{th}$ and $|y| < y_{th}$ to the right of x_{th} in which realizations of $\hat{B}^2$ and $\hat{\bar{f}}$ give rise to the decision H_0, and R_1 is the remainder of the plane. Optimal partitioning of the decision space would no doubt involve more complex analytical boundaries. Nevertheless, the performance of detector 2, which uses the suboptimal decision scheme in (4.387) provides clearly superior performance to that of detector 1. This is demonstrated below in Section 4.4.2.4.2.2.

The performance of detector 2 is evaluated by utilizing the two conditional pdf's

$$p(x,y|H_j) \qquad j = 1,2 \tag{4.388}$$

for the observation variables $\hat{B}^2$ and $\hat{\bar{f}}$. The conditions are, once again, the two events H_0 (no interference) and H_1 (interference present). The probability of a false alarm error, which occurs when H_0 is true and the observations fall in R_1, is given by

$$P_F = \iint_{R_1} p(x,y|H_0)\, dx\, dy \tag{4.389}$$

As in Section 4.4.2.4.1.1, it is a prespecification of this quantity that determines the thresholds, x_{th} and y_{th}. To simplify the analysis, it is helpful to utilize P_{FX}, the false alarm probability that would result if we were using just the rms bandwidth estimate, and P_{FY}, the false alarm probability for the centroid estimate alone. These are given, respectively, by

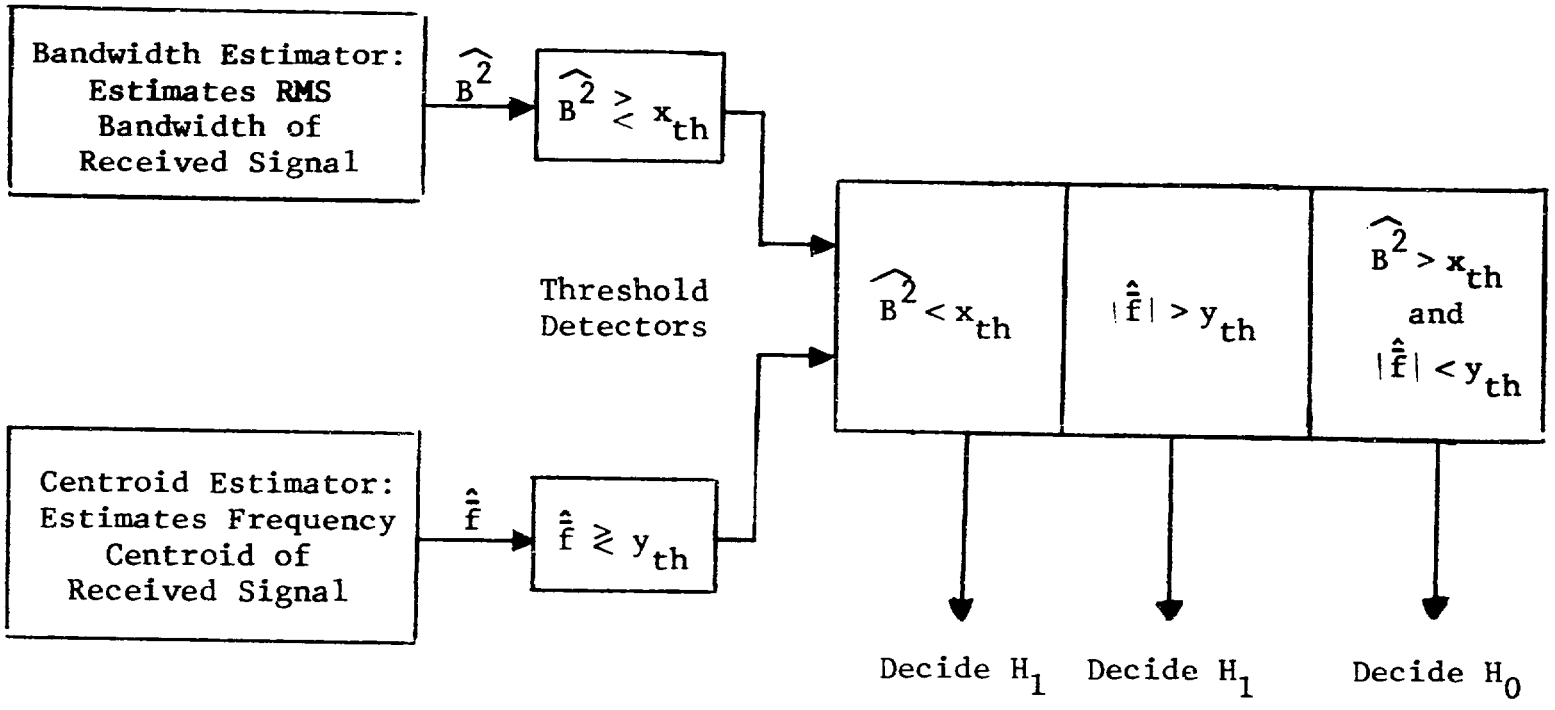

H_0 = No interference present

H_1 = Interference present

Figure 4.21 Schematic of Interference Detector 2

$$P_{FX} = \int_{-\infty}^{x_{th}} p(x|H_0)\,dx \tag{4.390}$$

and

$$P_{FY} = 1 - \int_{-y_{th}}^{+y_{th}} p(y|H_0)\,dy \tag{4.391}$$

Now, modifying (4.389) we have

$$\begin{aligned} P_F &= 1 - \iint_{R_0} p(x,y|H_0)\,dx\,dy \\ &= 1 - \int_{-y_{th}}^{+y_{th}} \int_{x_{th}}^{\infty} p(x,y|H_0)\,dx\,dy \end{aligned} \tag{4.392}$$

Now, making use of the independence of the two random variables as discussed at the end of Section 4.4.2.3.4, we obtain

$$\begin{aligned} P_F &= 1 - (1 - P_{FX})(1 - P_{FY}) \\ &= P_{FX} + P_{FY} - P_{FX}P_{FY} \end{aligned} \tag{4.393}$$

It is clear that a specification of P_F leaves somewhat arbitrary [within the constraint (4.393)] the choice P_{FX} and P_{FY}. This is a consequence of the nonoptimality of our decision scheme. Dividing the specified P_F equally between P_{FX} and P_{FY}, we choose

$$P_{FX} = P_{FY} = 1 - \sqrt{1 - P_F} \tag{4.394}$$

Thus, the thresholds, x_{th} and y_{th}, are completely specified by (4.394) and the by relations

$$P_{FX} = \int_{-\infty}^{x_{th}} p(x|H_0)\, dx \tag{4.395}$$

and

$$P_{FY} = 1 - \int_{-y_{th}}^{+y_{th}} p(y|H_0)\, dy \tag{4.396}$$

It is in this way that a specification of P_F leads, through (4.394), to the determination of x_{th} and y_{th}.

Once the thresholds have been determined through the procedures outlined above, the decision is completely specified and one can determine the detector operating characteristic (DOC) directly. The probability of detection is found by integrating the joint probability density function of the two observation variables (conditioned on the event H_1) over the region R_1. Equivalently, one can use the relation

$$P_D = 1 - P_M \tag{4.397}$$

where P_M is the probability of a "miss" error given by

$$P_M = \int_{-y_{th}}^{+y_{th}} \int_{x_{th}}^{\infty} p(x,y|H_1)\, dx\, dy \tag{4.398}$$

The numerical computation of x_{th} and y_{th}, from (4.390) - (4.398) has been facilitated by modifying existent routines [4.21] [4.21]. Detector operating characteristics for various physical situations of interest are presented in the following section.

4.4.2.4.2.2 Numerical Results for Detector 2

Detector 2, which utilizes two observation variables, rms bandwidth and centroid, compensates for the poor performance of detector 1 at high values of the frequency offset, f_Δ. The improvement in performance is clear from Figure 4.22 which has been plotted for the same values of interference parameters, f_Δ and B_I, but for an even lower value of fractional interference power, p.

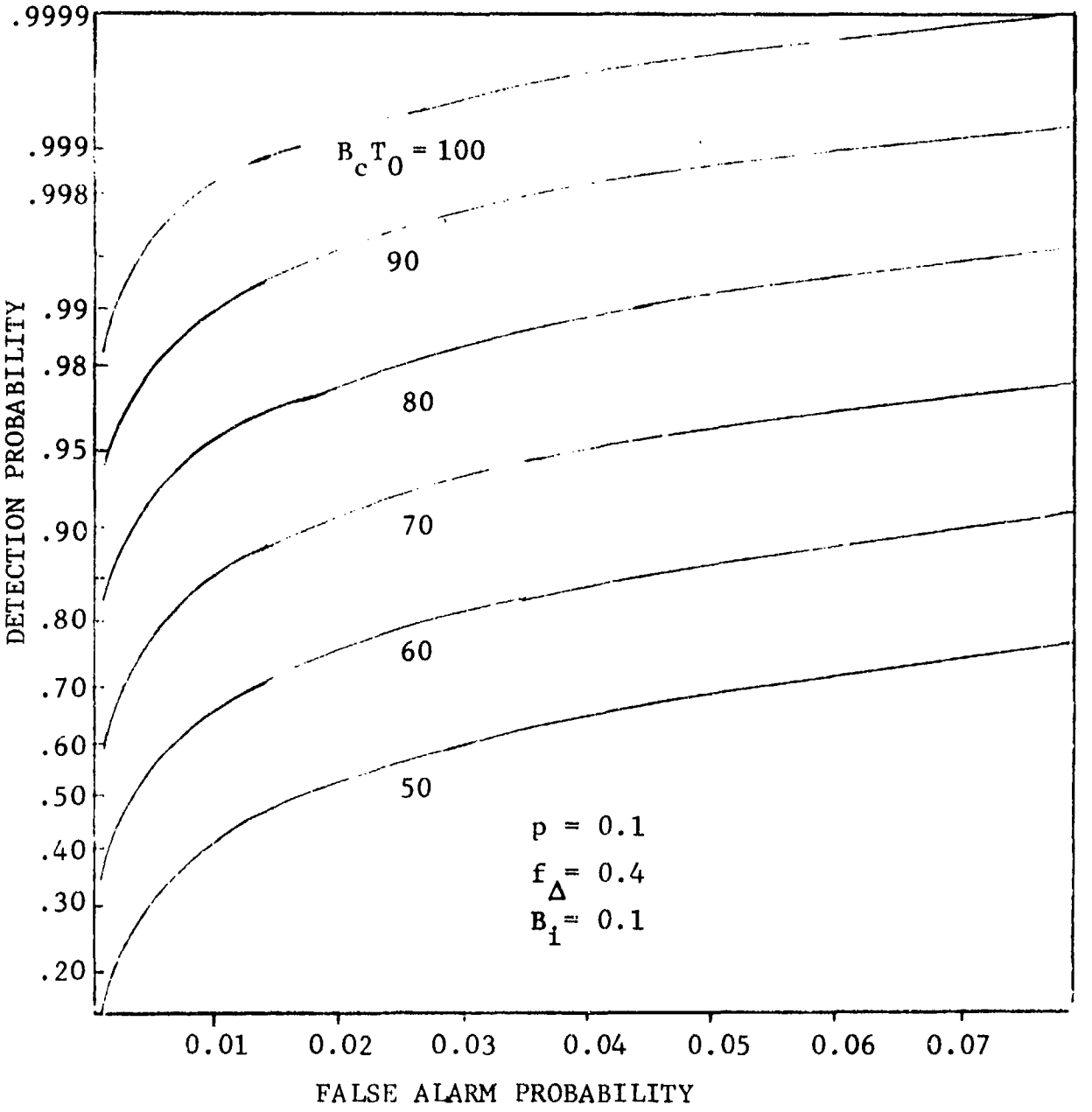

$$B_i = \frac{\text{RMS BANDWIDTH OF INTERFERENCE}}{\text{RMS BANDWIDTH OF DATA}}$$

$$p = \frac{\text{INTERFERENCE POWER}}{\text{TOTAL POWER IN RECEIVED SIGNAL}}$$

$$f_\Delta = \frac{\text{DIFFERENCE IN CARRIER FREQUENCIES OF INTERFERENCE \& DATA}}{\text{RMS BANDWIDTH OF DATA}}$$

B_c = CHANNEL DOPPLER SPREAD

T_0 = INTEGRATION TIME USED TO PROCESS

Figure 4.22 Detector 2 Operating Characteristic

It is clear from examination of this figure that the performance is far superior to that illustrated in Figure 4.20.

As one would expect, the performance of each test depends on the amount of time used to acquire the estimates (integration time, T_0), the narrowband interference bandwidth, the ratio of the interference power to total power in the received signal (fractional power ratio, p), and f_Δ, the offset frequency of the narrowband interference.

The curves we have presented here, and many others that have been calculated to cover a wide variety of interference conditions, indicate the feasibility of using rms bandwidth and centroid measurements (via detector 2) to indicate system degradation due to the presence of strong narrowband interference as source of system degradation.

4.4.2.4.2.3 Comparison with RMS Bandwidth Detector (Detector 1)

It is clear that the extra observation variable available to detector 2 can provide an extreme advantage in terms of performance. In fact, the performance of detector 2 is inferior to that of detector 1 only in one rare situation; this is when f_Δ is extremely close to zero. This is illustrated in Figure 4.23 where we have plotted the performance of both detectors for $f_\Delta = 0$. This minor degradation of detector 2 occurs at $f_\Delta = 0$ because the centroid is the same under each hypothesis and its measurement provides no information at all about the existence of narrowband interference. Fortunately, f_Δ must be very close to zero for this to happen. In fact, when f_Δ equals just 5% of the data bandwidth, detector 2 is once again superior, as is clear from the curve in the upper left-hand corner of Figure 4.23.

4.4.2.5 Summary

In order to obtain methods for detecting narrowband interference, decision-theoretic concepts have been applied to the development of detection techniques utilizing measurements of rms bandwidth and frequency centroid. As discussed in the previous sections, the success of any such scheme must necessarily depend on the reliability of the measurements and, hence, on the total processing time. It must also depend on the extent to which the observation variables are affected by the presence of the narrowband interference. Thus, the rms bandwidth and power of the interfering signal have the predominant effects on its detectability. The detector utilizing only the rms bandwidth measurements was found to be deficient because of the fact that the rms bandwidth is affected in different ways by interference at

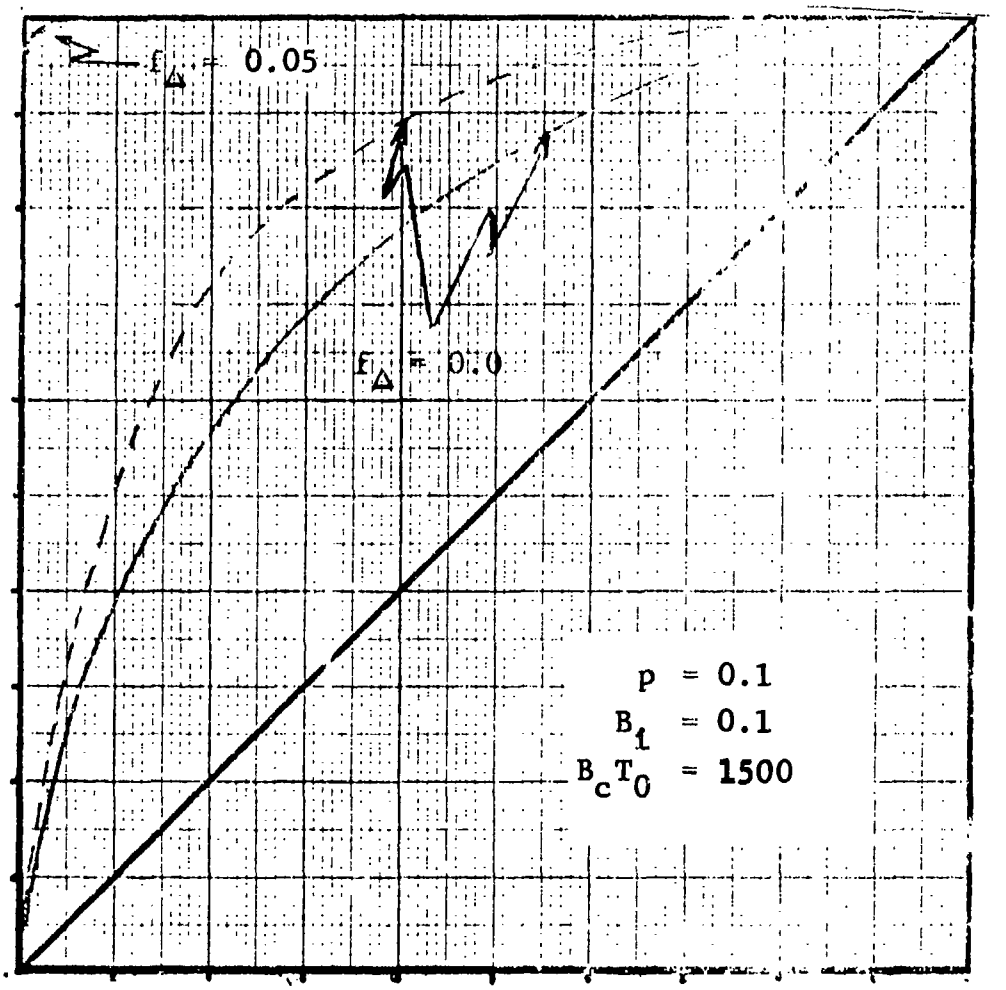

Note: Detector 1 Operating Characteristic (dotted line)
Detector 2 Operating Characteristic (solid lines)

B_i = $\frac{\text{rms bandwidth of interference}}{\text{rms bandwidth of data}}$

p = $\frac{\text{interference power}}{\text{total power in received signal}}$

f_Δ = $\frac{\text{difference in carrier frequencies of interference and data}}{\text{rms bandwidth of data}}$

B_c = channel Doppler spread

T_0 = integration time used to process

Figure 4.23 Comparison of Detector 1 and Detector 2 Operating Characteristics for Small Frequency Offset

different frequency centroid values. A detector using both measurements, detector 2, was found to be clearly superior.

4.4.3 Measurement of Changes in Receiver Power Level as an Indicator of the Presence of Interference

4.4.3.1 Introduction

In this section we discuss the use of power measurements of the received signal to indicate the presence of interference. For our power measurements, we will use the output signal of the configuration illustrated in Figure 4.1. Since our goal is to use this signal, $\nu(t)$, to determine the presence of interference, we can view $\nu(t)$ as being the desired signal (interference) corrupted by a noisy additive (channel-passed data). The use of special probing signals (idle slots in data) for uncorrupted measurements of the interference is discussed in Section 6.

We note here that this scheme does not depend so much on a classification of the interference according to bandwidth as was the case in Section 4.4.2.

For purposes of analysis, we assume that there is available a "recent" time record, presumably free of interference, against which "present" measurements can be compared when it is suspected that there is strong interference in the received signal. Obviously, for the zero interference reference, it is advantageous to use as recent a time record as possible in order to minimize the extent to which nonstationary changes in the channel can cause the observed power changes. This question is given a detailed treatment in Section 4.4.3.5.

From Section 4.1 we have the estimator output

$$\nu(t) = |T(F,t)y(t) + J_2(t)|^2 \otimes k(t) \qquad (4.399)$$

where $y(t)$ is the response of the predetection filter, $h(t)$, to a frequency shifted version of the data $z(t)$.

$$y(t) = h(t) \otimes z(t)\, e^{-j2\pi Ft} \qquad (4.400)$$

and $T(F,t)$ represents the channel transfer function at the particular frequency F. $J_2(t)$ represents the interference output of the predetection filter, $h(t)$. The interference at the input to this filter is given by

$$J_1(t) = N(t) + I(t) \tag{4.401}$$

where N(t) represents the previously assumed receiver noise and I(t) represents an additional, perhaps strong, interfering signal of unknown origin. Thus,

$$J_2(t) = n(t) + i(t) \tag{4.402}$$

where

$$n(t) = N(t) \otimes h(t) \tag{4.403}$$

and

$$i(t) = I(t) \otimes h(t) \tag{4.404}$$

Since k(t) performs a time-average of its input, i.e.,

$$k(t) = \begin{cases} \frac{1}{T_0} & 0 \le t \le T_0 \\ 0 & \text{otherwise} \end{cases} \tag{4.405}$$

the function in (4.399) can be viewed simply as a random variable which it is here convenient to index with the time instant, t_p. We designate this quantity, $\nu(t_p)$

$$\nu(t_p) = |T(F,t_p)y(t_p) + J_2(t_p)|^2 \otimes k(t_p) \tag{4.406}$$

and refer to it in the sequel as the sampled power at time t_p.

Clearly, a single sample is not of much use because of the time variation of T(f,t). It is far more useful to deal with some measurement involving power observations over several time instants. In Section 4.4.3.2, we will make use of the arithmetic mean

$$\hat{\nu} = \frac{1}{M} \sum_{p=1}^{M} \nu(t_p) \tag{4.407}$$

Before proceeding with the analysis, we mention that the nomenclature will be the same as that used previously. Since the problem can be formulated as a problem in detection theory, we refer to the two hypotheses:

H_0: strong interfering signal, I(t), is not present

H_1: strong interfering signal, I(t), is present

The primary consideration of this section is in determining whether or not the extent to which $\hat{\nu}$ in (4.407) is affected by the interference is great enough to allow an accurate determination of which condition holds - especially when there are nonstationary changes in the channel.

4.4.3.2 A Method by which the Interference can be Detected

It is clear that the effectiveness of any scheme for detecting the presence of interference must depend on the statistics of the measurement, primarily its mean and variance. Taking care to retain the possibility of channel nonstationarity, we note that the ensemble average of the power measurements in (4.407) is given by

$$\bar{\hat{\nu}} = \frac{1}{M} \sum_{p=1}^{M} \overline{\nu(t_p)} \tag{4.408}$$

where it has been assumed that the power samples are independent. Each ensemble average on the right-hand side of (4.408) depends of course on the time instant, t_p, and will be different under the two interference hypotheses. For the variance of the power measurement, we obtain

$$\sigma^2 = \overline{|\hat{\nu} - \bar{\nu}|^2} = \frac{1}{M^2} \sum_{p=1}^{M} \sigma^2(t_p) \tag{4.409}$$

where

$$\sigma^2(t_p) = \overline{|\nu(t_p) - \bar{\nu}(t_p)|^2}$$

The variance also exhibits dependence on the time instants at which each of the power samples were taken.

We recall from Section 4.4.3.1 that the effectiveness of the power measurements as an indicator of interference will be determined by comparing a "present" time record with an "earlier" one that is interference-free. In fact, one can easily design a threshold test to detect the interference; if we use $\hat{\nu}_P$ to represent the present power measurement and $\hat{\nu}_E$ to represent the earlier (interference-free) measurement, the test consists of comparing the difference of the two measurements against a threshold, d. Symbolically, we have

$$\hat{\nu}_P - \hat{\nu}_E \underset{H_0}{\overset{H_1}{\gtrless}} d \tag{4.410}$$

which indicates that we should decide H_1 (interference now present) if the power difference exceeds d and H_0 (no interference) if the power difference falls below d. The configuation of this detector is illustrated in Figure 4.24. Denoting the observation variable $\hat{\theta} = \hat{\nu}_P - \hat{\nu}_E$, we note as before that there can be two types of errors, or there can be detection. These events and their probabilities are:

1) "False Alarm" Error (probability P_F):

   $\hat{\theta} > d$ when, in fact, H_0 is true.

2) "Miss" Error (probability P_m):

   $\hat{\theta} < d$ when, in fact, H_1 is true.

3) Detection (probability P_D):

   $\hat{\theta} > d$ when H_1 is, indeed, true.

The error probabilities are expressed in terms of the probability density functions conditional on each of the hypotheses. They are given by

$$P_F = \int_d^\infty p_{\hat{\theta}/H_0}(x)\, dx \tag{4.411}$$

$$P_m = \int_{-\infty}^d p_{\hat{\theta}/H_1}(x)\, dx \tag{4.412}$$

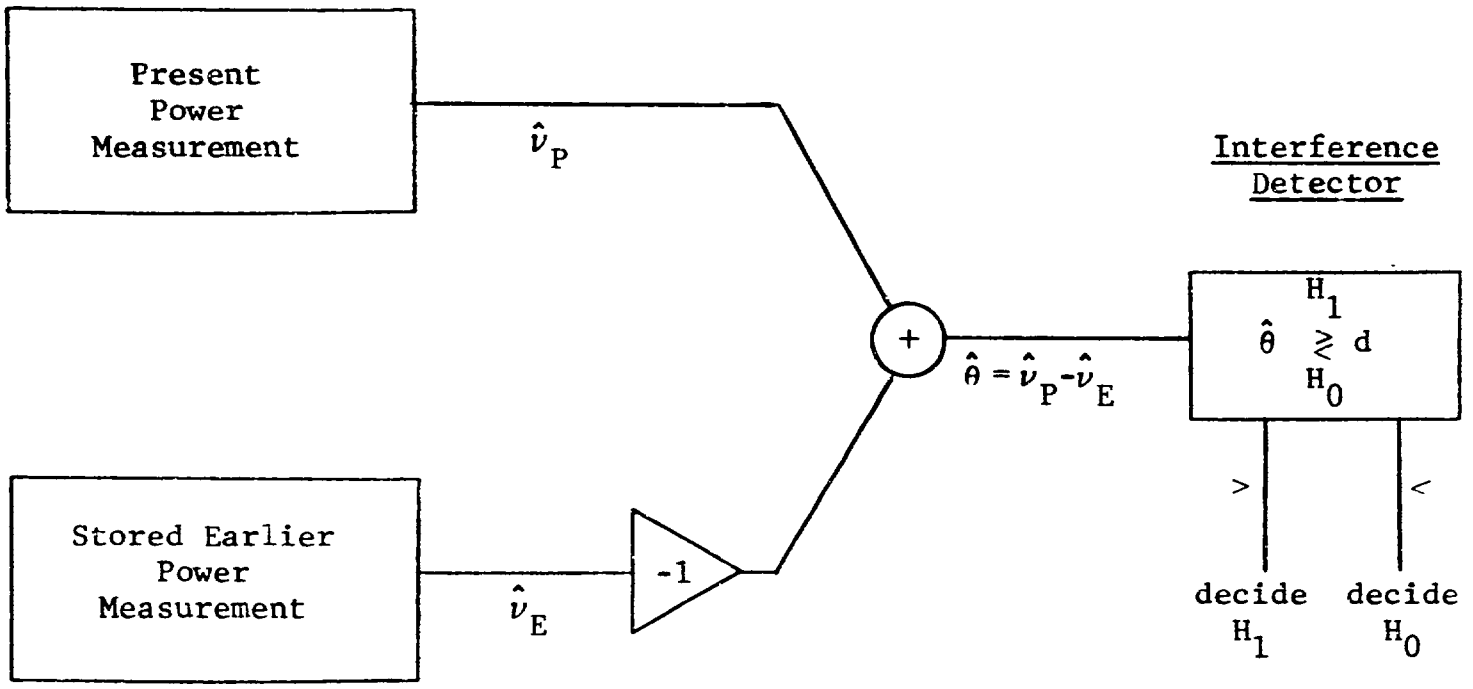

H_0: Interference Not Present

H_1: Interference Now Present
Where Previously It Was Not

Figure 4.24 Detection of Interference Using Power Measurements

$$P_D = \int_d^\infty P_{\hat{\theta}/H_1}(x)\, dx$$

$$= 1 - P_m \tag{4.413}$$

It is necessary to make a more precise definition of what is meant by "present" and "earlier" in reference to the different power measurements. For the "earlier" time measurements, we use the time record starting at sample instant t_1,

$$\hat{\nu}_E = \frac{1}{M} \sum_{p=1}^{M} \nu(t_p) \tag{4.414}$$

For the "present" measurement, we use a time record starting τ seconds later

$$\hat{\nu}_P = \frac{1}{M} \sum_{p=1}^{M} \nu(t_p + \tau) \tag{4.415}$$

At this point, the only restriction that we put on τ is that $\tau > t_M - t_1$. This is just to guarantee that we avoid the possibility of overlapping samples. Combining (4.414) and (4.415) the observation variable is just

$$\hat{\theta} = \frac{1}{M} \sum_{p=1}^{M} \left[\nu(t_p + \tau) - \nu(t_p)\right] \tag{4.416}$$

For a stationary channel, it is clear that the average value of the observation variable will be zero if H_0 is true and some non-zero constant if H_1 is true. For the more realistic nonstationary channel, the statistics of $\hat{\theta}$ will exhibit a dependence on τ that under certain circumstances may seriously weaken the effectiveness of interference detection. Averaging, we have

$$\bar{\hat{\theta}} = \frac{1}{M} \sum_{p=1}^{M} \left[\overline{\nu(t_p + \tau)} - \overline{\nu(t_p)}\right] \tag{4.417}$$

Denoting the deviation from the mean at any time instant, t, as D(t),

$$D(t) = \nu(t) - \overline{\nu(t)} \tag{4.418}$$

we have

$$\hat{\theta} - \bar{\hat{\theta}} = \frac{1}{M} \sum_{p=1}^{M} D(t_p + \tau) - D(t_p) \tag{4.419}$$

and, for the variance of this quantity,

$$\sigma^2_{\hat{\theta}} = \frac{1}{M^2} \sum_{p=1}^{M} \left[\overline{|D(t_p+\tau)|^2} + \overline{|D(t_p)|^2} \right] \tag{4.420}$$

Since the set of samples $\{\nu(t_p);\ p=1,M\}$ are all taken under an H_0 condition, we subscript their variance $\sigma_0^2(t_p)$ with a zero; i.e.,

$$\sigma_0^2(t_p) = \overline{|D(t_p)|^2} = \overline{|\nu(t_p) - \overline{\nu_0(t_p)}|^2} \tag{4.421}$$

The set of measurements taken τ seconds later is taken under either the H_0 or H_1 condition. Thus, the variance term

$$\sigma_j^2(t_p+\tau) = \overline{|D(t_p+\tau)|^2} = \overline{|\nu(t_p+\tau) - \overline{\nu(t_p+\tau)}|^2}$$

$$\begin{pmatrix} j = 0 & \text{under condition } H_0 \\ j = 1 & \text{under condition } H_1 \end{pmatrix} \tag{4.422}$$

is subscripted appropriately with 0 or 1. The same comments apply to the mean values $\nu(t)$, the subscript just indicating the condition under which the expectation is evaluated.

The observation variable statistics are summarized briefly below. Under the H_0 hypothesis, the mean and variance are given by

$$\bar{\hat{\theta}}_0 = \frac{1}{M} \sum_{p=1}^{M} \left[\overline{\nu_0(t_p+\tau)} - \overline{\nu_0(t_p)} \right] \tag{4.423}$$

and

$$\sigma^2_{\hat{\theta}/H_0} = \frac{1}{M^2} \sum_{p=1}^{M} \left[\sigma_0^2(t_p+\tau) + \sigma_0^2(t_p) \right] \tag{4.424}$$

respectively. Under the hypothesis H_1, we have

$$\bar{\hat{\theta}}_1 = \frac{1}{M} \sum_{p=1}^{M} \overline{\nu_1(t_p+\tau)} - \overline{\nu_0(t_p)} \tag{4.425}$$

$$\sigma^2_{\hat{\theta}/H_1} = \frac{1}{M^2} \sum_{p=1}^{M} \left[\sigma_1^2(t_p+\tau) + \sigma_0^2(t_p) \right] \tag{4.426}$$

All of the terms in the above sums can be calculated from the representation for $\nu(t)$ in (4.399). This problem is addressed in the next section.

4.4.3.3 Calculation of Measurement Statistics

In this section we calculate the means and variances listed in (4.423) - (4.426) above. We will use a specific predetection filter in the following analysis, whereas the integrate-and-dump filter has already been specified in (4.405). The impulse response of the predetection filter is given by

$$h(t) = \pi^2 W^2 t \, e^{-\pi W t} \, U(t) \tag{4.427}$$

and W is its 6 dB bandwidth, which can easily be proved by evaluating H(f), the Fourier transform of (4.427). We will find it helpful to use the following relations:

$$\int |H(f)|^2 \, df = \frac{\pi W}{4} \tag{4.428}$$

and

$$\int |H(f)|^4 \, df = \frac{5}{32} \pi W \tag{4.429}$$

Using the k(t) in (4.405), it is straightforward to calculate the value of (4.399). Under the entirely reasonable assumption that T(f,t) does not change significantly during an integration interval, we obtain the result

$$\nu(t) = |T(F,t)|^2 \frac{1}{T_0} \int_0^{T_0} |y(t-\xi)|^2 \, d\xi + \frac{1}{T_0} \int_0^{T_0} |J_2(t-\xi)|^2 \, d\xi$$

$$+ 2 \, \mathrm{Re}\left\{ T^*(F,t) \frac{1}{T_0} \int_0^{T_0} y^*(t-\xi) \, J_2(t-\xi) \, d\xi \right\} \qquad (4.430)$$

The ensemble average of this expression is given by

$$\bar{\nu}(t) = \overline{|y|^2} \; \overline{|T(F,t)|^2} + \overline{|J_2|^2} \qquad (4.431)$$

Turning now to the calculation of $\overline{|\nu|^2} - |\bar{\nu}|^2$, we obtain after some manipulation of (4.430) (and assumed independence of channel, data, and interference) the result

$$\overline{|\nu|^2} - |\bar{\nu}|^2 = \overline{|T(F,t)|^4} \left\{ \frac{1}{T_0^2} \int_0^{T_0} \int_0^{T_0} \overline{|y(t-\xi)|^2 |y(t-\eta)|^2} \, d\xi \, d\eta - \overline{|y^2|}^2 \right\}$$

$$+ \left\{ \frac{1}{T_0^2} \int_0^{T_0} \int_0^{T_0} \overline{|J_2(t-\xi)|^2 |J_2(t-\eta)|^2} \, d\xi \, d\eta - \overline{|J_2|^2} \right\}$$

$$+ \overline{|T(F,t)|^2} \frac{1}{T_0^2} \int_0^{T_0} \int_0^{T_0} \overline{y^*(t-\xi) y(t-\eta) \, J_2(t-\xi) J_2^*(t-\eta)} \, d\xi \, d\eta \qquad (4.432)$$

If we assume, as in Section 4.1, that y and J are both complex Gaussian random processes, then

$$\overline{|y_1|^2 |y_2|^2} = \overline{|y_1|^2} \; \overline{|y_2|^2} + |\overline{y_1^* y_2}|^2 \qquad (4.433)$$

where we have indicated the argument $t-\xi$ with a subscript 1 and the argument $t-\eta$ with a subscript 2, e.g., $\overline{y_1^* y_2} = R_y(\xi-\eta)$. Using (4.433) to evaluate (4.432), we obtain

$$\overline{|\nu|^2} - |\bar{\nu}|^2 = |T(F,t)|^4 \frac{1}{T_0^2} \int_0^{T_0}\int_0^{T_0} |R_y(\xi-\eta)|^2 \, d\xi \, d\eta$$

$$+ \frac{1}{T_0^2} \int_0^{T_0}\int_0^{T_0} |R_2(\xi-\eta)|^2 \, d\xi \, d\eta$$

$$+ |T(F,t)|^2 \frac{1}{T_0^2} \int_0^{T_0}\int_0^{T_0} R_y(\xi-\eta) R_2[-(\xi-\eta)] \, d\xi \, d\eta \qquad (4.434)$$

where $R_2(\tau)$ represents the correlation function of the total filtered interference, $J_2(t)$. The integrals in (4.434) can be evaluated with the aid of the double-to-single integral transformation

$$\frac{1}{T_0^2} \int_0^{T_0}\int_0^{T_0} f(\xi-\eta) \, d\xi \, d\eta \approx \frac{1}{T_0} \int_{-T_0}^{+T_0} f(\tau) \, d\tau \qquad (4.435)$$

which is an excellent approximation when T_0 is greater than the duration of $f(\tau)$. Since the data and interference decorrelate well within the T_0 band we apply (4.435) to (4.434) and, after using Parseval's relation, obtain

$$\overline{|\nu(t) - \bar{\nu}(t)|^2} = \overline{|T(F,t)|^4} \frac{1}{T_0} \int |P_y(f)|^2 \, df$$

$$+ \frac{1}{T_0} \int |P_2(f)|^2 \, df$$

$$+ \overline{|T(F,t)|^2} \frac{1}{T_0} \int P_y(f) P_2^*(f) \, df \qquad (4.436)$$

$P_y(f)$ represents the power spectrum of the filtered data and $P_2^y(f)$ the power spectrum of the filtered interference,

$$P_y(f) = |H(f)|^2 P_z(f - F)$$

$$\approx P_z(F)|H(f)|^2 \tag{4.437}$$

Thus, from (4.428)

$$\overline{|y|^2} = \frac{\pi W}{4} P_z(F) \tag{4.438}$$

The power spectrum, $P_2(f)$, in (4.436), is

$$P_2(f) = |H(f)|^2 P_1(f) \tag{4.439}$$

where $P_1(f)$ is the power spectrum of the interference input to the filter h(t). The terms in (4.436) can be given a simpler form by defining a filtered data power term P_D, a filtered interference term P_I, and a cross-power term P_X. These are

$$P_D = |P_z(F)|^2 \int |H(f)|^4 \, df$$

$$P_I = \int |H(f)|^4 \, |P_1(f)|^2 \, df$$

$$P_X = P_z(F) \int |H(f)|^4 P_1^*(f) \, df \tag{4.440}$$

Now, (4.436) takes on the simple form

$$\overline{|\nu(t) - \overline{\nu(t)}|^2} = \frac{1}{T_0} \overline{|T(F,t)|^4} P_D + \frac{1}{T_0} P_I + \frac{1}{T_0} \overline{|T(F,t)|^2} P_X \tag{4.441}$$

The data term, P_D, will remain unchanged under the different hypotheses, but P_I and P_X may change markedly. P_D retains the value

$$P_D = \frac{5}{32} \pi W |P_z(F)|^2 \tag{4.442}$$

From (4.401) the total interference $J_1(t)$ is the sum of $N(t)$, which is assumed to have a flat spectrum of constant power, $2N_0$, across the whole data band, and an interfering signal, $I(t)$, which changes under the different hypotheses. Under the zero hypothesis,

$$P_I^{(0)} = \frac{5}{8} N_0^2 \pi W$$

$$P_X^{(0)} = \frac{5}{16} N_0 \pi W P_z(F) \tag{4.443}$$

Assuming that $P_1(f)$ is flat across the bandwidth of $h(t)$, we obtain under hypothesis 1, the result

$$P_I^{(1)} = \frac{5}{32} |2N_0 + P_I(F)|^2 \pi W$$

$$P_X^{(1)} = \frac{5}{32} P_z(F) \left[2N_0 + P_I^*(F)\right] \pi W \tag{4.444}$$

If the strong interfering signal $I(t)$ can be characterized as wideband, of flat power spectrum $2N_1$, then under hypothesis 1 the power factors become

$$P_I^{(1)} = \frac{5}{8} N_0^2 \pi W + \frac{5}{8} N_1^2 \pi W + \frac{5}{4} N_0 N_1 \pi W$$

$$P_X^{(1)} = \frac{5}{16} N_0 P_z(F) \pi W + \frac{5}{16} N_1 P_z(F) \pi W \tag{4.445}$$

which we use subsequently in our calculations.

These factors can now be inserted, under the appropriate hypotheses, into (4.441). Using (4.441) and (4.431), we can now calculate each of the terms appearing in the sums of (4.423) - (4.426). To do this, we make use of some simple relations involving the random variable

$$\gamma = |T(F,t)|^2 \tag{4.446}$$

Because the channel is Rayleigh fading, γ has an exponential pdf

$$p_\gamma(x) = \frac{1}{\bar{\gamma}} e^{-\frac{\chi}{\bar{\gamma}}} \tag{4.447}$$

Thus, if we use q(t) to denote the time-varying mean of $|T(F,t)|^2$ we have

$$\overline{|T(F,t)|^2} = q(t) \tag{4.448}$$

and

$$\overline{|T(F,t)|^4} = 2q^2(t) \tag{4.449}$$

This is the notation that will be used below.

For the observation variable statistics in (4.423) - (4.426), we now obtain the results

$$\bar{\hat{\theta}}_0 = \frac{\pi W}{4M} P_z(F) \sum_{p=1}^{M} \left[q(t_p+\tau) - q(t_p)\right] \tag{4.450}$$

$$\bar{\hat{\theta}}_1 = \bar{\hat{\theta}}_0 + \left(\frac{\pi W}{4}\right) 2N_1 \tag{4.451}$$

$$\sigma^2_{\hat{\theta}/H_0} = \frac{1}{M^2 T_0} \left(\frac{5}{16}\pi W\right) S_M(\tau) + \frac{1}{MT_0} \frac{10}{8} N_0^2 \pi W \tag{4.452}$$

$$\begin{aligned}\sigma^2_{\hat{\theta}/H_1} &= \frac{1}{M^2 T_0} \left(\frac{5}{16}\pi W\right) S_M(\tau) \\ &\quad + \frac{1}{M^2 T_0} \left(\frac{5}{16}\pi W\right) \sum_{p=1}^{M} q(t_p+\tau) P_z(F) N_1 \\ &\quad + \frac{1}{MT_0} \left(\frac{5}{16}\pi W\right) \left[2N_0^2 + 2(N_0+N_1)^2\right]\end{aligned} \tag{4.453}$$

where

$$S_M(\tau) \triangleq |P_z(F)|^2 \sum_{p=1}^{M} \left[q^2(t_p+\tau) + q^2(t_p)\right]$$

$$+ N_0 P_z(F) \sum_{p=1}^{M} \left[q(t_p+\tau) + q(t_p)\right] \qquad (4.454)$$

4.4.3.4 Detection Effectiveness

A detector built to determine the presence of interference according to the decision rule in (4.410) would exhibit the usual dependence on the estimate mean values and variances. Note from (4.450) and (4.451) that the mean values of the observation variables differ by an amount depending on the interference to be detected, i.e.,

$$\bar{\hat{\theta}}_1 - \bar{\hat{\theta}}_0 = \left(\frac{\pi W}{4}\right) 2N_1 \qquad (4.455)$$

Obviously, the ability to resolve between interference and no-interference conditions depends significantly on the interference power $2N_1$ and on the variances in (4.452) and (4.453) which, in turn, depend most importantly on M, the number of independent samples taken.

We now turn to considerations of channel nonstationarity. As a simple model of the nonstationarity, we use a Taylor expansion for q(t), and neglect terms of higher than second order, i.e.,

$$q(t_p+\tau) = q(t_p) + \tau q'(t_p) \qquad (4.456)$$

For $q^2(t)$, we have

$$q^2(t_p+\tau) = q^2(t_p) + 2q(t_p)\, q'(t_p)\, \tau \qquad (4.457)$$

One of the most important effects of the channel nonstationarity is that it may render detection procedures nonoptimal. A threshold chosen to give optimum detector operation at one time may be decidedly suboptimal at a slightly later time. Since the threshold is set by placing a constraint on P_F in (4.411), the

effect of nonstationarity on the optimality of the detection procedures can be determined by considering only changes in the mean and variance conditional on the noninterference event, H_0.

The most impc : ant change of this type is in the mean value of the observation variable. By substituting (4.456) and (4.457) into (4.450), we find that the nonstationary change in $\bar{\hat{\theta}}_0$ is given by

$$\Delta\left(\bar{\hat{\theta}}_0\right) = \frac{\pi W}{4M} P_z(F) \sum_{p=1}^{M} \tau\, q'(t_p) \tag{4.458}$$

Assuming local stationarity, $q'(t_p)$ is a constant, and we have the result

$$\Delta\left(\bar{\hat{\theta}}_{0/}\right) = \frac{\pi W}{4} P_z(F)\, \tau\, q' \tag{4.459}$$

The channel nonstationarity will have a pronounced effect if this change in the mean value of the observation variable is a sizable fraction A of the separation of the two mean values given in (4.455). Defining

$$\delta_T \triangleq \tau\, q' \Big/ \sqrt{|T|^2} \tag{4.460}$$

this event occurs when

$$\delta_T = A\,\Psi \tag{4.461}$$

where Ψ is the interference-to-signal ratio

$$\Psi \triangleq \frac{2N_1}{|T|^2\, P_z(F)} \tag{4.462}$$

Nonstationary channel changes are often characterized in terms of a change in the "transmission loss" of the channel [4.22]. This value (in dB) and the value of δ_T (not in dB) are related through

$$L = 10 \log_{10}(1 + \delta_T) \tag{4.463}$$

where the change is that observed over some standard interval (20 minutes in the case of the tropo channel). A reasonable choice for A in (4.461) is $A = 1/2$. The implication of (4.461), then, is that nonstationary channel changes will have a pronounced effect when the interval between observations is great enough so that the change in transmission loss becomes as large as

$$L' = 10 \log_{10}(1 + \Psi/2) \tag{4.464}$$

For a nonstationary channel changing + 2 dB over the standard 20-minute period, a change as large as that specified in (4.464) would take place in approximately 1000 seconds for $\Psi = 0$ dB and 250 seconds for $\Psi = -6$ dB. These numbers follow directly from (4.464), (4.463), and (4.456).

Because of the large measurement times required to obtain accurate estimates of channel parameters, a case of practical interest here occurs when the "present" power measurement is taken immediately after the "earlier" one with no intervening time at all. For this situation, there is essentially zero probability that the change to the interference condition will take place exactly between the intervals. For the numerical example calculated here, this is remedied by considering a "worst-case" situation; the interference goes on halfway into the second observation interval. It can be shown, by retracing the steps leading to (4.450) - (4.453), that the only significant modification introduced by this change in the problem affects (4.451); the contribution of the noise term is reduced by a factor 1/2.

The approach to the numerical problem is greatly facilitated by neglecting the receiver noise N_0 and normalizing the observation variable to

$$\left(\frac{\pi W}{4}\right) \overline{|T(F,t)|^2} \, P_z(F) \tag{4.465}$$

We now have

$$\bar{\hat{\theta}}_0 = \delta \tag{4.466}$$

$$\bar{\hat{\theta}}_1 = \delta + \frac{\Psi}{2} \tag{4.467}$$

$$\sigma^2_{\hat{\theta}/H_0} = \frac{(1+\delta_T)^2}{BT} \tag{4.468}$$

$$\sigma^2_{\hat{\theta}/H_1} = \frac{1}{BT}\left(\frac{1}{1+\Psi}\right)\left[(1+\delta_T)^2 + \Psi^2 + 2\Psi(1+\delta_T)\right] \tag{4.469}$$

where δ_T and Ψ were defined in (4.460) and (4.462), respectively, and M, the number of independent samples in a given observation interval of length T, has been replaced by BT, where B is the Doppler spread (1 Hz for tropo channel).

Some information regarding nonstationary changes in the channel is available from Bello et al. [4.22, Fig. 3-27]. The curves there indicate that 3% to 96% cumulative distribution of the transmission loss change is contained roughly in the - 3 dB to + 3 dB range and 1% to 99% in the $\pm$ 4 dB range (for the 20-minute period). As a typical large value for the curves that follow, we have used the values $\pm$ 2 dB/20 minutes.

Numerical results are indicated in Figures 4.25 and 4.26 where it has been assumed that the decision statistic is Gaussian (valid for large M). The curves marked "0" indicate the performance that would be obtained in the absence of any channel nonstationarities. For this case, the symmetry in the P_F and P_D curves exists because the initial threshold was chosen so that the (P_F, P_D) pair fell along the line $P_D = 1 - P_F$ of the receiver operating characteristic. With the threshold so set, the other curves indicate how the detectability is affected by linear nonstationary changes with transmission slopes $\pm$ 2 dB/20 minutes. We see, in the case of + 2 dB/20 min and $\Psi = 0$ dB, that the detection probability rises slightly more rapidly than in the stationary case, but that P_F falls more slowly until finally it begins to rise with increasing observation time. By 1000 seconds, the nonstationarity has taken over fully. This is in agreement with our earlier estimate made in connection with (4.464). We note, however, that there is an "optimum" point on the P_F curve where it bottoms out. This point is at an observation time of 200 seconds and corresponds to $P_F = 0.0666$ and $P_D = 0.9985$ whereas the curves for - 2 dB have the values $P_F = 0.0065$ and $P_D = 0.96$ at the same point.

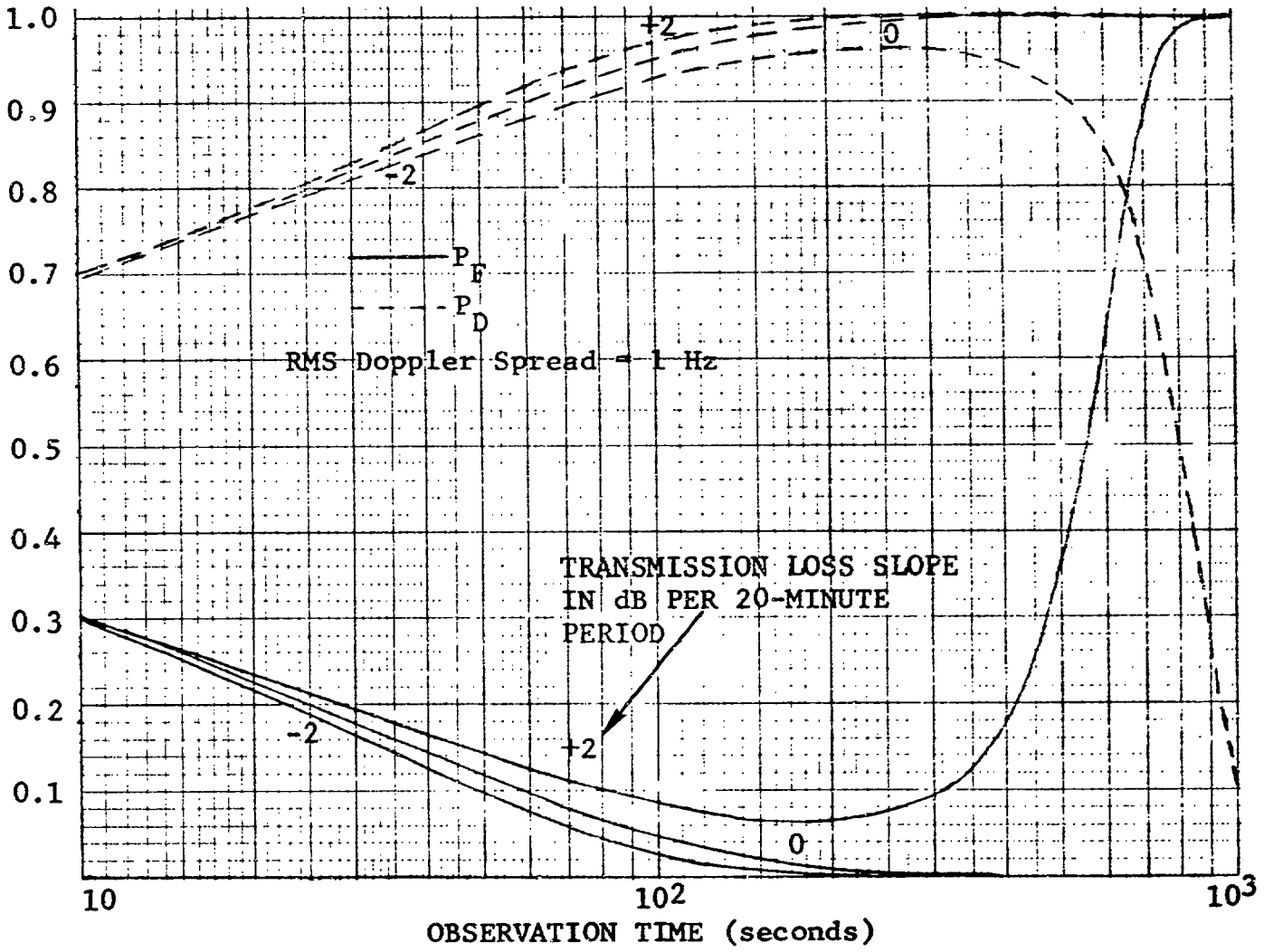

Figure 4.25 Plots of Interference Detectability for Nonstationary Changes on Tropo Channel. Inteference Power = Signal Power

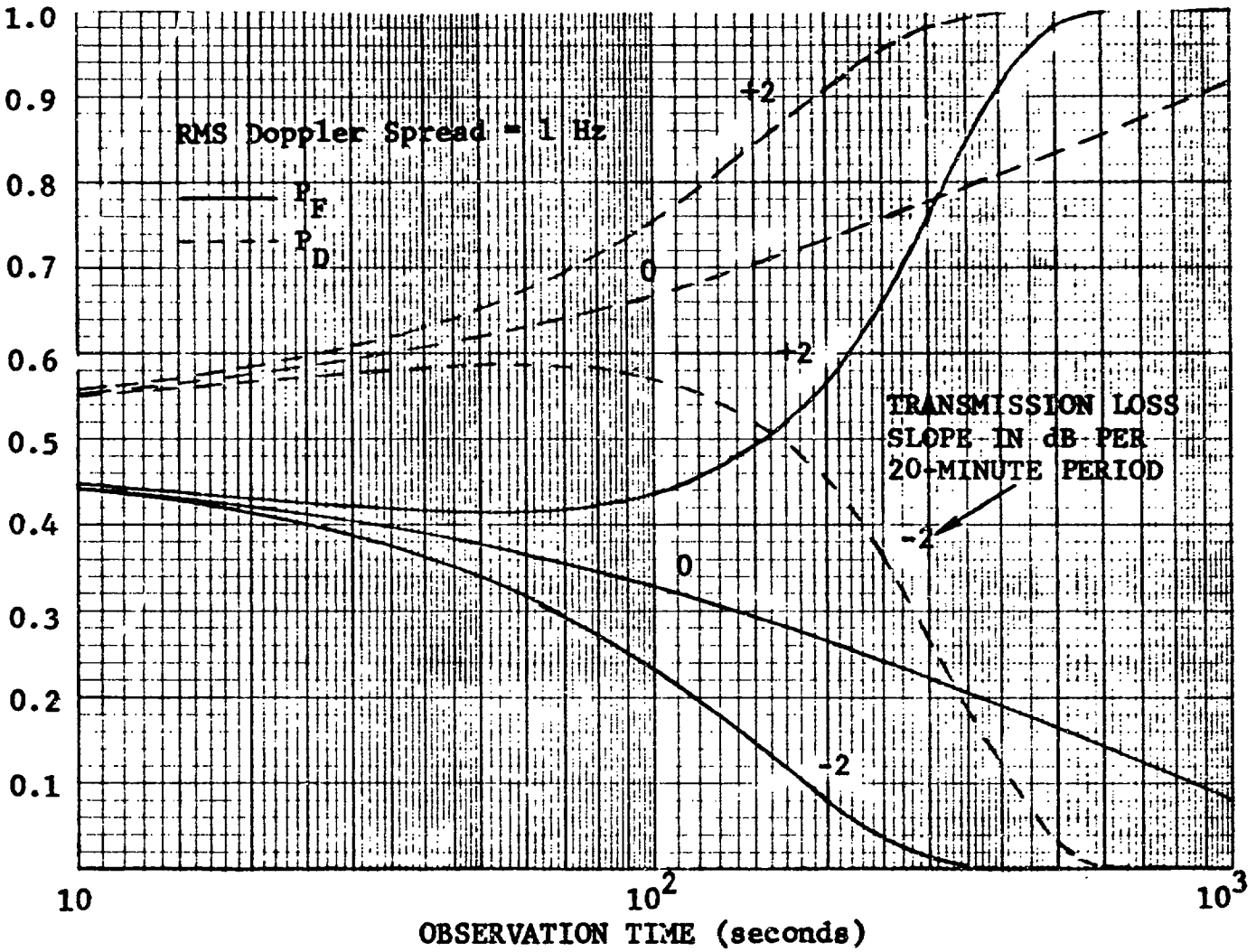

Figure 4.26 Plots of Interference Detectability in the Presence of Nonstationary Changes on Tropo Channel. Interference Power is 6 dB Down from Signal Power

Detector performance decreases markedly when the interference is weak with respect to the signal. This is evident in the curves of Figure 4.26 where now $\Psi = -6$ dB. We note that the nonstationarity has developed completely by 250 seconds, in agreement with our earlier rough estimate based on (4.464). This performance is unacceptable since the +2 dB/20-minute change P_F never goes below 0.4.

The performance improves when the fading is faster. This is clear from an examination of the curves in Figure 4.25. We note first that the performance curve corresponding to a transmission slope of 0 dB/20 minutes can be viewed as a general curve for a channel with arbitrary Doppler spread if one just replaces the abscissa T with BT.* This modification cannot be made for the curves including the nonstationarities because these occur in absolute time, i.e., vs. T as opposed to BT. It is easy to see that better performance can be expected at B = 10 Hz. This is borne out by the curve of Figure 4.27 which shows a plot of P_F vs. processing time. It is clear that the "optimum" time takes place at T = 200 seconds as before; this time, however, the probability of false alarm has decreased to 0.109×10^{-5} whereas the probability of detection is essentially unity near the optimum point (to within five decimal places).

The above results indicate that there are important situations where nonstationary channel changes can disrupt fixed threshold schemes to detect a weak interfering signal but that performance in the presence of nonstationarities improves as Ψ or B increases. We point out, however, that the channel nonstationarity, discussed herein, does not in itself place <u>fundamental</u> limits on the performance of the interference detectors. Improved detectors, using measurements of the gradual changes in the channel gain, could, by using adaptive procedures, appropriately change the threshold against which θ is compared, and hence provide detector performance much closer to the optimal. In fact, such a scheme would allow the accumulation of measurements under what is <u>known</u> to be a noninterference conditions, against which all future measurements could be compared.

*We recall that a value of 1 Hz (tropo channel) was used for Figure 4.25.

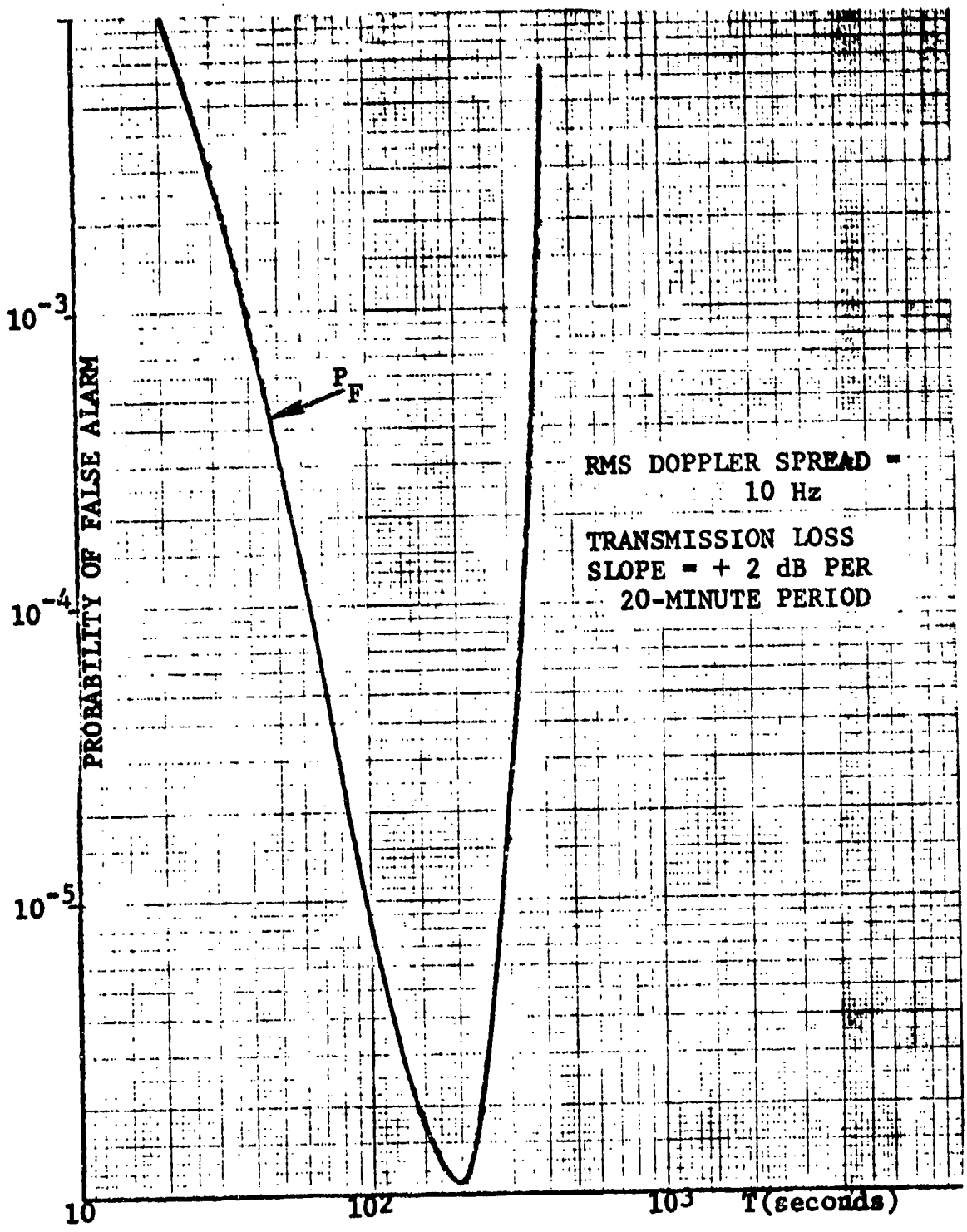

Figure 4.27 Probability of False Alarm vs. Observation Time for Nonstationary Changes in Power Level with Doppler Spread = 10 Hz and Interference Power Equal to Signal Power

4.5 Interference Measurement in the Absence of Signal

4.5.1 Introduction

In this section we analyze techniques for interference measurement when idle frequency or time slots are available. By the latter it is meant that the transmitted data signals have frequency slots or time slots that are idle in the sense that they carry no data power. One useful variant of the time slot idea is the "temporary-service-interrupt". This can provide a rapid means of determining, in the presence of communication impairment, whether or not additive interference is the main contributor to the degradation. It also provides the means of developing estimates for error rate bounds, even in the presence of interference for which there is available only a bare minimum of statistical information. This latter topic is discussed at some length in Section 5.7.

In Section 4.5.2 we detail the analytical forms for the interference in different communication systems. We conclude that the decision rule (probability of error calculation) can be put into a general framework that depends only on two generalized interference variables, U and V. The advantages that accrue from this general type of formulation are important. This is clear when one considers the variety of interference models, e.g., white noise, "colored" Gaussian noise, lognormally distributed atmospheric interference, impulsive noise, and the even greater variety of interference for which there are no models, e.g., jamming and various combinations of the naturally-occurring interferences. An error rate estimate based on any one model would be totally unreliable in the presence of another type of interference and it is safe to say that the sudden presence of a new strong interfering signal at the receiver, which the receiver was not designed to handle, will by definition be unpredictable and not amenable to simple modeling. It is to include just such unpredictable situations that we have used the general approach taken here.

In Sections 4.5.3 and 4.5.4 we discuss some possible structures for signals to be used in the measurement of interference; these methods involve, respectively, the use of idle frequency slots in the data and the use of idle time slots, even to the point of a "service interrupt".

Because of special difficulties which arise when the interference has a pulse-like character, pulse interference is given a separate treatment in Section 4.5.5.

The results and their implications are summarized in Section 4.5.6.

4.5.2 Generalized Interference Variables

In this section we define and develop explicit expressions for the interference variables. We concentrate on the receiver configurations illustrated in Figure 4.28. We note that only the in-phase modulation component of the PSK system is shown; there will also be a demodulator for the quadrature component when the system is running quaternary.

Assuming that conditions are statistically stationary and that a received signaling element occupies the time interval $0 < t < T$, it can be shown that the sampled outputs of each of the systems can be represented as a quadratic form of the type

$$q_L = \sum_{p=1}^{L} |G_p + \xi_p|^2 - \sum_{p=1}^{L} |\eta_p|^2 \qquad (4.470)$$

where L is the order of diversity, G_p is a complex signal term due to the p^{th} diversity receiver, and ξ_p, η_p are complex interference terms due to the p^{th} diversity receiver.

We first discuss the FSK system. We note that square law envelope detection is employed in this system. The diversity combiners simply add corresponding components of the various diversity receivers. After sampling the diversity combined output, the result is compared to a zero threshold. When there is no distortion, the complex envelope of the received signal is given by

$$s(t) = \sum_{q=-\infty}^{q=+\infty} Q(t - qT) \exp\left[j2\pi\left(\frac{\alpha_q}{2T}\right) t\right] \qquad (4.471)$$

mark: $\alpha_q = +1$

space: $\alpha_q = -1$

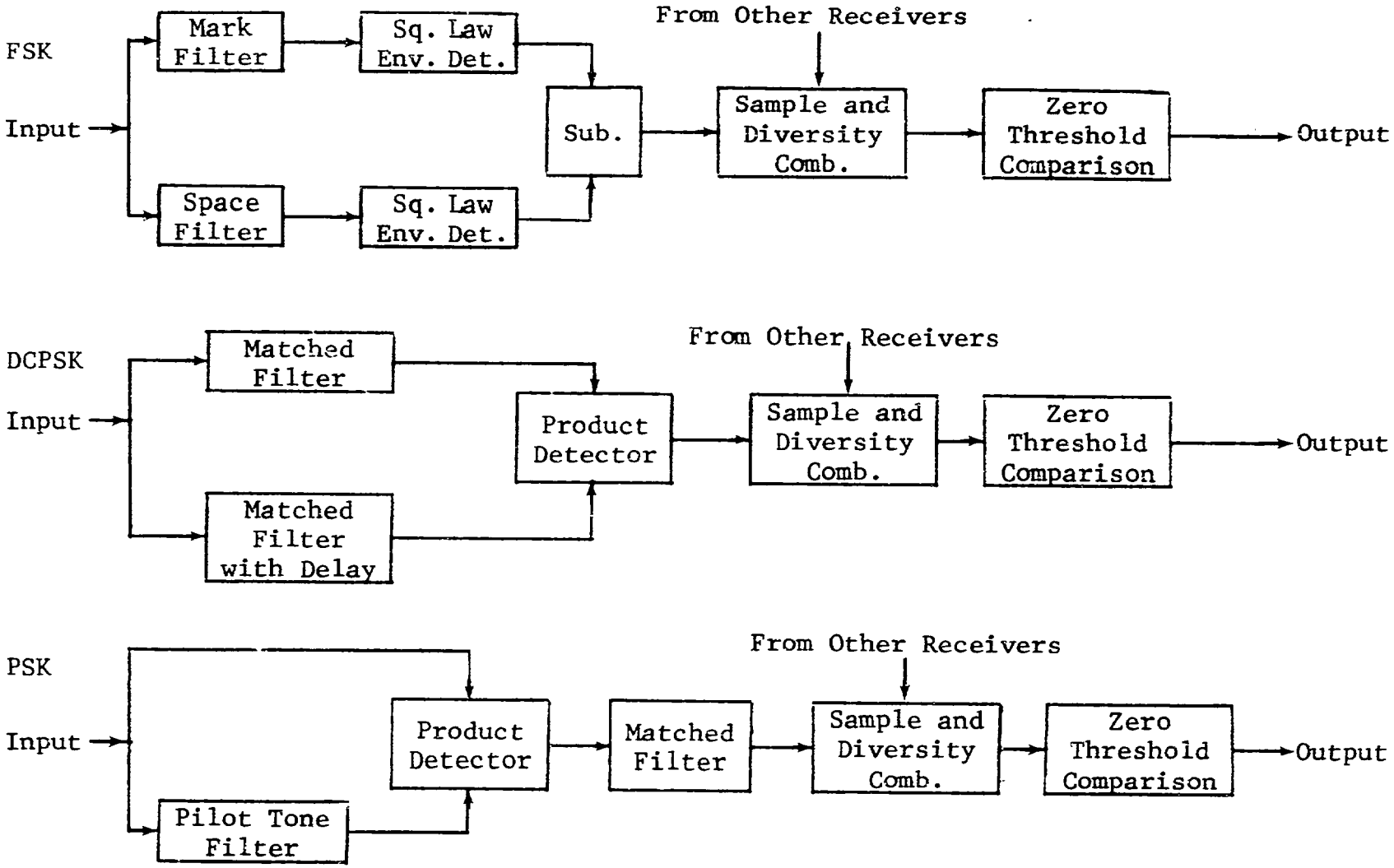

Figure 4.28 Simplified Block Diagram of FSK, DCPSK, and Coherent PSK Receivers

and Q(t) is a rectangular pulse of duration T

$$Q(t) = \begin{cases} 1 ; & 0 < t < T \\ 0 ; & t \le 0,\ t \ge T \end{cases} \tag{4.472}$$

and $\frac{1}{T}$ is the mark-space separation frequency.

The complex envelope of the received waveform for a particular diversity channel, including frequency flat fading and additive interference, is given by

$$y(t) = g(t)s(t) + n(t) \tag{4.473}$$

where n(t) is the complex envelope representation of the additive interference and g(t) is a complex valued Gaussian process characterizing the fading.

Since the mark and space filters are assumed to be matched filters, the sampled output of the receiver is given by

$$q = \left| \int_0^T y(t)\, e^{-j\pi t/T}\, dt \right|^2 - \left| \int_0^T y(t)\, e^{+j\pi t/T}\, dt \right|^2 \tag{4.474}$$

This is evaluated simply by substituting from (4.473) and (4.471). Symmetry arguments dictate that we need only consider the evaluation of error probability for the case in which a mark has been received in the interval $0 < t < T$. In this case, q is given by

$$q = \left| \int_0^T g(t)dt + \int_0^T g(t)e^{j2\pi t/T}\, dt + \int_0^T n(t)e^{-j\pi t/T} \right|^2 - \left| \int_0^T e^{j\pi t/T}\, n(t)\, dt \right|^2 \tag{4.475}$$

and the slow fading approximation allows us to write

$$G = \int_0^T g(t)\, dt \approx g(0)\, T \tag{4.476}$$

and

$$\int_0^T g(t)\, e^{j2\pi t/T}\, dt \approx 0 \tag{4.477}$$

Defining

$$\eta = \int_0^T e^{j\pi t/T}\, n(t)\, dt$$

and

$$\xi = \int_0^T e^{-j\pi t/T}\, n(t)\, dt \tag{4.478}$$

we see that q has the form

$$q = |G+\xi|^2 - |\eta|^2 \tag{4.479}$$

which upon summing for all diversity channels gives the result in (4.470).

We now turn to the last system illustrated in Figure 4.28, the coherent PSK receiver. A transmitted pilot tone provides the phase reference, and neglecting noise on the received pilot tone, it can be assumed that the complex envelope of the tone is proportional to g(t) and that the proportionality constant is T.* Thus, the sampled output of the in-phase channel, in terms of complex envelopes, is given by

$$q = \mathrm{Re}\left\{\sqrt{2} \int_0^T T\, g^*(t)\, y(t)\, dt\right\} \tag{4.480}$$

where y(t) is given in (4.473). The received signal without distortion (unity gain channel and no additive noise) is given by

$$s(t) = \sum_{-\infty}^{+\infty} Q(t - qT)\, \alpha_q \tag{4.481}$$

*This results in no loss of generality in terms of final results.

where

$$\alpha_q = \pm \frac{1}{\sqrt{2}} \pm j \frac{1}{\sqrt{2}} \tag{4.482}$$

for the quaternary case, and

$$\alpha_q = \pm 1 \tag{4.483}$$

for the binary case.

It is a simple matter to show for quaternary PSK that q can be expressed in the form of (4.479) with

$$\xi = \frac{\theta}{\sqrt{2}} \qquad \eta = j \frac{\theta}{\sqrt{2}} \tag{4.484}$$

where θ is given by

$$\theta = \int_0^T n(t)\, dt \tag{4.485}$$

whereas for the binary coherent PSK case, the variables are given by

$$\xi = \frac{\theta}{2} = \eta \tag{4.486}$$

Determining the interference variables when a differentially coherent PSK system is used is considerably more complex and the reader is referred elsewhere [4.23].

For later use, though, we have included these results in Table 4-3, which is a summary of the generalized noise variables for all the modulation formats that were earlier pictured in Figure 4.28.

The remainder of this section is related to our contention that the primary statistical quantity of interest in Table 4-3 is θ. The statistics of the other quantities can all be related to the behavior of θ. This is not very important from a measurement viewpoint since the other noise variables in Table 4-3 can be measured as easily as θ, but it is important in the sense that it considerably simplifies some of the work that follows; it puts

TABLE 4-3

GENERALIZED INTERFERENCE VARIABLES

Modulation Scheme	Generalized Interference Variable		Comment
	ξ	η	
Binary FSK	$\int_0^T e^{-j\pi t/T} n(t)\, dt$	$\int_0^T e^{+j\pi t/T} n(t)\, dt$	—
Quaternary DCPSK	$\frac{\alpha_0^* \gamma + \alpha_{-1}^* \theta}{\sqrt{2}}$	$\frac{\alpha_0^* \gamma + j\alpha_{-1}^* \theta}{\sqrt{2}}$	$\alpha_{-1}^* \alpha_0 = \frac{1}{\sqrt{2}} + j\frac{1}{\sqrt{2}}$ $\lvert\alpha_j\rvert^2 = 1$
Binary DCPSK	$\frac{\alpha_0^* \gamma + \alpha_{-1}^* \theta}{2}$	$\frac{\alpha_0^* \gamma - \alpha_{-1}^* \theta}{2}$	$\alpha_{-1}^* \alpha_0 = +1$ $\lvert\alpha_j\rvert^2 = 1$
Quaternary Coherent PSK	$\frac{\theta}{\sqrt{2}}$	$j\frac{\theta}{\sqrt{2}}$	—
Binary Coherent PSK	$\frac{\theta}{2}$	$\frac{\theta}{2}$	—

Definitions: $\theta = \int_0^T n(t)\, dt$, $\gamma = \int_{-T}^0 n(t)\, dt$

us in the position of not having to evaluate measurement errors for all of the noise variables in Table 4-3.

First, we note that the mean values of all the entries for ξ and η are directly proportional to $\overline{\theta}$. Now, turning to the second-order statistics, we note first, in order to simplify things, that

$$\overline{|\theta|^2} = \int_0^T \int_0^T R_n(t-s)\,dt\,ds \tag{4.487}$$

where we have defined the correlation function

$$R_n(t-s) = \overline{n^*(t)\,n(s)} \tag{4.488}$$

which assumes stationarity of n(t). Integrating out the dependence on one variable, we obtain

$$\overline{|\theta|^2} = T \int_{-T}^{+T} R_n(\tau)\,d\tau \tag{4.489}$$

For both the quaternary and binary coherent PSK systems, the relationship between $\overline{|\xi|^2}$, $\overline{|\eta|^2}$, and $\overline{|\theta|^2}$ is immediately apparent from examination of Table 4-3; for the quaternary we have

$$\overline{|\xi|^2} = \overline{|\eta|^2} = \overline{|\theta|^2}/2 \tag{4.490}$$

whereas for the binary we have

$$\overline{|\xi|^2} = \overline{|\eta|^2} = \overline{|\theta|^2}/4 \tag{4.491}$$

For the other modulation schemes there are similar relations; e.g., for the binary FSK we can proceed in exactly the same way as above and obtain

$$\overline{|\xi|^2} = T \int_{-T}^{+T} \left(1 - \frac{|\tau|}{T}\right) R_n(\tau)\, e^{j\frac{\pi}{T}\tau}\,d\tau \tag{4.492}$$

For interference that decorrelates rapidly within the T-interval we have the approximation

$$\overline{|\xi|^2} \approx T \int_{-T}^{+T} R_n(\tau)\, d\tau$$

$$= \overline{|\theta|^2} \qquad (4.493)$$

Turning to the DCPSK modulation schemes, we examine the binary case; it is easy to show that

$$\overline{|\xi|^2} = \frac{\overline{|\gamma|^2} + \overline{|\theta|^2} + 2\mathrm{Re}\{\overline{\theta\gamma^*}\}}{4} \qquad (4.494)$$

We note that $\overline{|\gamma|^2} = \overline{|\theta|^2}$ and that use of the same representations that led to (4.487) and (4.492) here gives

$$\overline{\theta\gamma^*} = T \int_{-T}^{+T} \left(1 - \frac{|\tau|}{T}\right) R_n(\tau + T)\, d\tau \qquad (4.495)$$

Now, if n(t) decorrelates well within a T interval, the main contributions to the integral in (4.495) arise from τ values near $-T$, and $\overline{\theta\gamma^*}$ is very small. We obtain

$$\overline{|\xi|^2} \approx \overline{|\theta|^2}/2 \qquad (4.496)$$

Finally, we are able to summarize for the binary alphabet:

$$\overline{|\xi|^2} \approx \overline{|\theta|^2}/4 \qquad \text{(coherent PSK)}$$

$$\overline{|\xi|^2} \approx \overline{|\theta|^2} \qquad \text{(FSK)}$$

$$\overline{|\xi|^2} \approx \overline{|\theta|^2}/2 \qquad \text{(DCPSK)} \qquad (4.497)$$

Examination of Table 4-3 indicates that similar results will be obtained for the quaternary case.

The fact that $\bar{\xi}$ is directly proportional to $\bar{\theta}$ for each of the modulation schemes and the mean square values of ξ and θ are related through (4.497) indicates strongly that θ alone provides a complete characterization of interference. This is especially important in the present context because it justifies the assumption that reliable estimates of θ imply reliable estimates of ξ (and η) for each of the modulation formats.

Without any further justification, future sections relating to interference measurement will focus on determining the reliability with which θ can be estimated, and the uses to which the interference measurements can be put.

4.5.3 Use of Idle Frequency Slots: Power Estimate

In conjunction with measurements of the channel transfer function, the direct measurement of interference power can be used to provide SNR estimates on each branch of a diversity receiver. The interference estimator configuration on a single branch is shown in Figure 4.29. Note that there are effectively no data inputs to the noise monitor. This is because the filters are centered on frequencies for which there is no enegy in the data; this comes about either because of the intentional introduction of "idle" slots into the data, or because the interference is monitored outside the information band. It is assumed that the interference monitored in this way is wideband; i.e., the power level in an idle band indicates closely its power level across the data band.

As Figure 4.29 indicates, the noise monitor analysis is considerably simpler than the channel estimator analysis documented in Section 4.1. The analysis here is an obvious outgrowth of the earlier one. In fact, the resulting percentage estimation errors are almost identical. The present section, aside from establishing a formalism for the interference measurement problem, points out the different sets of assumptions under which the result holds (considerably less restrictive here) and the different character of the estimate (unbiased here).

By first utilizing the equivalent system pictured in Figure 4.29 for purposes of analysis, we note that the output of the system is given by

$$\nu(t) = |\eta(t)\, e^{-j2\pi F_m t} \otimes h(t)|^2 \circledast k(t) \qquad (4.498)$$

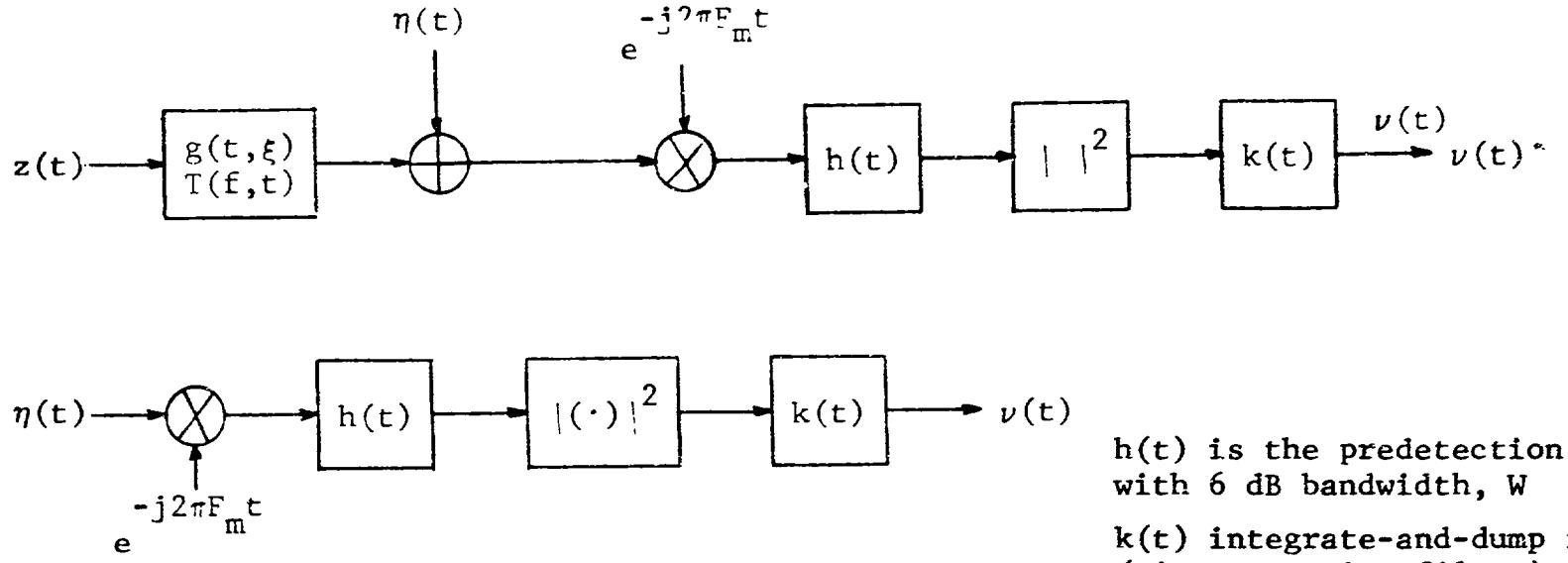

h(t) is the predetection filter with 6 dB bandwidth, W

k(t) integrate-and-dump filter (time-averaging filter)

(a) Equivalent Systems for Analyzing Interference Estimator

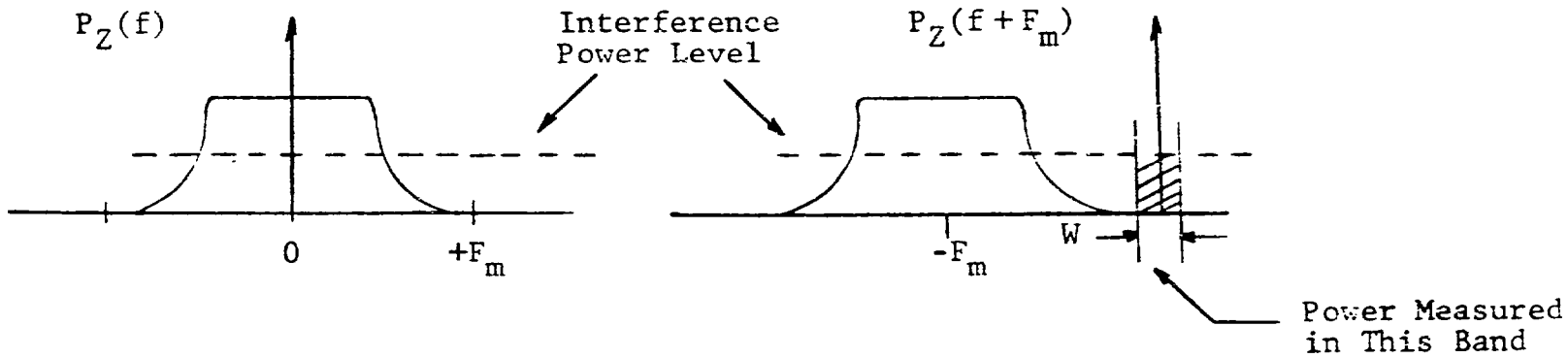

(b) Illustration of Spectral Relationships (Out-of-Band Monitoring)

Figure 4.29 Interference Monitoring

It is useful to define a filtered noise variable, n(t),

$$n(t) = \eta(t)\, e^{-j2\pi F_m t} \circledast h(t) \tag{4.499}$$

so that now

$$\nu(t) = |n(t)|^2 \circledast k(t) \tag{4.500}$$

The mean of our estimate is given by

$$\bar{\nu}(t) = \overline{|n|^2}\, K(0) \tag{4.501}$$

where K(f) is the Fourier transform of k(t). Hence, the output of the interference monitor in Figure 4.29(a) gives an unbiased estimate of the interference power.

In order to determine estimate error variance, we now evaluate

$$\begin{aligned} |\nu(t)|^2 &= \overline{\left| \int |n(t-\xi)|^2 k(\xi)\, d\xi \right|^2} \\ &= \iint \overline{|n(t-\xi)|^2 |n(t-\eta)|^2}\, k(\xi)\, k(\eta)\, d\xi\, d\eta \end{aligned} \tag{4.502}$$

which, by utilizing the fourth-moment formula for Gaussian random variables used in (4.33), we find to have the value

$$\overline{|\nu(t)|^2} = \int |R_n(\tau)|^2 R_k(\tau)\, d\tau + \overline{|n^2|}^2 K^2(0) \tag{4.503}$$

where $R_k(\tau)$ was defined earlier in (4.32). Combining (4.503) and (4.32) we have

$$\begin{aligned} \overline{|\nu(t)|^2} - |\bar{\nu}|^2 &= \int |R_n(\tau)|^2 R_k(\tau)\, d\tau \\ &\approx R_k(0) \int |R_n(\tau)|^2\, d\tau \end{aligned} \tag{4.504}$$

The last assumption follows because of the wideband nature of n(t), i.e., the time constant of k(t) is assumed to be much larger than that of h(t).

It remains to evaluate the correlation function for n(t), and its integral as presented in (4.504).

From (4.499) we note that the power spectrum of the output of the filter h(t) in Figure 4.29 is given by

$$P_n(f) = |H(f)|^2 P_\eta(f + F_m)$$

$$\approx P_\eta(F_m) |H(f)|^2 \tag{4.505}$$

This last approximation arises because the interference will have a flat spectrum across the narrow passband of any reasonably designed filter [see Figure 4.29(b)]. Thus, from Parseval's relation

$$\int |R_n(\tau)|^2 \, d\tau = \int |P_n(f)|^2 \, df$$

$$= |P_\eta(F_m)|^2 \int |H(f)|^4 \, df \tag{4.506}$$

an expression which can be easily evaluated for specific implemented filters.

We now assume specific transfer functions for the filters illustrated in Figure 4.29 so that we can calculate (4.506). The predetection filter is lowpass with impulse response given by

$$h(t) = \pi^2 W^2 t \, e^{-\pi W t} \, u(t) \tag{4.507}$$

where u(t) is the unit step function. For this expression it can be shown, by Fourier transforming, that W is the 6 dB bandwidth of the filter. The output filter is an integrate-and-dump filter (time-averager) with impulse response

$$k(t) = \begin{cases} \frac{1}{T} & 0 \le t \le T \\ 0 & \text{otherwise} \end{cases} \tag{4.508}$$

We can now evaluate the integral in (4.506). We have, using Parseval's relation,

$$\int |H(f)|^4 \, df = \int |h_2(\tau)|^2 \, d\tau \tag{4.509}$$

where

$$h_2(t) = h(t) \otimes h(t)$$

$$= \frac{\pi^4 w^\pi}{6} t^3 e^{-\pi w t} u(t) \tag{4.510}$$

which can be obtained by direct calculation. Substituting in (4.509) we now have the result

$$\int |H(f)|^4 \, df = \frac{5}{32} \pi w \tag{4.511}$$

A more direct application of Parseval's relation leads to another needed result

$$\int |H(f)|^2 \, df = \frac{\pi w}{4} \tag{4.512}$$

Finally, we note from (4.508) that K(0) is just unity. The specific filter impulse responses and various filter parameters which enter into the power calculations can now be applied to the estimator in Figure 4.29 in order to determine estimate error statistics.

We first note that $\overline{|n|^2}$ in (4.501) is just the integral of the power spectrum $P_n(f)$ in (4.505). By using (4.512), we find

$$\overline{|n|^2} = \frac{\pi w}{4} P_\eta(F_m) \tag{4.513}$$

Because K(0) = 1, this is just the mean of the estimate

$$\bar{\nu} = \frac{\pi w}{4} P_\eta(F_m) \tag{4.514}$$

The variance can be calculated by combining (4.504), (4.505),

(4.506), and (4.511) and also utilizing the fact from (4.32) and (4.508) that $R_k(0) = 1/T$. The result is

$$|\nu(t) - \bar{\nu}|^2 = \frac{5}{32} \frac{\pi w P^2(F_m)}{T} \tag{4.515}$$

Thus, defining a normalized error

$$\epsilon = \frac{\nu(t) - \bar{\nu}}{\bar{\nu}} \tag{4.516}$$

we have for its variance, the rms fractional error

$$\sigma_\epsilon = \sqrt{|\epsilon|^2}$$

$$= \sqrt{\frac{5}{2\pi}} \quad \frac{1}{\sqrt{WT}} \tag{4.517}$$

One immediate conclusion about the above analysis is that there are no assumptions about the nature of channel fading ... simply by virtue of the fact that the interference measurements are made in frequency intervals for which there is no data power. Thus, there is considerable flexibility in the adjustment of the filter parameters W and T. The integration time must be adjusted with two criteria in mind: T must be long enough to achieve the desired accuracy, but short enough so as not to include non-stationary changes in interference level. Neither of these restrictions on T seem very stringent. For the lowpass filter, h(t), W must be large enough to allow substantial power levels at the filter output but small enough so that the interference level is constant across the band. Another restriction on the wideness of h(t) bandwidth (when idle slots are used) relates to the amount of spectral space available in the data band for interference monitoring.

As a numerical example, we see that for W = 0.25 MHz (typical value of this parameter for power measurements on tropo channel - see Table 4-2) we have

$$\sigma_\epsilon \approx \frac{2}{\sqrt{T}} \qquad T \text{ in } \mu s \tag{4.518}$$

which corresponds to an error of 1% at 40 ms integration time.

It should be clear for out-of-band interference measurements that a very high measurement accuracy can be obtained, since restrictions on W would then be minimal. Unfortunately, however, the whole idea of using frequency band measurements only applies to the case of wideband interference that has a flat spectrum across the data band, i.e., is characterized as white noise as in Section 4.1.3. There is, of course, a wide variety of situations for which this characterization is valid. In such cases, the use of out-of-band measurements is sufficient and the use of idle frequency slots within the data band has little to recommend it, except, perhaps, its possibilities as a check on the flatness of the spectrum.

4.5.4 Use of Idle Time Slots: General Problems

4.5.4.1 Preliminary Comments

In this section we demonstrate that the use of idle time slots in the data (with a temporary service interrupt being a special case) is the most general and useful method for accumulating interference data. The reason for this, as developed later, is that the interference is picked off and analyzed in just such a way that its final form coincides exactly with the form it takes on in the receiver's decision circuitry. The manner in which this interference variable is processed, and the reliability of the measurements of the various pertinent interference parameters, is discussed in detail in the following sections.

We point out, here, an important fact which will be used extensively in Section 5.7; this is the fact that the probability of error for each of the communication systems listed in Table 4-3 depends directly and exactly on the joint probability density function of the generalized interference variables U and V, where U and V are given by

$$U = \sum_{k=1}^{k=L} |\xi_k|^2 \qquad V = \sum_{k=1}^{k=L} |\eta_k|^2 \tag{4.519}$$

In this expression, the index k just indicates summation over the L diversity branches, whereas the value of ξ and η can be found from Table 4-3 for a particular modulation format. Clearly, then, a totally accurate measurement of the joint pdf for U and V would lead to accurate predictions of error rate. This could be accomplished by the determination of a two-dimensional histogram for U and V, e.g., for bin resolutions ΔU and ΔV the entry in the ij^{th} bin would represent

$$p_{ij} = \text{Prob.}\left\{(i-1)\Delta U \le U \le i\Delta U, (j-1)\Delta V \le V \le j\Delta V\right\} \quad (4.520)$$

and would be estimated by counting all the pairs of samples $\{U_n, V_n\}$ which jointly satisfy the above inequalities and dividing by the total number of sample pairs to determine the relative frequency. Such a scheme, of course, is subject to errors that depend on the number of samples available and the bin resolution. The major drawback to this scheme (if high bin resolution is desired) is its complexity. Much simpler approaches, which lead to reliable bounds on the error rate, are available. These are discussed in Section 5.7. It should be pointed out, however, that these schemes are not totally unrelated to the problem of developing interference variable pdf's. In fact, the last procedure for developing error bounds, discussed in Section 5.7, makes direct use of a simple two-bin histogram of just one of the interference variables, U or V.

The requirements of measuring U and V under a variety of interference conditions rules out the use of frequency slots. This is because of the inherent distortion that n(t) and each of the noise variables in Table 4-3 would be subject to, were n(t) to be first passed through a narrowband filter. The use of idle time slots in the data, even to the point of a temporary service interrupt, is clearly superior in this respect. The interference can be processed in such a way that it appears for statistical processing at baseband in exactly the form that it would take on in the decision circuitry of the receiver. A block diagram, illustrating the processing procedures, is given in Figure 4-30. We note that the system pictured operates on θ only, i.e., $U = |\theta|^2$, and applies exactly to the coherent PSK case only. Similar processing schemes, for the other modulation formats, can easily be contrived using the interference variable definitions given in Table 4-3. We note, however, that the analysis only requires consideration of the noise variable θ. The justification of this approach was given at the end of Section 4.5.2.

In Sections 4.5.4.2 and 4.5.4.3 we explore some problems associated with measuring the mean and maximum value of U. In Section 4.5.4.4 we determine the reliability with which $\hat{p}$ can be estimated, where $\hat{p}$ is the measurement of the probability that U' exceeds some threshold. As discussed in Section 5.7, these topics relate very closely to the reliability with which the bounds on error probability can be determined. Because of time limitations, the calculations have been simplified to include only single diversity operation; the extension to more than one branch is conceptually straightforward.

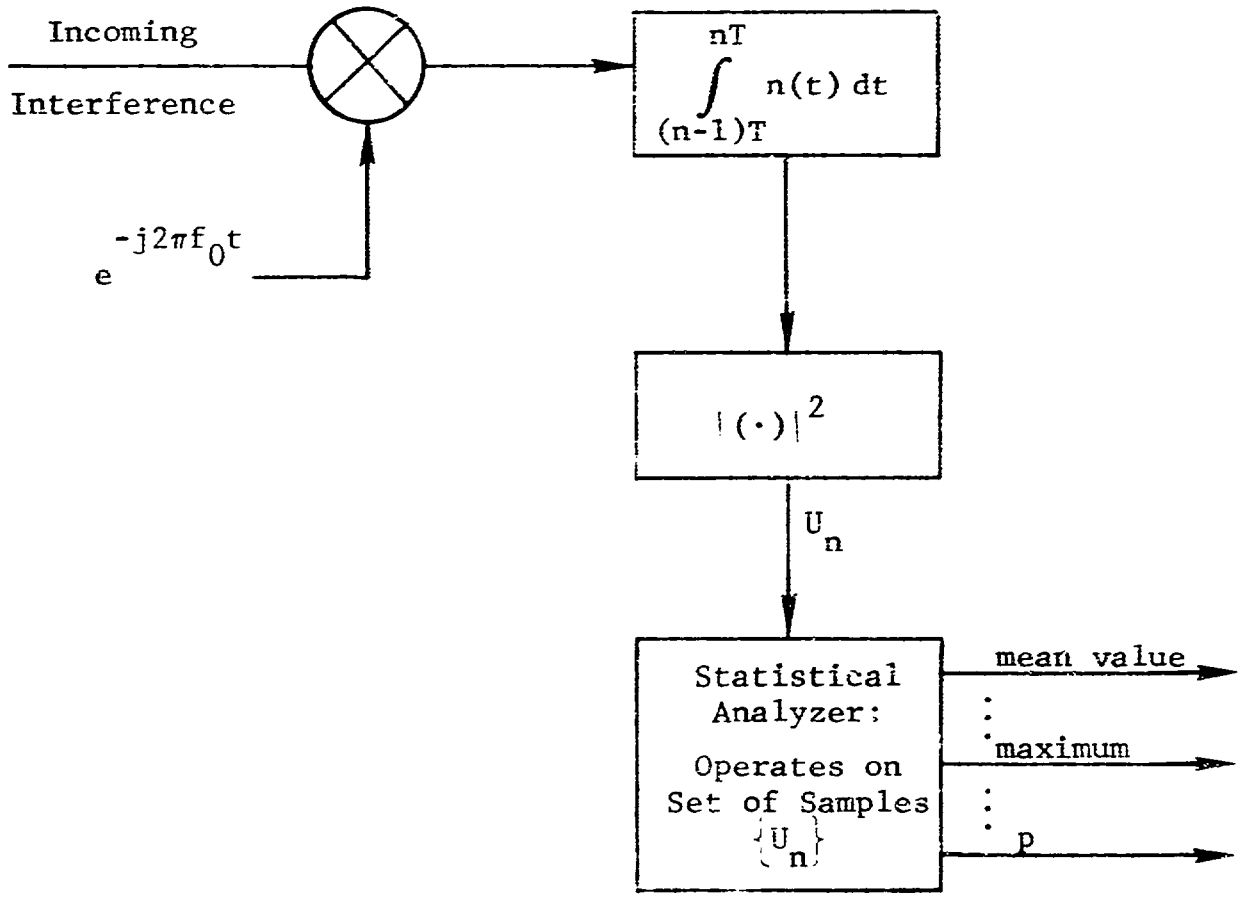

Figure 4.30 Interference Measurement during Service Interrupt

The detailed structure of the statistical analyses which generates the estimates of mean value, maximum, and threshold probability, p, are given in Figure 4.31. Examination of Figures 4.30 and 4.31 indicates clearly that the signal processing operations and the statistical analysis could be implemented in a straightfoward manner.

4.5.4.2 Reliability of Estimate of the Mean Value

It will be seen in Section 5.7 that the assigning of reliable bounds to error rate requires, as one would expect, reliable measurements of the signal-to-noise ratio, ρ. The problem of estimating the channel transfer function (and, hence, the average power of the received signal) has already been discussed in Section 4.3.4;this will not be further treated here.* In this section we determine the reliability with which the "noise" part of the signal-to-noise ratio can be measured. As in Section the noise power is denoted α and has the value

$$\alpha = \overline{U} \tag{4.521}$$

where

$$U = \left| \int_0^T n(t)\, dt \right|^2 \tag{4.522}$$

In the remainder of this section, emphasis is placed on the problem of determining the reliability with which α can be estimated.

Assuming the availability of a complete set of M interference samples $\{U_n\}$ at the input of the statistical process in Figure 4.30 the most direct (and reasonable) approach to generating an estimate of α is to perform an arithmetic average of the samples. As our estimate, denoted $\hat{\alpha}$, we then have

$$\hat{\alpha} = \frac{1}{M} \sum_{i=1}^{M} U_i \tag{4.523}$$

It can be noted immediately that the estimate is unbiased, i.e.,

$$\overline{\hat{\alpha}} = \overline{U} = \alpha \tag{4.524}$$

---

*The channel transfer function measurements will be reconsidered in Section 5.7 when we examine the way that probability of error bounds depends on measurement accuracy.

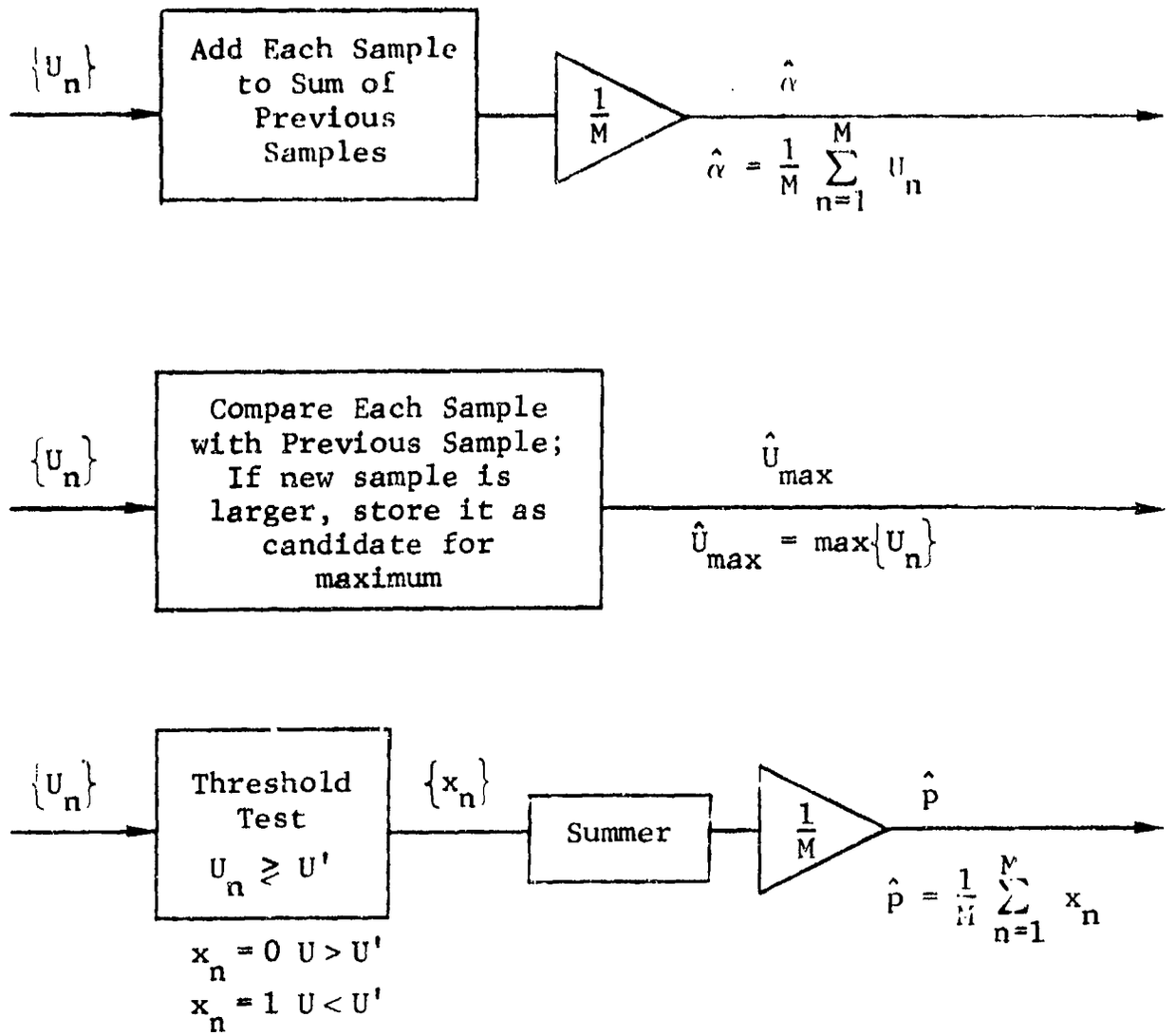

Figure 4.31 Illustration of Operations Used to Estimate Mean Value, Maximum Value, and Probability, p

The normalized estimation error is defined according to

$$\epsilon_\alpha = \frac{\hat{\alpha} - \alpha}{\alpha} \tag{4.525}$$

Its mean-squared value is simply

$$\overline{\epsilon_\alpha^2} = \frac{\overline{\hat{\alpha}^2} - \alpha^2}{\alpha^2} \tag{4.526}$$

The first term in the numerator is easily evaluated by squaring (4.523) and then averaging. We obtain

$$\overline{\hat{\alpha}^2} = \left(\frac{M-1}{M}\right)\bar{U}^2 + M\overline{U^2} \tag{4.527}$$

Substituting in (4.526) the normalized mean-squared error follows directly; the result for the rms fractional estimation is

$$\sqrt{\overline{\epsilon_\alpha^2}} = \sqrt{\frac{1}{M}\left\{\frac{\mathrm{Var}(U)}{(\bar{U})^2}\right\}} \tag{4.528}$$

where Var(U) is just used to denote the variance of U.

In view of (4.528), one can argue that the normalized root mean-squared error goes roughly as $1/\sqrt{M}$. In fact, if n(t) is a Gaussian noise process, then the fact that the integral in Figure 4.30 is the sampled output of a linear system responding to n(t) indicates that θ in

$$U = \left|\int_0^T n(t)\,dt\right|^2 = |\theta|^2 \tag{4.529}$$

is a complex Gaussian random variable. For such a random variable

$$\overline{|\theta|^4} = 2\left(\overline{|\theta|^2}\right)^2 \tag{4.530}$$

Hence,

$$\overline{U^2} = 2(\bar{U})^2 \tag{4.531}$$

and

$$\sqrt{\overline{\epsilon_\alpha^2}} = \frac{1}{\sqrt{M}}$$

and the normalized rms error goes <u>exactly</u> as $1/\sqrt{M}$.

4.5.4.3 Reliability of Estimate of the Crest Factor (Maximum)

Schemes for developing bounds on error rate will be discussed in Section 5.7. One of these schemes makes use of the crest factor, β_L. This factor is used in the probability of error bound calculations as a constraint on the values which the generalized noise variables, U can take on. Its definition is given by

$$\beta_L \triangleq \text{Max}\left\{\frac{\text{Peak U}}{\alpha_L}\right\} \tag{4.532}$$

where, as before, α_L represents the average noise "power".

$$\alpha_L = \bar{U} \tag{4.533}$$

and U is the generalized noise variable.

$$U = \sum_{k=1}^{L} |\xi_k|^2 \tag{4.534}$$

The summation over k refers to the different diversity branches, and the specific form of ξ_k depends on the particular modulation format as discussed earlier.

In order to establish bounds on probability of error through observations of special probing signals, estimates of both β_L and α_L are required. Estimation of α_L is straightforward and was discussed in the previous section. In this section we discuss the problems associated with estimating the maximum in (4.532); this problem is approached in a general context and results will be applied later.

It is clear that errors in estimating α_L and β_L have the effect of weakening the bounds on probability of error. The exact manner in which the bounds are affected by estimation errors will be discussed in Section 5.7.

The maximum, x_{max}, for a random variable, x, must satisfy three major conditions. In terms of the pdf, p(x), these conditions are:

1) $p(x) = 0 \qquad \text{for } x > x_{max}$
2) $P_r(x \leq x_{max}) = 1$
3) $P_r(x \leq x') < 1 \quad \text{where } x' < x_{max}$

For our purposes, it is only necessary to use the working definition that x_{max} is the largest value that any realization of the random variable can take on. Also, we make use, in the following, of the cumulative distribution

$$F_Z(z) \triangleq P_r\{Z \leq z\} \tag{4.535}$$

It will be clear from the ideas developed in the previous section that the estimate of the crest factor will be achieved by drawing on a set of M, identically distributed, random variables. These will be in the form of a collection of measurements made in separate and nonoverlapping time intervals. Now, the problem of determining an estimate for x_{max} is a simple one. The most direct approach is to just choose the maximum of all the realizations, i.e., as our estimate we use

$$\hat{x} = \max\{x_1, x_2, x_3, \ldots, x_M\} \tag{4.536}$$

where $\{x_1, \ldots, x_M\}$ is the set of M observations. Less, direct schemes, would use modified versions of (4.536) above, perhaps adding a small correction depending on M. Unfortunately, such tricks, if they are to be at all useful, require some prior knowledge of the pdf for each of the random variables. The nature of the problem here does not allow this assumption.

$F_{\hat{x}}(z)$ for the random variables in (4.536) can be calculated easily. We note simply that the region of M-dimensional space in which

$$\max\{x_1, \ldots, x_M\} \leq z \tag{4.537}$$

is identical with that for which

$$x_j \leq z \qquad j = 1,M \tag{4.538}$$

Hence,

$$F_{\hat{x}}(z) = F_{x_1,x_2,\ldots,x_M}(z, \ldots, z) \tag{4.539}$$

Now, utilizing the fact that the random variables are independent and identically distributed, we obtain the result

$$F_{\hat{x}}(z) = F_x^M(z) \tag{4.540}$$

The density function (pdf) follows immediately after differentiating (4.540)

$$f_{\hat{x}}(z) = M F_x^{(M-1)}(z) f_x(z) \tag{4.541}$$

It is from this expression that the various moments

$$\overline{\hat{x}^k} = M \int_{-\infty}^{+\infty} z^k F_x^{(M-1)}(z) f_x(z) \, dz \tag{4.542}$$

must be calculated.

To get a clear idea of how well the maximum can be estimated it is necessary to turn to some examples. So that we can present the rms errors for maximum and mean value together, the examples are treated in a separate section, Section 4.5.4.4, below.

4.5.4.4 Some Specific Examples

In this section, we analyze the reliability with which the mean values and maximum can be estimated for the specific pdf's illustrated in Figure 4.32.

As our first example, we consider the case of a random variable uniformly distributed between 0 and some upper limit x_{max}. For this distribution, it is a simple matter to calculate the variance and mean value required in (4.528). This gives for the rms fractional error in estimating the mean value, α, the result

$$\sqrt{\overline{\epsilon_\alpha^2}} = \frac{1}{\sqrt{3M}} \tag{4.543}$$

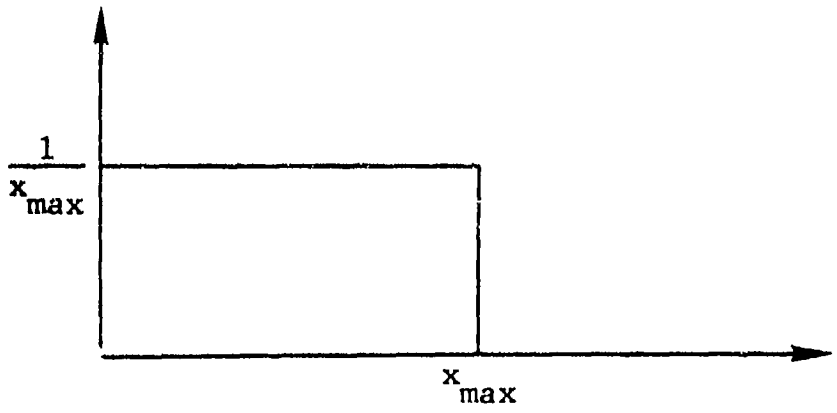

(a) Uniform Distribution

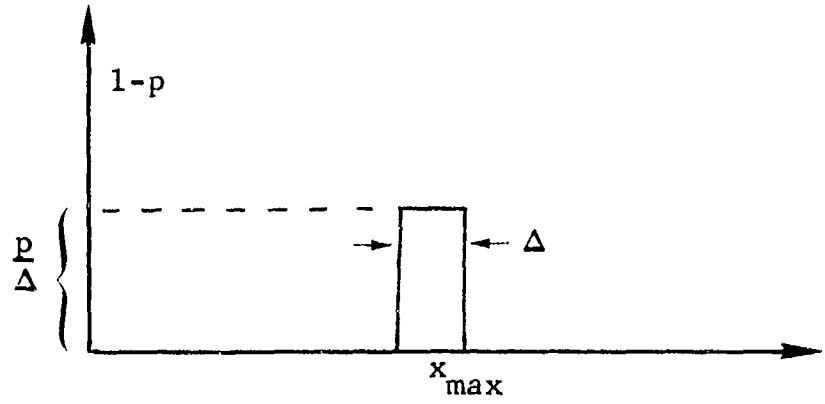

(b) Mixed pdf

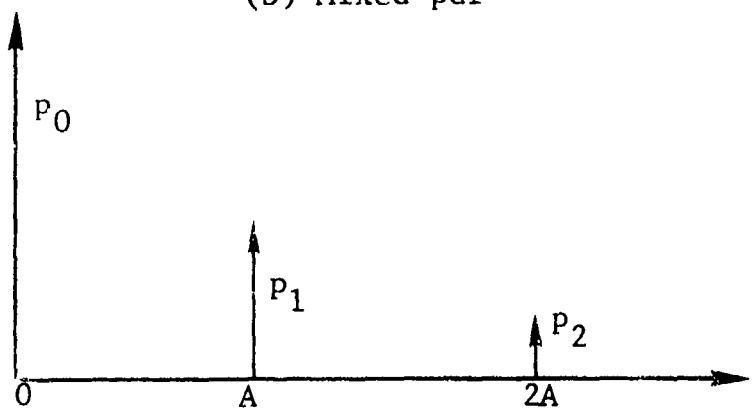

(c) Discrete pdf (Pulse Noise Jamming)

Figure 4.32 Probability Distributions Used as Examples for Calculating Measurement Errors

The rms fractional error in estimating the maximum is determined directly from substitution in (4.542). We obtain

$$\overline{\hat{x}} = \left(\frac{M}{M+1}\right) x_{max} \tag{4.544}$$

and

$$\overline{\hat{x}^2} = \left(\frac{M}{M+2}\right) x_{max}^2 \tag{4.545}$$

and utilizing the definition for the rms fractional error

$$\sqrt{\epsilon_u^2} = \sqrt{\overline{|\hat{x}_{max} - \hat{x}|^2}\Big/ x_{max}^2} \tag{4.546}$$

and normalized variance

$$\frac{\sigma_x}{x_{max}} = \sqrt{\overline{|\hat{x}_{max} - \bar{\hat{x}}|^2}\Big/ x_{max}^2} \tag{4.547}$$

we obtain the result

$$\overline{\epsilon_u^2} = \sqrt{\frac{2}{(M+1)(M+2)}} \sim \frac{\sqrt{2}}{M} \tag{4.548}$$

and

$$\frac{\sigma_x}{x_{max}} = \frac{M}{(M+1)^2(M+2)} \sim \frac{1}{M} \tag{4.549}$$

From (4.548) it is clear that choosing the maximum of the realizations is a procedure that gives rapid convergence to the true value, x_{max}, in the case of the uniform distribution. As (4.544) indicates, however, the estimate is biased, i.e., its mean value is not x_{max}. This could be remedied by choosing

$$\hat{x} = \left(1 + \frac{1}{M}\right) \max\{x_1, \ldots, x_M\} \tag{4.550}$$

for which it is easy to see

$$\overline{\hat{x}} = x_{max}$$

$$\overline{\hat{x}^2} = \frac{(M+1)^2}{M(M+2)} \; x_{max}^2 \tag{4.551}$$

and

$$\frac{\sigma_x}{x_{max}} = \sqrt{\overline{\epsilon_u^2}} = \sqrt{\frac{1}{M(M+2)}} \sim \frac{1}{M} \tag{4.552}$$

Tricks to improve the estimate, such as that given above, are not available if the pdf is not known, and one must settle for the estimate error given in (4.548). Clearly, the difference is negligible at large values of M.

The uniform distribution discussed above leads to an optimistic prediction of the estimator performance. This is because of the pdf's sharp cutoff at x_{max}, which means that there is always a reasonably high probability that realizations near x_{max} will actually occur. For pdf's that taper off more slowly, i.e., that have a low probability of realizations near x_{max}, the situation can be different. In fact, some analytical pdf's have no x_{max} value at all.

To get a clearer picture of the situation that exists when the probability of events near x_{max} is lower than it was for the uniform distribution, we examine the mixed pdf illustrated in Figure 4.32(b). For this pdf, there is a discrete probability of 1-p for zero values and a probability p of higher values. The higher values are uniformly distributed over an interval extending from $x_{max}-\Delta$ to x_{max}. The specific form for this pdf is given by

$$f_x(x) = (1 - p)\,\delta(x) + g(x) \tag{4.553}$$

where

$$g(x) = \begin{cases} \frac{p}{\Delta x} & , \; x_{max} - \Delta \leq x \leq x_{max} \\ \\ 0 & \text{otherwise} \end{cases} \tag{4.554}$$

The cumulative distribution defined in (4.535) is given by

$$F_x(z) = \begin{cases} 0 & z < 0 \\ (1-p) + \frac{p}{\Delta x}(x - x_{max} + \Delta) & x_{max} - \Delta < z < x_{max} \\ 1 & z \geq x_{max} \end{cases} \tag{4.555}$$

Physically, the statistical description given above could relate to the occurrence of pulse noise; the pulse is "on" with probability, p, but spread somewhat in pulse height over an amplitude range, Δx. Apart from this, though, the main interest here is in the mathematical properties of the pdf. In particular, we investigate the way the mean-squared error (M.S.E.) is altered when high amplitude values have a low probability of occurring.

We turn first to the calculation of the rms fractional error in estimating the mean value. It is a simple matter to utilize (4.554) for the moment calculations required in (4.528). The mean-squared fractional error is then given by

$$\overline{\epsilon_\alpha^2} = \frac{(1-p) - (1-p)\frac{\Delta}{x_{max}} + \frac{\Delta^2}{3x_{max}^2}\left(1 - \frac{3}{4}p\right)}{Mp\left[1 - \frac{\Delta}{x_{max}} + \frac{\Delta^2}{4x_{max}^2}\right]} \tag{4.556}$$

For small Δ relative to x_{max} this expression simplifies; for the rms fractional error in estimating the mean, we obtain

$$\sqrt{\epsilon_\alpha^2} \approx \sqrt{\frac{(1-p)}{Mp}} \tag{4.557}$$

The error in estimating the maximum can also be calculated easily. We need only substitute the density of (4.553) and the distribution of (4.555) into (4.542) and evaluate the integral for k=1 and k=2.

We find

$$\bar{\bar{x}} = \frac{\Delta x^2}{p^2}\left\{\frac{p(M+1)-1}{M+1} + \frac{1}{(M+1)}(1-p)^{M+1}\right\}$$

$$+ \frac{(x_{max} - \Delta x)}{p}\Delta x\left\{1 - (1-p)^M\right\} \qquad (4.558)$$

Though mildly biased at low values of n, this estimate is asymptotically unbiased, i.e., $\bar{\bar{x}} \to x_{max}$ as $M \to \infty$. Evaluating the M.S.E. we find, after considerable simplification, neglecting all terms that go as $1/M^2$ and using the large M approximation $(1/M+1) \approx 1/M$, that

$$\text{M.S.E.} \approx \frac{(\Delta x)^2}{p^2}\left\{-\frac{2p}{M} + p^2\right\} + \frac{2(x_{max} - \Delta x)\Delta x}{p}\left\{p - \frac{1}{M} + \frac{(1-p)^{M+1}}{M}\right\}$$

$$+ (x_{max} - \Delta x)^2\left\{1 - (1-p)^M\right\} - \frac{2\Delta x}{p}\left\{p - \frac{1}{M} + \frac{(1-p)^{M+1}}{M}\right\}$$

$$- 2(x_{max} - \Delta x)x_{max}\left\{1 - (1-p)^M\right\} + x_{max}^2 \qquad (4.559)$$

From this expression, it is easy to show that

$$\lim_{M\to\infty} \text{M.S.E.} \to 0 \qquad (4.560)$$

The rate at which the M.S.E. decreases can be determined by retaining the dominant terms in (4.559). We obtain

$$\text{M.S.E.} \approx x_{max}^2\left[1 - \left(\frac{\Delta x}{x_{max}}\right)^2\right](1-p)^M \qquad (4.561)$$

which, in turn, is approximately equal to $x_{max}^2(1-p)^M$ if the pulse amplitude spread is small. The normalized M.S.E., or fractional error, is obtained by dividing by x_{max} and taking the square root.

We have finally

$$\sqrt{\overline{\epsilon_u^2}} \approx (1-p)^{M/2} \tag{4.562}$$

This result indicates clearly that it is difficult to estimate x_{max} accurately when there is a low probability of the higher amplitude events occurring [small p in (4.562)].

To give an idea of the numbers involved, we have calculated some numerical values for a pulse probability, $p = 0.01$. These are entered in Table 4-4.

It is clear from the above analysis that effective estimation can be made of the maximum for a random variable with the pdf given in (4.553), provided a sufficient, but not unreasonable, number of samples are available. For probability density functions that taper off slowly at high values, the situation could be much more pessimistic, since x_{max} could be far removed from all those values which occur with significant probability. In fact, for some analytical forms, there are no upper bounds at all, and the problem is not meaningful. We note, however, that all experimental pdf's have bounding values due to dynamic range limitations in receivers, and that the problem is always meaningful from this viewpoint.

Comparing our ability to estimate the mean value with our ability to estimate the maximum value, we note from (4.557) that the fractional error in estimating the mean can also be large at small p. For the mean, however, the rms fractional error is large because of normalization by a small quantity. If we were to have normalized with x_{max} rather than the mean value $\bar{x}$, the rms fractional error in estimating the mean value would have been considerably smaller; in fact, the fractional error normalized to x_{max} would have had the value

$$\sqrt{\overline{\epsilon_\alpha^2}} \approx \sqrt{\frac{(1-p)}{M}} \tag{4.563}$$

which, in terms of absolute values, indicates more rapid convergence of the mean value estimate at small values of p than for the maximum value estimate.

TABLE 4-4

FRACTIONAL ERROR IN ESTIMATING x_{max} WHEN "PULSE PROBABILITY", p, IS 0.01

Number of Samples	RMS Fractional Estimation Error
100	0.606
200	0.367
300	0.221
400	0.134
500	0.083
600	0.042

$p = 0.01$

We turn now to the final pdf illustrated in Figure 4.32(c). This pdf will take on practical significance in Section 4.5.5. Analytically, it has the form

$$f(x) = p_0\delta(x) + p_1\delta(x - A) + p_2\delta(x - 2A) \tag{4.564}$$

It is a simple matter to calculate the moments

$$\bar{x} = A(p_1 + 2p_2) \tag{4.565}$$

and

$$\overline{x^2} = A^2(p_1 + 4p_2) \tag{4.566}$$

Direct substitution in (4.528) now gives

$$\sqrt{\epsilon_\alpha^2} = \sqrt{\frac{p_1 + 4p_2 - p_1^2 - 4p_2^2 - 4p_1p_2}{M\left(p_1^2 + 4p_2^2 + 4p_1p_2\right)}} \tag{4.567}$$

for the rms fractional error in estimating the mean value. Presentation of numerical results is deferred until Section 4.5.5.

Turning now to the measurement of the maximum value, we note immediately that one of the inherent difficulties associated with (4.564) is that it is not directly amenable to calculation using (4.542) because the impulses in $f_x(x)$ occur at exactly the same locations as the discontinuities in $F_x^{(n-1)}(x)$. This is remedied by using a limiting form for the impulsive contributions; we use

$$f_x(x) = p_0\delta(x) + p_1g_1(x) + p_2g_2(x) \tag{4.568}$$

where

$$g_1(x) = \begin{cases} \dfrac{p_1}{2\Delta} & A-\Delta \le x \le A+\Delta \\ 0 & \text{otherwise} \end{cases} \tag{4.569}$$

and

$$g_2(x) = \begin{cases} \frac{p_2}{2\Delta} & 2A-\Delta \le x \le 2A+\Delta \\ 0 & \text{otherwise} \end{cases} \tag{4.570}$$

and, at the completion of the calculations, will take the limit $\Delta \to 0$. By utilizing (4.535) and integrating the expressions above, we obtain

$$F(x) = \begin{cases} 0 & x < 0 \\ p_0 & 0 \le x < A-\Delta \\ p_0 + \frac{p_1}{2\Delta}[x - (A - \Delta)] & A-\Delta \le x < A+\Delta \\ p_0 + p_1 & A+\Delta \le x < 2A-\Delta \\ p_0 + p_1 + \frac{p_2}{2\Delta}[x - (2A - \Delta)] & 2A-\Delta \le x < 2A+\Delta \\ 1 & x \ge 2A+\Delta \end{cases} \tag{4.571}$$

If we now substitute this expression in (4.542) we obtain the approximate result (exact as $\Delta \to 0$)

$$\overline{\hat{x}^k} \approx \frac{M p_1}{2\Delta} A^k \int_{A-\Delta}^{A+\Delta} \left\{ p_0 + \frac{p_1}{2\Delta}[x - (A - \Delta)] \right\}^{M-1} dx$$

$$+ \frac{M p_2}{2\Delta} (2A)^k \int_{2A-\Delta}^{2A+\Delta} \left\{ p_0 + p_1 + \frac{p_2}{2\Delta}[x - (2A - \Delta)] \right\}^{M-1} dx \tag{4.572}$$

The integrals can be easily calculated, with the final result

$$\overline{\hat{x}^k} = A^k\left[(p_0+p_1)^M - p_0^M\right] + (2A)^k\left[1 - (p_0+p_1)^M\right] \quad (4.573)$$

a relation which is exact in the limit $\Delta \to 0$.

This moment relation, for the maximum of M independent samples, can be used to calculate the mean-squared fractional error

$$\overline{\epsilon_u^2} = \overline{\left(\hat{x}_{max} - x_{max}\right)^2} \Big/ x_{max}^2 \quad (4.574)$$

where, here, x_{max} is the maximum 2A. We have

$$\overline{\epsilon_u^2} = \frac{\overline{\hat{x}^2}}{(2A)^2} - \frac{\overline{\hat{x}}}{A} + 1 \quad (4.575)$$

Specifically, for the problem at hand, we have as the rms fractional error

$$\sqrt{\overline{\epsilon_u^2}} = \sqrt{1 - \left[1 - (p_0+p_1)^M\right] - \frac{3}{4}\left[(p_0+p_1)^M - p_0^M\right]} \quad (4.576)$$

By considering the case $p_2 = 0$, it can be shown by using the expressions for $\overline{\hat{x}^2}$ and $\overline{\hat{x}}$, and the fact $p_0 + p_1 = 1$, that the rms fractional error is given by

$$\sqrt{\overline{\epsilon^2}} = \left(1 - p_1\right)^{M/2} \quad (4.577)$$

This reinforces the intuitive notion that the reliability of the estimate of the maximum must decrease with decreasing probability, p_1, of events near the maximum.

The practical importance of this pdf and the results of some numerical calculations will be presented in Section 4.5.5.

4.5.4.5 Reliability of Probability Estimate

In Section 5.7, we will examine a scheme for developing error probability bounds that makes use of measurements of the probability that the generalized noise variable, U, exceeds some threshold, U'. In this section we determine the accuracy with which such measurements can be made.

Assuming the availability of a set of M independent interference measurements $\{U_n\}$, we denote as x_n the binary random variable

$$x_n = \begin{cases} 0 & U_n < U' \\ 1 & U_n \geq U' \end{cases} \tag{4.578}$$

which results directly from comparisons of the noise realization with the fixed threshold U'; then we note immediately that

$$\overline{x_n} = 0 \cdot (1 - p) + 1 \cdot p = p \tag{4.579}$$

and, similarly, that

$$\overline{x_n^2} = p \tag{4.580}$$

Clearly, a useful measurement of the probability, p, can be obtained by forming the arithmetic average of the random variables x_n; denoting the estimate of p as $\hat{p}$, we have

$$\hat{p} = \frac{1}{M} \sum_{n=1}^{M} x_n \tag{4.581}$$

This is an unbiased estimate because of the fact that

$$\overline{\hat{p}} = p$$

which follows directly from (4.579). Hence, the mean-squared fractional error in estimating p is given by

$$\overline{\epsilon_p^2} = \frac{\mathrm{Var}(\hat{p})}{p^2} \tag{4.582}$$

where Var is just the variance of $\hat{p}$.

$$\mathrm{Var}(\hat{p}) = \overline{(\hat{p} - p)^2} = \overline{\hat{p}^2} - p^2 \tag{4.583}$$

The second moment of $\hat{p}$ is easily evaluated by squaring (4.581) and utilizing (4.579) and (4.580). For the variance of $\hat{p}$, we obtain

$$\mathrm{Var}(\hat{p}) = \frac{p(1 - p)}{M} \tag{4.584}$$

Thus, the rms fractional error is given by

$$\sqrt{\overline{\epsilon_p^2}} = \sqrt{\frac{1}{M}\left(\frac{1 - p}{p}\right)} \tag{4.585}$$

Clearly, when U' is near the median, the rms fractional error goes as 1/M, whereas when p is smaller, e.g., $p = 0.01$, we have

$$\sqrt{\overline{\epsilon_p^2}} \approx \sqrt{\frac{100}{M}} \tag{4.586}$$

We recall that interference data can be accumulated at the data rate during an out-of-service look. Thus on the slowest channel, HF, at about 100 bits per second, the rms error for $p = 0.01$ can be reduced to 1% in about 100 seconds, whereas on the tropo channel, which is capable of megabit operation, the same accuracy could be obtained in 10 milliseconds.

These general conclusions, which for the most part are independent of particular interference models, motivate the development of error rate bounds using measurements of p as a possible alternative to using measurements of the maximum. This question is explored further in Section 5.7.

We note, finally, that there are certain types of interference that require separate examination; these are slowly varying interference and pulse noise. The first poses a special

problem because the elements in a set of samples $\{U_n\}$ collected at the data rate need not be independent. The question here just breaks down to that of finding out how long a time span is required to obtain independent samples; the result in (4.585), which is framed solely in terms of the number of such samples, still holds.

4.5.5 A Special Problem: Pulse Noise Jamming

In order to obtain a clearer view of the reliability with which estimates of interference mean and maximum values can be obtained, we treat a special problem in this section, that of pulse noise jamming.

It is assumed that the jamming signal consists of wideband pulses which appear at the receiver with more or less constant amplitude but a pseudo-random distribution in time; the jamming signal has periodicity in the sense that a jamming pulse is launched every periodic interval, T_p, but is randomly located somewhere within the interval. Additionally, the jamming pulse has unknown synchronization, i.e., unknown time origin.

Because of the wideband nature of the jamming pulses, the interference processor of Figure 4.30 responds to the input pulses as if they were impulsive. Because of time limitations, we will treat the case of n(t) real. The use of a complex n(t) would, through the random phase, result in a continuous distribution for which the true maximum would occur with probability zero. Nevertheless, some important insights into the measurement reliability can be determined by using an analytical representation for the interference of the form

$$n(t) = \sum_{k=-\infty}^{+\infty} A\, \delta(t - kT_p - \xi_k - \xi) \qquad (4.587)$$

where T_p is the period of the jamming pulse train, ξ is the unknown synchronization (time origin) and is a random variable uniformly distributed between 0 and T_p, and ξ_k represents the deliberately randomized pulse location within each period and is a random variable uniformly distributed between kT_p and $(k+1)T_p$.

The incoming interference is observed over a time interval (0,T) where T is much smaller than the pulse period, T_p. This implies that the probability density function of the detected noise variable

$$U = \int_0^T n(t)\, dt \qquad (4.588)$$

has the form

$$p_U(x) = p_0\delta(x) + p_1\delta(x - A) + p_2\delta(x - 2A) \tag{4.589}$$

The third term in this expression occurs because of the small but non-negligible probability of two pulses occurring in the interval (0,T). This event, of course, can only happen in the event that ξ falls in the interval (0,T).

Turning now to calculation of the probabilities p_1 and p_2, we note that

$$p_1 = \Pr\{N=1 \mid \xi \text{ not in } (0,T)\} \Pr\{\xi \text{ not in } (0,T)\}$$
$$+ \Pr\{N=1 \mid \xi \text{ in } (0,t)\} \Pr\{\xi \text{ in } (0,T)\} \tag{4.590}$$

and

$$p_2 = \Pr\{N=2 \mid \xi \text{ in } (0,T)\} \Pr\{\xi \text{ in } (0,T)\} \tag{4.591}$$

It is noted immediately that

$$\Pr\{\xi \text{ in } (0,T)\} = T/T_p \tag{4.592}$$

and

$$\Pr\{\xi \text{ not in } (0,T)\} = 1 - T/T_p \tag{4.593}$$

For simplicity of notation, we now define the event

$$A = \{N=2 \mid \xi \text{ in } (0,T)\} \tag{4.594}$$

and calculate the probability of the event A given ξ. It is easy to see that this event can be framed in terms of a single joint event involving the ξ_k. We have

$$\Pr\{A|\xi\} = \Pr\{\xi_{-1} \text{ in } (0,T)\,,\, \xi_0 \text{ in } (0,T)\}$$

$$= \frac{\xi(T-\xi)}{T_p^2} \tag{4.595}$$

Utilizing the mixed probability expression

$$\Pr\{A|\xi\}\; p(\xi) = p(\xi|A)\; \Pr(A) \tag{4.596}$$

and the fact that

$$p(\xi|A) = p[\xi|\xi \text{ in } (0,T)] = \begin{cases} \frac{1}{T} & 0 \le \xi \le T \\ 0 & \text{elsewhere} \end{cases} \tag{4.597}$$

we can integrate both sides of (4.596) to obtain the result

$$\Pr(A) = \int_0^T \Pr(A|\xi)\, p(\xi)\, d\xi = \frac{1}{6}\left(\frac{T}{T_p}\right)^3 \tag{4.598}$$

Thus, from (4.591) and (4.592)

$$p_2 = \frac{1}{6}\left(\frac{T}{T_p}\right)^4 \tag{4.599}$$

We now turn to calculation of p_1. Clearly

$$\Pr\{N=1 \mid \xi \text{ not in } (0,T)\} = \frac{T}{T_p} \tag{4.600}$$

We now need only calculate the probability of the event

$$B = \{N=1 \mid \xi \text{ in } (0,T)\} \tag{4.601}$$

which is most easily accomplished by calculating the probability of the condition event $\{B|\xi\}$, i.e.,

$$\Pr\{B|\xi\} = \Pr\{\xi_{-1} \text{ in } (0,\xi)\} \cdot \left[1 - \Pr\{\xi_0 \text{ in } (\xi,T)\}\right]$$

$$+ \left[1 - \Pr\{\xi_{-1} \text{ in } (0,\xi)\}\right] \cdot \Pr\{\xi_0 \text{ in } (\xi,T)\}$$

$$= \left(\frac{\xi}{T_p}\right)\left(1 - \frac{T-\xi}{T_p}\right) + \left(1 - \frac{\xi}{T_p}\right)\left(\frac{T-\delta}{T_p}\right)$$

$$= \frac{T}{T_p} - 2\left[\frac{\xi(T-\xi)}{T_p}\right] \qquad (4.602)$$

Thus

$$\Pr\{N=1 \mid \xi \text{ in } (0,T)\} = \frac{T^2}{T_p^2}\left[1 - \frac{1}{3}\frac{T}{T_p}\right] \qquad (4.603)$$

and, finally,

$$p_1 = \left(\frac{T}{T_p}\right)\left[1 - \frac{T}{T_p} + \left(\frac{T}{T_p}\right)^2 - \frac{1}{3}\left(\frac{T}{T_p}\right)^3\right] \qquad (4.604)$$

The value of p_0 is specified immediately from knowledge of p_1 and p_2. These results can now be summarized; defining $\lambda T = T/T_p$ where λ takes on the meaning of a rate parameter (jamming pulses per second) for the incoming interference, we have

$$p_0 = 1 - (\lambda T)\left[1 - (\lambda T) + (\lambda T)^2 - \frac{1}{6}(\lambda T)^3\right]$$

$$p_1 = (\lambda T)\left[1 - (\lambda T) + (\lambda T)^2 - \frac{1}{3}(\lambda T)^3\right]$$

$$p_2 = \frac{1}{6}(\lambda T)^4 \qquad (4.605)$$

Thus, for a given value of λ, the three probabilities in (4.605) are completely specified. The resulting pdf of (4.589) is completely specified and is the same as that treated earlier [see (4.564)]. The rms fractional errors in measuring the mean value and maximum [see (4.567) and (4.576)] are plotted in Figure 4.33 for $\lambda T = 0.1$. This corresponds to the physical situation wherein one jamming pulse occurs on the average every ten data pulse intervals of length T.

4.5.6 Summary and Recommendations

We have seen that interference data can be rapidly and reliably collected in a wide variety of circumstances.

In Section 4.5.2 we reviewed the concept of generalized interference variable, and documented the specific forms in certain modulation schemes.

In Section 4.5.3 we described how measurements of interference can be accomplished by using idle frequency slots in the data; these measurements are essentially just power measurements and their utility is limited to those situations wherein it can be safely assumed that the interference is white Gaussian noise. In view of the wide variety of naturally-occurring and man-made interferences, this could be an extreme limitation.

Because of the fact that the effect of interference on error rate in communication receivers can be characterized in terms of certain generalized interference variables (as discussed in Section 4.5.2), it was found in Section 4.5.4 that the use of idle time slots in the data can lead to interference measurements of just such a form that simple statistical processing provides estimates and bounds on error rate. These measurements can take the form of a temporary service interrupt ("quick-look-out-of-service") or the form of idle time slots multiplexed into the data. Implementation of this latter scheme would require some practical investigations into the possibility and/or extent of intersymbol interference (resulting in data corruption of the idle slot) though one ramification is immediately transparent; if the idle slots are made to occur in blocks, e.g., three, and only the central one is used for the interference measurement in order to avoid data symbol overlaps, then the required number of idle slots must go up correspondingly, e.g., by a factor of 3.

Because of the digital character, the interference measurements seem especially amenable to processing with a small computer. Additionally, their direct relation to the form that the interference actually takes on in the decision circuitry of the receiver indicates that this approach to interference measurement

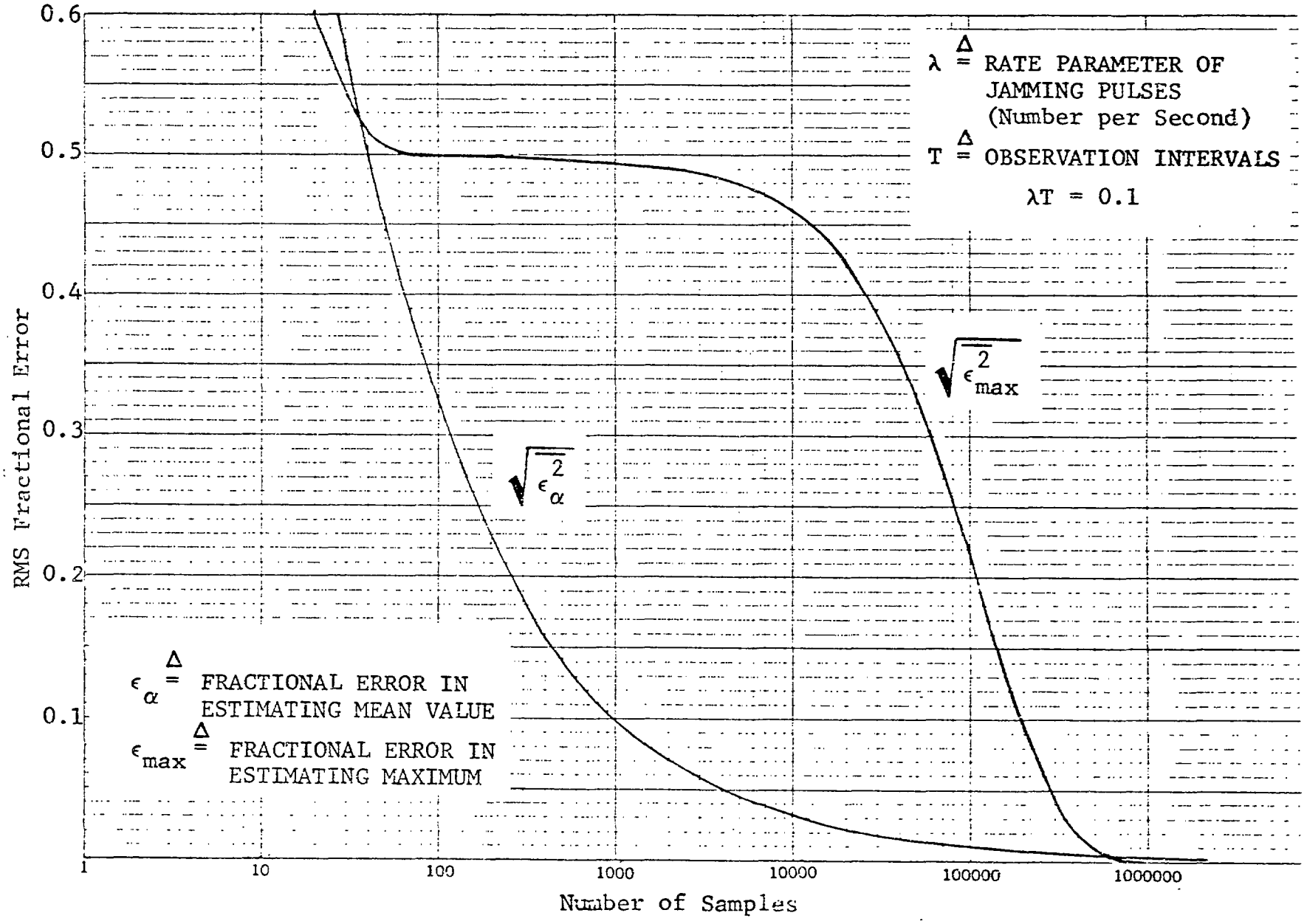

Figure 4.33 RMS Fractional Measurement Errors for Pulse Jamming ($\lambda T = 0.1$)

can be used as the building block for monitoring systems that use a more sophisticated statistical analyzer than that studied in this report. Ideally, a more complete computational ability of the processor could lead to generation of probability density functions for the interference variables. Because of the general approach taken here, these probability density functions could then be used to generate estimates of error probability. This topic is discussed at greater length in Section 5.7.

In this report we concentrated on the measurement of interference mean value, maximum value, and threshold probability. These were covered in Sections 4.5.4.2, 4.5.4.3, and 4.5.4.5, respectively. (The method by which error rate bounds can be generated from measurements of interference mean value and maximum value is deferred until Section 5.7.) It was found that reliable estimates could be obtained in processing times that vary with the type of interference. The reliability of the estimation schemes was treated at an elementary theoretical level in Section 4.5.4.3 and was applied to a special problem, that of pulse noise jamming, in Section 4.5.5.

REFERENCES FOR SECTION 4

[4.1] R. Arens, "Complex Processes for Envelopes of Normal Noise," IRE Trans. on Information Theory, pp. 204-207 (September 1957).

[4.2] K. S. Miller, "Moments of Complex Gaussian Noise," Proc. of the IEEE, pp. 83-84 (January 1968).

[4.3] A. H. Nuttall, "High-Order Covariance Functions for Complex Gaussian Processes," IRE Trans. on Information Theory, pp. 255-256 (April 1962).

[4.4] I. S. Reed, "On a Moment Theorem for Complex Gaussian Processes," IRE Trans. on Information Theory, pp. 194-195 (April 1962).

[4.5] P. A. Bello, "Time-Frequency Duality," IEEE Trans. on Information Theory, pp. 18-33 (January 1964).

[4.6] P. A. Bello, "Characterization of Randomly Time-Variant Linear Channels," IEEE Trans. on Communication Systems, pp. 360-393 (December 1963).

[4.7] P. A. Bello and L. Ehrman, "Error Rates in Diversity FDM-FM Digital Troposcatter Transmission," IEEE Comm. Tech., pp. 184-191 (April 1969).

[4.8] P. Bello, "Aeronautical Channel Characterization," IEEE Trans. on Comm., pp. 548-563 (May 1973).

[4.9] R. S. Lawrence, C. G. Little, and H. J. A. Chivers, "A Survey of Ionospheric Effects Upon Earth-Space Radio Propagation," Proc. of the IEEE, pp. 4-27 (January 1964).

[4.10] R. R. Taur, "Ionospheric Scintillation at 4 and 6 GHz," COMSAT Technical Review, pp. 145-163 (Spring 1973).

[4.11] P. A. Bello, "Some Techniques for the Instantaneous Real-Time Measurement of Multipath and Doppler Spread," IEEE Trans. on Comm. Tech., pp. 285-292 (September 1965).

[4.12] P. A. Bello, "Joint Estimation of Delay, Doppler, and Doppler Rate," IRF Trans. on Information Theory, pp. 330-341 (June 1960).

[4.13] P. A. Bello and R. Esposito, "Measurement Techniques for Time-Varying Dispersive Channels," Alta Frequenza, Vol. XXXIX, pp. 980-996 (1970).

[4.14] P. A. Bello, "On the RMS Bandwidth of Nonlinearly Envelope Detected Narrow-Band Gaussian Noise," IEEE Trans. on Information Theory, pp. 236-239 (April 1965).

[4.15] L. Ehrman and R. Esposito, "On the Accuracy of the Envelope Method for the Measurement of Doppler Spread," IEEE Trans. on Comm. Tech., pp. 578-581 (October 1969).

[4.16] K. A. Norton, et al., "The Rate of Fading in Propagation Through a Turbulent Atmosphere," Proc. IRE, Vol. 43, pp. 1341-1353 (October 1955).

[4.17] S. O. Rice, "Distribution of the Duration of Fades in Radio Transmission: Gaussian Noise Model," BSTJ, pp. 581-635 (May 1958).

[4.18] S. O. Rice, "Statistical Properties of a Sine Wave Plus Random Noise," BSTJ, pp. 109-157 (January 1948).

[4.19] R. Cox, Renewal Theory, Halsted Press (1962).

[4.20] H. L. VanTrees, Detection Estimation and Modulation Theory, Part I, John Wiley & Sons, New York (1968).

[4.21] C. Hastings, Approximations for Digital Computers, Princeton University Press, Princeton, N.J. (1955)

[4.22] P. A. Bello, et al., "Modeling and Data Analysis -- Short and Medium Range Digital Troposcatter Tests," Signatron, Inc., Final Technical Report, RADC-TR-69-233, Vol. 1 (October 1969). (AD862767)

[4.23] P. A. Bello, "Error Probabilities Due to Atmospheric Noise and Flat Fading in HF Ionospheric Communication Systems," IEEE Trans. on Communication Technology, Vol. COM-13, No. 3, pp. 266-279 (September 1965).

MISSION
of
Rome Air Development Center

RADC is the principal AFSC organization charged with planning and executing the USAF exploratory and advanced development programs for information sciences, intelligence, command, control and communications technology, products and services oriented to the needs of the USAF. Primary RADC mission areas are communications, electromagnetic guidance and control, surveillance of ground and aerospace objects, intelligence data collection and handling, information system technology, and electronic reliability, maintainability and compatibility. RADC has mission responsibility as assigned by AFSC for demonstration and acquisition of selected subsystems and systems in the intelligence, mapping, charting, command, control and communications areas.